LIÈGE université
Gembloux
Agro-Bio Tech

Rapid detection and biocontrol of *Fusarium verticillioides*, a major pathogen of maize ear and stalk rot

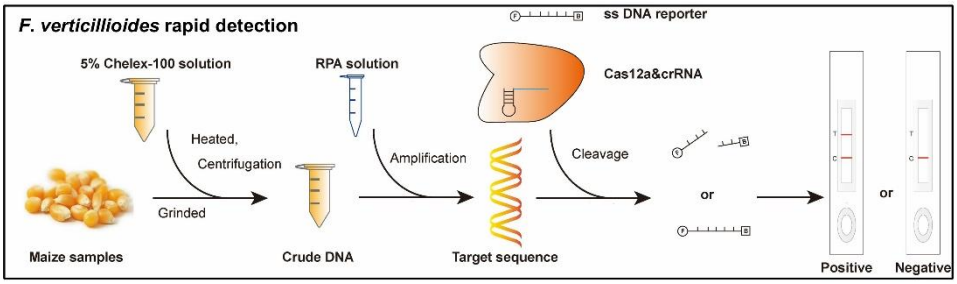

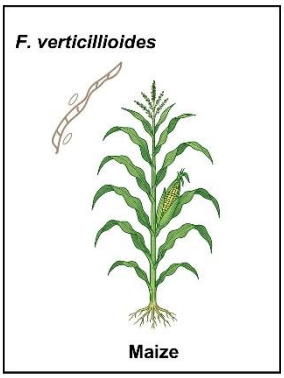

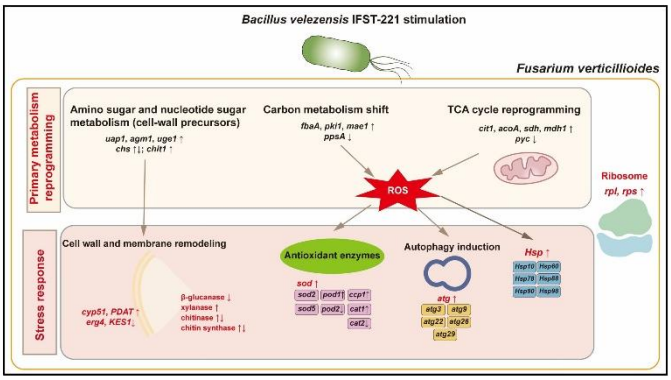

Author: Xiaoyan LIANG

Supervisor: Prof. M. Haïssam Jijakli

Co-supervisor: Prof. Wei GUO

Year: 2026

COMMUNAUTÉ FRANÇAISE DE BELGIQUE
UNIVERSITÉ DE LIÈGE – GEMBLOUX AGRO-BIO TECH

Rapid detection and biocontrol of *Fusarium verticillioides*, a major pathogen of maize ear and stalk rot

Xiaoyan LIANG

Dissertation originale présentée (ou essai présenté) en vue de l'obtention du grade de doctorat en sciences agronomiques et ingénierie biologique

Promoteur(s) : Prof. M. Haïssam Jijakli
Prof. Wei GUO

Année civile : 2026

Copyright

Citation: Liang Xiaoyan, 2026. From Rapid detection and biocontrol of *Fusarium verticillioides*, a major pathogen of maize ear and stalk rot. PhD Thesis. University of Liège - Gembloux Agro-Bio Tech, Belgium.

Abstract

Maize (*Zea mays* L.) is one of the world's most important cereal crops, providing a major source of food, animal feed, and industrial raw materials globally. *Fusarium verticillioides*, the primary causal agent of maize ear and stalk rot, threatens maize production due to its pathogenicity and fumonisin production, which poses serious risks to food safety and international trade. This study developed a field-deployable molecular diagnostic platform and characterized an effective biocontrol agent for the management of *F. verticillioides*.

A rapid, sensitive, and minimal-equipment assay was developed based on Chelex-100 resin-based DNA extraction, *FUM1* gene targeting, and recombinase polymerase amplification coupled with CRISPR/Cas12a-based cleavage and lateral flow detection. This assay demonstrated an analytical sensitivity close to one genomic equivalent and completed the diagnostic process within 73 minutes. In field validation with diseased maize kernels from Shanxi Province, the assay identified two positive samples, which were confirmed as *F. verticillioides* by single-spore isolation and *TEF-1α* sequencing.

A promising biocontrol strain, *Bacillus velezensis* IFST-221, isolated from the maize rhizosphere, exhibited broad-spectrum antifungal activity, inhibiting the mycelial growth of *F. verticillioides* by 62.63% in plate confrontation assays. In maize kernel assays, FB_1 levels decreased from 5,700 to 19.6 ppb after pretreatment with IFST-221. In greenhouse trials against cotton Verticillium wilt, pretreatment with IFST-221 reduced disease severity index from 73.21% to 8.93% and disease incidence from 85.71% to 14.29%, while also promoting better plant growth. IFST-221 additionally stimulated seedling growth in maize, tomato, and broccoli. Genome sequencing revealed a 3.86 Mb genome encoding nine secondary metabolite clusters, including surfactin, fengycin, bacillibactin, macrolactin H, difficidin, bacillaene, bacilysin, butirosin A/B, andalusicin A/B, and three unknown secondary metabolites, along with PGPR-related genes such as nitrogen fixation, indole-3-acetic acid biosynthesis, phosphate solubilization, and biofilm formation.

To elucidate the antifungal mechanism of IFST-221, liquid chromatography-tandem mass spectrometry (LC-MS/MS) and gene knockout analyses were conducted. Surfactins were detected in the crude extract, and deletion of the *srfAA* gene reduced the antifungal activity of mutant extracts; however, overall biocontrol efficacy remained largely unaffected in dual culture and maize kernel infection assays, suggesting that surfactin plays only a partial role. Further transcriptomic profiling of *F. verticillioides* under bacterial challenge revealed reprogramming of primary metabolism, ribosome-related genes, cell wall- and membrane-associated processes, and stress-adaptive pathways such as antioxidant defense, autophagy, and heat shock proteins. These findings illustrate the dynamic interaction between *B. velezensis* IFST-221 and its fungal target and provide a molecular framework for optimizing biocontrol efficacy.

Collectively, this study presents a robust framework for sustainable maize protection by advancing both rapid molecular diagnostic and the mechanistic

characterization of a promising biocontrol agent. The findings lay a strong foundation for the application of *B. velezensis* IFST-221 in integrated disease management strategies.

Résumé

Xiaoyan Liang (2025). "Détection rapide et biocontrôle de *Fusarium verticillioides*, un agent pathogène majeur de la pourriture des tiges et des épis du maïs" (thèse de doctorat en anglais).

Gembloux, Belgique, Gembloux Agro-Bio Tech, Université de Liège.

Le maïs (*Zea mays* L.) est l'une des principales céréales au niveau mondial, constituant une source essentielle d'alimentation humaine, de fourrage et de matières premières industrielles. *Fusarium verticillioides*, agent causal majeur de la pourriture des épis et des tiges, compromet fortement la production de maïs en raison de sa pathogénicité et de la production de fumonisines, ce qui représente un risque sérieux pour la sécurité alimentaire et le commerce international. Cette étude a développé une plateforme moléculaire de diagnostic sur le terrain et caractérisé un agent de biocontrôle efficace pour la gestion de *F. verticillioides*.

Un test rapide, sensible et nécessitant peu d'équipement a été mis au point, reposant sur l'extraction d'ADN par résine Chelex-100, le ciblage du gène *FUM1*, l'amplification par recombinase polymérase (RPA) couplée au clivage CRISPR/Cas12a et à la détection par flux latéral. L'analyse a montré une sensibilité analytique proche d'un équivalent génomique et permet d'obtenir un diagnostic complet en 73 minutes. Lors de la validation sur le terrain avec des grains de maïs infectés provenant de la province du Shanxi, le test a identifié deux échantillons positifs, confirmés comme *F. verticillioides* par isolement monospore et séquençage du gène *TEF*-1α.

Une souche prometteuse de biocontrôle, *Bacillus velezensis* IFST-221, isolée de la rhizosphère du maïs, a montré une activité antifongique à large spectre, inhibant la croissance mycélienne de *F. verticillioides* de 62,63 % en confrontation sur boîte de Petri. Dans des tests sur grains de maïs, les niveaux de FB_1 ont diminué de 5 700 à 19,6 ppb après prétraitement avec IFST-221. En conditions de serre, l'application d'IFST-221 a réduit l'indice de sévérité de la verticilliose du coton de 73,21 % à 8,93 % et l'incidence de la maladie de 85,71 % à 14,29 %, tout en favorisant une meilleure croissance des plantes. IFST-221 a également stimulé la croissance des plantules de maïs, de tomate et de brocoli. Le séquençage du génome a révélé un génome de 3,86 Mb codant pour neuf clusters de métabolites secondaires (surfactine, fengycine, bacillibactine, macrolactine H, difficidine, bacillaène, bacillysine, butirosine A/B et andalusicine A/B, ainsi que trois clusters inconnus), ainsi que des gènes liés aux fonctions PGPR tels que la fixation de l'azote, la biosynthèse de l'acide indole-3-acétique, la solubilisation du phosphate et la formation de biofilms.

Afin de préciser le mécanisme antifongique, des analyses par LC-MS/MS et des délétions géniques ciblées ont été réalisées. Les surfactines ont été détectées dans les extraits bruts, et la délétion du gène *srfAA* a réduit l'activité antifongique des extraits mutants; toutefois, l'efficacité globale du biocontrôle est restée largement inchangée en double culture et lors d'infections sur grains de maïs, suggérant que la surfactine

ne joue qu'un rôle partiel. Le profil transcriptomique de *F. verticillioides* exposé à IFST-221 a révélé une reprogrammation du métabolisme primaire, des gènes liés au ribosome, des processus associés à la paroi et à la membrane cellulaires, ainsi que de voies d'adaptation au stress telles que la défense antioxydante, l'autophagie et les protéines de choc thermique. Ces résultats illustrent l'interaction dynamique entre *B. velezensis* IFST-221 et sa cible fongique et fournissent un cadre moléculaire pour optimiser l'efficacité du biocontrôle.

Collectivement, cette étude propose un cadre robuste pour une protection durable du maïs en faisant progresser à la fois le diagnostic moléculaire rapide et la caractérisation mécanistique d'un agent de biocontrôle prometteur. Ces résultats constituent une base solide pour l'application de *B. velezensis* IFST-221 dans des stratégies intégrées de gestion des maladies.

Acknowledgement

This Ph.D. thesis was carried out at Integrated and Urban Plant Pathology Laboratory, University of Liège, and Plant Health and Food Safety Laboratory, Institute of Food Science and Technology, Chinese Academy of Agriculture Science, from 2021 to 2025, under the Uliège-GSCAAS Joint PhD Program.

I would like to acknowledge the financial support provided by Agricultural Science and Technology Innovation Program of Institute of Food Science and Technology, Chinese Academy of Agricultural Sciences (Grant No. CAAS-ASTIP-G2022-IFST-01), and the China Scholarship Council. These supports enabled me to pursue a Ph.D. without undue financial concern and allowed me to focus fully on my research.

I am deeply grateful to my supervisors, Prof. M. Haïssam JIJAKLI and Prof. Wei GUO, for their continuous guidance, valuable insights, and unwavering encouragement throughout my PhD journey. I would also like to express my sincere thanks to my thesis committee members, Prof. Sébastien MASSART, Prof. Pierre Delaplace, and Prof. Caroline De Clerck, for their constructive feedback and kind support during each of my annual progress meetings. Their suggestions greatly enriched this thesis.

I have also received great kindness from all the members of Integrated and Urban Plant Pathology Laboratory. When I first arrived in Belgium, I was overwhelmed by the unfamiliar environment. However, the warmth and friendliness of the people around me made me feel welcome rather than like an outsider. Whenever I made unintentional mistakes, they reassured me that it was okay. As someone who is often afraid of bothering others, their support made me feel at home.

I am equally grateful to all members of Plant Health and Food Safety in Beijing. We accompanied, studied, conducted experiments, and solved problems together, fostering a spirit of mutual support and collaboration. My heartfelt thanks go to all my colleagues and labmates for their help and companionship throughout this journey.

Most importantly, I would like to thank my family for their unconditional love, patience, and unwavering belief in me. To my parents, who have always stood by my side, this achievement would not have been possible without your endless support. Even though they may not understand English and read this acknowledgement, I will make sure my love and gratitude reach them.

This has been a meaningful and transformative journey. I have learned how to conduct research and how to get along with friends. Now, I think I am ready for the next chapter in my life.

Table of contents

Abstract i

Résumé iii

Acknowledgement v

Table of contents vii

List of figures xv

List of tables xvii

List of acronyms i

Chapter 1: Rapid detection, biological approaches, and their modes of action against *Fusarium verticillioides* in maize 1

1. Context 2

2. Maize: Importance and challenges 2

2.1. Global significance of maize as a crop 2

2.2. Major biotic threats to maize with an emphasis on *Fusarium* ear and stalk rot 3

3. *Fusarium verticillioides*: A major pathogen of maize ear and stalk rot. 4

3.1. Biological features and life cycle 4

3.2. Mycotoxin contamination and implications for human and animal health 6

4. Current detection methods for *F. verticillioides* 7

4.1. Traditional morphological and culture-based methods 7

4.2. Molecular detection approaches 8

4.3. Recent advances in rapid diagnostics (RPA-CRISPR/Cas12a system) 11

5. Integrated management of *F. verticillioides* in maize 12

5.1. Agronomic and cultural practices 12

5.2. Breeding for genetic resistance 13

5.3. Chemical control measures 14

5.4. Biological control approaches 15

6. Mechanisms of antifungal activity of *Bacillus* spp 20

6.1. Production of bioactive metabolites 20

6.2. Hydrolytic enzyme-mediated cell wall degradation 21

6.3. Induction of systemic resistance in plants 21

6.4. Competition for nutrients and ecological niches 22

6.5. Interference with pathogen quorum sensing 22

6.6. Modulation of rhizosphere microbiota 23

6.7. Summary 23

Chapter 2: Research objectives and thesis structure.....25

1. Research questions and hypotheses.....26

2. Objectives.....26

3. Thesis structure.....27

Chapter 3: Development of an RPA-based CRISPR/Cas12a assay in combination with a lateral flow strip for rapid detection of toxigenic *Fusarium verticillioides* in maize 29

1. Introduction 31

2. Materials and methods.....32

2.1. Fungal strains.....32

2.2. Preparation of DNA extracts for pathogen detection.....33

2.3. Design of primers and crRNA 33

2.4. RPA-Cas12a-LFD reaction.....36

2.5. Specificity and sensitivity of the RPA-Cas12a-LFD assay for *F. verticillioides* detection 36

2.6. Detection of *F. verticillioides* in artificially diseased maize stalks and kernels 36

2.7. The developed RPA-Cas12a-LFD assay for the diagnosis of field maize samples 37

2.8. Statistics and reproducibility 37

3. Results 37

3.1. Design and optimization of detection primers and crRNA 37

3.2. Specificity and sensitivity of RPA-Cas12a-LFD assay for the detection of *F. verticillioides* 38

3.3. Analytical performance of RPA-Cas12a-LFD assay on maize stalks and kernels artificially infected with *F. verticillioides* 39

3.4. Diagnosis of diseased maize ears in the field 40

4. Discussion 41

5. Conclusion 43

Chapter 4: Identification and genomic insights into a strain of *Bacillus velezensis* with phytopathogen-inhibiting and plant growth-promoting properties 45

1. Introduction 47

2. Materials and methods 48

2.1. Strains 48

2.2. Identification of IFST-221 49

2.3. *In vivo* anti-*F. verticillioides* assay of IFST-221 49

2.4. The biocontrol activity of IFST-221 against *Verticillium* wilt of cotton 51

2.5. Plant growth-promoting assays.....51

2.6. Genomic sequencing, annotation, and prediction of secondary metabolites.....53

2.7. Statistical analysis and data availability 53

3. Results 54

3.1. Isolation of an antifungal strain IFST-221.....54

3.2. IFST-221 is a strain of *B. velezensis*.....55

3.3. *B. velezensis* IFST-221 is a putative biological control agent for plant disease 58

3.4. *B. velezensis* IFST-221 promotes plant seedlings' growth 60

3.5. Genomic feature of *B. velezensis* IFST-221 and comparative genomics analysis of *B. velezensis* IFST-221, SQR9, FZB42^T, *B. amyloliquefaciens* DSM7^T, and *B. subtilis* 168^T.....61

3.6. Prediction of the antimicrobial characteristic of IFST-221 65

3.7. Global screening of genes potentially contributing to plant growth-promoting activities in IFST-221 68

4. Discussion 69

5. Conclusion.....72

Chapter 5: Antifungal mechanism of *Bacillus velezensis* IFST-221 against *Fusarium verticillioides*: transcriptomic insights and surfactin contribution 73

1. Introduction 75

2. Materials and methods 76

2.1. Mutant construction 76

2.2. Lipopeptide extraction and analysis 78

2.3. Maize kernels inoculation assay 78

2.4. Transcriptome sequencing and data analysis 79

2.5. Quantitative real-time polymerase chain reaction 80

3. Results 81

3.1. *srfAA* was knocked out from *B. velezensis* IFST-221 81

3.2. Inhibitory ability of *srfAA* deletion mutants on the growth of *F. verticillioides* 82

3.3. Transcriptome sequencing of *F. verticillioides* under IFST-221 treatment 84

4. Discussion 94

5. Conclusion 97

Chapter 6: General discussion, conclusion, and perspectives 99

1. General discussion 100

1.1. Context....100

1.2. Rapid detection of *F. verticillioides* 100

1.3. Biocontrol potential of *B. velezensis* IFST-221 103

1.4. Fungal transcriptomic responses....106

2. Conclusion....107

3. Perspectives....108

3.1. Practical challenges and validation needs for assay deployment....108

3.2. Clarifying the role of iturin and fengycin in IFST-221 antagonism ..108

3.3. Toward practical application strategies of IFST-221 109

3.4. Future directions for omics integration and functional validation....110

Chapter 7: Reference 113

Appendix 1: Gene-by-gene annotation of biosynthetic gene clusters predicted by antiSMASH in *B. velezensis* IFST-221 141

Appendix 2: Differentially expressed genes related to ribosome, carbon metabolism, amino sugar and nucleotide sugar metabolism, and stress responses....149

Appendix 3: Scientific publications 155

List of figures

Figure 1-1 The maize production of the World and China from 1994 to 2023 (FAOStat, 2023). 2
Figure 1-2 Morphological characteristics of *F. verticillioides*, including colony morphology on PDA and microscopic features of macroconidia and microconidia. ..5
Figure 1-3 *Fusarium verticillioides* infection cycle in maize.....6
Figure 1-4 Schematic representation of the multiple biological protective mechanisms of *Bacillus* spp. 24
Figure 3-1 Schematic diagram of RPA-Cas12a-LFD assay and minimal time required for the detection of *F. verticillioides*. 32
Figure 3-2 The primer and crRNA design for *F. verticillioides*. 35
Figure 3-3 Specificity and sensitivity of RPA-Cas12a-LFD assay for *F. verticillioides* detection. 38
Figure 3-4 Early detection of *F. verticillioides* in artificially diseased maize stalks and kernels using the developed RPA-Cas12a-LFD assay. 39
Figure 3-5 On-site detection of *F. verticillioides* using the RPA-Cas12a-LFD assay. 40
Figure 4-1 Antagonistic activity of strain IFST-221 against eight different phytopathogens. 54
Figure 4-2 Scanning electron microscopy of the morphology of IFST-221 after incubation in LB broth at 37 °C for 12 hours. 55
Figure 4-3 A neighbor-joining phylogenetic tree was constructed using the 16S rDNA gene sequence of IFST-221 and other closely related *Bacillus* species. 57
Figure **4-4** A phylogenetic tree of IFST-221 constructed using the nucleotide sequences of *gyrB* based on the neighbor-joining method. 58
Figure 4-5 The inhibitory effects of IFST-221 against ear rot of maize and Verticillium wilt of cotton plants. 59
Figure 4-6 The plant growth-promoting activity of IFST-221. 61
Figure 4-7 Comparative genomic analysis of *Bacillus velezensis* IFST-221 with *B. velezensis* SQR9 and FZB42^T, *B. amyloliquefaciens* DSM7^T, and *B. subtilis* 168^T. .62
Figure 4-8 Heatmap of the ANI values for the genomes of five *Bacillus* strains, including *B. velezensis* IFST-221, SQR9, FZB42^T, *B. amyloliquefaciens* DSM7^T, and *B. subtilis* 168^T. 64
Figure 4-9 Classification of annotated gene functions in the (A) COG, (B) GO, and (C) KEGG database for the whole genome of *B. velezensis* IFST-221. 66
Figure 4-10 The key genes potentially participating in antimicrobial secondary metabolites (green color), plant growth promotion (yellow color), cellulase and xylose degradation (pink color), and biofilm formation (blue color) in the IFST-221 genome. 69
Figure 5-1 Generation of the *srfAA* deletion mutant by homologous recombination. 82

Figure 5-2 The biological activity of IFST-221 and its *srfAA* mutants (Δ*srfAA* 4# and 9#). 83
Figure 5-3 The antifungal activity and mass spectrum of the crude extract of IFST-221 and its *srfAA* mutants (Δ*srfAA* 4# and 9#). 84
Figure 5-4 The gene expression distribution across samples, shown as boxplots (A) and density plots (B) of $\log_2$(FPKM+1). 85
Figure 5-5 Sample-to-sample relationship of gene expression profiles between Fv and Fv+221 groups. 86
Figure 5-6 Venn diagram of total expressed genes in Fv and Fv+221 groups. 86
Figure 5-7 Differential expression analysis in the Fv vs. Fv+221 comparison. ... 87
Figure 5-8 The GO (A) and KEGG (B) enrichment analyses in the Fv vs. Fv+221 comparison. 88
Figure 5-9 Hyphal and conidia morphology of *F. verticilllioides* co-cultivated with (B) or without (A) strain IFST-221. Scale bar, 20 μm. 91
Figure 5-10 qRT-PCR was performed to validate the RNA-Seq-based differential gene expression analysis in *F. verticillioides* following exposure to *B. velezensis* IFST-221..... 93
Figure 5-11 Integrated transcriptomic response model of *F. verticillioides* under IFST-221 treatment..... 94

List of tables

Table 1-1 Fumonisin contamination in maize kernels across major producing regions (dsm-firmenich, 2024) 4
Table 1-2 Global prevalence of major mycotoxins in all raw commodities and finished feed (dsm-firmenich, 2024) 7
Table 1-3 Comparison of existing detection methods for *F. verticillioides* and emerging isothermal platforms (RPA-Cas12a). 10
Table 1-4 Representative biocontrol agents effective against *Fusarium* spp., mechanisms of antifungal action, and key bioactive traits. 16
Table 3-1 Fungal strains used in this study and their results in the RPA-Cas12a-LFD assay. 33
Table 3-2 Primers and guide RNA used in this study 34
Table 4-1 Primers used in this study 50
Table 4-2 Physiological and biochemical results of strain IFST-221. 55
Table 4-3 Genomic comparison between *B. velezensis* IFST-221, *B. velezensis* SQR9, *B. velezensis* FZB42^T, *B. amyloliquefaciens* DSM7^T, and *B. subtilis* 168^T ...63
Table 4-4 Comparison of predicted and known secondary metabolites between *B. velezensis* IFST-221, *B. velezensis* SQR9, *B. velezensis* FZB42^T, *B. amyloliquefaciens* DSM7^T, and *B. subtilis* 168^T 66
Table 4-5 Manual confirmation of biosynthetic gene clusters (BGCs) identified in *B. velezensis* IFST-221. 67
Table 5-1 Primers used in this study 77
Table 5-2 The active peaks and their assignments 81
Table 5-3 Summary of RNA-seq data quality and read statistics for Fv and Fv+221 samples. 84
Table 5-4 Summary of read mapping statistics for Fv and Fv+221 samples. 85

List of acronyms

ANI	Average nucleotide identity
ATG	Heat shock proteins
BCAs	Biological control agents
bp	Base pair
BP	Biological process
Cas	CRISPR-associated proteins
CAT	Catalase
CC	Cellular component
CDS	Coding sequence
cfu	Colony-forming units
CLA	Carnation leaf agar
CLP	Cyclic lipopeptide
CM	Complete media
COG	Clusters of orthologous groups
CRISPR	Clustered regularly interspaced short palindromic repeats
CTAB	Cetyltrimethylammonium bromide
ddH_2O	Double-distilled water
DEGs	Differentially expressed genes
DETECTR	DNA endonuclease-targeted CRISPR trans reporter
DI	Disease incidence
dpi	Days post inoculation
DSI	Disease severity index
ELISA	Enzyme-linked immunosorbent assay
ESI	Electrospray ionization
FAO	Reactive oxygen species
FB_1	Fumonisin B_1
FDR	False discovery rate
FFSC	*Fusarium fujikuroi* species complex
FPKM	Fragments per kilobase of transcript per million mapped reads
FUM	Fumonisins
GO	Gene ontology

gyrB	DNA gyrase subunit B
HCA	Hierarchical cluster analysis
HDA	Helicase-dependent amplification
HOLMES	one-HOur Low-cost Multipurpose highly Efficient System
hpi	Hours after inoculation
HPLC-MS	High-performance liquid chromatography coupled with mass spectrometry
IAA	Indole-3-acetic acid
IAM	Indole-3-acetamide
IAN	Indole-3-acetonitrile
IARC	International Agency for Research on Cancer
IGS	Intergenic spacers
IPyA	Indole-3-pyruvic acid
ISR	Induced systemic resistance
ITS	Internal transcribed spacers
JA	Jasmonic acid
KEGG	Kyoto encyclopedia of genes and genomes
LAMP	Loop-mediated isothermal amplification
LB	Luria-Bertani
LC-MS/MS	Liquid chromatography-tandem mass spectrometry
LFD	Lateral flow dipsticks
MAPK	Mitogen-activated protein kinase
MF	Molecular function
MQTLs	meta-QTLs
MR	Methyl red
NAAT	Nucleic acid amplification technique
NCBI	National Center for Biotechnology Information
NRPS	Non-ribosomal peptide synthetases
NRPs	Non-ribosomal peptides
ONPG	O-nitrophenyl-β-D-galactopyranoside
PAM	Protospacer adjacent motif
PCA	Principal component analysis

PCR	Polymerase chain reaction
PDA	Potato dextrose agar
PGP	Plant growth-promoting
PGPR	Plant growth-promoting rhizobacteria
PKs	Polyketides
POD	Peroxidase
ppb	Parts per billion
qPCR	Quantitative PCR
qRT-PCR	Quantitative real-time polymerase chain reaction
QS	Quorum sensing
QTL	Quantitative trait locus
RCA	Rolling circle amplification
RNA-seq	RNA sequencing
ROS	Reactive oxygen species
RPA	Recombinase polymerase amplification
RPA-Cas12a-LFD	Recombinase polymerase amplification coupled with CRISPR/Cas12a-based cleavage and lateral flow detection
RT	Room temperature
SA	Salicylic acid
SEM	Scanning electron microscopy
SHERLOCKv2	Specific high-sensitivity enzymatic reporter unlocking version 2
SMRT	Single-molecule real-time
SOD	Superoxide dismutase
ssDNA	Single-stranded DNA
TEF-1α	Translation elongation factor-1 alpha
TetR	Tetracycline resistance
TrxR	Thioredoxin reductases
VOCs	Volatile organic compounds
VP	Voges Proskauer

Chapter 1

Rapid detection, biological approaches, and their modes of action against *Fusarium verticillioides* in maize

1. Context

Maize (*Zea mays* L.) is one of the world's most important cereal crops, providing a major source of food, animal feed, and industrial raw materials all over the world. As a staple crop grown on every continent, maize plays a critical role in ensuring global food security and supporting agricultural economies. However, maize production is severely threatened by a range of fungal pathogens, among which *Fusarium verticillioides* (synonym: *Fusarium moniliforme* Sheldon; teleomorph: *Gibberella moniliformis*) is particularly notorious. This filamentous fungus not only causes ear and stalk rot, leading to substantial yield losses, but also produces harmful mycotoxins such as fumonisins, which pose serious health risks to humans and animals. The widespread occurrence of *F. verticillioides* in maize-growing regions worldwide, coupled with its dual impact on crop productivity and food safety, underscores the urgent need for effective detection and management strategies.

In recent years, research has increasingly focused on developing rapid diagnostic tools and environmentally friendly biological control measures to combat *F. verticillioides* infections in maize. While traditional chemical fungicides have shown limited success and raise concerns over environmental and health impacts, biological control agents, especially beneficial bacteria like *Bacillus* spp., have emerged as promising alternatives. Understanding the mechanisms by which these biocontrol agents inhibit fungal pathogens is crucial for optimizing their application and achieving sustainable disease management. This introduction provides an overview of the importance of *F. verticillioides* in maize, current detection methods, biological control strategies, and the underlying antifungal mechanisms, setting the stage for a comprehensive exploration of integrated solutions for managing this major crop pathogen.

2. Maize: Importance and challenges

2.1. Global significance of maize as a crop

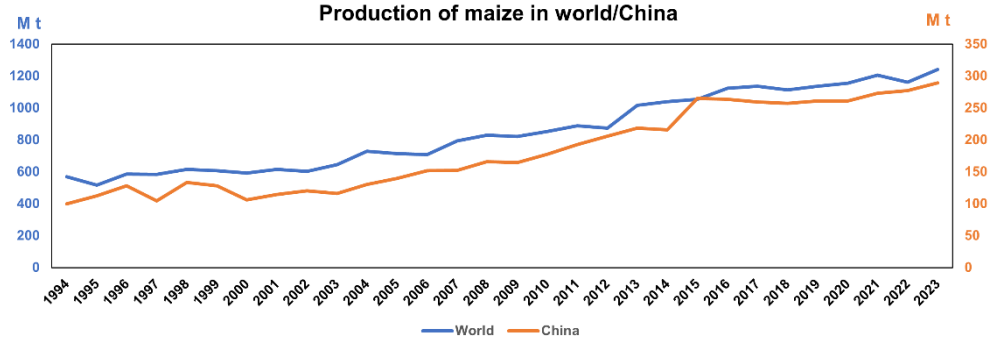

Figure 1-1 The maize production of the World and China from 1994 to 2023 (FAOStat, 2023).

Maize is one of the world's most important cereal crops, serving as a major source of human food, animal feed, and industrial raw materials globally. Maize was first domesticated more than 9,000 years ago in southern Mexico/Meso America. Recent research has revealed that modern maize originated from an admixture event between ancient maize and *Zea mays* ssp. *mexicana* in the highlands of Mexico, occurring approximately 4000 years after initial domestication began (Bai et al., 2019). According to data from the Food and Agriculture Organization (FAO) of the United Nations, global maize production reached approximately 1.24 billion tons in 2023, surpassing the production of rice, wheat, and other staple crops. Historical data spanning from 1994 to 2023 also indicate a steady increase in maize production and yield quantities (Figure 1-1). Globally, approximately 61% of global maize (dry grain) production is primarily utilized as animal feed, 16% for biofuel production, 13% directly for human food, and the remaining 10% for other purposes (FAOStat, 2023). Although direct dietary use accounts for only a fraction, maize contributes substantially to human nutrition through animal-derived products and by-products from industrial processing.

In China, maize is the most extensively cultivated cereal crop, with a harvested area of 43 million hectares and an annual production of approximately 289 million tons in 2023, representing more than 23% of global output. Production is concentrated in the northeastern provinces (Heilongjiang, Jilin, Liaoning) and the North China Plain (He et al., 2020). Given China's dual role as both a major producer and consumer of maize, ensuring the safety and sustainability of maize production is therefore of critical importance for national food security.

2.2. Major biotic threats to maize with an emphasis on Fusarium ear and stalk rot

Maize production is challenged by a wide range of biotic stresses, including fungal, bacterial, and viral pathogens, insect pests, and weeds (Matos et al., 2024). Together, these agents significantly reduce yield and compromise grain quality, thereby threatening food security on local and global scales. Long-term monitoring in China revealed that the occurrence area of crop pests and diseases increased nearly fourfold between 1970 and 2016, at an average annual growth rate of 3.1% (Wang et al., 2022). This demonstrates the escalating burden of biotic stresses under changing agricultural and climatic conditions.

At the global level, an expert survey conducted from November 2016 to January 2017 estimated average maize yield losses of 22.5% (range: 19.5-41.1%), ranking second among the five major food crops after rice (30.0%) and before wheat (21.5%), soybean (21.4%), and potato (17.2%) (Savary et al., 2019). Regionally, yield reductions in maize reached 30.1% in Sub-Saharan Africa, 41.1% in the Indo-Gangetic Plain, and 21.3% in the United States Midwest and Canada (Savary et al., 2019). These estimates, derived from expert elicitation rather than long-term field monitoring, provide the most comprehensive global comparison of crop losses currently available.

National-scale data from China (1970-2016) further indicated that maize is predominantly affected by insect pests (mainly Lepidoptera and Homoptera, about 60% of total occurrence area) and fungal diseases (about 25-30%), whereas bacterial, viral, and other stresses contributed comparatively little (Wang et al., 2022). This pattern corroborates global analyses that consistently rank insects and fungi as the dominant biotic threats to maize. In particular, *Fusarium* and *Gibberella* ear and stalk rots have repeatedly ranked among the top contributors to maize yield losses across diverse production regions. According to global surveys, *Fusarium* and *Gibberella* stalk rots accounted for 4.54% yield losses in the United States Midwest and Canada, 4.15% in South Brazil, Paraguay, Uruguay, and Argentina, and 5.84% in the Indo-Gangetic Plain (Savary et al., 2019). These diseases were consistently listed alongside fall armyworm as the two most important maize yield-reducing factors globally.

Table 1-1 Fumonisin contamination in maize kernels across major producing regions (dsm-firmenich, 2024)

	North America	Central America	South America	Asia
Number of tested samples	460	237	2617	1,129
% contaminated samples	68%	98%	84%	85%
Average of positive (ppb)	3,995	5,189	2,413	3,455
Median of positive (ppb)	1,143	1,976	1,859	1,740
Maximum (ppb)	96,316	244,701	17,820	489,698

One predominant causal agent of *Fusarium* ear and stalk rot is *F. verticillioides*, which not only reduces yield but also contaminates kernels with fumonisins, a group of mycotoxins classified as possible human carcinogens (Group 2B) by the International Agency for Research on Cancer (Gai et al., 2018). Large-scale surveys demonstrate that fumonisin contamination is pervasive in maize across major producing regions (Table 1-1). For example, 85% of tested samples in Asia were contaminated, with maximum levels reaching 489,698 ppb (dsm-firmenich, 2024). Such widespread and severe contamination underscores the dual threat posed by *F. verticillioides*, affecting both productivity and safety, and justifies its central focus in this thesis. The combination of yield reduction and fumonisin contamination makes *F. verticillioides* one of the most critical pathogens of maize, and thus the central focus of this thesis.

3. *Fusarium verticillioides*: A major pathogen of maize ear and stalk rot

3.1. Biological features and life cycle

F. verticillioides belongs to *Fusarium fujikuroi* species complex (FFSC), one of the largest and most extensively studied groups within the genus *Fusarium* (Qiu et al.,

2020). Morphologically, *F. verticillioides* shared similarities with related species such as *F. proliferatum* and *F. fujikuroi*. On the Potato Dextrose Agar (PDA) plates, colonies initially appear white or light purple and gradually darken to deep purple in the later stages. The fungus produces microconidia on PDA and both macroconidia and microconidia on carnation leaf agar (CLA) plates. The macroconidia are typically sickle-shaped, straight, slender, with 3-5 septa, measuring approximately 30.4-52.3 μm in length and 2.6-4.0 μm in width, while the microconidia are club-shaped, mostly aseptate or with one septum, and measure 4.4-11.1 μm in length and 1.5-3.7 μm in width (Figure 1-2). When *F. verticillioides* infects maize plants, it causes a notable decrease in chlorophyll concentration, leading to reduced photosynthetic efficiency and water loss. The pathogen induces root rot, ear rot, stalk rot, and seedling blight, resulting in stunted plant growth and chlorosis (Omotayo & Babalola, 2023).

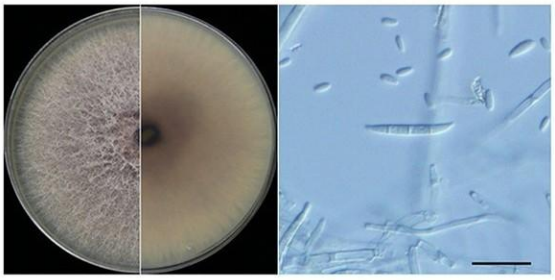

Figure 1-2 Morphological characteristics of *F. verticillioides*, including colony morphology on PDA and microscopic features of macroconidia and microconidia. Scale bar = 20 μm. Figure reproduced from (Xi et al., 2021), *Frontiers in Microbiology*, licensed under CC BY 4.0.

F. verticillioides is a soilborne fungal pathogen capable of long-term survival in the maize residues, persisting in stalk pieces on the soil surface or buried at various soil depths (including 15 and 30 cm) for up to 630 days (Cotten & Munkvold, 1998). During its saprophytic phase, the fungus develops thickened hyphae to enhance survival, although it does not typically form chlamydospores (Kant et al., 2017). The life cycle of *F. verticillioides* involves multiple infection routes (Figure 1-3) (Xu et al., 2023). Germinating seeds in infested soils or using infected seeds (whether externally contaminated or harboring endophytic infections) can lead to early root and mesocotyl colonization, followed by systemic movement through the vasculature into the stalk, causing stalk rot (Blacutt et al., 2017; Machado et al., 2013). Wounds from mechanical damage or insect feeding can serve as additional entry points, facilitating external infections (Blacutt et al., 2017; Sobek & Munkvold, 1999). At the reproductive stage, particularly during silking, airborne spores colonize maize silks, and fungal mycelia subsequently invade kernels, often resulting in the characteristic "starburst" pattern of *Fusarium* ear rot (Duncan & Howard, 2009). Kernel infection is frequently exacerbated by insect feeding, bird pecking, or hail damage (Mesterházy et al., 2012). Systemic infections originating from seedborne or soilborne inoculum

can also spread upward through the plant, eventually reaching cobs and kernels (Murillo-Williams & Munkvold, 2008). Furthermore, airborne microconidia can directly infect maize leaves via stomata and trichomes, providing another pathway for cob and kernel infection (Nguyen et al., 2016a, 2016b). Kernel infection may manifest as ear rot, seed rot, or asymptomatic endophytic presence (Xu et al., 2023). Importantly, during seed storage, seedborne *F. verticillioides* or latent endophytic infections can develop into visible rot under favorable conditions, significantly reducing seed viability, vigor, and germination rates, and potentially initiating a new systemic infection cycle in the subsequent planting season (Ma et al., 2022).

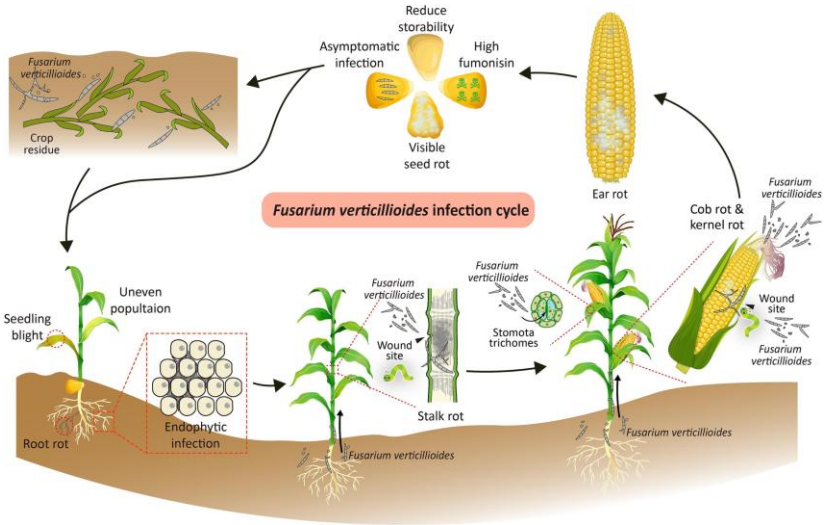

Figure 1-3 *Fusarium verticillioides* infection cycle in maize.
Figure reproduced from (Xu et al., 2023), *The Crop Journal*, licensed under CC BY 4.0.

3.2. Mycotoxin contamination and implications for human and animal health

Beyond its impact on crops, *F. verticillioides* poses significant risks to human and animal health through the production of various mycotoxins, including fumonisins, fusaric acid, fusarins, zearalenone, and potentially beauvericin (Qu et al., 2024). Among these, fumonisins are the most notorious mycotoxins. Fumonisins were first isolated and identified in 1988 and have since been recognized as a major group of mycotoxins associated with *F. verticillioides* contamination (Gelderblom et al., 1988). To date, at least 28 fumonisin analogs have been identified, which are classified into four main series: fumonisin A, B, C, and P (Keawmanee et al., 2021). Among these, fumonisin B_1 (FB_1) is the most abundant, biologically significant, and widely distributed fumonisin detected in contaminated maize (Ekwomadu et al., 2021; Samyal & Sharma, 2023). Fumonisin production is primarily attributed to species within the *Fusarium fujikuroi* species complex, particularly *F. verticillioides* and *F. fujikuroi*. Although some studies have reported variation in fumonosin production or production potential in other species, such as *F. thapsinum* and *F. oxysporum*, these

findings are less consistent. Additionally, while fumonisin biosynthetic gene clusters have been identified in *F. chlamydosporum* and *F. hostae*, there are currently no confirmed reports of actual fumonisin production by these species (Qu et al., 2024).

Fumonisins, particularly FB_1, pose significant health risks to both humans and animals. In animals, FB_1 is known to cause porcine pulmonary edema, equine leukoencephalomalacia, liver cancer in rodent models, and kidney damage in various species, including rabbits, rodents, and sheep (Samyal & Sharma, 2023). In humans, chronic fumonisin exposure, primarily through consumption of contaminated maize, has been linked to esophageal and liver cancers, with notable epidemiological evidence from regions such as South Africa, China, and Iran (Yu et al., 2021). At the cellular level, fumonisins exert toxicity largely by disrupting sphingolipid metabolism (Riley & Voss, 2006). Due to their structural similarity to sphingoid bases, FB_1 and FB_2 competitively inhibit ceramide synthase, leading to the accumulation of sphinganine and sphingosine in cells (Voss et al., 2007). This metabolic interference not only compromises membrane integrity but also induces oxidative stress, lipid peroxidation, apoptosis, and disturbances in cellular processes such as growth, differentiation, and immune function (Voss et al., 2007). Importantly, fumonisins are classified as Group 2B compounds, meaning they are possibly carcinogenic to humans. In contrast to many other organic solvents, the unique water solubility of soluble mycotoxins poses additional challenges for detection and removal in food processing (Chen et al., 2021). While some reduction in toxicity occurs during heat processing (Humpf & Voss, 2004), covalently bound fumonisin derivatives may persist in processed foods, maintaining a residual health risk.

Table 1-2 Global prevalence of major mycotoxins in all raw commodities and finished feed (dsm-firmenich, 2024)

	Afla	ZEN	DON	T-2	FUM	OTA
Global prevalence	29%	60%	63%	23%	61%	17%
Average of positive (ppb)	18	110	730	32	1,516	11

According to the dsm-firmenich world mycotoxin survey, fumonisins (FUM) were detected in 61% of raw commodities and finished feed samples in 2024, with an average positive concentration of 1,516 ppb (dsm-firmenich, 2024). Among the major mycotoxins, deoxynivalenol (DON, 63%), fumonisins (61%), and zearalenone (ZEN, 60%) showed the highest global prevalence, whereas aflatoxins (Afla, 29%), T-2 toxin (T-2, 23%), and ochratoxin A (OTA, 17%) were less frequently detected (Table 1-2). These findings emphasize fumonisins as a critical global threat to food and feed safety, not only due to their high prevalence but also because of their severe toxicological implications.

4. Current detection methods for *F. verticillioides*

4.1. Traditional morphological and culture-based methods

Traditional diagnosis of *F. verticillioides* has long relied on morphological and culture-based methods. Symptomatic observation in the field, such as the “starburst”

pattern on kernels or internal stalk discoloration, provides an initial indication of infection but varies depending on genotype, climate, and disease severity, requiring skilled expertise (Qiu et al., 2025; Xu et al., 2023).

Cultivation-based methods are generally considered the gold standard for the detection and identification of fungal pathogens. In the laboratory, morphological identification for *F. verticillioides* relies on single-spore isolation followed by morphological characterization (Xi et al., 2021). In this approach: 1) diseased maize samples are surface-sterilized and cultured on agar medium to induce sporulation; 2) a colony is selected, and conidia were suspended in sterile distilled water and spread onto fresh PDA plates; 3) after incubation at 25 °C for 16-18 h, individual germinating spores are identified under the microscope; 4) a small agar block containing a single germinated spore is excised and transferred to a new PDA plate, where it developed into a pure colony. Morphological assessment is then based on mycelial growth rate, colony pigmentation, macroconidial shape and size, microconidial shape and production, as well as the presence of chlamydospores, sclerotia, and sexual stages (Ekwomadu & Mwanza, 2023; Noman et al., 2018) (see section 2.1 for detailed description). And the sexual reproduction stages (perithecia and ascospores) have differences in *F. verticillioides* isolates, and no formation of chlamydospores and sclerotia was reported (F. Zhang et al., 2023). However, accurate morphological and microscopic identification can be challenging, as it relies heavily on the interpretative skills, expertise, and experience of the analyst (Rajapaksha et al., 2019).

To improve the recovery of *Fusarium* from complex samples, a variety of selective media have been developed, including Nash and Snyder medium, dichloran–chloramphenicol peptone agar, modified Czapek-Dox agar, Czapek Dox iprodione dichloran agar, potato dextrose iprodione dichloran agar, and malachite green agar (Bragulat et al., 2004). Among these media, malachite green agar exhibits stronger selectivity in natural samples, whereas other media often allow substantial growth of non-*Fusarium* fungi such as yeasts and *Zygomycetes*. Thus, selective culture media can serve as a useful complementary tool for preliminary identification before morphological or molecular confirmation.

Overall, although morphological and culture-based methods remain valuable reference approaches for the detection of *F. verticillioides*, their reliance on skilled expertise, limited selectivity, and relatively low sensitivity highlight the necessity of integrating them with modern molecular diagnostics.

4.2. Molecular detection approaches

Although morphological identification alone can be problematic, it remains useful in practice and is often employed in combination with molecular methods, particularly for species within the genus *Fusarium*. Molecular systematics was first applied to the identification of *Fusarium* in 1989 (Guadet et al., 1989). Subsequently, O'Donnell conducted extensive phylogenetic studies using molecular techniques to clarify species-level and intraspecific relationships, as well as to elucidate connections between sexual and asexual forms (O'Donnell, 1996; O'Donnell & Cigelnik, 1997; O'Donnell et al., 1998). These foundational works established the theoretical basis for

the rapid detection and accurate identification of *Fusarium* species. Key gene regions employed in O'Donnell's phylogenetic research included β-tubulin, mitochondrial small subunit (mtSSU) rDNA, 28S rDNA, internal transcribed spacers (ITS), translation elongation factor-1 alpha (TEF-1α), and intergenic spacers (IGS) regions. By analyzing combined sequences of RNA polymerase II largest subunit (RPB1) and second largest subunit (RPB2) genes, O'Donnell et al. classified *Fusarium* into 20 species complexes, enabling molecular detection approaches to differentiate species based on genetic diversity (O'Donnell et al., 2013; O'Donnell et al., 2015).

For the early detection of fumonisin-producing *F. verticillioides*, various molecular methods have been developed, including conventional PCR polymerase chain reaction (PCR) and its variants, such as nested PCR, multiplex PCR, real-time PCR, PCR-ELISA (Enzyme-linked immunosorbent assay), as well as DNA fingerprinting techniques (random amplified polymorphic DNA, restriction fragment length polymorphism, and amplified fragment length polymorphism) (Deepa & Sreenivasa, 2019). These methods are faster and more sensitive than the culture-based method (Table 1-3). For example, PCR-ELISA targeting the *FUM21* gene achieved a detection limit as low as 2.5 pg and was 100-fold more sensitive than conventional PCR, capable of detecting down to 1×10^4 conidia per gram of maize samples (Omori et al., 2018). Similarly, a real-time PCR assay targeting the calmodulin gene enabled group-specific detection with a sensitivity of approximately eight *F. verticillioides* genomes, corresponding to 0.11 pg DNA (Nutz et al., 2011).

Although DNA fingerprinting techniques have also been applied, they are less commonly used in routine diagnostics (Deepa & Sreenivasa, 2019). Despite the accuracy and sensitivity of PCR-based methods, the abovementioned molecular techniques generally require purified DNA, thermal cyclers, and laboratory instruments, which limit their field applicability. Moreover, they are relatively time-consuming and costly compared to emerging isothermal amplification systems. Therefore, although PCR-based methods remain important reference tools, there is a clear need for rapid, portable, and user-friendly diagnostic assays that can be deployed under resource-limited conditions.

In addition to PCR-based methods, isothermal amplification techniques have also been explored (Ivanov et al., 2021). Among them, a kind of isothermal amplification technology, loop-mediated isothermal amplification (LAMP), has been developed for the detection of *F. verticillioides*. A LAMP assay targeting the 3-phosphoglyceric phosphokinase gene employed three primer pairs and required approximately 120 min for DNA extraction (CTAB method) plus 70 min for isothermal amplification at 62 °C. However, the assay required over three hours in total and involved complex primer design, which limits its field applicability. Other isothermal amplification approaches have not yet been reported for this pathogen.

Table 1-3 Comparison of existing detection methods for *F. verticillioides* and emerging isothermal platforms (RPA-Cas12a).

Detection method	Limit of detection	Specificity	Total time	Cost	Field applicability	Advantages	Limitations	Reference
Culture-based	-	Low	Several days	Low	No	Simple, cheap	Slow, low specificity	(Xi et al., 2021)
PCR	0.1~ 1 ng DNA	High	60 min DNA extraction, 150 min reaction time, and 60 min agarose gel electrophoresis	Low	No (lab-based)	Differentiate *F.v* and fumonisin-producing *F. v* strains; relatively low cost	Slow; requires lab equipment	(Patiño et al., 2004)
Semi-nested PCR	1:100 diluted samples	High	93 min DNA extraction, 210 min reaction time, and 60 min agarose gel electrophoresis	Low	No (lab-based)	Differentiate *F. v* and fumonisin-producing *F. v* strains; relatively low cost;	Slow; requires lab equipment	(Nagaraj et al., 2016)
Multiplex PCR	0.5 ng	High	140 min DNA extraction, 150 min reaction time, and 60 min agarose gel electrophoresis	Low	No (lab-based)	Specific identification of *F. v* and other strains of Gibberella fujikuroi complex.	Slow; requires lab equipment	(Faria et al., 2012)
Real-time PCR	~13 fg	High	120 min DNA extraction and 150 min reaction time	Moderate	No (lab-based)	High sensitivity and specificity; quantitative; objective LOQ by ROC analysis	Requires lab equipment; relatively costly	(Nutz et al., 2011)
PCR-ELISA	2.5 pg	High	60 min DNA extraction and 120 min reaction time	High	No (lab-based)	Allows semi-quantitative estimation; suitable for high throughput	Labor-intensive; requires hybridization steps	(Omori et al., 2018)
LAMP	100 pg	High	120 min DNA extraction and 70 min reaction time	Moderate	Yes (portable)	Isothermal amplification; simple equipment; rapid	Risk of cross-contamination; lower specificity than qPCR	(Zeng et al., 2018)
RPA-Cas12a (emerging platform)	-	High	60 min DNA extraction, 10 min amplification, and 60-120 min Cas12a detection	High	Yes (portable, field-deployable)	Rapid, portable, highly sensitive SNP discrimination	Risk of non-specific amplification	(Chen et al., 2018)

4.3. Recent advances in rapid diagnostics (RPA-CRISPR/Cas12a system)

Nevertheless, RPA has recently gained increasing attention as a versatile isothermal method for nucleic acid detection. RPA utilizes a recombinase, single-stranded DNA-binding proteins (SSBs), and a strand-displacing DNA polymerase to amplify DNA at a constant low temperature of 37-42 °C within 15-30 minutes (Lobato & O'Sullivan, 2018). The recombinase forms complexes with primers and mediates their invasion into double-stranded DNA at homologous sites, while SSBs stabilize the displaced strands, and the polymerase extends the primers without the need for thermal cycling (Piepenburg et al., 2006). Its short reaction time and low temperature requirement make RPA much faster than LAMP (about 1 hour) and particularly suitable for point-of-care applications. In addition, RPA requires minimal equipment, tolerates crude DNA extracts, and is therefore highly compatible with portable diagnostic platforms (Tan et al., 2022). However, RPA also presents certain drawbacks, including the relatively high cost of reagents and a tendency toward non-specific amplification that may lead to false-positive signals if stringent assay optimization is not performed.

While RPA alone provides rapid amplification, its integration with CRISPR/Cas systems has revolutionized nucleic acid diagnostics by adding highly specific target recognition and signal generation. A breakthrough in CRISPR-based diagnostics was reported to demonstrate that Cas12a, upon recognition of a target DNA sequence, exhibits collateral cleavage activity against surrounding single-stranded DNA. In their study, human anal swab samples were subjected to proteinase K treatment at 56 °C for one hour to rapidly obtain human papillomavirus (HPV) 16 or 18 DNA templates without conventional extraction, followed by RPA at 37 °C within 10 minutes. The amplified products were then recognized by Cas12a-crRNA complexes, which triggered indiscriminate cleavage of fluorophore-quencher (FQ) labeled single-stranded DNA reporters. Cleavage of the reporters generated a detectable signal that could be measured either as fluorescence or lateral flow test lines (Chen et al., 2018; Gootenberg et al., 2018). This RPA-Cas12a platform provided highly sensitive detection of HPV, with results obtained in 130 minutes, and offered superior specificity by distinguishing single-nucleotide polymorphisms.

Beyond clinical diagnostics, CRISPR-based assays have also been applied in plant pathology. For example, Cas12a-based platforms have been developed for the detection of fungal pathogens such as *F. oxysporum* f. sp. *cubense*, *F. temperatum*, and *F. graminearum* (Li et al., 2023; Matthews et al., 2025; Mu et al., 2022), bacterial pathogens including *Xanthomonas oryzae* (Buddhachat et al., 2022), and several plant viruses such as Tomato yellow leaf curl virus and Tobacco mosaic virus (Mahas et al., 2021; Marqués et al., 2022). These examples highlight the broad applicability of CRISPR systems in plant disease diagnostics.

The combination of rapid DNA extraction, rapid RPA reaction, rapid detection, Cas12a's unique collateral cleavage activity, and flexible readout formats established RPA-Cas12a as a powerful tool for point-of-care diagnostics. Nevertheless, the implementation of RPA-CRISPR systems in agriculture still faces challenges, such as

limited validation with diverse field samples, the need for cost-effective reagent formats, and ensuring assay robustness under variable on-site conditions. Building on this conceptual framework, our study applies the RPA-Cas12a system to *F. verticillioides*, where rapid, sensitive, and field-deployable detection remains urgently needed.

5. Integrated management of *F. verticillioides* in maize

5.1. Agronomic and cultural practices

Since complete management is neither feasible nor economically practical, agronomic and cultural management practices aim to reduce pathogen levels to acceptable thresholds. These strategies include sanitation measures, such as removing diseased plants or plant parts, eliminating living plants that carry pathogens, and destroying crop residues, as well as cultural practices such as crop rotation, optimizing sowing dates, maintaining low crop density, and soil management (Dale & Ogle, 1997; Dinolfo et al., 2022).

The long-term survival of *Fusarium* strains in buried maize residues, which can persist for up to 630 days, represents a major inoculum source for subsequent crops (Cotten & Munkvold, 1998). While residue burial can maintain pathogen inoculum, certified seeds and superficial tillage provide preventive tools to reduce inoculum pressure. Certified seeds help avoid the introduction of contaminated propagules into the field (Wimalasekera, 2015). In addition, incorporating crop residues into the topsoil through superficial tillage can accelerate their decomposition and promote the development of suppressive soils. For example, incorporation of pineapple residues rather than banana residues into *Fusarium*-infected soils significantly reduced pathogen density and *Fusarium* wilt disease by enriching antagonistic fungal taxa, such as *Aspergillus fumigatus* and *Fusarium solani*, which inhibited the pathogen through antimicrobial secretion and nutrient competition (Yuan et al., 2021). Such findings demonstrate that combining superficial tillage with residue incorporation can stimulate beneficial microbial communities and accelerate residue decomposition, thereby lowering *Fusarium* inoculum pressure.

Soil amendments such as compost, biochar, or organic fertilizers have also been reported to suppress *Fusarium* populations by enhancing microbial antagonism, altering soil physicochemical properties, or promoting host plant growth (Jin et al., 2023; Markakis et al., 2016; Xiong et al., 2017) In addition, proper irrigation and drainage management can lower the risk of *Fusarium* infection, since excessive soil moisture and poor drainage favor fungal growth and dissemination (Barker, 2007; Cowger et al., 2009). Although none of these practices can eliminate the pathogen, they help reduce soil inoculum pressure and therefore complement crop rotation and residue management.

The choice of sowing date is another important tool for reducing *Fusarium* presence. A study by Krnjaja et al. showed that early sowing combined with mid-maturity hybrid ZP 560 achieved high maize grain yields with lower contamination by *F.*

verticillioides and fumonisins, compared to late sowing with the late-maturity hybrid ZP 666 (Krnjaja et al., 2022). Similar results were observed in Brazil and Italy, where an earlier sowing season resulted in lower fungal incidence than a later sowing season (Berghetti et al., 2020; Blandino et al., 2017). Another cultural practice affecting *Fusarium* occurrence is crop density; the highest plant density (75,000 plants·ha^{-1}) has been associated with increased fumonisins (Krnjaja et al., 2019).

Overall, while agronomic and cultural practices play a key role in reducing *Fusarium* infection and mycotoxin contamination, they are most effective when integrated with other management strategies, such as chemical treatments and biological control, to achieve more reliable disease suppression.

5.2. Breeding for genetic resistance

The breeding of disease-resistant cultivars has long been recognized as an economical and effective way for controlling plant diseases and improving crop yields. In China, several multi-resistant or broad-spectrum resistant maize inbred lines have been developed, including Xianyu 335, TL10B-6903-134, and the Indonesian line 1, all of which exhibit high resistance to *Fusarium* stalk rot (Xi, 2016). Additionally, using natural inoculation methods at multiple locations in China (Hainan and Nantong), ten stable and highly resistant maize inbred lines were identified from a collection of 144 commonly used maize inbred lines, including Dan598, F2, 7922, DH02, Zhong128, T1014, R3, R10, N16, and T3012 (Q. Wu et al., 2018). The use of maize varieties with high resistance to stalk rot can effectively reduce disease incidence and thereby improve maize yield and quality.

Apart from domestic breeding initiatives, global research efforts have increasingly concentrated on mapping quantitative trait loci (QTLs) and identifying resistance-associated genes that contribute to *Fusarium* tolerance. Innovative tools such as molecular marker-assisted selection and genomic prediction are accelerating the release of improved maize varieties with enhanced resistance profiles. For instance, Akohoue and Miedaner (2022) reported the discovery of 40 meta-QTLs (MQTLs) linked to *Fusarium* ear rot and *Gibberella* ear rot. These MQTLs overlapped with key agronomic and biochemical traits, including kernel dry-down rate and husk coverage, and three of them (ZmMQTL2.2, ZmMQTL9.2, and ZmMQTL9.4) exhibited constitutive and strong expression patterns in the resistant maize line CO441, marking them as particularly promising targets for breeding programs (Akohoue & Miedaner, 2022).

Nonetheless, the long-term effectiveness of genetic resistance can be undermined by the rapid evolution and adaptability of *Fusarium* populations, making it imperative to continuously introduce diverse genetic resources and maintain dynamic breeding strategies. In the broader context of integrated pest management, host resistance remains a pivotal and environmentally sound approach, complementing chemical, biological, and agronomic interventions to safeguard crop health and productivity.

5.3. Chemical control measures

Chemical control remains an inexpensive and effective strategy widely used in current agricultural practices to manage *Fusarium* species. Different types of fungicides, including systemic, non-systemic, and combination fungicides, have been widely employed as seed or soil treatments to manage *Fusarium* infections (Sahane, 2020; Saravanakumari et al., 2019).

Numerous studies have evaluated the efficacy of chemical fungicides against *Fusarium* species under laboratory or greenhouse conditions. For example, systemic fungicides such as carbendazim (a methyl benzimidazole carbamate targeting β-tubulin) and tebuconazole (a demethylation inhibitor acting on C14-demethylase in sterol biosynthesis) at 250 ppm markedly inhibited the growth of *F. oxysporum*, while non-systemic fungicides like captan and mancozeb (multi-site inhibitors of sulfhydryl enzymes) at 1,000 ppm also showed suppressive effects (Ayer et al., 2021; W. Chen et al., 2022; Vela-Corcía et al., 2018). Combination fungicides, including carbendazim + mancozeb, tebuconazole + trifloxystrobin (a QoI fungicide inhibiting mitochondrial respiration at the Qo site), and carboxin + thiram (with carboxin acting as a succinate dehydrogenase inhibitor), often achieved complete inhibition at higher concentrations (Luo & Ning, 2022; Macar et al., 2022; Sahane, 2020). For *F. verticillioides*, trifloxystrobin (25%) + tebuconazole (50%) at 60 ppm was reported to strongly suppress radial growth in the plate test (Wajid et al., 2024). Greenhouse experiments further confirmed the potential of fumigants such as formaldehyde and phosphine in reducing *Fusarium* inoculum (El-Aswad et al., 2023).

In agricultural practice, fungicides are widely applied as seed dressings, soil treatments, or foliar sprays to mitigate fungal disease (Ayesha et al., 2021). However, systematic field evaluations specifically targeting *F. verticillioides* are less compared with the abundance of *in vitro* assays. Available evidence suggests that fungicide performance in the field is often less consistent than under laboratory conditions, largely due to the pedoclimatic and agronomic factors. For instance, prothioconazole and thiophanate-methyl exhibited strong inhibitory effects against *Fusarium* species (*F. graminearum*, *F. proliferatum*, and *F. verticillioides) in vitro*, but field trials revealed differential performance among species, with *F. verticillioides* not effectively suppressed (Masiello et al., 2019). Moreover, field studies have also demonstrated that insect management plays a decisive role in reducing *F. verticillioides* infection and fumonisin accumulation. For example, application of chlorantraniliprole at 25 $g \cdot hm^{-2}$ and emamectin benzoate at 30 $g \cdot hm^{-2}$ significantly decreased ear rot incidence, fumonisin levels, and insect damage, leading to yield improvements (Li et al., 2021). Notably, this addition of fungicides to insecticide treatments did not provide further benefits, underscoring the critical role of insect infestation in facilitating *F. verticillioides* infection (Li et al., 2021).

Overall, these results highlight the practical value of chemical fungicides but also reveal their limitations. Many modern fungicides act on single molecular targets, such as β-tubulin, C14-demethylase in sterol biosynthesis, or mitochondrial respiration complexes. This unisite action makes them particularly prone to resistance

development in pathogen populations. In addition, their extensive use is increasingly constrained by residue accumulation and environmental risks. These limitations reinforce the need to complement chemical control with more sustainable alternatives. Biocontrol agents, in contrast, typically rely on multisite action, including the secretion of diverse metabolites, competition for resources, and induction of host resistance, making them less likely to drive resistance.

5.4. Biological control approaches

5.4.1. Principles of biological control

Naturally occurring antagonistic microorganisms can suppress plant pathogens through diverse mechanisms. These include competition for ecological niches and nutrients, parasitism or predation, the production of antimicrobial compounds, and the induction of systemic resistance within the host plant (Elnahal et al., 2022). Notably, some biological control agents (BCAs) also function as plant growth-promoting rhizobacteria (PGPR), which, during the plant-microbe interactions, can act as biofertilizers, rhizoremediators, phytostimulators, and stress controllers, thereby enhancing plant growth in the absence of pathogens (Lugtenberg & Kamilova, 2009). A key advantage of biological control is ecological safety; unlike chemical fungicides, biocontrol agents leave no harmful residues and pose minimal risk to non-target organisms (Ons et al., 2020). Furthermore, they are less likely to drive the development of pathogen resistance due to their multifaceted modes of action. Beyond disease suppression, biological control also contributes to soil and plant health by enhancing microbial diversity, improving nutrient cycling, and supporting the overall resilience of agroecosystems.

Despite these advantages, biological control also faces several challenges. The inconsistency of field performance, strong dependence on environmental conditions, limited persistence of inoculants, and difficulties in large-scale formulation and commercialization have restricted its broad adoption. Moreover, compared with chemical pesticides, which often act through a single-site mechanism and therefore face a high risk of resistance development, biocontrol agents such as *Bacillus* spp. generally act through multiple mechanisms. This multi-site mode of action greatly reduces the likelihood of resistance development relative to chemical fungicides, although adaptive responses of pathogens cannot be completely excluded. In addition, although generally considered safer than synthetic pesticides, BCAs and their metabolites are not universally risk-free; certain strains may harbor toxin-encoding or antibiotic resistance genes, and some natural compounds (e.g., essential oils or microbial metabolites) can cause non-target toxicity or phytotoxicity under specific conditions (Ajayi, 2024; Cui et al., 2020). These considerations highlight that while biological control offers an environmentally friendly alternative to chemical control, rigorous strain-specific and ecological safety assessments remain essential for its successful and sustainable application.

Table 1-4 Representative biocontrol agents effective against *Fusarium* spp., mechanisms of antifungal action, and key bioactive traits.

Biocontrol agents	Mechanisms of action	Key bioactive compounds or traits	References
***Bacillus* genus** (e.g., *B. subtilis*, *B. amyloliquifaciens*, *B. velezensis,*)	Antimicrobial compounds production, niches and nutrients competition, induction of systemic resistance, pathogen quorum sensing interference, modulation of rhizosphere microbiota	Lipopeptides (surfactin, iturin, and fengycin), polyketides (difficidin and macrolactin), volatile organic compounds (2-nonanone, 2-decanone, 2-propanone, benzaldehyde, 1,2-benzothiazole-3(2H)-one, 1,3-butadiene, etc.), hydrolases	(N. Zhang et al., 2023)
***Trichoderma* genus** (e.g. *T. harzianum*, *T. virens*, *T. atroviride*)	Mycoparasitism, secondary metabolites production; competition, activation of plant defense system induction, production of hydrolytic enzymes	Azaphilones, viridins, nitrogen heterocyclic compounds, volatile terpenes, hydrolytic enzymes, proteases	(Guzmán-Guzmán et al., 2023)
***Pseudomonas* genus** (e.g., *P. fluorescens*, *P. aeruginosa*, *P. protegens*)	Antibiotic and siderophore production, disruption of redox balance, membrane and cell wall damage, interference with fungal metabolism and gene expression, and plant immune stimulation	Phenazine-1-carboxylic acid, phenazine-1-carboxamide, 2,4-diacetylphloroglucinol, pyrrolnitrin, brasmycin, braspeptin, orfamides, sessilins, nunamycin, nunapeptin	(Dimkić et al., 2022)
Non-toxigenic strains (*F. verticillioides*, *Aspergillus flavus*)	Competitive exclusion of toxigenic strains	N/A	(Tang et al., 2024)
Essential oils (e.g., *Cinnamomum* spp., *Rosmarinus officinalis*, *Perilla frutescens*, *Matricaria chamomilla*)	Disruption of membrane integrity, inhibition of mitochondrial enzymes, generation of ROS, interference with fungal homeostasis, TCA cycle inhibition, inhibition of mycelial growth, and spore germination	Cinnamaldehyde, thymol, carvacrol, camphor, 1,8-cineole, perillaldehyde	(Almeida et al., 2024)

5.4.2. Promising biocontrol agents, with a focus on *Bacillus* spp.

Biological control has emerged as a highly attractive and sustainable strategy for managing *Fusarium* diseases in maize. By harnessing the natural activities of beneficial microorganisms, such as bacteria and fungi, mycoviruses, and non-toxigenic strains, as well as other biocontrol agents including antioxidants, plant extracts, and plant-based essential oils, these approaches offer environmentally friendly solutions that reduce reliance on chemical treatments (N et al., 2021; Tariq et al., 2020).

A wide range of bacterial and fungal strains have been evaluated for their biocontrol potential to control *F. verticillioides* in maize. Among them are bacterial and fungal agents such as *Bacillus* spp., *Pseudomonas* spp., and *Trichoderma* spp. being the most prominent (Table 1-4). These organisms employ diverse mechanisms, including the production of antimicrobial metabolites, competition for nutrients and colonization sites, interference with pathogen quorum sensing, and induction of plant systemic resistance.

Bacillus strains in particular have attracted great attention due to their ability to produce stable endospores, which enhance survival and facilitate large-scale formulation (Biermann & Beutel, 2023; Duré et al., 2025). They also synthesize a broad spectrum of secondary metabolites, such as lipopeptides, polyketides, and volatile organic compounds that effectively inhibit fungal pathogens. Notably, *B. cereus* RC1 was reported to produce diketopiperazines that modulate pathogen metabolic pathways by disrupting signal transduction or enzymatically degrading QS molecules (Kachhadia et al., 2022). In addition, *B. amyloliquefaciens* W19, an efficient antagonist of *Fusarium oxysporum* f. sp. *cubense* in banana, was shown to reshape the resident soil microbiome following inoculation, particularly enriching beneficial *Pseudomonas* populations, highlighting microbiome modulation as a novel and ecologically significant mode of action (Tao et al., 2020).

Besides *Bacillus*, other microbes such as *Trichoderma harzianum* have also demonstrated antagonistic activity against *Fusarium* spp. in maize, though their application in field conditions remains variable (Guzmán-Guzmán et al., 2023). Non-toxigenic strains represent another promising approach, acting through competitive exclusion of toxigenic *Fusarium* populations and thereby reducing fumonisin accumulation. For example, the co-cultivation of *F. verticillioides* wild-type strains with the *FUM* gene deletion mutants led to a 97% reduction in FB_1 production, suggesting that non-toxigenic strains may disrupt fumonisin biosynthesis pathways via competitive mechanisms (Tang et al., 2024).

In addition to microbial antagonists, plant-derived antifungal agents such as essential oils and extracts from *Cinnamomum*, *Rosmarinus officinalis*, *Perilla frutescens*, and *Matricaria chamomilla* have been tested for potential activity against *Fusarium* spp. These compounds act mainly by membrane disruption, mitochondrial damage, and oxidative stress induction, and some have shown strong *in vitro* activity (Almeida et al., 2024; Kocevski et al., 2013). These natural compounds offer eco-friendly

alternatives or complementary strategies to microbial biocontrol and mycotoxin contamination reduction.

Overall, a variety of biological agents have been explored for the management of *F. verticillioides* in maize, and *Bacillus* spp. are one of the most promising due to their ability to produce a wide spectrum of antimicrobial compounds, form resilient endospores, and modulate plant-associated microbiomes. These multifaceted traits not only suppress fungal growth but also contribute to plant health and resilience, making *Bacillus* a valuable candidate for sustainable disease management. However, as for most biocontrol agents, field performance can be inconsistent, reflecting the complexity of agroecosystems. This underlines the importance of mechanistic studies under controlled conditions, which provide critical insights into how *Bacillus* antagonizes pathogens and pave the way for future applications in more complex environments.

5.4.3. Application methods of *Bacillus*-based BCAs

BCAs can be applied through various methods depending on the target pathogen, crop growth stage, and environmental conditions. Selecting an appropriate application strategy is critical to maximizing the efficacy of biocontrol against *F. verticillioides* in maize. Since *F. verticillioides* is capable of infecting maize at all developmental stages, from seed germination to ear formation, BCAs can be applied via various methods, including seed treatment, root inoculation, cutting and seedling root dip, soil treatment, plant inoculation, furrow application, and wound application (Gai et al., 2018; N et al., 2021; Tsegaye et al., 2018).

Seed coating has emerged as a widely accepted strategy for protecting germinating seeds and ensuring early seedling vigor. Recent studies demonstrated that incorporating *B. subtilis* QST 713 spores into a bioplastic-based coating matrix on maize seeds significantly enhanced seedling growth, with stem and root lengths increased by 18.0% and 21.4%, respectively, compared with untreated controls in the greenhouse experiment. Importantly, the coating did not reduce germination or seedling establishment and also generated substantially less dust during handling compared with commercial coatings, thereby improving safety (Accinelli et al., 2018). These results indicate that *Bacillus*-based seed coating represents a promising and practical delivery method for maize protection.

Soil inoculation is another effective strategy to deliver *Bacillus* strains into the maize rhizosphere, thereby suppressing *F. verticillioides* and improving plant growth. For example, prophylactic treatment of soil and maize seeds with *B. safensis* RF69, *Bacillus* sp. RP103 and RP242, either individually or as a combined bacterial mixture, significantly reduced fungal density in both bulk soil and the rhizosphere while promoting seedling growth (Einloft et al., 2021).

Foliar sprays of *Bacillus* have also been evaluated as a means to reduce *F. verticillioides* infection in maize. In tropical field trials, two applications of *B. subtilis* BIOUFLA2 significantly increased the proportion of native phylloplane antagonistic bacteria and fungi by 25% and 27.3%, respectively, compared with the control, while fungicide sprays with a triazole + strobilurin mixture reduced these beneficial

communities. Moreover, most antagonists subsequently isolated from the phylloplane originated from plants treated with BIOUFLA2, and acted through antibiosis, competition, and parasitism. These results indicate that foliar *Bacillus* treatments not only directly suppress *F. verticillioides* but also recruit indigenous microbial antagonists, thereby enhancing the overall resilience of the phylloplane community (Perrony et al., 2023).

In addition to single-strain applications, combining *Bacillus* with other beneficial microbes has shown promise in enhancing disease suppression and stability under variable soil conditions. For example, greenhouse studies demonstrated that a consortium of *B. velezensis* NWUMFkBS10.5 and *Pseudomonas fulva* PS9.1 effectively colonized maize roots, promoted plant growth, and suppressed *F. graminearum* infection. Notably, the combined treatment performed consistently well in both sterilized and non-sterilized soils, indicating resilience in the presence of complex resident microbiota (Adeniji & Babalola, 2022). These findings suggest that microbial consortia may represent a robust strategy for integrated maize disease management, although further formulation and field-scale evaluations are required.

Overall, *Bacillus*-based BCAs can be applied through multiple strategies, including seed coating, soil inoculation, foliar sprays, and consortia-based applications. These methods allow targeting different infection stages of *F. verticillioides* and provide flexibility in maize protection. However, the success of such applications depends on factors such as formulation stability, persistence under field conditions, and compatibility with other agronomic practices. Optimizing application methods, together with selecting robust and safe strains, will be crucial for improving the reliability of *Bacillus*-based biocontrol.

5.4.4. Limitations of *Bacillus*-based BCAs

Bacillus-based BCAs can be applied through multiple delivery strategies that target different infection stages of *F. verticillioides*, offering considerable flexibility for maize protection. Nevertheless, their practical use also faces several limitations. Field performance is often less consistent than in controlled experiments, largely due to environmental variability, formulation instability, and competition with resident microbiota (He et al., 2021). Stable colonization of *Bacillus* on plant tissues remains difficult to achieve, and their efficacy can be strongly influenced by soil type, pH, and climatic conditions (Charron-Lamoureux et al., 2024). In addition, biocontrol agents usually act more slowly than chemical fungicides and may require repeated applications to achieve satisfactory protection (Tyagi et al., 2024).

Although *Bacillus* species are generally regarded as safe, strain-specific evaluation is still essential. Some strains may harbor toxin-encoding or antibiotic resistance genes, and some metabolites can exhibit non-target toxicity or even phytotoxic effects under specific conditions (Cui et al., 2020). As a contrasting example, *B. subtilis* MB40, a probiotic strain for dietary use, was confirmed to lack toxin and mobile antibiotic resistance genes and showed no adverse effects in animal and human trials (Spears et al., 2021). This positive case illustrates that *Bacillus*-based BCAs should also undergo rigorous safety assessment before large-scale agricultural application.

These drawbacks highlight the importance of continued research to develop optimized formulations, select robust and safe strains, and integrate *Bacillus*-based BCAs with other disease management strategies.

6. Mechanisms of antifungal activity of *Bacillus* spp.

6.1. Production of bioactive metabolites

Bacillus spp. produce a lot of secondary metabolites that contribute significantly to their antifungal activity, including lipopeptides, polyketides, hybrid polyketide-nonribosomal peptides, and volatile organic compounds (Kaspar et al., 2019). Genes responsible for the biosynthesis of these metabolites constitute approximately 5%-10% of the *Bacillus* genome (Comba-González et al., 2024).

Among them, lipopeptides are the most extensively studied and synthesized by non-ribosomal peptide synthetases (NRPSs). These mainly include: the surfactin family, known for its surfactant activity and ability to disrupt microbial membranes, commonly produced by *B. subtilis*, *B. velezensis*, *B. amyloliquefaciens*, and *B. licheniformis* strains (Qi et al., 2023); the iturin family (e.g., iturins, bacillomycin, mycosubtilin, mojavensin), exhibiting antifungal activity against *Fusarium* spp. and other phytopathogens (Dunlap et al., 2019); the fengycin family, effective against soil-borne phytopathogens, such as *F. oxysporum* and *Verticillium dahliae*. Due to their small and amphiphilic structure, lipopeptides can insert into fungal membranes, disrupting membrane integrity by forming pores or altering permeability, which ultimately leads to cytoplasmic leakage and cell death (Sreedharan et al., 2023).

Additionally, polyketides such as difficidin and macrolactin are synthesized by polyketide synthases. Difficidin, produced by *B. velezensis* FZB42, suppresses bacterial blight of rice by downregulating genes related to virulence, cell division, and cell wall and protein synthesis (Wu et al., 2015). Macrolactin possesses broad-spectrum antibacterial activity by interfering with DNA replication and cell wall formation (Vasilchenko et al., 2025).

Bacillus spp. also produce hybrid metabolites, such as bacillaene, which combine polyketide and lipopeptide biosynthesis pathways and exhibit wide-ranging antimicrobial effects (Butcher et al., 2007).

Besides these contact-mediated compounds, *Bacillus* spp. also produce volatile organic compounds (VOCs) into the surrounding environment, including alcohols, hydrocarbons, esters, ketones, aldehydes, nitrogen-containing compounds, organic acids, sulfur-containing compounds, and terpenes (Rani et al., 2023). These VOCs can enhance plant growth, suppress pathogens, and act as signaling molecules during plant and microorganism interactions.

Together, these diverse secondary metabolites offer *Bacillus* spp. with powerful and multifaceted antifungal capabilities. Their combined actions make *Bacillus* a promising and versatile agent for sustainable biocontrol in agriculture.

6.2. Hydrolytic enzyme-mediated cell wall degradation

In addition to producing antifungal secondary metabolites, *Bacillus* spp. also exert biocontrol effects through the secretion of hydrolytic enzymes, often at relatively high concentrations (Ajuna et al., 2023). These enzymes include chitinases, cellulases, xylanases, glucanases, and proteases, which can degrade structural components of fungal cell walls (chitin, glucans, and proteins). By cleaving glycosidic and peptide bonds, these enzymes compromise cell wall integrity, ultimately leading to inhibited fungal growth and cell lysis (N. Zhang et al., 2023). For example, treatment of tomato seeds infected by *V. dahliae*, *Alternaria citri*, *A. solani*, *F. solani*, *F. sambucinum*, *Penicillium occitanis*, and *Aspergillus nidulans* using chitinase derived from *B. cereus* IO8 significantly improved seed germination rates, increasing from 0-35% in untreated controls to 45-85% (Hammami et al., 2013). Similarly, β-1,3-1,4-glucanase produced by *B. velezensis* ZJ20 was shown to disrupt hyphal morphology, contributing to antifungal activity (Xu et al., 2016).

6.3. Induction of systemic resistance in plants

As a key group of PGPR, *Bacillus* spp. not only facilitate plant growth and development but also enhance resistance to environmental stress through activation of ISR. ISR is a plant defense mechanism triggered by beneficial microbes and provides broad-spectrum protection against various pathogens (Yu et al., 2022). Unlike systemic acquired resistance, which is mediated by salicylic acid and pathogen-related proteins, ISR is predominantly regulated through jasmonic acid and ethylene signalling pathways (Knoester et al., 1999; Pieterse et al., 1996).

Several mechanisms underlie PGPR-induced ISR: 1) Induction of plant volatiles: PGPR can enhance the emission of host-derived volatiles like indole and β-caryophyllene, which deter pathogens and pests; 2) Emission of bacterial VOCs: Bacterial volatiles such as 2,3-butanediol and acetoin can activate host hormone signaling pathways (JA, ET, and SA), thereby priming ISR responses; 3) QS signaling: PGPR can secrete quorum sensing signals such as N-acyl-homoserine lactones, which trigger mitogen-activated protein kinase (MAPK) cascades and oxylipin pathways, leading to stomatal closure, ROS accumulation, lignification, and callose deposition; 4) Modulation of plant microRNAs: PGPR can suppress specific defense-supressing plant microRNAs (e.g., miR825/825*, miR472, miR1918), thereby upregulating resistance-related genes such as those encoding jacalin lectins, RING-H2 finger proteins, and NBS-LRR protein (Zhu et al., 2022). Together, these ISR-triggering responses contributed to enhancing immunity and overall plant health, demonstrating the multifaceted role of *Bacillus* in maize.

The effectiveness of ISR has been clearly demonstrated under controlled laboratory or greenhouse conditions. For example, *B. aryabhattai* LAD, isolated from maize rhizosphere soil, activated root immunity by stimulating reactive oxygen species (ROS) accumulation. This oxidative burst subsequently promotes the bacterial synthesis of indole-3-acetic acid (IAA), enhancing plant growth. In co-culture experiments, LAD significantly improved maize seedling growth, primary root length

increased by 197%, seedling height by 107%, root surface area by 89%, and root volume by 75% (Deng et al., 2024).

More recently, field-relevant evidence has also emerged. Resistant maize cultivars were shown to selectively recruit *Bacillus* spp. from the rhizosphere to the stem, where they induced host metabolic defenses against maize stalk rot. Specifically, *Bacillus* isolates activated TYDC1, a gene encoding tyrosine decarboxylase, leading to the biosynthesis of alkaloids with inhibitory activity against *F. graminearum* (Xia et al., 2024). This study demonstrates that ISR-like mechanisms can indeed function under field conditions, although their stability and reproducibility are influenced by host genotype and environmental variability.

Together, these findings illustrate the multifaceted role of *Bacillus* spp. in priming plant immunity and highlight both the promise and the challenges of translating ISR from controlled settings to agricultural fields.

6.4. Competition for nutrients and ecological niches

Nutrients and ecological niches are critical for the establishment of epiphytic microorganisms, including pathogens and beneficial microbes (Roussin-Léveillée et al., 2024). Competition for these resources is therefore an indirect but important antagonistic strategy by PGPR, such as *Bacillus* spp. This can take the form of exploitative competition, where microbes rapidly acquire essential nutrients, or interference competition, where they inhibit competitors through antimicrobial compounds (Cornforth & Foster, 2013). *Bacillus* strains secrete siderophores such as bacillibactin that chelate ferric iron with high affinity, thereby depriving fungal pathogens of this vital nutrient (Schalk, 2025). For instance, *B. subtilis* CAS15 produced bacillibactin and significantly inhibited the growth of multiple fungal pathogens *in vitro*. Moreover, its biocontrol efficacy against *Fusarium* wilt of pepper was reduced by iron supplementation, confirming that disease suppression was mediated by iron competition (Yu et al., 2011).

Niche colonization traits such as motility, chemotaxis, biofilm formation, and exopolysaccharide production determine the ecological success of PGPR (Liu et al., 2024). Mutants of *Pseudomonas* spp. impaired in motility or other colonization traits exhibited reduced rhizosphere competitiveness and failed to control *Fusarium* diseases, even though they still produced antifungal metabolites (Barahona et al., 2011; Chin et al., 2000). These findings demonstrate that effective colonization provides the foundation for biocontrol, ensuring the delivery and activity of antifungal compounds. Similar principles apply to *Bacillus* spp., where motility, biofilm formation, and exopolysaccharide production are essential for rhizosphere competence.

6.5. Interference with pathogen quorum sensing

Quorum sensing (QS) in *Bacillus* is a communication mechanism that enables populations to coordinate essential behaviors such as competence, sporulation, virulence, and biofilm formation (Anju et al., 2018). A striking example of the ecological relevance of quorum sensing comes from the interaction between *B. subtilis* and the soil fungal pathogen *Setophoma terrestris*. After contact with the

fungus, heritable phenotypic variants of *B. subtilis* lost the ability to produce surfactin and plipastatin, yet paradoxically acquired strong antifungal activity. Metabolomic profiling revealed that these variants secreted elevated levels of the ketones 2-heptanone and 2-octanone, both of which displayed potent antifungal effects that were abolished by the addition of exogenous surfactin. Whole-genome sequencing identified mutations in the ComQXPA QS system as the genetic basis for this conversion, demonstrating how alterations in quorum sensing can reprogram *Bacillus* metabolism and redirect secondary metabolite output towards effective antifungal compounds during antagonistic interactions (Albarracín Orio et al., 2020).

6.6. Modulation of rhizosphere microbiota

A recent study in banana fields affected by *Fusarium* wilt demonstrated that *Bacillus subtilis* R31 can sustainably reshape the rhizosphere microbiota under continuous cropping. Inoculation with R31 enriched the core beneficial taxa such as *Burkholderia-Dyella*, *Arthrobacter-Ralstonia*, and *Streptomyces*, while weakening pathogen-associated networks of *Burkholderia*. Functional profiling further revealed enhanced correlations between *Rhizobium* and secondary metabolism pathways, suggesting that R31 improved the ecological functionality of the rhizosphere. Remarkably, even though R31 was undetectable in the second year, its modulation of community structure persisted as a "legacy effect," consistent with priority effects that allow early colonizers to resist pathogen invasion. These findings highlight that *Bacillus* can drive long-lasting shifts in microbial community assembly, thereby contributing to broad-spectrum disease suppression and offering a basis for the design of synthetic bacterial consortia for sustainable biocontrol (Shao et al., 2025).

6.7. Summary

Overall, *Bacillus* spp. employ multiple and complementary mechanisms to suppress fungal pathogens, including the production of diverse secondary metabolites, secretion of hydrolytic enzymes that degrade fungal cell walls, induction of systemic resistance in host plants, competition for nutrients and ecological niches, interference with pathogen quorum sensing, and modulation of rhizosphere microbiota (N. Zhang et al., 2023). These mechanisms jointly weaken fungal growth and virulence while enhancing plant defense capacity.

Recent omics-based studies, particularly transcriptomics, have expanded this classical framework by revealing large-scale reprogramming of fungal gene expression in response to *Bacillus* (C. Wang et al., 2019). Pathogens often downregulate toxin biosynthetic and metabolic pathways, while upregulating stress adaptation and detoxification genes, reflecting costly survival trade-offs (Liang et al., 2023). Meanwhile, *Bacillus* itself undergoes feedback adjustments in metabolism, sporulation, and colonization traits during these interactions.

Beyond biological insights, transcriptomics, as a high-throughput sequencing approach, provides a powerful means to capture genome-wide gene expression changes under biotic interactions. Its advantages include the unbiased coverage of coding transcripts, the ability to identify differentially expressed genes and enriched

pathways, and the opportunity to generate new hypotheses on cellular responses at a systems level. However, transcriptome data also have inherent limitations: RNA abundance does not necessarily reflect protein levels or enzymatic activity, the measurements represent only a snapshot of dynamic processes, and results are sensitive to sample quality and sequencing depth (Manzoni et al., 2018). Therefore, transcriptomic analyses are most informative when integrated with complementary omics approaches, such as proteomics and metabolomics, and validated by functional assays.

Together, these findings reveal that *Bacillus* antagonism is not limited to metabolite and enzyme activity but extends to systems-level reprogramming of fungal metabolism, stress adaptation, and nutrient responses, while also reshaping *Bacillus* physiology. This reciprocal transcriptional remodeling underscores the complexity of cross-kingdom interactions and provides a molecular basis for understanding and optimizing *Bacillus* as a biocontrol agent.

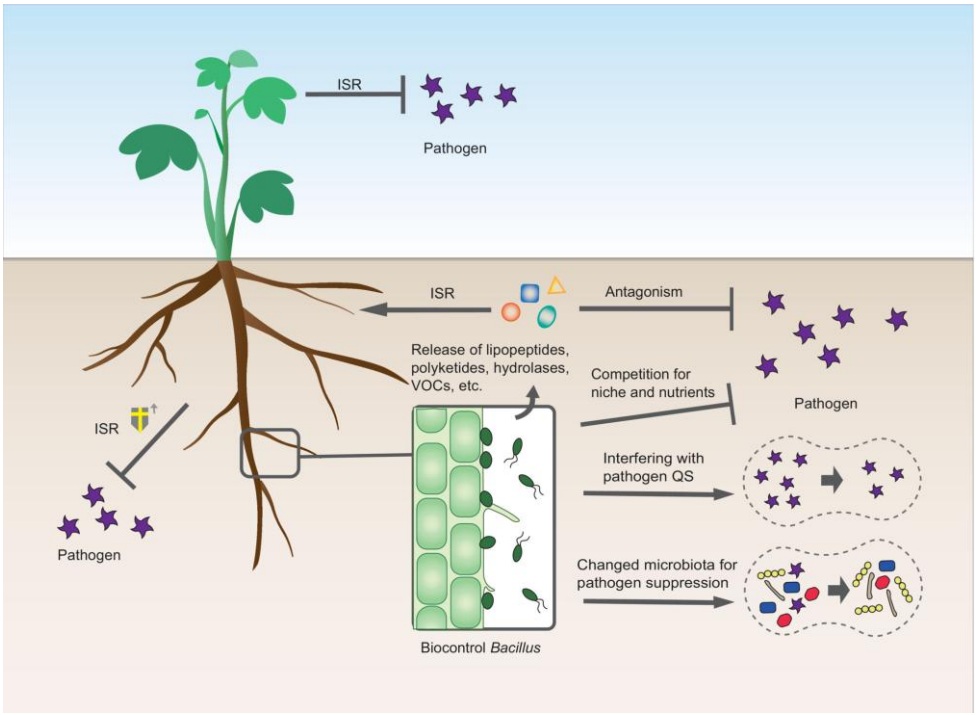

Figure 1-4 Schematic representation of the multiple biological protective mechanisms of *Bacillus* spp.
Figure reproduced from (N. Zhang et al., 2023), *Microbial Biotechnology*, licensed under CC BY 4.0.

Chapter 2

Research objectives and thesis structure

1. Research questions and hypotheses

Fusarium verticillioides is a major pathogen of maize, particularly in warm and humid regions such as northern China, where it frequently causes ear and stalk rot and contaminates kernels with fumonisins. The strain used in this study (FvLNF15-11) was isolated from diseased maize kernels collected in northern China, a region with recurrent outbreaks of *F. verticillioides*. This isolate was selected because of its high virulence and fumonisin production potential, ensuring that it is representative of local pathogen populations. While the geographical focus is on northern China, the findings are broadly relevant since *F. verticillioides* is among the most widespread maize pathogens worldwide. Current diagnostic methods for *F. verticillioides* are either time-consuming, labor-intensive, or lack the portability required for field application. In terms of biological control, most studies have focused on *in vitro* antagonistic activity, with less attention given to plant growth-promoting traits or to the molecular responses of the pathogen under biocontrol pressure.

This thesis addresses these gaps through two main innovations. First, the development of a CRISPR/Cas12a-based RPA assay provides a rapid, sensitive, and potentially field-deployable method for detecting *F. verticillioides*. Second, the previously isolated strain IFST-221 is evaluated for its biocontrol efficacy and plant growth-promoting properties, and its antagonistic mechanism is dissected at the molecular level through transcriptomic analysis. Guided by these gaps and innovations, the research questions and hypotheses of this thesis are:

1) Can a CRISPR/Cas12a-based RPA assay provide a rapid, sensitive, and potentially field-ready tool for detecting *F. verticillioides*?

2) Does *B. velezensis* IFST-221 possess both antagonistic activity and plant growth-promoting traits that support its potential as a biocontrol agent against *F. verticillioides*?

3) Does the antagonism of IFST-221 depend on multiple metabolites and trigger adaptive transcriptomic responses in *F. verticillioides*?

2. Objectives

The primary objective of this study is to establish a comprehensive strategy for the detection and biocontrol of *F. verticillioides* in maize. Taken together, these objectives aim not only to advance rapid detection and biocontrol independently, but also to highlight their complementary roles in sustainable management. Specifically, it aims to:

1) Develop a rapid, sensitive, and field-deployable detection method for *F. verticillioides* based on RPA-CRISPR/Cas12a technology coupled with lateral flow dipsticks.

2) Evaluate the biocontrol efficacy and plant growth-promoting properties of *B. velezensis* IFST-221 through *in vitro* and *in planta* assays.

3) Investigate the antifungal mechanism of IFST-221, focusing on secondary metabolites and the transcriptomic responses of *F. verticillioides* under biocontrol pressure.

3. Thesis structure

Chapter 1 provides a literature review on recent advances in the detection and management of *F. verticillioides*.

Chapter 2 outlines the general objectives and structure of the thesis, setting the stage for the main research questions and methodological framework.

Chapter 3 describes the development of a rapid detection method of *F. verticillioides* based on recombinase polymerase amplification combined with CRISPR/Cas12a with lateral flow dipsticks, providing a sensitive and portable solution suitable for field application.

Chapter 4 evaluates the biocontrol potential and plant growth-promoting traits of IFST-221, identified as *Bacillus velezensis*. Its antifungal activity was assessed through inhibitory spectrum assays, morphological observation via scanning electron microscopy (SEM), and in planta disease control tests. The plant growth-promoting traits of IFST-221 were preliminarily evaluated based on its effects on various seedlings, as well as its abilities in nitrogen fixation, phosphate and potassium solubilization, and biofilm formation. Genomic analysis was further conducted to identify key genes or pathways responsible for its biocontrol potential.

Chapter 5 investigates the antifungal mechanism of IFST-221. The main active compound was identified from crude extract using LC-MS/MS, followed by gene knockout via homologous recombination and functional validation. Transcriptomic analysis was conducted to elucidate the response of *F. verticillioides* under the biocontrol stress of IFST-221.

Chapter 6 provides the general discussion, conclusion, and perspectives, integrating results and highlighting future directions.

Chapter 7 lists all the references cited in this thesis.

Chapter 3

Development of an RPA-based CRISPR/Cas12a assay in combination with a lateral flow strip for rapid detection of toxigenic *Fusarium verticillioides* in maize

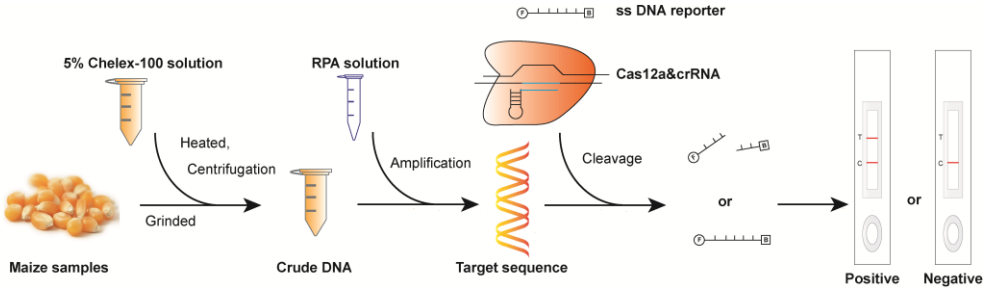

The work from this chapter was published in *Food Control* and adapted from Liang, X., Zhang, X., Xi, K., Liu, Y., Jijakli, M. H., & GUO, W. (2024). Development of an RPA-based CRISPR/Cas12a assay in combination with a lateral flow strip for rapid detection of toxigenic *Fusarium verticillioides* in maize. *Food Control*, 157, 110172.

Abstract

Fusarium verticillioides is an important phytopathogenic fungus that poses a threat to maize yield and quality in global maize-growing regions by causing *Fusarium* ear and stalk rot. The fungus is known to produce fumonisins, which are toxic secondary metabolites and have been associated with high incidences of esophageal cancer. The *FUM1* gene is responsible for producing a crucial polyketide synthase required for fumonisin biosynthesis and is present in all pathogenic strains of *F. verticillioides*. This study aims to develop a rapid and accurate detection assay for *F. verticillioides* by utilizing Chelex-100 resin for DNA extraction, recombinase polymerase amplification coupled with CRISPR/Cas12a cleavage, and lateral flow detection (RPA-Cas12a-LFD) assay based on the *FUM1* gene. The developed RPA-Cas12a-LFD assay exhibited remarkable specificity for *F. verticillioides*, with an analytical sensitivity close to one genome equivalent. The entire diagnostic process was completed in just 73 minutes, including sample DNA extraction, RPA reaction, Cas12a cleavage, and result readout. Furthermore, the RPA-Cas12a-LFD assay was found to be equivalent to single-spore isolation and partial translation elongation factor 1α gene sequencing in identifying diseased samples in the field. In summary, this accurate and portable detection equipment has great potential for detecting and recognizing *F. verticillioides*, especially in areas where advanced lab equipment is not available.

Keywords: Cas12a, *Fusarium verticillioides*, lateral flow detection, maize, recombinase polymerase amplification

1. Introduction

Fusarium verticillioides is a major pathogen that affects the maize crop worldwide, leading to significant qualitative and quantitative losses (Liu et al., 2022). In China, *F. verticillioides* is commonly responsible for maize ear and stalk rot (Duan et al., 2016; L. Li et al., 2019). The infection of *F. verticillioides* can disrupt the structure of maize starch and alter its physicochemical qualities, reducing its suitability for both food and non-food industries (Wei et al., 2022). It is important to note that the maize kernels infected by fungi are highly dangerous for human consumption, as they contain fumonisins that are carcinogenic (Braun & Wink, 2018). According to the 2022 World Mycotoxin Survey, the prevalence of fumonisin contamination in China is alarmingly high at 93% (dsm-firmenich, 2022). Additionally, most of the maize produced worldwide is used as animal feed, which not only poses a threat to animal health but also increases the likelihood of indirect mycotoxin contamination in humans. Therefore, early diagnosis techniques to identify *F. verticillioides* are crucial in preventing maize ear and stalk disease, thus benefiting the food and feed industry.

In the past, identifying *F. verticillioides* through its morphological characteristics was a lengthy and complex process that required expensive equipment and well-trained staff (Guarro & Gené, 1992). As an alternative approach, contemporary nucleic acid amplification techniques (NAATs) such as real-time PCR, nested PCR, or a combined culture and NAAT approach provide fast and accurate results as compared to culture-based methods (Campos et al., 2019; Omori et al., 2018; Patiño et al., 2004). For example, LAMP and RPA are accurate and sensitive isothermal amplification technologies (Wigmann et al., 2020; Xu et al., 2022). Performing LAMP can be quick and efficient, taking only 30-60 minutes at 65 °C. However, when using 4-6 primers to target 6 or 8 regions within a small region, there is an increased chance of primer-primer hybridization, leading to template-free amplification. Additionally, the high efficiency of the LAMP technique increases the risk of carry-over contamination, which can cause false-positive results (Nzelu et al., 2019). Compared to LAMP technology, RPA employs two primers to obtain amplicons within 30 min at a lower temperature, leading to fewer false-positive results, making it a suitable amplification method for this study (Figure 3-1 “RPA reaction”).

Recent studies have shown that the clustered regularly interspaced short palindromic repeats - Cas system-based nucleic acid detection technology can accurately recognize target sequences better than other previously developed methods (Gootenberg et al., 2018; Li et al., 2018). This detection method is based on the crRNA-guided Cas12a (Cpf1) protein that has shown non-target DNase activity to single-stranded DNA when binding to target DNA containing a protospacer-adjacent motif (PAM) site (5’-TTTN-3’) (Figure 3-1 “Cas12a cleavage”) (Chen et al., 2018). RPA product with the PAM site aforementioned could activate Cas12a cleavage (Figure 3-1). Combining Cas12a cleavage with RPA reaction products has created a versatile rapid and specific platform for pathogens detection, such as HPV16 (25/25 agreement) and HPV18 (23/25 agreement) using DNA Endonuclease-Targeted CRISPR Trans Reporter (DETECTR) with fluorescence readout, *Mycoplasma*

contamination detection with 100% accuracy from cell culture using Cas12a-based Visual Detection (Cas12VDet) with fluorescence readout, 10 aM of African swine fever virus DNA detection using Cas12a-based On-site and Rapid Detection System (CORDS) along with lateral-flow strip readout, multiplexed nucleic acid detection platform with Specific High-sensitivity Enzymatic Reporter unlocking version 2 with fluorescence and lateral-flow strip readout (SHERLOCKv2), citrus scab diagnosis using an RPA-CRISPR/Cas12a combined with a lateral flow assay, 0.3072 fg/μL of *Alternaria* DNA detection using RPA-CRISPR/Cas12a combined with rolling circle amplification and so on (Bai et al., 2019; Chen et al., 2018; Gootenberg et al., 2018; Liu et al., 2023; Shin et al., 2021; B. Wang et al., 2019). The lateral-flow strip readout is superior to the fluorescence readout as it doesn't require any laboratory equipment.

In this study, we present an approach to rapidly detect *F. verticillioides* on-site using the CRISPR/Cas12a system. This involves combining rapid nucleic acid extraction, RPA reaction, Cas12a cleavage after target recognition, and lateral flow dipstick visualization. The whole procedure can be completed within 73 min, and the results can be visualized by the naked eye (Figure 3-1). Due to its portability, this method can improve quality management in the field and storage facilities without expensive equipment.

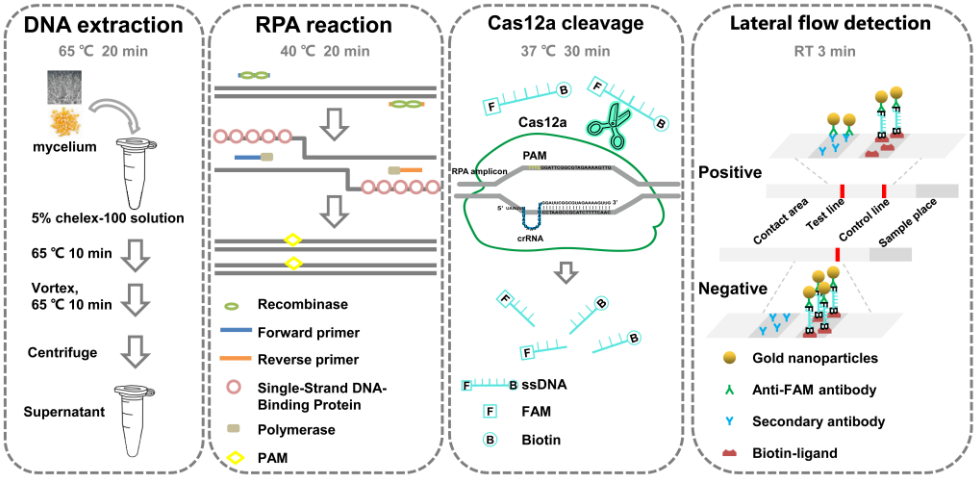

Figure 3-1 Schematic diagram of RPA-Cas12a-LFD assay and minimal time required for the detection of *F. verticillioides*.

2. Materials and methods

2.1. Fungal strains

The *Fusarium* and non-*Fusarium* strains were obtained from diseased maize stalks and kernels that were collected from different regions of China, including Jilin Province, Inner Mongolia, Shandong Province, Liaoning Province, Shanghai City, Gansu Province, Henan Province, Shanxi Province, and Yunnan Province, and were

maintained in our laboratory (Table 3-1). All of the *Fusarium* strains used in this study were identified based on their morphological characteristics and partial sequences of the translation elongation factor 1α gene, whereas all of the non-*Fusarium* strains were identified based on the partial sequences of the internal transcribed spacer.

Table 3-1 Fungal strains used in this study and their results in the RPA-Cas12a-LFD assay.

Species	Number	Host	Location in China	RPA-Cas12a-LFD
***Fusarium* strains**				
F. verticillioides	12	Maize	Jilin, Inner Mongolia, Shandong, Liaoning, Shanghai, Gansu, Henan	+
F. proliferatum	1	Maize	Liaoning, Henan	-
F. fujikuroi	1	Maize	Henan	-
F. graminearum	1	Maize	Jilin	-
F. oxysporum	1	Maize	Liaoning	-
F. temperatum	1	Maize	Yunnan	-
F. subglutinans	1	Maize	Inner Mongolia	-
F. andiyazi	1	Maize	Inner Mongolia	-
***Non-Fusarium* strains**				
Aspergillus niger	1	Maize	Shanxi	-
Alternaria sp.	1	Maize	Shanxi	-

2.2. Preparation of DNA extracts for pathogen detection

The strains were grown at 25 °C until the PDA plates were full. For crude DNA extraction, the hyphae were scraped with toothpicks into the tube containing 100 µL of 5% Chelex-100 solution (Chelex® 100 sodium form, Sigma-Aldrich, Germany) and incubated at 65 ℃ for 20 min. The supernatant was collected and used as crude DNA for the RPA reaction. To detect the sensitivity, DNA was extracted using the CTAB (Cetyltrimethylammonium bromide) method (Pahlich & Gerlitz, 1980). The quality and quantity of the extracted DNA were assessed using P200/P200+ microvolume spectrophotometers (Pultton Technology, California, USA). The DNA concentration was adjusted to 10 ng/µL with ddH_2O and stored at -20 ℃ for further use.

2.3. Design of primers and crRNA

The primers FUM1-F/R were used to amplify the partial *FUM1* sequence of *F. verticillioides* LNF15-11 (Table 3-2). A polymerase chain reaction assay was conducted in the thermal cycler with a reaction mixture of 25 µL 2× TaKaRa Ex Taq®, 1 µL forward primer (FUM1-F), 1 µL reverse primer (FUM1-R), 1 µL *F. verticillioides* LNF15-11 DNA, and the final volume was adjusted by adding 22 µL ddH_2O. The PCR products were purified using the HiPure Gel Pure DNA Mini Kit (Magen Biotech, Guangzhou, China) and sequenced by Sangon Biotech (Beijing, China). Homologous sequences of the partial *FUM1* gene for alignment were obtained

from the National Center for Biotechnology Information (NCBI) website (https://blast.ncbi.nlm.nih.gov/Blast.cgi). The sequence alignment was performed using Clustal X version 2 and Jalview version 2.11.2.5 (Larkin et al., 2007; Waterhouse et al., 2009). After that, the conservative region of *F. verticillioides* but the variant region for other strains was chosen to design three primer pairs RPA-FUM1-1-F/R, RPA-FUM1-2-F/R, and RPA-FUM1-3-F/R, according to the manual of TwistAmp® DNA Amplification Kits (Figure 3-2). To evaluate the specificity of the designed primer pairs, the genomic DNA of *F. verticillioides*, *F. fujikuroi*, *F. proliferatum*, *F. temperatum*, and *F. graminearum* was amplified by using three primer pairs in the RPA reaction. The amplified PCR products were then electrophorized on 2% agarose gel. Additionally, we ensured that the ideal amplicon contained at least one protospacer adjacent motif (PAM) site (5'-TTTN-3') to facilitate recognition by Cas12a (Chen et al., 2018).

Table 3-2 Primers and guide RNA used in this study.

Name	Sequence (5'-3')	Length (bp)
FUM1-F	GCCGGCACGAACCTTGTA	18
FUM1-R	AGGCAACTCCCACACCCTCAA	21
RPA-FUM1-1-F	TAACCTTGGACATAGCGAGGGTGCTTCAGGC	31
RPA-FUM1-1-R	CTCTTCCAGAGTTTCTATGATGCAATGGGC	30
RPA-FUM1-2-F	GGCAAATCGAAGAGAGCATTTGTCGCATCG	30
RPA-FUM1-2-R	CCCATTGGGCACCTTGTCCAGTGAAGATCA	30
RPA-FUM1-3-F	TGGGCAAAGAGCTCATGGACGAATATGAGA	30
RPA-FUM1-3-R	CAAGTGGCTGGGAGAATTCGGCGCGGCCAA	30
RPA-FUM1-crRNA	UAAUUUCUACUAAGUGUAGAUGGAUUCGGC GUAGAAAAGUUG	42
ssDNA reporter	5'-FAM-TTATT-biotin-3'	5
Fv-TUB-F	CCCCGAGGACTTACGATGTC	20
Fv-TUB-R	CGCTTGAAGAGCTCCTGGAT	20
Maize-EF-1α-F	TGGGCCTACTGGTCTTACTACTGA	24
Maize-EF-1α-R	ACATACCCACGCTTC-+`AGATCCT	22

For Cas12a cleavage, the crRNA for the CRISPR detection system was designed based on the amplified product from *F. verticillioides* and synthesized by Sangon Biotech. As in Figure 3-2, the noted "PAM" site "CAAA" was not the actual PAM site. The reverse complementary sequence "TTTG" was the true PAM site. The complete sequence of crRNA included a direct repeat sequence for Cas12a recognition "5'-UAAUUUCUACUAAGUGUAGAU-3' " (scaffold sequence) and spacer sequence "5'-GGAUUCGGCGUAGAAAAGUUG-3' " (guide sequence).

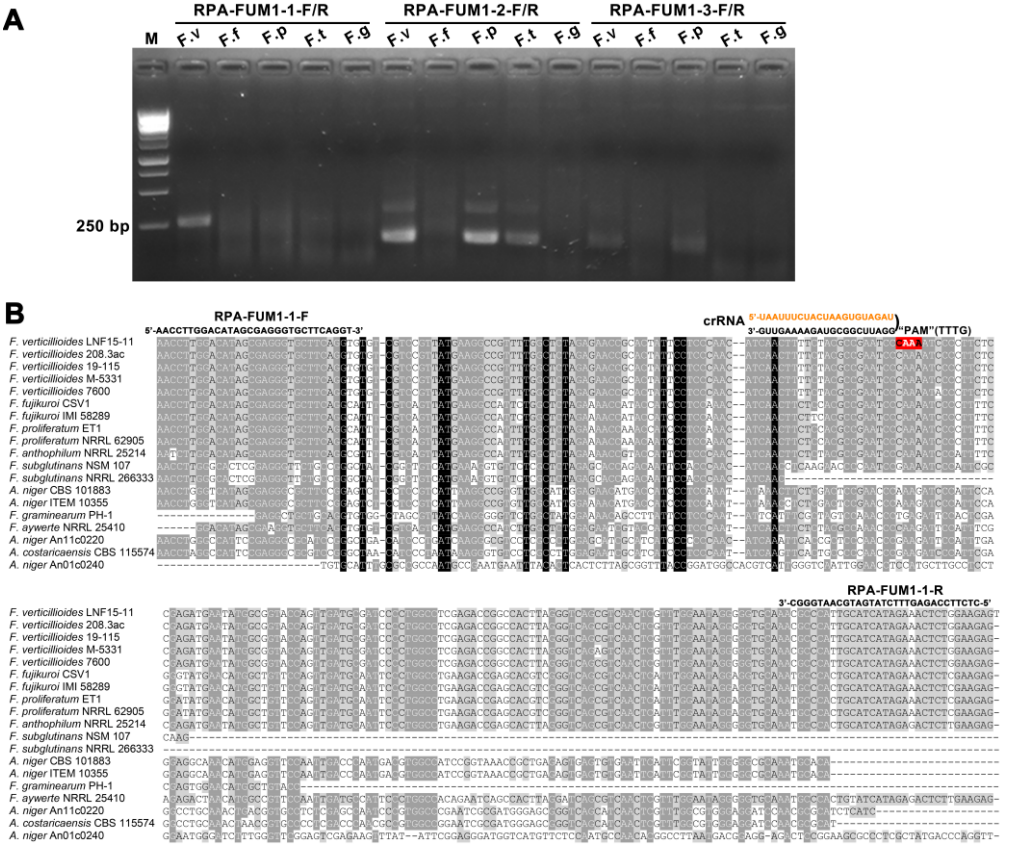

Figure 3-2 The primer and crRNA design for *F. verticillioides*.
(A) Screening of the optimal amplification primer pairs by RPA. The agarose gel electrophoresis showed the amplification results of the three designed primer pairs using RPA. Each primer pair is indicated above the corresponding lane. *F. v*, *F. f*, *F. p*, *F. t*, and *F. g* indicate *F. verticillioides*, *F. fujikuroi*, *F. proliferatum*, *F. temperatum*, and *F. graminearum*, respectively. M represents a marker of 1 kb molecular weight. (B) Location of the primer pair and crRNA in the *FUM1* gene of *F. verticillioides*. The crRNA consists of a constant scaffold sequence (orange) and a 20-nt spacer (black) complementary to the target site adjacent to the PAM. The site labeled as "PAM" (CAAA) corresponds to the reverse complement of the actual protospacer-adjacent motif (TTTG).

2.4. RPA-Cas12a-LFD reaction

The RPA reaction was prepared using the TwistAmp™ basic Kit (TwistAmp® basic kits. TwistDx™, Cambridge, United Kingdom). The reaction mixture was prepared by adding RPA enzyme powder, followed by 2.4 μL forward primer (10 μM), 2.4 μL reverse primer (10 μM), 29.5 μL primer-free rehydration buffer, and 11.2 μL ddH_2O. The resulting mixture was thoroughly mixed and then centrifuged, and the volume was divided into five RPA reactions (9.1 μL per reaction). Then, 0.4 μL crude DNA and 0.5 μL Magnesium Acetate (MgOAc, 280 mM) were added to the RPA reaction. The mixture was then incubated on a dry heating block at 40 ℃ for 20 min. Next, a single Cas12a-crRNA reaction was prepared by combining 16.875 μL ddH_2O, 0.125 μL crRNA (10 μM), 2 μL 10×NEBuffer™ r2.1, and 1 μL EnGen® Lba Cas12a (Cpf1) (1 μM) (New England Biolabs, Ipswich, MA, USA) and incubated at 37 ℃ for 10 min. Afterward, 17 μL Cas12a-crRNA reaction, 2 μL RPA product, and 1 μL ssDNA reporter were transferred into a new tube. The mixture was incubated at 37 ℃ to perform a CRISPR/Cas12a cleavage assay. After 30 minutes' incubation, 30 μL ddH_2O was added to 50 μL of the product. Then, the lateral flow strip (Cat. No. JY0301; Tiosbio Biotechnology Co., Ltd., Beijing, China) was inserted into the tube and incubated at room temperature (RT) for 3 min. If two lines appeared on the strip, it indicated a positive result, while a single line meant a negative result. The strip was then removed for inspection and photographed using a Canon EOS 80D camera.

2.5. Specificity and sensitivity of the RPA-Cas12a-LFD assay for F. verticillioides detection

To confirm the accuracy of the RPA-Cas12a-LFD assay developed for detecting *F. verticillioides* strain, crude DNA from various *F. verticillioides* strains, as well as additional *Fusarium* strains, and other fungal species from different regions of China were analyzed (Table 3-1). The results were then visualized by using the RPA-Cas12a-LFD assay.

To determine the sensitivity of the RPA-Cas12a-LFD assay for *F. verticillioides* detection, different concentrations of genomic DNA were tested, i.e., 10 ng/μL, 1 ng/μL, 100 pg/μL, 10 pg/μL, 1 pg/μL, 100 fg/μL, 10 fg/μL, 1 fg/μL, 100 ag/μL, and 10 ag/μL. The genomic DNA was extracted using the CTAB method, and then it was diluted with ddH_2O, and the sensitivity of the RPA reaction was tested by adding 0.2 μL DNA. The amount of DNA used in the RPA reaction was 2 ng, 200 pg, 20 pg, 2 pg, 200 fg, 20 fg, 2 fg, 200 ag, 20 ag, and 2 ag, respectively. The results were visualized using the RPA-Cas12a-LFD assay.

2.6. Detection of F. verticillioides in artificially diseased maize stalks and kernels

To ensure the application of the RPA-Cas12a-LFD assay for *F. verticillioides* detection in the field, we artificially inoculated *F. verticillioides* into maize stalks and kernels. At the 10^{th} leaf stage, 100 μL of the conidial suspension with a concentration of 1×10^6 conidia/mL was inoculated into the maize stalks. For maize kernels, 100 μL

of the aforementioned conidial suspension was inoculated into 5 g of the sterilized maize kernels and cultured at 25 ℃, and then collected at different inoculation times, including 24 h, 48 h, 72 h, 96 h, and 120 h. The sterilized maize kernels were prepared in accordance with the method described by Liang et al. (2022). Maize stalks and kernels inoculated with ddH_2O served as a negative control. Three replications of each experiment were made. After inoculation, the crude genomic DNA was extracted from ground stalks at 7 days post-inoculation (dpi) and kernels at different times using a 5% Chelex-100 solution, respectively. The RPA-Cas12a-LFD assay was used for visual detection of the results. To determine fungal biomass in maize kernels, total genomic DNA was extracted from kernels at different growth stages and quantified using qPCR as previously described (Gao et al., 2007). The *β-tubulin* gene of *F. verticillioides* was used to quantify fungal colonization, while the *EF1-α* gene of maize served as an endogenous plant control.

2.7. The developed RPA-Cas12a-LFD assay for the diagnosis of field maize samples

Field samples were collected from Taiyuan City, Shuozhou City, and Yangquan City in Shanxi Province, China. The samples were subjected to crude DNA extraction using 5% chelex-100 solution. The detection results were obtained visually using the RPA-Cas12a-LFD assay. Furthermore, fungal isolation, purification, and molecular identification were carried out based on the previous study (Xi et al., 2021). Briefly, the samples were cut into small pieces, surface sterilized, and then cultured on potato dextrose agar plates. Fungal isolates with different morphological characteristics were selected and cultured after single spore purification. To identify fungal isolates, their morphological features were observed on PDA and CLA plates. Furthermore, molecular identification was done using *ITS* and *TEF1-α* sequencing.

2.8. Statistics and reproducibility

All experiments were performed in at least three independent replicates. Data from qPCR assays used to determine the relative fungal biomass in maize kernels at different post-inoculation times are presented as the mean ± standard error (SE). Graphing was carried out using GraphPad Prism 6.0.1.

3. Results

3.1. Design and optimization of detection primers and crRNA

Following the guidelines of RPA primer designing, three sets of primer pairs, RPA-FUM1-1-F/R, RPA-FUM1-2-F/R, and RPA-FUM1-3-F/R were manually designed from the *FUM1* gene of *F. verticillioides* (Table 3-2). To evaluate the specificity of the designed three primer pairs, the RPA amplification was carried out using *F. verticillioides*, *F. fujikuroi*, *F. proliferatum*, *F. temperatum*, and *F. graminearum* as templates. Among the three designed primer pairs, RPA-FUM1-1-F/R was considered the optimal pair due to its lack of non-specific amplification and optimal amplicon length as compared to other fragments (Figure 3-2A). After selecting the detection primer pairs, one of the PAM sites (5'-TTTG-3') in the amplicon was chosen, and the

following sequence was selected as the target sequence of crRNA for *F. verticillioides* detection (Figure 3-2B).

3.2. Specificity and sensitivity of RPA-Cas12a-LFD assay for the detection of F. verticillioides

The specificity of the RPA-Cas12a-LFD assay for *F. verticillioides* was initially tested by mycelial DNA from various *F. verticillioides* strains, which were isolated from diseased maize samples from Jilin Province, Inner Mongolia, Shandong Province, Liaoning Province, Shanghai City, Gansu Province, and Henan Province in China (Table 3-1). The results showed that the RPA-Cas12a-FLD assay was able to accurately diagnose all strains of *F. verticillioides* regardless of their origins (Figure 3-3A). Meanwhile, the RPA-Cas12a-LFD assay was tested for its capability to differentiate nine other species. The test results showed that there was no cross-reaction among all the tested strains, including seven different *Fusarium* species and two non-*Fusarium* species (Figure 3-3A). Based on these findings, it can be concluded that the RPA-Cas12a-LFD assay could successfully distinguish *F. verticillioides* from other *Fusarium* and non-*Fusarium* fungal species.

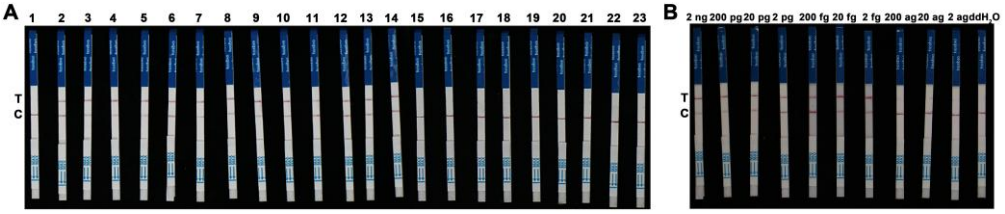

Figure 3-3 Specificity and sensitivity of RPA-Cas12a-LFD assay for *F. verticillioides* detection.

(A) Specificity analysis of the developed assay using DNA from different fungal strains. Lane 1, ddH_2O (negative control); lanes 2-3, *F. verticillioides* isolates from Shandong province; lanes 4-5, isolates from Jilin province; lanes 6-7, isolates from Inner Mongolia; lanes 8-9, isolates from Liaoning province; lanes 10-11, isolates from Henan province; lanes 12-13, isolates from Gansu province; lane 14, *F. verticillioides* reference strain 7600; lanes 15-21 closely related *Fusarium* species (*F. proliferatum*, *F. fujikuroi*, *F. graminearum*, *F. oxysporum*, *F. temperatum*, *F. subglutinans*, and *F. andiyazi*); lane 22, *Aspergillus niger*; lane 23, *Alternaria* sp. (B) Sensitivity analysis of the assay using serially diluted genomic DNA of *F. verticillioides* LNF15-11 from 2 ng to 2 ag and ddH_2O served as the negative control.

To evaluate the sensitivity of the RPA-Cas12a-LFD assay, the genomic DNA of *F. verticillioides* at serial dilutions ranging from 2 ng to 2 ag was tested (Figure 3-3B). A clear and strong test band was consistently observed at 2 fg, indicating that the assay is capable of visually detecting DNA at extremely low concentrations. Below this level, the test line weakened markedly and became undetectable at 2 ag.

Thus, 2 fg represents the lowest DNA quantity at which a visible signal was observed in this study, although the statistically reliable limit of detection is expected to be higher (see Discussion).

3.3. Analytical performance of RPA-Cas12a-LFD assay on maize stalks and kernels artificially infected with F. verticillioides

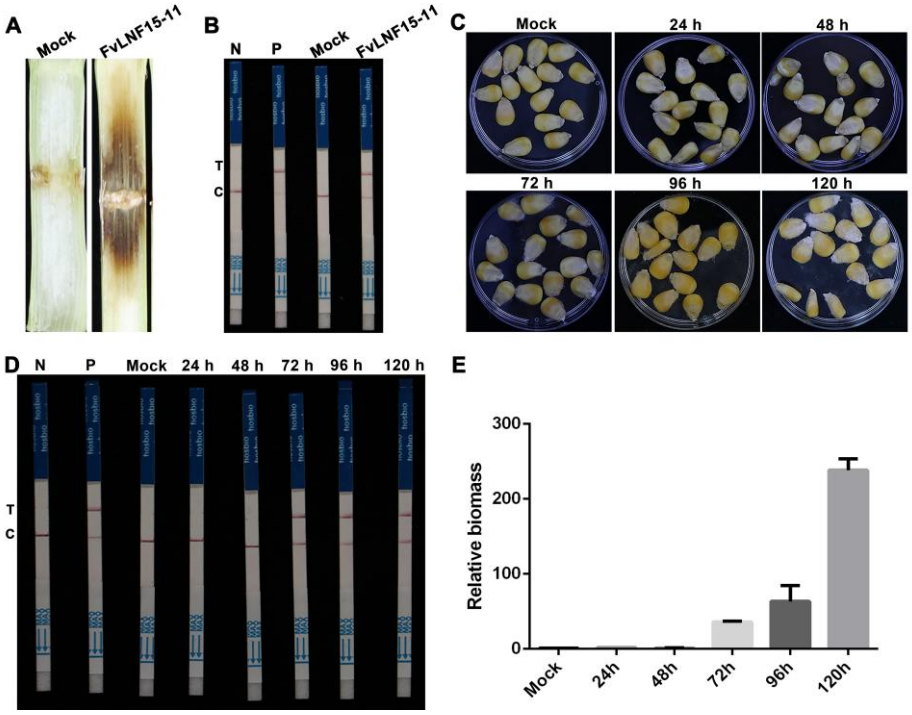

Figure 3-4 Early detection of *F. verticillioides* in artificially diseased maize stalks and kernels using the developed RPA-Cas12a-LFD assay.
(A) Longitudinally sectioned maize stalks at 7 dpi; no symptoms were observed in the control. (B) RPA-Cas12a-LFD detection of *F. verticillioides* in maize stalks. Lane 1, ddH_2O (negative control, N); lane 2, 10 ng/µL genomic DNA of *F. verticillioides* (positive control, P); lane 3, crude DNA from maize stalks inoculated by ddH_2O (Mock); lane 4, crude DNA from *F. verticillioides*- inoculated stalks. (C) Symptoms of maize kernels inoculated with *F. verticillioides* at 24 h, 48 h, 72 h, 96 h, and 120 h post-inoculation. (D) RPA-Cas12a-LFD detection of *F. verticillioides* in maize kernels. Lane 1, ddH_2O (N); lane 2, 10 ng/µL genomic DNA of *F. verticillioides* (P); lane 3, crude DNA extracted from uninfected maize kernels (Mock); lane 4-8, crude DNA extracted from kernels collected at 24 h, 48 h, 72 h, 96 h, and 120 h post-inoculation. (E) Relative fungal biomasses of the maize kernels at different post-inoculation times determined by qPCR. Error bars represent standard error.

The RPA-Cas12a-LFD detection assay was used to verify the feasibility of detecting *F. verticillioides* in maize samples (Figure 3-4A). Maize stalks inoculated with *F. verticillioides* were tested, and the assay successfully identified the presence of the

target strain in the infected sample, as indicated by the appearance of a second line on the lateral flow dipstick (Figure 3-4B). Therefore, the maize genomic DNA did not affect the detection results, and the RPA-Cas12a-LFD assay could identify *F. verticillioides* in the maize stalks.

F. verticillioides not only infects the maize kernels in the field, but also causes devastating losses during storage. To study this, maize samples were collected at different time points after inoculation (Figure 3-4C). The results revealed that there were no disease symptoms on the maize kernels at 24 h and 48 h post-inoculation, similar to the control (water). Additionally, the fungal relative biomass showed no significant difference between infected samples at 24 h, 48 h, and healthy samples, which resulted in negative results on the lipsticks test line (negative results) (Figure 3-4D and E). However, the diseased samples showed positive results when the relative biomass showed a significant difference between the inoculated maize kernels at 72 h, 96 h, 120 h, and the control (Figure 3-4C, D, and E). Based on these results, the RPA-Cas12a-LFD assay was found to be efficient for detecting *F. verticillioides*-infected maize kernels for more than 3 days.

3.4. Diagnosis of diseased maize ears in the field

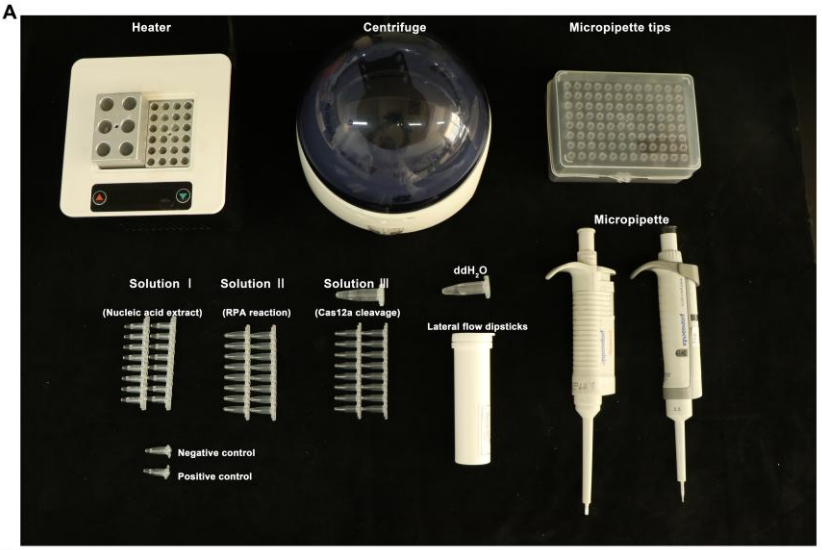

B

Diseased maize ears	Location	RPA-Cas12a-LFD results	*F. verticillioides* isolates
Sample 1	Taiyuan, Shanxi province	-	-
Sample 2	Shuozhou, Shanxi province	-	-
Sample 3	Yangquan, Shanxi province	+	+
Sample 4	Taiyuan, Shanxi province	-	-
Sample 5	Taiyuan, Shanxi province	+	+
Sample 6	Shuozhou, Shanxi province	-	-

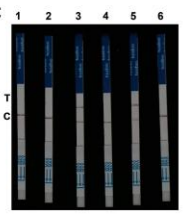

Figure 3-5 On-site detection of *F. verticillioides* using the RPA-Cas12a-LFD assay.

(A) Minimal instrument requirements of the developed RPA-Cas12a-LFD assay for detecting *F. verticillioides* in the field. (B) The infected maize ears were collected from three cities in Shanxi province. (C) The sample results were obtained using the developed RPA-Cas12a-LFD assay with minimal instrumentation.

To rapidly detect *F. verticillioides* in the field, the RPA-Cas12a-LFD assay equipment was further optimized as shown in Figure 3-5A. This equipment allows for the entire detection process to be completed in just 73 min, which includes 20 min for DNA extraction, 20 min for RPA reaction, 30 min for Cas12a cleavage, and 3 min of lateral flow detection (Figure 3-1). The efficacy of the detection kit was confirmed by collecting diseased maize ears from different cities of Shanxi province (as shown in Figure 3-5B and C). Furthermore, *F. verticillioides* strains were successfully isolated and identified from those two positive samples. Based on these results, it can be concluded that the kit is capable of detecting *F. verticillioides* in the field.

4. Discussion

F. verticillioides is the most prevalent strain responsible for maize ear and stalk rot in almost all maize-growing regions globally (Munkvold, 2003). However, other strains such as *F. proliferatum*, *F. fujikuroi*, *F. graminearum*, *F. oxysporum*, *F. temperatum*, *F. subglutinans*, *F. andiyazi*, *Aspergillus niger*, and *Alternaria sp.* have also been isolated from diseased maize samples (L. Li et al., 2019; Y. Li et al., 2019; Qin et al., 2014; Sun et al., 2017; Xi et al., 2021; Zhang et al., 2014). The prevalence of different pathogens varies by region, which is primarily influenced by geographic location and climate. In northern China, *F. verticillioides* is considered the most important pathogen of maize ear rot (Duan et al., 2016; Qiu et al., 2015).

To date, various molecular methods have been used to detect *F. verticillioides* based on different genes. The conventional PCR method, using the VER1/2 primer (based on calmodulin gene sequence), has successfully detected *F. verticillioides* with a sensitivity of 12.5 pg of pure total genomic DNA (Mulè et al., 2004). VERTF-1 and two reverse primers (VERTR and VERTF-2) have been used for the early detection of *F. verticillioides* in 1:100 diluted positive cereal samples by conventional PCR and semi-nested PCR (Nagaraj et al., 2016). For specific detection of *F. verticillioides* isolates, a PCR-ELISA assay was developed, which showed 100-fold higher sensitivity than conventional PCR (Omori et al., 2018; Patiño et al., 2004). However, these methods are difficult to apply in the field because of the need for various equipment such as a PCR machine, microwave, electrophoresis tank, and gel imaging systems. Other amplification methods are commonly used for DNA detection, including LAMP, RPA, HDA, and E-SDA (Exponential Strand Displacement Amplification). Among these methods, LAMP and RPA have higher efficiency (Zhao et al., 2015). A *FUM1*-specific assay based on LAMP has been developed to detect multiple fumonisin-producing strains with a detection limit of 5 pg genomic DNA at 65 ℃ in 60 min (Wigmann et al., 2020). However, the RPA-LFD assay demonstrated the capability to detect as low as 20 fg DNA of *F. graminearum* at 40 ℃ within 25 min, surpassing the detection limits, time duration, and operating temperature of LAMP methods (Liang et al., 2022). In this study, the *FUM1* target region, which is

present in all *F. verticillioides* strains and different from other fumonisin-producing strains like *F. proliferatum*, was selected for primer design, and this assay gave a relatively specific result for *F. verticillioides* by RPA reaction. Nevertheless, the aforementioned assays require the utilization of DNA extraction kits to acquire amplified templates (Mulè et al., 2004; Patiño et al., 2004; Wigmann et al., 2020). To efficiently implement such assays in the field, it becomes imperative convenient method for obtaining sufficient DNA from the sample for the RPA reaction. In this study, we have successfully devised a rapid extraction protocol employing chelex-100 resin, enabling the acquisition of a satisfactory quantity of total DNA for detection within 20 min. This approach helps the developed RPA-Cas12a-LFD to be suitable in field situations.

As *F. verticillioides* can frequently be isolated from symptomless kernels, more precise and sensitive methods are required to facilitate early diagnosis of *F. verticillioides* infection (Kant et al., 2017). This led to the development of advanced CRISPR-based diagnostic platforms such as Cas12a and Cas13, SHERLOCK, and HOLMES (one-HOur Low-cost Multipurpose highly Efficient System), which were originally established for clinical diagnostics but have since shown potential for plant pathogen detection as well (Chen et al., 2018; Gootenberg et al., 2018). Notably, HOLMES exhibited the capability to detect DNA concentration as low as 1-10 aM (1.0E-18 moles), which is lower than the normal RPA reaction (Li et al., 2018). By integrating the CRISPR-Cas12a system, the RPA assays have achieved detection limits down to 1 fg/μL of *F. graminearum* DNA (Mu et al., 2022).

In this study, the RPA-Cas12a-LFD assay produced clear visual bands at 2 fg of *F. verticillioides* genomic DNA. Given that the haploid genome size of *F. verticillioides* is about 46 Mb (≈47 fg DNA, based on the conversion 1 pg=978 Mbp) (Doležel et al., 2003), this concentration falls below one genome equivalent. Such sub-genome-equivalent detection can be explained by DNA fragmentation during extraction, as commonly observed in CTAB-based or kit-based protocols (Kang et al., 2023). Because RPA requires only short intact target regions rather than a complete genome, fragmented DNA molecules may still contain intact copies of the target sequence, allowing amplification at nominal DNA quantities below the theoretical genome weight.

One potential limitation of the RPA-Cas12a-LFD assay is the risk of false positives singals due to contamination. The high analytical sensitivity of isothermal amplification means that even trace amounts of carryover DNA can generate unintended test lines (Lobato & O'Sullivan, 2018). Although 2 fg consistently produced clear positive bands, concentrations below this level occasionally generated faint, non-reproducible shadows (e.g., 200 ag - 2 ag). These weak bands did not meet the predefined positivity criteria and were therefore considered background noise rather than true amplification (Ding et al., 2025). This highlights the importance of predefined interpretation criteria and contamination control measures, and results below the genome-equivalent range should be interpreted with caution.

Thanks to this high sensitivity, this assay enabled the detection of *F. verticillioides* infections in maize kernels as early as 72 hpi, when visible symptoms were still absent. In addition, it produced consistent positive results for the 13 different *F. verticillioides* strains isolated from the seven provinces, while yielding negative results for nine other species because of the high specificity of Cas12a recognition. These findings indicate that the RPA-Cas12a-LFD assay is an extraordinarily sensitive and specific tool for the efficient detection of *F. verticillioides*. Furthermore, two positive samples collected from Shanxi Province have been identified by using RPA-Cas12a-LFD developed in this assay, along with the traditional isolation procedure. However, it is important to note that all the field samples tested were maize ears collected from the same province. Given that *F. verticillioides* is widely distributed across maize-growing regions of China and other agroecological zones and is capable of contaminating not only maize tissues but also stored grains and processed food products (Nagaraj, 2017), further validation using multi-provincial and multi-matrix samples will be essential to confirm the robustness and broad applicability of the assay.

5. Conclusion

In this study, the developed RPA-Cas12a-LFD assay was designed, incorporating four essential components: Chelex-100 solution for rapid DNA extraction, RPA reaction for efficient amplification of target DNA, CRISPR/Cas12a system for cleaving of the target sequence and producing a detectable signal, and lateral flow detection for visualizing the results. The developed RPA-Cas12a-LFD assay exhibits tremendous potential as a valuable tool for swift and on-site diagnosis of *F. verticillioides*, eliminating the requirement for specialized equipment. Furthermore, it can also be deduced that the developed RPA-Cas12a-LFD assay has the potential to evaluate the quality of raw materials in food and feed products, thereby mitigating the risk associated with mycotoxin contamination.

Chapter 4

Identification and genomic insights into a strain of *Bacillus velezensis* with phytopathogen-inhibiting and plant growth-promoting properties

The work from this chapter was published in *Microbiological Research* and adapted from Liang, X., Ishfaq S., Liu, Y., Jijakli, M. H., Zhou, X., Yang, X., & Guo, W. (2024). Identification and genomic insights into a strain of *Bacillus velezensis* with phytopathogen-inhibiting and plant growth-promoting properties. *Microbiological Research*, 285, 127745.

Abstract

The use of biological agents offers a sustainable alternative to chemical control in managing plant diseases. In this study, *Bacillus velezensis* IFST-221 was isolated from the rhizosphere of a healthy maize plant in a field with severe disease incidence. The strain exhibited broad-spectrum antagonistic activity against eight pathogenic ascomycetes and oomycetes, and greenhouse assays further demonstrated its ability to mitigate maize ear rot and cotton Verticillium wilt. Additionally, IFST-221 significantly promoted the growth of maize, cotton, tomato, and broccoli seedlings, with improvements observed in plant height, root length, and dry biomass depending on the seedlings. *In vitro* assays further revealed several putative plant growth-promoting traits, including phosphate and potassium solubilization, growth on nitrogen-free medium, suggesting potential nitrogen fixation, indole-3-acetic acid (IAA) production, and biofilm formation under laboratory conditions. Whole genome sequencing revealed a genome size of 3.86 M bp with a GC content of 46.71% and identified nine known secondary metabolite biosynthetic clusters with antimicrobial properties, along with three predicted novel clusters. Genome mining also identified several key genes associated with plant growth regulation, colonization, and biofilm formation. Together, these results highlight the dual role of IFST-221 in plant growth promotion and disease suppression, supporting its potential application as an integrated biocontrol agent to enhance crop productivity.

Keywords: antifungal activity, *Bacillus velezensis*, genomic analysis, plant growth promotion, rhizobacterium

1. Introduction

Maize, a staple grain crop for both human and livestock consumption, faces significant threats from insects and pathogens, with ear and stalk rot caused by *Fusarium verticillioides* being among the most destructive. This pathogen can infect plants from the roots, spreading through the stalk and reaching the ear and kernels, leading to reduced yields and potential secondary infection (Gai et al., 2018). This disease not only results in a reduction in maize yield but also poses a threat to human and livestock health by producing mycotoxins (L. Li et al., 2019; Savary et al., 2019). Compounding the problem, *F. verticillioides* produces mycotoxins such as Fumonisin B_1, classified by the International Agency for Research on Cancer as a group 2B carcinogen, posing serious health risks to livestock and humans (Kujawa, 1994).

To combat maize ear and stalk rot, growers typically employ a mix of resistant cultivars, field management practices, and the application of chemical pesticides. However, it has been found that the resistance observed in specific cultivars under ideal experimental conditions may not be adequate for effectively managing the disease in the field (Dinolfo et al., 2022). Moreover, the excessive reliance on chemical fungicides for maize disease control has resulted in the emergence of resistance in certain fungal species. Additionally, this heavy use of chemicals raises environmental contamination and potential health risks for humans and animals (Pereira et al., 2021). Consequently, there's a growing demand for more sustainable solutions. Biological control methods, which rely on beneficial organisms to combat plant pathogens, present a promising alternative. They offer an environmentally and human-friendly approach to managing plant diseases, providing a sustainable path for controlling maize ear and stalk rot (González-Estrada et al., 2021; M. Gupta et al., 2021).

Plant growth-promoting rhizobacteria inhabit the rhizosphere, a narrow soil zone surrounding plant roots, where they provide various benefits to plant development (Kloepper et al., 1980). By colonizing plant roots, PGPR acts as a biofertilizer and biological control agent, protecting against a range of root pathogens, including bacteria, fungi, nematodes, and other harmful microorganisms (Haskett et al., 2021). A key group within this category is the genus *Bacillus*, renowned for its role in promoting plant growth and controlling pathogens. *Bacillus* species are capable of fixing atmospheric nitrogen, solubilizing phosphorus and potassium, and enhancing nutrient uptake in plants (K. Gupta et al., 2021). Moreover, these bacteria produce a range of phytohormones to stimulate plant growth, like auxins, cytokinins, gibberellins, ethylene, and abscisic acid. *Bacillus* also produces some secondary metabolites, which are crucial in preventing pathogen infection. Unlike primary metabolites, secondary metabolites are not essential for microbial growth and development but are synthesized in response to specific environmental conditions (Abdel-Aziz et al., 2017). They include various antibiotics, such as lipopeptides (surfactin, iturin, and fengycin), polyketides (macrolactin, bacillaene, and difficidin), and aminoglycosides (butirosin), which can alter cell membrane structures and inhibit the growth of pathogenic fungi and bacteria (Harwood et al., 2018; Heifetz et al.,

1972). In addition, lipopeptides produced by *Bacillus* can induce systemic resistance in plants, leading to the production of defense-related proteins such as peroxidase, lipoxygenase, chitinase, and β-1,3-glucanase, which enhance the plant's resistance to pathogens (Lin et al., 2019; Ongena et al., 2007; Tunsagool et al., 2019). Furthermore, *Bacillus* spp. can trigger the activation of enzymatic antioxidants crucial for plant defense, like phenylalanine ammonia-lyase and polyphenol oxidase (Wang et al., 2021). The chitinase and glucanase produced by *Bacillus* can degrade the fungal cell wall, directly inhibiting the growth of fungal hyphae (Tanaka & Watanabe, 1995).

Given the detrimental effects of *F. verticillioides* and its secondary metabolites, finding an eco-friendly method for disease management is crucial. In our investigation of maize ear and stalk rot in Yunnan Province, it was observed that a healthy maize plant was in the vicinity of others with severely diseased symptoms. This unique observation prompted our study with the following objectives: (i) to isolate and identify the potential antifungal strains from the rhizosphere of the healthy maize plant; (ii) to evaluate the biocontrol effects against *Fusarium* ear and stalk rot as well as other fungal disease; (iii) to assess its growth-promoting activity in crop plants; (iv) to explore the mechanisms of its biocontrol and growth-promoting activities through genome mining and comparative genome analysis. By examining this strain's efficacy as a biocontrol agent and gaining insights into the genetic basis of its beneficial properties, this study aims to discover an effective biocontrol agent that can both enhance plant growth and manage fungal diseases in crops, contributing to sustainable agricultural practices.

2. Materials and methods

2.1. Strains

B. velezensis IFST-221 was isolated from the rhizosphere soil collected from maize in an area affected by *Fusarium* ear and stalk rot in Yunnan Province, China. Using a serial dilution method, 5 g of soil was mixed with 50 mL of 0.9% NaCl solution and shaken at 30 °C for 30 minutes. A stepwise dilution (10^{-1}, 10^{-2}, 10^{-3}, 10^{-4}, 10^{-5}, 10^{-6}, and 10^{-7}) was carried out (Fang, 1998). For each dilution, 100 μL of solution was spread on Luria-Bertani (LB) medium and incubated at 30 °C for two days. After incubation, colonies were isolated, and a pure colony was obtained through streak plate preparation. To assess the strain's antifungal activity, a plate confrontation assay was performed. A 6 mm plug of *F. verticillioides* agar was placed in the center of the PDA plate, and 5 μL of bacterial culture was carefully added on both sides of the fungal agar plug, approximately 2.5 cm away. A control plate without bacterial culture was also prepared. All plates were incubated at 25 °C until the control plates exhibited full growth. The inhibition rate was calculated as inhibition rate (%) = (D1 - D2) / D2 ×100%, where D1 represents the diameter (mm) of the fungal colony in the control, and D2 represents the diameter (mm) of the fungal colony in the test plate. The experiment was conducted in triplicate and repeated three times. *B. velezensis* IFST-221's antimicrobial spectrum was evaluated against seven additional phytopathogens: *F. proliferatum*, *F. graminearum*, *F. oxysporum*, *F. solani*, *Botrytis cinerea*,

Phytophthora nicotianae, and *Verticillium dahliae. Fusarium* strains used in this study were preserved in our laboratory and identified by morphological features and translation elongation factor 1α sequence, while non-*Fusarium* strains were also maintained in our laboratory and were identified based on the partial sequences of the internal transcribed spacer region gene.

2.2. Identification of IFST-221

For identification, strain IFST-221 was subjected to morphological, biochemical, and molecular analysis. Colony morphology (color, shape, and surface) was observed on an LB plate. Cell morphology was examined by scanning electron microscope (S-570, Hitachi, Japan). Biochemical analysis followed protocols outlined in "Bergey's Manual of Systematic Bacteriology" (Madigan & Imhoff, 2001), evaluating growth at various NaCl concentrations (2%, 5%, 7%, and 10%), pH tolerance at 5.7 and 6.8, temperature tolerance at 15 °C, 25 °C, 30 °C, 37 °C, and 40 °C. Catalase activity was assessed, and utilization of various carbon sources (glucose, arabinose, xylose, mannitol, and starch) was examined. Citrate utilization, casein hydrolysis, the methyl red (MR) test, and the Voges-Proskauer (VP) test were conducted to determine the strain's biochemical profile (Madigan & Imhoff, 2001). Additionally, the O-nitrophenyl-β-D-galactopyranoside (ONPG) test for identifying *B. velezensis* CR502^T was performed as described by Ruiz-García et al. (2005).

For molecular identification, the genomic DNA of IFST-221 was extracted using the TIANamp Bacteria DNA Kit (TIANGEN Biotech Co., Ltd., Beijing, China). The partial 16S rRNA gene was amplified using the primers 27F and 1492R (Cheng et al., 2020), while the DNA gyrase subunit B (*gyrB*) gene was amplified using the primers UP1 and UP2R (Yamamoto & Harayama, 1995) (Table 4-1). The PCR reaction, in a 50 μL final volume, contained 25 μL Premix Taq (Takara Biomedical Technology Co., Ltd., Beijing, China), 1 μL forward primer and 1 μL reverse primer, 1 μL bacterial culture, and 22 μL ddH_2O under 35 cycles of 94 °C for 10 sec, annealing at 55 °C for 30 sec, and 72 °C for 2 min. After amplification, products were separated using 1% agarose gel electrophoresis and purified with HiPure Gel Pure DNA Mini Kit (Magen Biotech, Guangzhou, China). Purified PCR products were then ligated into the pMD18-T vector (Takara Biomedical Technology Co., Ltd., Beijing, China) and transformed into *E. coli* TG-1. Positive transformants were selected and sequenced by Sangon Biotech (Shanghai) Co., Ltd. using Sanger sequencing. The resulting gene sequences of 16S rRNA and *gyrB* were aligned manually. Phylogenetic analysis of partial 16S rRNA and *gyrB* gene sequences was performed separately using MEGA X. The neighbor-joining method was employed to construct the phylogenetic trees. Evolutionary distances were calculated with the Kimura two-parameter model, and a bootstrap analysis with 1000 replications was used to estimate the robustness of tree branches.

2.3. In vivo anti-F. verticillioides assay of IFST-221

To assess the inhibitory effect of IFST-221 on *F. verticillioides* in maize, *in vivo* assays were conducted using maize ears and kernels (Jannat et al., 2024). For the maize ears assay, the front husks of maize ears were carefully removed, and the ears

were sprayed with 2 mL IFST-221 culture at a concentration of 1 × 10^9 cfu/mL. A control group was treated with the same volume of distilled water. Three days later, the maize ears were inoculated with either 10 μL of *F. verticillioides* conidial suspension with a concentration of 1×10^6 conidia/mL or ddH_2O for the control. Following the inoculation, the maize ears were re-covered with the removed husks, placed in a box with wet paper towels at the bottom to maintain humidity, wrapped with plastic wrap, and incubated in the dark at 25 °C for five days. The experiment was performed in triplicate and repeated three times.

To evaluate the antifungal activity of IFST-221 against *F. verticillioides* in maize kernels, sterilized maize kernels were prepared following the previously described method (Liang et al., 2022). Briefly, IFST-221 was grown overnight in LB broth at 37 °C and 180 rpm. Cells were harvested by centrifugation (5,000 × g, 10 min), washed twice with sterile 0.9% NaCl, and resuspended in sterile 0.9% NaCl to a final concentration of 1 × 10^9 cfu/mL. After one hour, the immersed maize kernels were inoculated with either 10 μL of *F. verticillioides* conidial suspension or ddH_2O. Each treatment was conducted five times and repeated in triplicate. The kernels were then incubated for five days, and symptoms of infection were observed and photographed.

To measure the relative fungal biomass in maize kernels, quantitative PCR (qPCR) was conducted following the previous study (F. Zhang et al., 2023). The *β-tubulin* gene from *F. verticillioides* (*Fv_β-tubulin*) and the *gyrB* gene from *B. velezensis* (*Bv_gyrB*) were used to quantify fungal and bacterial colonization, respectively. The translation elongation factor 1α gene of maize (*Zm_TEF-1α*) served as an endogenous plant control. The qPCR was conducted using SYBR Green (NovoStart® SYBR qPCR SuperMix Plus, Suzhou, China) on a Quant Studio™ 6 Flex System Cycler (Applied Biosystems, Waltham, MA, USA). The experiment was performed in triplicate to ensure the robustness and accuracy of the data. The specific primer sequences used for the qPCR analysis are listed in Supplementary Table 4-1.

Table 4-1 Primers used in this study

Name	Sequences (5'-3')	Purpose
27F	AGAGTTTGATCCTGGCTCAG	Partial 16S rDNA gene amplification
1492R	TACGGCTACCTTGTTACGACTT	
UP1	GAAGTCATCATGACCGTTCTGCA YGCNGGNGGNAARTTYGA	Partial *gyrB* gene amplification
UP2R	AGCAGGGTACGGATGTGCGAGCC RTCNACRTCNGCRTCNGTCA	
*Zm_TEF-1α*_F	TGGGCCTACTGGTCTTACTACTGA	Relative biomass (endogenous control of plants)
*Zm_TEF-1α*_R	ACATACCCACGCTTCAGATCCT	
*Fv_β-tubulin*_F	CCCCGAGGACTTACGATGTC	Relative biomass (fungi)
*Fv_β-tubulin*_R	CGCTTGAAGAGCTCCTGGAT	
*Bv_gyrB*_F	CGTACGGTTCACAGGGACAG	Relative biomass (bacteria)
*Bv_gyrB*_R	ACACGGCCTTGGATCGTATG	

Note: R = A/G, Y = C/T, N = A/G/C/T

The content of FB_1 in maize kernels was quantified by SAX solid-phase extraction and high-performance liquid chromatography coupled with mass spectrometry (HPLC-MS) with slight modifications (Ding et al., 2024). Briefly, crude fumonisin was extracted by homogenizing 5 g of ground maize kernels in 20 mL of acetonitrile/water (50:50, v/v) for 30 min, followed by centrifugation at 4000 rpm for 5 min. The supernatant (3 mL) was mixed with 8 mL methanol/water solution (60:20, v/v) and passed through a SAX solid-phase extraction column (SAX-06-500mg, Bioland, China). Subsequently, the column was rinsed with 8 mL of methanol/water solution, 3 mL of methanol, and 10 mL of methanol/acetic acid solution (99:1, v/v). The elution buffer was collected, evaporated, and dissolved in 1 mL of acetonitrile/water (20:80, v/v). After filtering through a 0.22 μm membrane, the samples were subjected to HPLC-MS/MS analysis. For HPLC-MS/MS analysis, 2 μL of the processed sample was injected into a Waters 2695 separation module (Waters Corporation, Milford, MA, USA) equipped with an EC-C18 reverse-phase column (100 mm × 2.1 mm, 1.7 μm). The mobile phase consisted of 0.1 % formic acid in water (solvent A) and acetonitrile (solvent B, 50:50, v/v) with a flow rate of 0.3 mL/min. The column was maintained at 35 °C during the analysis. FB_1 in the samples was identified and quantified by comparing retention times with FB_1 standards (Sigma-Aldrich Co., St Louis, MO).

2.4. The biocontrol activity of IFST-221 against Verticillium wilt of cotton

To evaluate the effectiveness of IFST-221 in combating *Verticillium* wilt in cotton, an experiment using a root-dipping method (Zhang et al., 2020). Cotton plants, aged three weeks, were divided into two groups. One group of 28 plants was treated with a 40 mL culture of IFST-221 at a concentration of 1×10^9 cfu/mL, and the other group of 28 plants was treated with an equal volume of ddH_2O. After three days, both groups of 14 cotton plants were inoculated with a 20 mL suspension of *V. dahliae* conidia containing 5×10^6 conidia/mL, effectively introducing the pathogen into the plant roots. The other 14 cotton plants of both groups were inoculated with 20 mL ddH_2O. The experiment was repeated three times, and the severity of *Verticillium* wilt was evaluated based on disease incidence (DI) and disease severity index (DSI) (Zhu et al., 2013). Negative controls (cotton plants inoculated with ddH_2O only) and pathogen-only controls were included in each trial, and all treatments were conducted in parallel under identical conditions to ensure reliability and reproducibility of the results.

2.5. Plant growth-promoting assays

2.5.1. Greenhouse pot experiments

Seeds of maize, cotton, tomato, and broccoli were purchased from a local market and used without surface sterilization. Pots (9 × 9 cm; four pots per species) were filled with a non-sterile substrate consisting of Jiffy black peat (0-10 mm; Jiffy®, Netherlands), commercial horticultural nutrient soil, and vermiculite mixed at a 1:1:1 (v/v/v) ratio. Five seeds were sown per pot. Strain IFST-221 was cultured in LB broth

at 37 °C to late-log phase and adjusted to 1×10^9 cfu/mL. At the two-leaf stage, 40 mL per pot of the IFST-221 suspension was applied by soil drench (treatment). Control pots received 40 mL per pot of nutrient solution containing the commercial fertilizer Huabao No. 2 (HYPONeX, USA), a balanced NPK formulation (20-20-20; 20% N, 20% P_2O_5, 20% K_2O), at the manufacturer's recommended concentration. Plants were grown in a greenhouse under controlled conditions (25 ± 2 °C, 16 h light/8 h dark photoperiod, and 60-70% relative humidity); all pots received the same watering schedule.

At harvest (30 dpi), plants were gently removed from the substrate and rinsed under running tap water, followed by sterile distilled water to remove adhering particles. Excess surface moisture was removed with paper towels. Plant height (from the root-shoot junction to the apex) and primary root length (from the root-shoot junction to the tip) were recorded immediately using a stainless-steel ruler with 1 mm resolution. The roots and shoots were separated and weighed within 30 min of harvest on an analytical balance (readability 0.01 g). And for dry weight, tissues were first treated at 110 °C for 15 min to inactivate enzymes and then oven-dried at 60 °C to constant weight.

2.5.2. Growth on nutrient-deficient cultures

In vitro studies were designed to evaluate the nitrogen-fixing, phosphorus- and potassium-solubilizing ability of IFST-221. A single colony of IFST-221 was cultured individually in a nitrogen-free medium to evaluate the nitrogen-fixing ability. Phosphorus solubilizing capacity was tested using the National Botanical Research Institute's phosphate growth medium (NBRIP), where the insoluble phosphorus source was $Ca_3(PO_4)_2$. Potassium solubilization was assessed with potassium feldspar powder as the insoluble potassium source in a potassium bacteria medium. These cultures were maintained at 30 °C for approximately 3-7 days, as described in previous studies (Chen et al., 2011; Ma et al., 2013; Nautiyal, 1999). The culture medium without inoculation served as a control.

2.5.3. Biofilm formation assay

Biofilm formation of strain IFST-221 was evaluated on LBGM agar medium (LB supplemented with 1% glycerol and 100 μM $MnSO_4$). An overnight LB culture was adjusted to an OD_{600} of 0.5, and 2 μL of this suspension was spotted onto LBGM agar plates. Plates were incubated at 30 °C for 36 h, and colony surface morphology was visually assessed (D. C. Wang et al., 2019). Representative images were captured with a Canon EOS 80D camera.

2.5.4. IAA production

For assessing indole-3-acetic acid production, the Salkowski reaction was used with slight modifications (Fierro-Coronado et al., 2014). Briefly, a single colony of IFST-221 was cultured in LB medium supplemented with 100 mg/L L-tryptophan and incubated at 37 °C for two days. After centrifugation, 2 mL of the supernatant was mixed with an equal volume of Salkowski reagent and kept in the dark for 30 min. The absorbance of the resulting solution was measured at 530 nm using a spectrophotometer. The concentration of IAA production was estimated by comparing

the absorbance with an IAA standard curve. The experiment was conducted in triplicate and repeated three times to ensure the reliability of the results.

2.6. Genomic sequencing, annotation, and prediction of secondary metabolites

The genome of IFST-221 was sequenced using single-molecule real-time (SMRT) technology. This sequencing work was conducted by Beijing Novogene Bioinformatics Technology Co., Ltd (Beijing, China).To maintain data integrity, low-quality reads were filtered using SMRT Link v5.0.1, resulting in high-quality contigs. The assembly produced a single continuous contig without any gaps, indicating a high-quality genome assembly. For comparative analysis, the genomic sequences of related strains, including *B. velezensis* SQR9 (NZ_CP006890.1), *B. velezensis* FZB42^T (NC_009725.2), *B. amyloliquefaciens* DSM7^T (NC_014551.1), and *B. subtilis* 168^T (NC_000964.3), were downloaded from the NCBI website. These sequences were used as references to compare and analyze the genomic features and characteristics of IFST-221.

Various software tools were employed to perform comparative analyses and gene annotation. The BLAST Ring Image Generator (BRIG) 0.95 software was used to visualize genomic comparisons among the five *Bacillus* strains (Alikhan et al., 2011), while collinearity analysis was performed using TBtools-II (Chen et al., 2023). Whole-genome orthologous gene comparisons were done using OrthoVenn 2 (Xu et al., 2019). The coding sequences (CDS) of *B. velezensis* IFST-221, SQR9, and FZB42^T, *B. amyloliquefaciens* DSM7^T, and *B. subtilis* 168^T were used for this analysis. The related coding genes of IFST-221 were analyzed by BLAST search with specific parameters (E-value less than 1e-5, minimal alignment length percentage larger than 40%). After comparative analysis, the singletons in IFST-221 were annotated using eggNOG-mapper (Cantalapiedra et al., 2021). Gene annotation and function prediction were performed using a combination of GeneMarkS, Gene Ontology (GO), Kyoto Encyclopedia of Genes and Genomes (KEGG), and Clusters of Orthologous Groups (COG) databases.

To identify secondary metabolite biosynthetic gene clusters (BGCs), the genome sequence of IFST-221 was analyzed using antiSMASH version 6.0 (Blin et al., 2021). To ensure the reliability of BGC prediction, each antiSMASH-identified cluster was subsequently subjected to manual curation. This process included gene-by-gene inspection of cluster boundaries, identification of core biosynthetic genes, verification of conserved enzymatic domains (e.g., NRPS and PKS modules), and comparison with well-characterized reference clusters from *B. velezensis* FZB42. Only clusters containing complete core biosynthetic machinery and conserved functional domains were considered intact and potentially functional. Detailed gene-by-gene annotations of all predicted BGCs are provided in the supplementary materials.

2.7. Statistical analysis and data availability

All experiments were conducted with at least three independent biological replicates. For pot experiments, five plants per pot were measured, and the mean value

per pot was used as the experimental unit (n = 4 pots per treatment). Data are presented as mean ± standard error.

For pairwise comparisons between treatment and control groups (e.g., *in vitro* inhibition assays on agar plates, plant growth parameters, qPCR-based biomass quantification, and toxin production), significance was assessed using Student's t-test in Microsoft Excel, with a threshold of $p < 0.05$.

The genomic sequence of IFST-221 is available at the NCBI website with accession No. CP125283.1.

3. Results

3.1. Isolation of an antifungal strain IFST-221

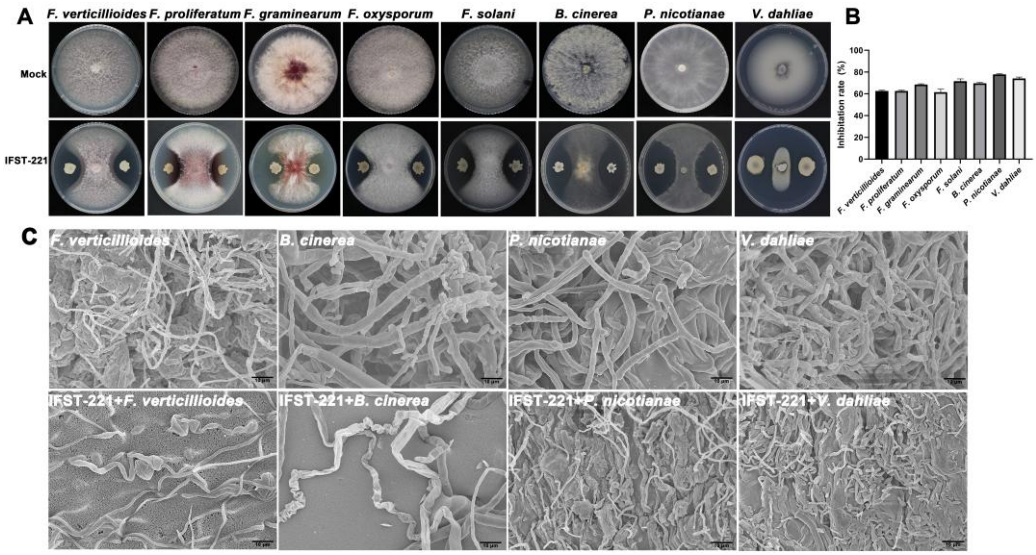

Figure 4-1 Antagonistic activity of strain IFST-221 against eight different phytopathogens. (A) The antagonistic spectrum of strain IFST-221 *in vitro*. *Fusarium verticillioides*, *F. proliferatum*, *F. graminearum*, *F. solani*, *Botrytis cinerea*, *Phytophthora nicotianae*, and *Verticillium dahliae* were used to test the antimicrobial activity. (B) Inhibition rates of strain IFST-221 against eight phytopathogens. Error bars represent standard errors. (C) Scanning electron microscopy images showing the morphological changes of *F. verticillioides*, *B. cinerea*, *P. nicotianae*, and *V. dahliae* after co-incubation with IFST-221. Scale bar, 10 μm.

To explore potential sources of disease resistance in maize, soil suspension from healthy maize rhizosphere in Yunnan Province was shaken at 30 °C for 20 min. Following a stepwise dilution method, a total of 156 strains were isolated. These strains were tested for their antifungal activity against *F. verticillioides* to identify potential disease resistance. IFST-221 exhibited the highest antifungal potential, inhibiting 62.63% of *F. verticillioides*. To further assess the broad-spectrum antimicrobial activity of IFST-221, additional tests were conducted using various

phytopathogens, including *F. proliferatum*, *F. graminearum*, *F. oxysporum*, *F. solani*, *B. cinerea*, *P. nicotianae*, and *V. dahliae*. The results revealed that IFST-221 exhibited robust antagonistic effects against all the tested pathogens, with relatively broad-spectrum activity against both ascomycetes and oomycetes, as shown in Figure 4-1A. Inhibition rates of up to 77.88% were observed against *P. nicotianae*, and up to 60% against other tested pathogens (Figure 4-1B).

Scanning electron microscopy was employed to examine the ultrastructural effect of IFST-221 on fungal hyphae, focusing on strains such as *F. verticillioides*, *B. cinerea*, *P. nicotianae*, and *V. dahliae*. SEM images of untreated *F. verticillioides* hyphae displayed smooth surfaces and intact hyphae. However, when treated with IFST-221, the hyphae exhibited notable morphological changes, appearing folded, twisted, and partially distended (Figure 4-1C). Similarly, irregular hyphae structures were observed in IFST-221-treated other pathogens (Figure 4-1C). These findings suggest that treatment with IFST-221 induces morphological alterations in the hyphae of the tested pathogens.

3.2. IFST-221 is a strain of B. velezensis

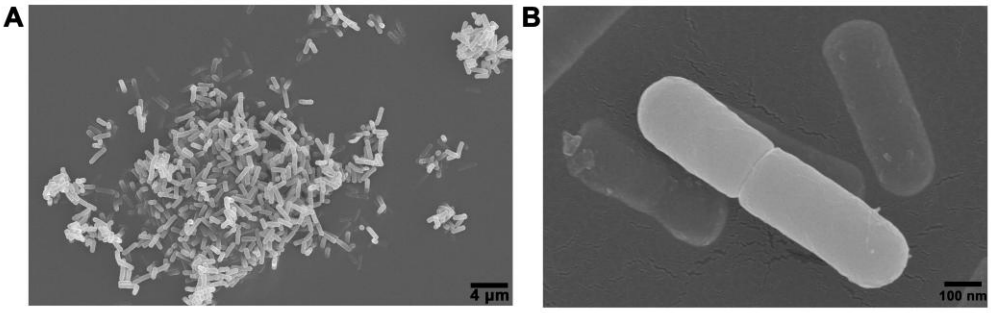

Figure 4-2 Scanning electron microscopy of the morphology of IFST-221 after incubation in LB broth at 37 °C for 12 hours.
(A) Scale bar, 4 µm (B) Scale bar, 100 nm.

Table 4-2 Physiological and biochemical results of strain IFST-221.

Tests	IFST-221	Tests	IFST-221
Gram stain	+	Dextrose	+
Growing at pH 5.7	+	L-Arabinose	+
Growing at pH 6.8	+	D-xylose	+
Growing at 15 °C	+	Mannitol	+
Growing at 40 °C	+	Starch	+
Growing in 10 % NaCl	-	Methyl red (MR) test	+
Growing in 7 % NaCl	+	Voges-Proskauer (VP) tests	+
Growing in 5 % NaCl	+	Casein hydrolysis	+
Growing in 2 % NaCl	+	Citrate utilization test	+
ONPG production test	+		

"+" represents "Positive" and "-" represents "Negative".

To determine the taxonomic classification of IFST-221, its morphology was initially examined. When cultured on the LB solid medium, a single colony of IFST-221 displayed characteristics such as being round, opaque, milky white to yellow, and possessing folded edges. Gram staining revealed that IFST-221 was a gram-positive bacterium, indicated by the purple color from crystal violet dye. SEM revealed that IFST-221 is a rod-shaped bacterium with a width ranging from 0.2-0.25 μm and a length ranging from 0.6-1.2 μm (Figure 4-2). To gain further insights into the physiological and biochemical characteristics of IFST-221, tests outlined in "Bergey's Manual of Systematic Bacteriology" were conducted. IFST-221 exhibited positive results in various tests, including catalase activity, carbon source utilization based on dextrose, arabinose, xylose, mannitol, and starch, citrate utilization, casein hydrolysis, MR test, and VP test. Moreover, IFST-221 demonstrated the ability to thrive under a range of growth conditions, including tolerating NaCl concentrations between 2% to 7%, pH levels ranging from 5.7 to 6.8, and temperatures within the range of 15 to 40 °C (Table 4-2). These findings collectively indicate that the IFST-221 belongs to the *Bacillus* group.

To ensure precise identification of the *Bacillus* strain IFST-221, a molecular phylogeny analysis was conducted. This method could overcome the limitations inherent in relying solely on morphological and physiological characteristics. The analysis focused on key genetic markers, particularly the 16S rRNA gene, a well-established marker for determining bacterial phylogenetic relationships. Comparing the 16S rDNA gene sequence of IFST-221, which had a length of 1,512 bp, to sequences from known *Bacillus* species revealed that IFST-221 shared up to 99% identity with the aligned type strains of different *Bacillus* species, including *B. subtilis* subsp. *spizizenii*, *B. rugosus*, *B. tequilensis*, *B. cabrialesii*, *B. inaquosorum*, *B. vallismortis*, *B. amyloliquefaciens*, *B. nematocida*, *B. velezensis*, and so on (Figure 4-3). This high degree of sequence similarity suggested a close relationship between IFST-221 and these *Bacillus* species. The phylogenetic analysis further confirmed a close relationship between IFST-221 and *B. velezensis* strains NRRL B-41580^T and BCRC 17467^T, but not CR-502^T (Figure 4-3). This outcome, however, highlighted the potential limitation of using the 16S rDNA marker for accurately differentiating between closely related *Bacillus* species. Another phylogenetic marker, the *gyrB* gene, which encodes the subunit B protein of DNA gyrase, was examined to provide additional clarity. The BLASTn analysis of *gyrB* sequences obtained from IFST-221 revealed a high level of identity, 98.87% with the type strain *B. velezensis* BCRC 17467^T. This strong similarity was further supported by the phylogenetic analysis, which showed that IFST-221 and *B. velezensis* BCRC 17467^T clustered together on the same branch (Figure 4-4). Furthermore, the ONPG production test was conducted to distinguish *B. amyloliquefaciens* and *B. velezensis*. IFST-221 exhibited ONPG production like that of *B. velezensis* CR-502^T (Table 4-2). The combined results from the 16S rRNA and *gyrB* genes, as well as the ONPG production test, confirmed that

IFST-221 is a strain of *B. velezensis*, providing a robust and multifaceted approach to the identification and classification of this strain.

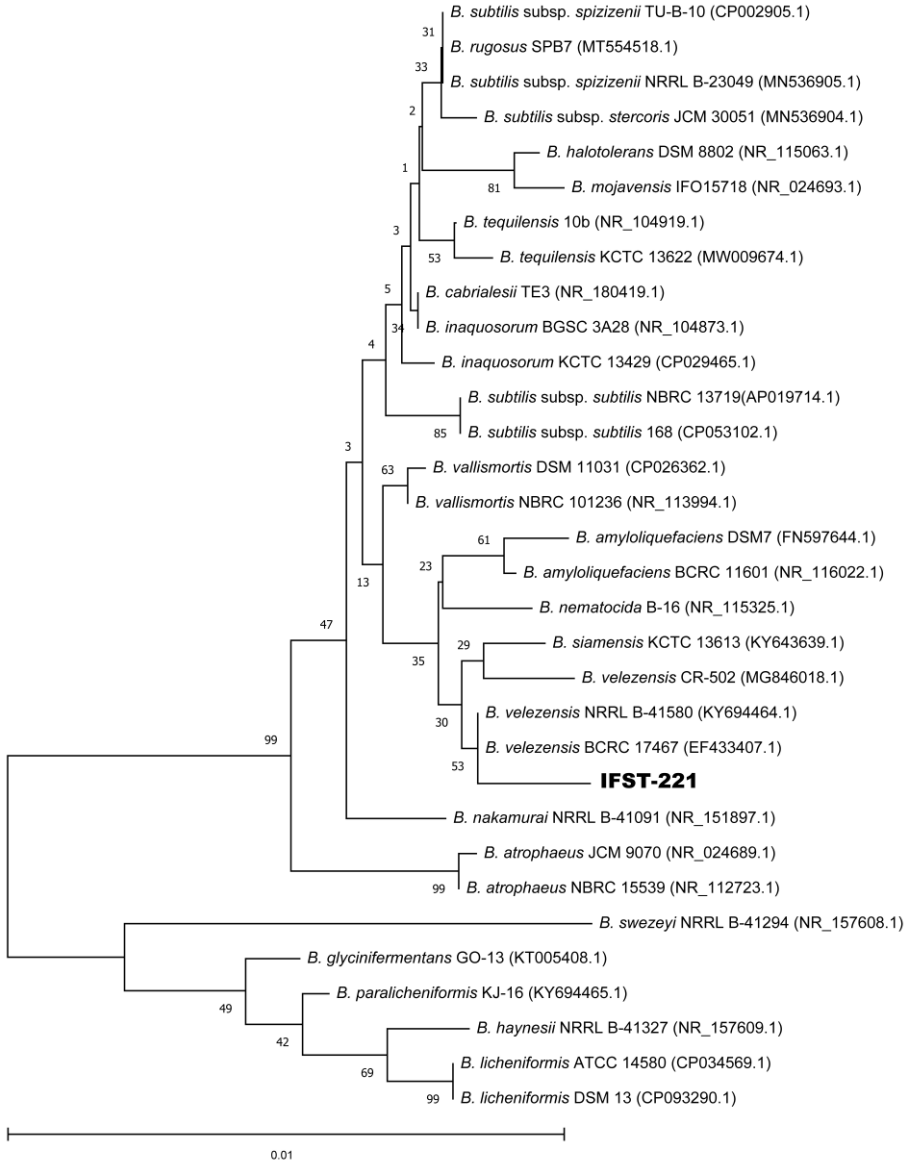

Figure 4-3 A neighbor-joining phylogenetic tree was constructed using the 16S rDNA gene sequence of IFST-221 and other closely related *Bacillus* species.
The significance of each branch is indicated by a bootstrap value (%) calculated for 1000 subsets. Genbank accession numbers are given in parentheses. Bar, 0.01 substitutions per nucleotide position.

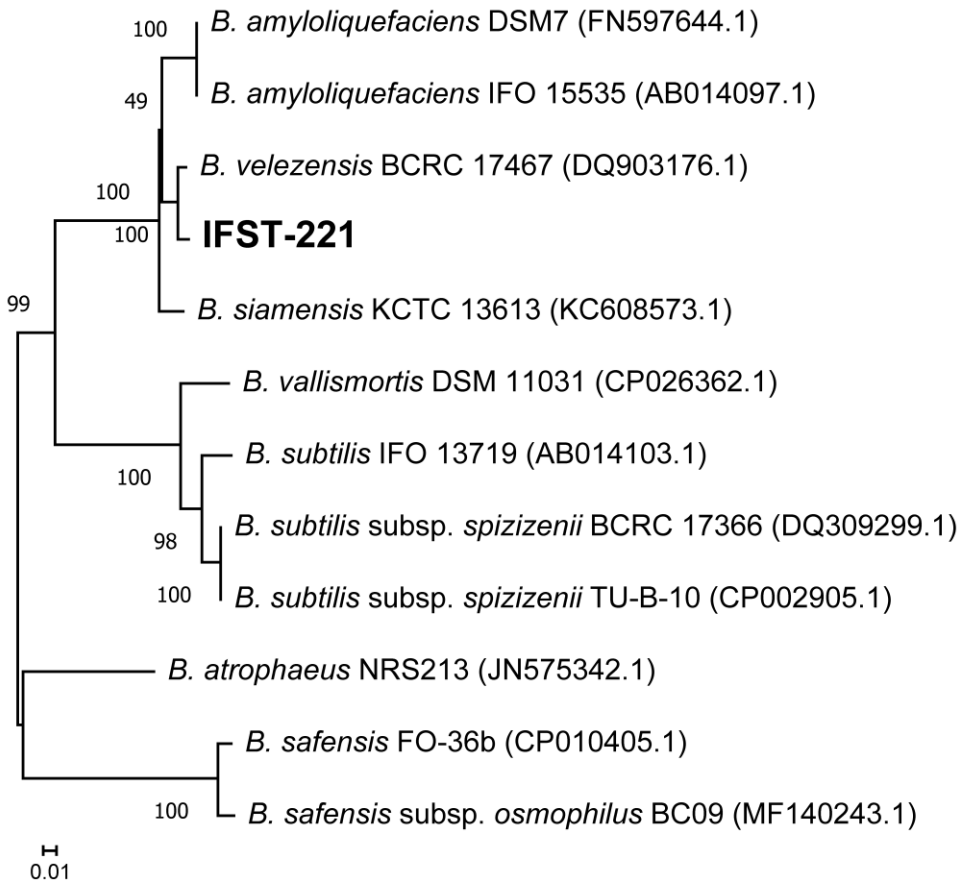

Figure **4-4** A phylogenetic tree of IFST-221 constructed using the nucleotide sequences of *gyrB* based on the neighbor-joining method.
The significance of each branch is indicated by a bootstrap value (%) calculated for 1000 subsets. Genbank accession numbers are given in parentheses. Bar represents 0.01 substitutions per nucleotide position.

3.3. B. velezensis IFST-221 is a putative biological control agent for plant disease

To evaluate the effectiveness of *B. velezensis* IFST-221 as a biological control agent, *in vivo* anti-phytopathogenic activity against *F. verticillioides* in maize ears and kernels. Maize ears and kernels were pre-sprayed with IFST-221 and ddH_2O before inoculating with *F. verticillioides*. The results showed a significant reduction in *F. verticillioides* infection in maize ears pre-sprayed with IFST-221 compared to those pre-sprayed with ddH_2O (Figure 4-5A). Similarly, when maize kernels were pre-immersed in ddH_2O and then inoculated with *F. verticillioides*, which exhibited visible hyphae formation, the kernels that were pre-immersed with IFST-221 and then inoculated with *F. verticillioides* did not show any visible fungal hyphae (Figure 4-5B). The qPCR analysis supported these observations, indicating a considerable

reduction in the biomass of *F. verticillioides* in kernels treated with IFST-221 compared to ddH_2O (Figure 4-5C). Moreover, the treatment of maize kernels with IFST-221 resulted in a significant reduction in the production of FB_1, a mycotoxin produced by *F. verticillioides*, with levels dropping from 5700.33 parts per billion (ppb) per gram of maize kernels in the control group to 19.63 ppb in the IFST-221-treated group (Figure 4-5D).

Similarly, IFST-221 demonstrated potential as a biocontrol agent against cotton Verticillium wilt (Figure 4-5E and F). At 30 days post inoculation of *V. dahliae*, cotton plants that were pre-treated with IFST-221 showed a significantly lower DSI (8.93%) compared to cotton plants without the pretreatment of IFST-221 (73.21%) (Figure 4-5F). The disease incidence of cotton plants inoculated with *V. dahliae* and treated with IFST-221 was 14.29%, whereas the DI of plants without treatment was 85.71% (Figure 4-5F). Furthermore, it is worth noting that cotton plants treated with IFST-221 exhibit better growth compared to those treated with ddH_2O (Figure 4-5E).

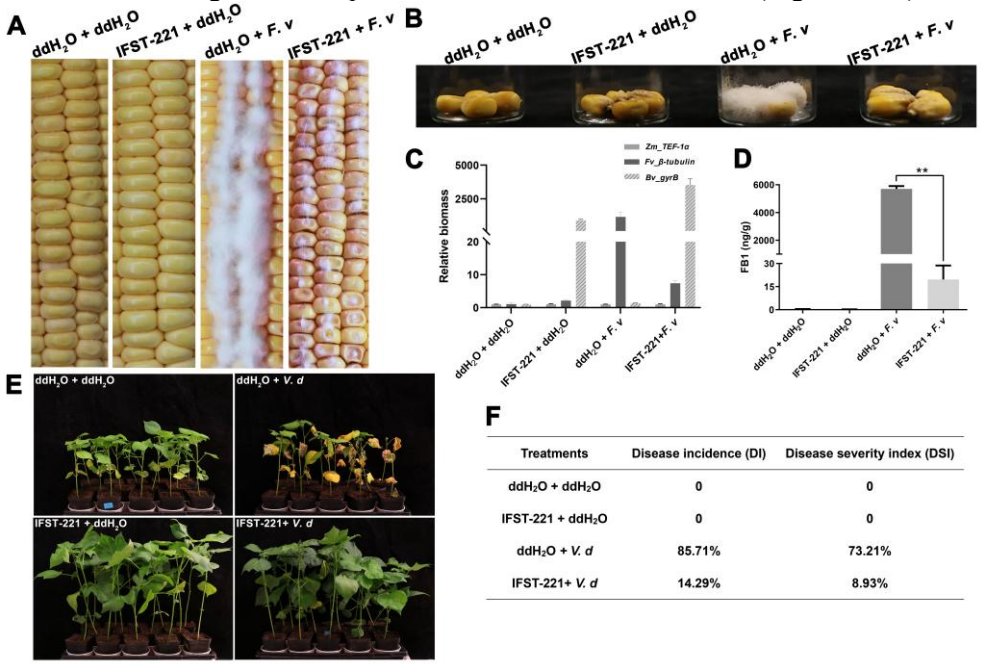

Treatments	Disease incidence (DI)	Disease severity index (DSI)
ddH_2O + ddH_2O	0	0
IFST-221 + ddH_2O	0	0
ddH_2O + *V. d*	85.71%	73.21%
IFST-221+ *V. d*	14.29%	8.93%

Figure 4-5 The inhibitory effects of IFST-221 against ear rot of maize and Verticillium wilt of cotton plants.

(A and B) Effect of IFST-221 on the development of *F. verticillioides* in maize ears and kernels, respectively. Maize ears and kernels pretreated with ddH_2O or IFST-221 were then inoculated with *F. verticillioides* or ddH_2O. Representative photos were captured at 5 days post-inoculation. (C) qPCR analysis of the fungal and bacterial biomass on maize kernels. Error bars represented standard errors. (D) HPLC-MS analysis of the level of FB_1 in maize kernels under different treatments. Double asterisks (**) indicate $p < 0.01$ determined by Student's *t*-test. (E) Assessment of the efficacy of IFST-221 in controlling Verticillium wilt of cotton plants. (F) The DI and DSI of Verticillium wilt under different treatments.

3.4. B. velezensis IFST-221 promotes plant seedlings' growth

To evaluate the potential of IFST-221 in promoting plant growth, experiments were conducted on maize, cotton, tomato, and broccoli seedlings with treatment and control groups. The treatment group was inoculated with IFST-221, while a commercial fertilizer served as the control. Plant growth was monitored over 30 days. The inoculation of IFST-221 resulted in an enhanced growth of the tested plants, as depicted in Figure 4-6A. After 30 days post-inoculation, plant height was significantly increased in maize and cotton. For maize, the average height was 11.57 ± 1.72 cm, compared to the control height of 10.17 ± 1.13 cm. Similarly, the height of treated cotton increased to 13.67 ± 1.67 cm, whereas the control group measured 11.30 ± 1.90 cm (Figure 4-6B).

More importantly, biomass accumulation was promoted by IFST-221, as reflected in increased dry weight of the aboveground part of broccoli (0.37 ± 0.13 g vs. 0.19 ± 0.13 g, $p < 0.05$). In addition, supportive measurements showed that the fresh weight for aboveground tissues also tended to increase across maize, cotton, tomato, and broccoli (Figure 4-6B). Although treatment with IFST-221 didn't significantly affect the underground parts of maize, tomato, and broccoli seedlings, cotton seedlings displayed a clear response, showing a 1.5-fold increase in root length and a 0.5-fold increase in fresh weight of the underground part compared with the control (Figure 4-6B).

These findings suggest that IFST-221 contributes to enhanced plant biomass, while the fresh weight data provide supportive evidence. Additionally, IFST-221 showed versatility by thriving in various nutrient-deficient cultures, suggesting its adaptability to different environmental conditions. This was observed in nitrogen-free cultures, NBRIP, and potassium bacteria medium, demonstrating that IFST-221 could grow in nutrient-limited environments (Figure 4-6C). Moreover, crystal violet staining of IFST-221 grown on LBGM medium revealed the formation of a wrinkled structure, a common phenotype observed in mature biofilms produced by various bacteria (Figure 4-6D). Additionally, when IFST-221 was cultured for 12 hours, it produced 5.59 mg/L of IAA as determined by the Salkowski reagent method.

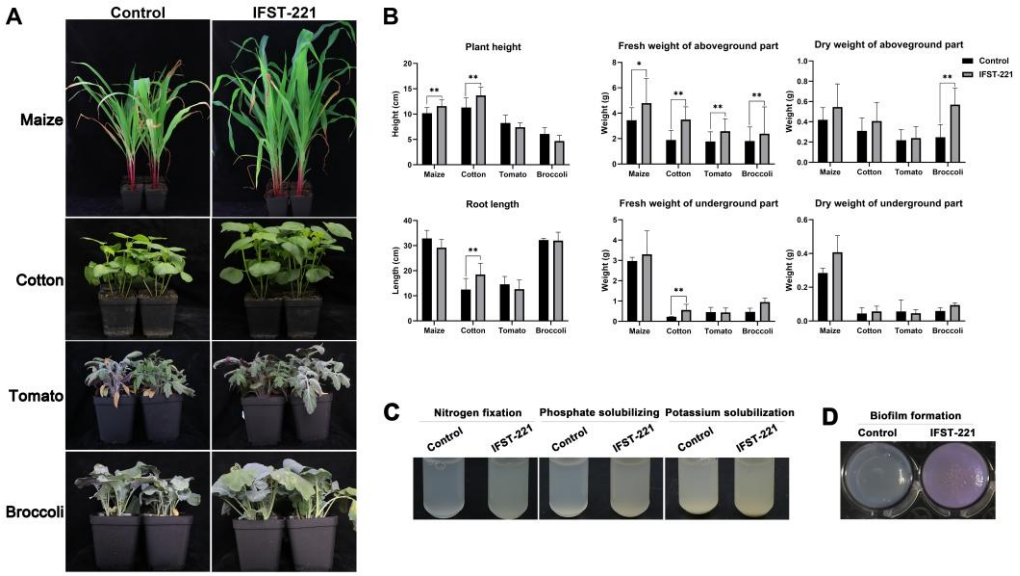

Figure 4-6 The plant growth-promoting activity of IFST-221.
(A) Effect of IFST-221 on the growth of maize, cotton, tomato, and broccoli seedlings. Photos were captured at 30 dpi. Seedlings exposed to the Fertilizer "HUABAO No. 2" were used as controls. (B) Measurements of plant height, fresh and dry weight of the aboveground, root length, and fresh and dry weight of the underground part of maize, cotton, tomato, and broccoli seedlings treated with IFST-221 or HUABAO Fertilizer "HUABAO No. 2" at 30 dpi. Error bars indicate standard errors. A single asterisk (*) indicates a significant difference of $p < 0.05$. Double asterisks (**) indicate a highly significant difference of $p < 0.01$. (C) Ability of IFST-221 to fix nitrogen and to solubilize phosphate and potassium *in vitro*. The IFST-221 was cultivated under different cultures, with ddH_2O serving as the control. (D) Biofilm formation of IFST-221 stained with crystal violet.

3.5. Genomic feature of B. velezensis IFST-221 and comparative genomics analysis of B. velezensis IFST-221, SQR9, FZB42^T, B. amyloliquefaciens DSM7^T, and B. subtilis 168^T

The whole genome sequencing of IFST-221 yielded significant insights into the genomic features. Following the sequencing and quality assessment of the original reads, the assembled genome consisted of one contig with an N50 length of 3,874,945 base pairs (bp). The entire genome of IFST-221 comprised a circular chromosome with a length of 3,858,300 bp and a GC content of 46.71% (Figure 4-7A). Within this genome, a total of 3,973 genes were identified, accounting for approximately 90.06% of the total genome length with a combined gene length of 3,474,660 bp. Additionally, the genome analysis predicted the presence of 86 tRNA structures, nine rRNA operons (i.e., 5S, 16S, and 23S structures), and six sRNAs were also predicted in the genome of IFST-221 (Table 4-3). The genome sequencing data of IFST-221 have been

deposited in the National Center for Biotechnology Information under the GenBank BioProject number CP125283.1.

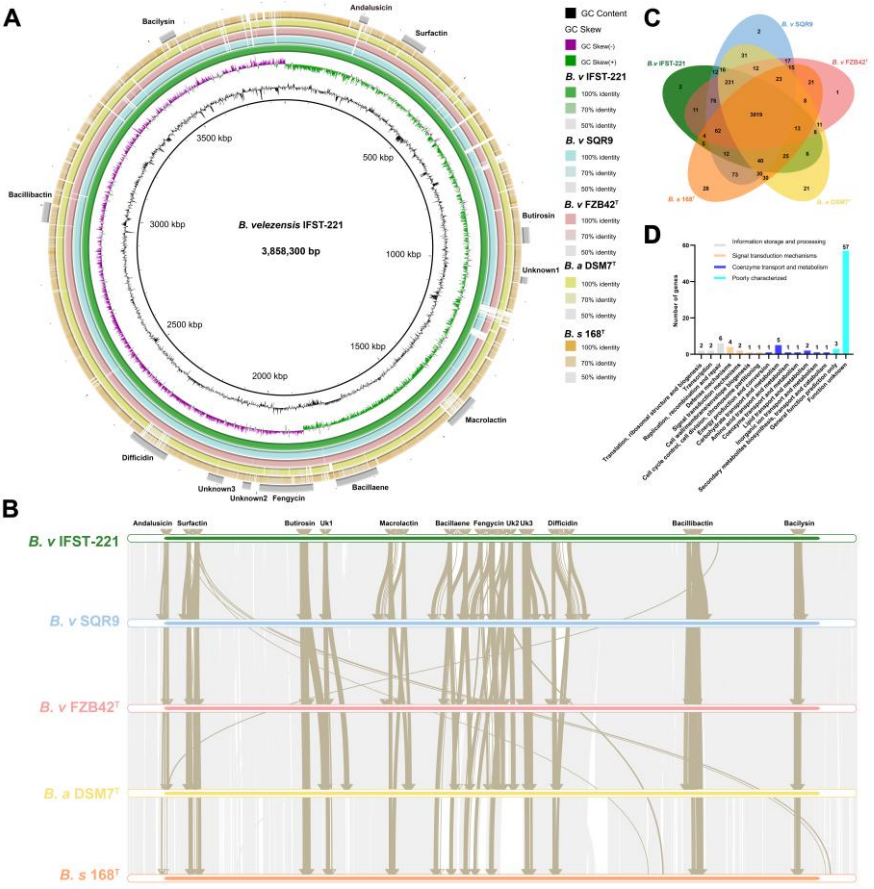

Figure 4-7 Comparative genomic analysis of *Bacillus velezensis* IFST-221 with *B. velezensis* SQR9 and FZB42^T, *B. amyloliquefaciens* DSM7^T, and *B. subtilis* 168^T.
(A) The comparative genomic circle map was constructed using BRIG v0.95. The features are as follows (from center to outside): circle 1 is genome size; circle 2 is GC Content; circle 3 is GC Skew; circles 4 to 8 are the comparative genomic maps of *B. velezensis* IFST-221, SQR9, FZB42^T, *B. amyloliquefaciens* DSM7^T, and *B. subtilis* 168^T, respectively; the outermost circle indicates the positions of gene clusters of predicted secondary metabolites. (B) Synteny analysis of five strains and the IFST-221 genome was used as the reference genome. Grey indicated a sequence with synteny, and the genes of secondary metabolites were shown in brown. (C) Venn diagram showing the number of unique, accessory, and core genes shared by *B. velezensis* IFST-221, SQR9, FZB42^T, *B. amyloliquefaciens* DSM7^T, and *B. subtilis* 168^T. The core and accessory genes are those located at the intersection of the five circles. The number of unique genes of each species is shown in each corresponding circle. Annotation was performed using OrthoVenn2. (D) Classification of annotated singleton (genes for which no orthologs could be found in other species) functions in the COG database for *B. velezensis* IFST-221.

Table 4-3 Genomic comparison between *B. velezensis* IFST-221, *B. velezensis* SQR9, *B. velezensis* FZB42^T, *B. amyloliquefaciens* DSM7^T, and *B. subtilis* 168^T

Features	*B. velezensis* IFST-221	*B. velezensis* SQR9	*B. velezensis* FZB42 ^{T}	*B. amyloliquefaciens* DSM7^T	*B. subtilis* 168^T
Genome size (bp)	3,858,300	4,117,023	3,918,600	3,980,200	4,215,606
GC content (mol%)	46.71	46.1	46.5	46.1	43.5
Protein-coding sequences	3,659	4,078	3,693	3,921	4,237
Average CDS size (bp)	875	916	933	888	895
Percent of coding region	90.06	89.0	88.0	87.0	87.2
Number of tRNAs	86	72	88	93	86
Ribosomal RNA operons	9	7	10	10	10

Note: The genomic information of IFST-221 was predicted by GeneMarkS software (http://topaz.gatech.edu/). And the genomic information of *B. velezensis* SQR9, *B. velezensis* FZB42^T, *B. amyloliquefaciens* DSM7^T, and *B. subtilis* 168^T were obtained from Chen et al. (2007) and Zhang et al. (2015).

To deeply understand the genetic characteristics of IFST-221, a comparison of gene features was made using the nucleotide sequence of well-studied and standard *Bacillus* strains, including *B. velezensis* SQR9, *B. velezensis* FZB42^T, *B. amyloliquefaciens* DSM7^T, and *B. subtilis* 168^T. Compared to other strains, IFST-221 exhibited a smaller genome size, lower GC content, fewer CDS, a smaller average CDS size, and a higher percentage of coding region (Table 4-3). Based on the Average Nucleotide Identity (ANI) value of these strains, it was confirmed that IFST-221 belongs to the *B. velezensis* strain because of the high ANI value between IFST-221 and *B. velezensis* SQR9 and FZB42^T (Figure 4-8). Also, a collinearity analysis was performed to examine the genomic similarities and variations among the five strains. The analysis revealed a generally collinear relationship among the genomes, indicating that the gene order and arrangement were largely conserved. Despite this overall collinearity, some genome rearrangement events, such as inversions and translocations, were observed among the five *Bacillus* genomes (Figure 4-7B). Among these strains, IFST-221 showed the highest synteny with SQR9.

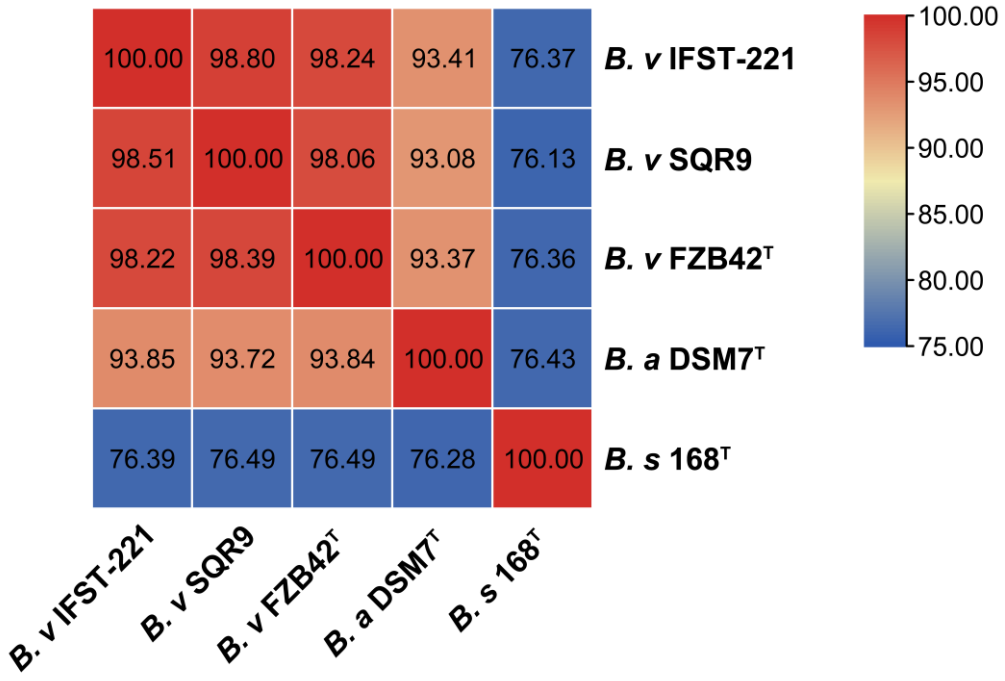

Figure 4-8 Heatmap of the ANI values for the genomes of five *Bacillus* strains, including *B. velezensis* IFST-221, SQR9, FZB42^T, *B. amyloliquefaciens* DSM7^T, and *B. subtilis* 168^T.

In addition to collinearity, a comprehensive protein sequence analysis using OrthoVenn2 was performed to compare the orthologous and paralogous clusters across the five strains. Out of the 3,659 proteins identified in IFST-221, 3,542 clusters were generated by comparing orthologs and paralogs among the five *Bacillus* strains. Additionally, 90 singletons were observed, representing genes that did not have orthologs in other species (Figure 4-7C and D). Additionally, 3,019 clusters were common to all five strains, indicating a significant overlap in genetic content (Figure 4-7C). A total of 3,468 overlapping clusters were common between IFST-221 and *B. velezensis* SQR9. IFST-221 shared 3,424 clusters with *B. velezensis* FZB42^T and 3,358 clusters with *B. amyloliquefaciens* DSM7^T, while sharing 3,180 clusters with *B. subtilis* 168^T. Additionally, two unique clusters were identified for IFST-221 (Figure 4-7C). These unique clusters contained four proteins (IFST-221_GM001075, IFST-221_GM001077, IFST-221_GM001080, and IFST-221_GM001084) involved in ATP and DNA binding, which were important biological processes. Furthermore, 90 singletons found in IFST-221 were annotated using eggNOG-mapper. The results revealed that ten proteins were associated with information storage and processing, eight proteins were involved in signal transduction and mechanisms, 12 proteins were associated with coenzyme transport and metabolism, and 60 proteins had unknown functions (Figure 4-7D).

3.6. Prediction of the antimicrobial characteristic of IFST-221

Functional annotation of protein-coding genes is crucial for understanding the molecular functions of the species. In the case of IFST-221, 2,574, 3,810, and 2,846 protein-coding genes were annotated in the GO, KEGG, and COG databases, respectively (Figure 4-9).

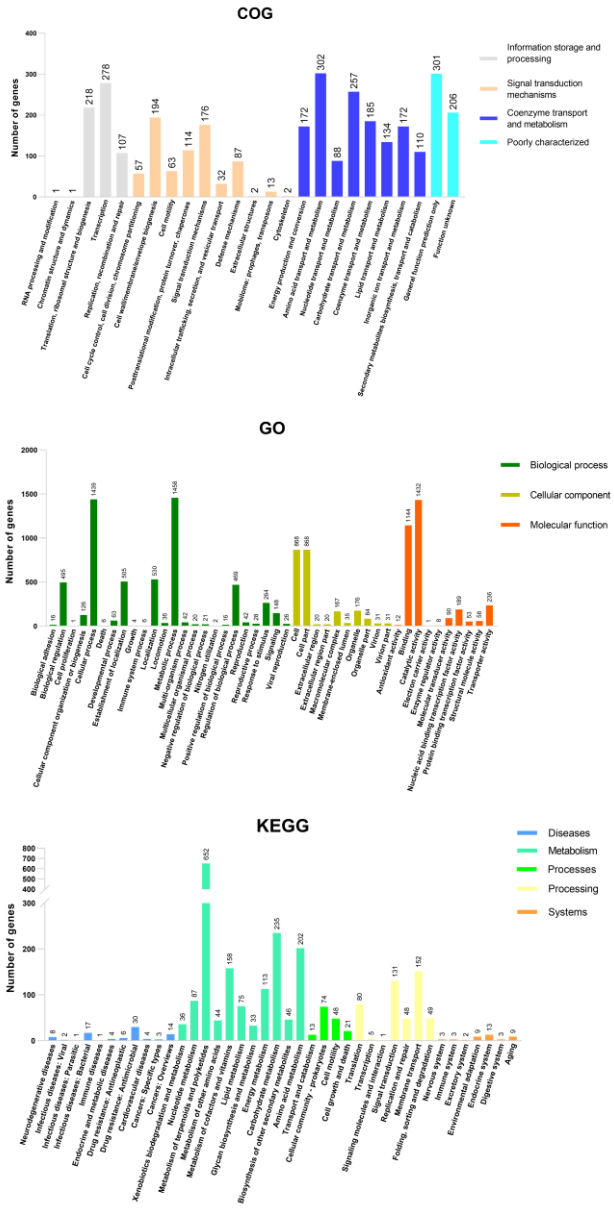

Figure 4-9 Classification of annotated gene functions in the (A) COG, (B) GO, and (C) KEGG database for the whole genome of *B. velezensis* IFST-221.

To investigate the genetic basis underlying the antimicrobial activity of IFST-221, biosynthetic gene clusters (BGCs) were first predicted using antiSMASH version 6.0. In total, 13 putative BGCs were identified across the genome (Table 4-4; Figure 4-7A and B), including clusters encoding nonribosomal peptides (NRPS), polyketides (PKS), hybrid NRPS-PKS systems, ribosomally synthesized and post-translationally modified peptides (RiPPs), and terpene-related metabolites.

Table 4-4 Comparison of predicted and known secondary metabolites between *B. velezensis* IFST-221, *B. velezensis* SQR9, *B. velezensis* FZB42^T, *B. amyloliquefaciens* DSM7^T, and *B. subtilis* 168^T.

Cluster	*B. velezensis* IFST-221	*B. velezensis* SQR9	*B. velezensis* FZB42^T	*B. amyloliquefaciens* DSM 7^T	*B. subtilis* 168^T
1	Surfactin	Surfactin	Surfactin	Surfactin	Surfactin
2	Fengycin	Fengycin	Fengycin	Fengycin	Fengycin
3	Bacillibactin	Bacillibactin	Bacillibactin	Bacillibactin	Bacillibactin
4	Macrolactin H	Macrolactin H	Macrolactin H	Unknown	Subtilosin A
5	Difficidin	Difficidin	Difficidin	Unknown	Sporulation killing factor
6	Bacillaene	Bacillaene	Bacillaene	Bacillaene	Bacillaene
7	Bacilysin	Bacilysin	Bacilysin	Bacilysin	Bacilysin
8	Butirosin A/B	Butirosin A/B	Butirosin A/B	Butirosin A/B	Sublancin 168
9	Andalusicin A/B	Dumulmycin/ Shuangdaolide A/B/C/D	Plantazolicin	Unknown 1	1-carbapen-2-em-3-carboxylic acid
10	Unknown 1	Unknown 1	Bacillothiazol A/B/C/ D/E/F/G//H/I/J /K/L/M/N	Unknown 2	Pulcherriminic acid
11	Unknown 2	Unknown 2	Unknown 1	Unknown 3	Thailanstatin A
12	Unknown 3	Unknown 3	Unknown 2	-	Unknown 1
13	-	-	Unknown 3	-	Unknown 2
14	-	-	-	-	Unknown 3

-, Not applicable

To validate these predictions, each BGC was subsequently subjected to manual, gene-level curation. Cluster boundaries, core biosynthetic genes, conserved enzymatic domains (e.g., NRPS adenylation domains and PKS ketosynthase domains), and operon organization were examined and compared with well-characterized reference clusters from *B. velezensis* FZB42. Only clusters containing complete core biosynthetic machinery and conserved functional domains were considered intact and potentially functional.

Table 4-5 Manual confirmation of biosynthetic gene clusters (BGCs) identified in *B. velezensis* IFST-221.

No.	Predicted product	Similarity confidence	Type	Length	Gene number	Core biosynthetic gene number	Additional biosynthetic gene number	Key biosynthetic genes confirmed	Integrity
1	andalusicin A/B	High	lanthipeptide-class-iii	22,610	21	1	6	class III lanthipeptide, lanKC, class I SAM-dependent methyltransferase	Intact and Functional
2	Surfactin	High	NRPS	65,408	40	3	13	srfAA, srfAB, srfAC, srfAD (4 core NRPS modules)	Intact and Functional
3	-	-	PKS-like	41,245	41	1	6	-	-
4	-	-	terpene	20,741	23	1	1	-	-
5	macrolactin H	High	transAT-PKS	88,216	44	7	12	Seven core PKS genes. Confirmed KS, AT, ACP, KR, ER domains.	Intact and Functional
6	bacillaene	High	transAT-PKS, T3PKS, NRPS	110,112	52	9	11	Complete PKS, NRPS, and T3PKS systems. Confirmed A/C and KS/AT/ACP domains.	Intact and Functional
7	fengycin	High	NRPS, transAT-PKS, betalactone	137,833	65	11	15	Complete fenA-E operon, PKS, and NRPS modules confirmed.	Intact and Functional
8	-	-	terpene	21,884	22	1	2	-	-
9	-	-	T3PKS	41,101	49	1	4	-	--
10	difficidin	High	transAT-PKS	106,183	59	8	17	Complete PKS system. Confirmed KS, ER, KR, cMT domains.	Intact and Functional
11	-		terpene-precursor	20,891	23	1	2	-	-
12	bacillibactin	High	terpene-precursor, NRP-metallophore, NRPS, RiPP-like	65,351	63	5	12	Confirmed core Adenylation (A) domain. All necessary NRPS modules for trimeric synthesis are present.	Intact and Functional
13	bacilysin	High	other	41,419	42	1	10	Confirmed core bacA-E synthetase and anticapsin pathway genes.	Intact and Functional

Based on this systematic analysis, eight BGCs were confirmed to encode complete and functionally credible biosynthetic pathways, including those responsible for the production of andalusicin A/B, surfactin, macrolactin H, bacillaene, fengycin, difficidin, bacillibactin, and bacilysin (Table 4-5). In contrast, the remaining clusters lacked identifiable core biosynthetic genes or complete enzymatic modules and were therefore classified as putative or incomplete.

The andalusicin A/B cluster represents a distinctive feature of IFST-221 compared with the other four reference strains, as this RiPP-type cluster was absent or

incomplete in the genomes of *B. velezensis* SQR9, FZB42^T, *B. amyloliquefaciens* DSM7^T, and *B. subtilis* 168^T.

Collinearity analysis further revealed that the genomic organization of secondary metabolite gene clusters was largely conserved among the five strains (Figure 4-7B). Gene clusters encoding bacillibactin, bacilysin, and butirosin displayed particularly high conservation, whereas clusters encoding surfactin, fengycin, macrolactin, bacillaene, and difficidin exhibited greater sequence divergence, suggesting strain-specific variation in secondary metabolite biosynthesis.

Collectively, these results demonstrate that IFST-221 harbors a diverse and largely intact repertoire of antimicrobial biosynthetic gene clusters, providing a robust genetic basis for its broad-spectrum antagonistic activity against plant pathogens.

3.7. Global screening of genes potentially contributing to plant growth-promoting activities in IFST-221

The annotation results from eggNOG and GO databases offer valuable insights into the potential roles of genes within the IFST-221 genome, especially regarding plant growth promotion, colonization, and biofilm formation. In addition to the genes responsible for antimicrobial secondary metabolites production (*srf*, *fen*, *dhb*, *btr*, *bac*, *ancKC/anCMT*, *bae*, *mln*, and *dif*), there are numerous additional genes that directly or indirectly contribute to plant promotion (Figure 4-10). IFST-221 possesses genes involved in the synthesis of indole-3-acetic acid (IAA), including *yhcX*, which encodes a putative nitrilase participating in the indole-3-acetamide (IAM) pathway, and *ysnE*, an IAA transacetylase that may function in the indole-3-pyruvate (IPA) and tryptamine (TAM) pathways (Shao et al., 2021). Furthermore, IFST-221 carries the *phy* gene, which is responsible for phytase production. It also possesses the genes involved in acquiring and utilizing PO_4^{3-} (*pstABCS*), K^+ (*ackA*, *gltA*, and *mdh*), Fe^{3+} (*yclNOPQ*), and N_2 (*nifU*). The synthesis of plant cell wall-degrading enzymes is another important trait for colonization in the rhizosphere. IFST-221 carries genes such as *bglC5*, *bglS*, and *yhfE* involved in the coding of endo-β-glucanase, *bglA* and *licH* related to endo-β-glucosidase, Additionally, IFST-221 possesses genes (*xylA/B* and *xynA/B)* involved in the coding of xylanase. Moreover, the IFST-221 genome contains a complete pathway for biofilm formation, including *kinC/D*, *spo0A*, *abbA*, *abrB*, *sinI/R*, *eps*, and *yqxM/tapA-sipW-tasA*. Overall, the comprehensive analysis of the IFST-221 genome demonstrates its potential as a biological control agent and hopefully enables its use in the future with capabilities in plant growth promotion, colonization, and biofilm formation.

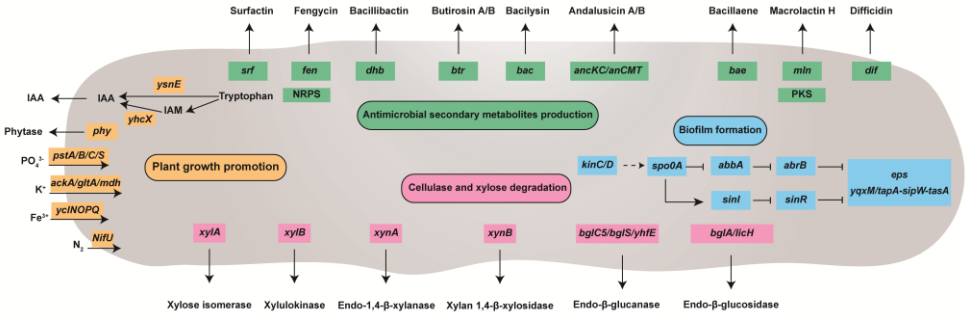

Figure 4-10 The key genes potentially participating in antimicrobial secondary metabolites (green color), plant growth promotion (yellow color), cellulase and xylose degradation (pink color), and biofilm formation (blue color) in the IFST-221 genome.

4.Discussion

Plant growth-promoting rhizobacteria play a dual role in agriculture, functioning as biocontrol agents that protect plants from pathogens and as beneficial microbes that enhance crop performance by stimulating growth, increasing yields, improving seedling vigor, and promoting seed germination (Tabassum et al., 2017). In this study, we isolated and identified *B. velezensis* IFST-221 from the healthy maize rhizosphere in the field with a high incidence of *Fusarium* ear and stalk rot. IFST-221 exhibited broad-spectrum antimicrobial activity against both oomycetes and ascomycetes in the plates. When applied to crops, IFST-221 significantly reduced maize ear rot and cotton Verticillium wilt. Moreover, seedlings of maize, cotton, tomato, and broccoli treated with IFST-221 showed enhanced growth compared to untreated controls, highlighting its dual potential as a biocontrol agent and plant growth promoter.

Historically, *B. velezensis* was long regarded as a heterotypic synonym of *B. amyloliquefaciens* (Borriss et al., 2011; Wang et al., 2008). Genomic studies in 2016, however, confirmed *B. velezensis* as a distinct species, and in 2017 it was grouped with *B. amyloliquefaciens*, *B. velezensis*, and *B. siamensis* as an "operational group *B. amyloliquefaciens*" within the *B. subtilis* species complex (Dunlap et al., 2016; Fan et al., 2017). While the 16S rRNA gene is widely used for bacterial phylogenetic analysis, its high sequence similarity across *Bacillus* species limits its resolution. This limitation was evident in our 16S rRNA-based phylogeny of IFST-221, which failed to clearly differentiate it from closely related taxa. In contrast, *gyrB*-based phylogeny provided higher resolution (Wang et al., 2007), with IFST-221 clustering tightly with the *B. velezensis* type strain BCRC 17467^T. Additional support came from the ONPG biochemical testing and the comparative genomics, which revealed a higher ANI value and greater numbers of shared gene clusters between IFST-221 and *B. velezensis* SQR9 and FZB42^T, confirming its taxonomic placement.

The *Bacillus* genus, especially *B. velezensis*, has attracted considerable attention due to its capacity to produce various antimicrobial secondary metabolites (Chowdhury et al., 2015). FZB42^T, the first *B. velezensis* strain with a fully annotated genome, was

isolated from the maize rhizosphere (Chen et al., 2007). Since then, many strains have been recovered from the rhizosphere of various plants, such as tomato, wheat, cucumber, polar, and lettuce. As of 2024/04/25, the NCBI database contained 859 genome assemblies for *B. velezensis*. These strains differ in the repertoire of secondary metabolites they produce, which typically fall into two major categories: polyketides and non-ribosomal synthetic peptides. Polyketides such as bacillaene, macrolactin, and difficidin are synthesized by polyketide synthase gene clusters *bae* (formerly *pks1*), *mln* (formerly *pks2*), and *dif* (formerly *pks3*), respectively (Chen et al., 2006). Non-ribosomal peptide synthetases (NRPSs) produce numerous lipopeptides, including iturins, surfactins, and fengycins, as well as the siderophore bacillibactin (Cochrane & Vederas, 2016; Mongkolthanaruk, 2012). Although both IFST-221 and FZB42^T were isolated from the maize rhizosphere, comparative secondary metabolite profiles revealed differences in their biosynthetic gene cluster profiles. Both strains encode surfactin, fengycin, bacillibactin, macrolactin H, difficidin, bacillaene, bacilysin, and butirosin A/B. However, FZB42^T additionally harbors clusters for plantazolicin and bacillothiazol, whereas IFST-221 encodes unique clusters for andalusicin A/B and several uncharacterized metabolites. It is noteworthy that although FZB42^T has been experimentally confirmed to produce bacillomycin D, a member of the iturin family (Assena et al., 2024), the corresponding NRPS cluster was not detected by antiSMASH (bacterial version 6.0). Moreover, in other *Bacillus* genomes, the bacillomycin gene cluster has been found embedded within the fengycin cluster rather than annotated as a separate entity by antiSMASH, likely due to overlapping NRPS modules or contig boundary issues (Blin et al., 2013; Stincone et al., 2020). Such discrepancies highlight a known limitation of antiSMASH, which relies on homology-based domain prediction and may underestimate or misclassify NRPS clusters with highly conserved modular architectures. Therefore, in the present study, antiSMASH predictions were not interpreted in isolation but were combined with manual gene-level curation and comparative analysis against well-characterized reference clusters. This integrative approach allowed a more reliable assessment of the biosynthetic capacity of IFST-221 and reduced the risk of overestimating or misclassifying secondary metabolite gene clusters.

Collinearity analysis further indicated that secondary metabolites gene clusters have become more compact throughout evolutionary transitions from *B. subtilis* 168, *B. amyloliquefaciens* DSM7^T, to subsequently *B. velezensis* FZB42^T, SQR9, and IFST-221. Such compact organization may allow IFST-221 to retain more metabolite clusters while simultaneously deleting or integrating less essential genes to adapt to challenging environments. Among the predicted metabolites, IFST-221 produces andalusicin A/B, a class III lanthipeptide known to inhibit Gram-positive bacteria (Grigoreva et al., 2021). Since related metabolites such as surfactin, fengycin, bacillibactin, macrolactin, difficidin, bacillaene, and bacilysin have been successfully extracted from *B. velezensis* SQR9 using reverse-phase high-pressure liquid chromatography analysis (Li et al., 2014; G. Wu et al., 2018; Xu et al., 2013), similar approaches may be applied to characterize novel and known IFST-221 metabolites.

Notably, the variation detected in the collinearity analysis suggests IFST-221 could harbor additional, yet undiscovered, novel compounds.

In the pot experiment, IFST-221 promoted the growth of maize, cotton, tomato, and broccoli seedlings, leading to significant increases in plant height and shoot fresh weight compared with controls. This growth promotion appears partly attributable to IAA production in the IFST-221 culture. Gram-positive bacteria can synthesize IAA through various tryptophan-dependent pathways, including the indole-3-acetamide (IAM) pathway, indole-3-pyruvic acid (IPyA) pathway, indole-3-acetonitrile (IAN) pathway, as well as an acetyltransferase (*ysnE*) mediated route (Keswani et al., 2020). In IFST-221, the *yhcX* gene encoding a nitrilase (indole-3-acetonitrile nitrilase) suggests IAN-to-IAA conversion potential, while ysnE was predicted to participate in the conversion of IPA and tryptamine (TAM) to indole-3-acetaldehyde (IAAld), and of indole-3-lactic acid (ILA) to tryptophol (TOL). However, some genes associated with the other pathways are absent. In addition to auxin synthesis, IFST-221 harbors a *nif* gene cluster containing *nifU* and *nifS*, which encode iron-sulfur cluster assembly proteins involved in nitrogen fixation (Ryu et al., 2020). Although *nifU* is not essential for all nitrogen-fixation strains (Wang et al., 2013), its presence indicates potential nitrogen-fixation capabilities. Further validation using acetylene reduction or isotopic labeling assays will be necessary to determine the actual nitrogen-fixation capacity of the strain.

Beyond nitrogen metabolism, IFST-221 displays traits typical of PGPR. It solubilizes insoluble phosphate and potassium, supported by genomic evidence such as the phytase-encoding *phy* gene for organic phosphate solubilization (Torres et al., 2024). Additionally, the high-affinity phosphate transport system (*pst*) is essential for phosphate uptake in a nutrient-deficient environment (Moreno-Letelier et al., 2011). Genes involved in potassium solubilization, such as *ackA*, *gltA*, and *mdh,* have also been described in the potassium-solubilizing strain *B. aryabhattai* SK1-7 (Y. Chen et al., 2022). However, IFST-221 lacks the *ktrAB* and *ktrCD* genes encoding the high-affinity and low-affinity potassium transporters, respectively (Gundlach et al., 2017). While siderophore production was not directly observed in our assays, genomic analysis revealed a bacillibactin biosynthesis cluster (*dhb*) and the *yclNOPQ* operon encoding a petrobactin transporter (Zawadzka et al., 2009). Moreover, IFST-221 contains enzymes such as cellulases specialized in cellulose degradation, β-glucanases, and β-glucosidases involved in glucan degradation, which play a significant role in bacterial colonization of the rhizosphere of plants (Sritongon et al., 2023). Biofilm formation in IFST-221 adds to its ecological adaptability, enhancing its resilience in challenging environmental conditions.

Overall, IFST-221 demonstrates multiple mechanisms for disease suppression, plant growth promotion, and environmental adaptability. While our results confirm its PGPR potential under controlled conditions, future work should assess its performance under diverse abiotic stresses and field environments to fully evaluate its utility in sustainable crop production.

5. Conclusion

B. *velezensis* IFST-221 is a promising PGPR with a broad spectrum of antimicrobial activity and notable plant growth-promoting abilities. Comparative genomic analysis of IFST-221 and related strains revealed the presence of 12 secondary metabolites, including surfactin, fengycin, bacillibactin, macrolactin H, difficidin, bacillaene, bacilysin, butirosin A/B, andalusicin A/B, and three unknown secondary metabolites. Notably, the IFST-221 exhibited three unidentified secondary metabolites as well as a distinctly known metabolite, andalusicin A/B. Furthermore, the deep mining of the IFST-221 genome has provided insights into the genetic potential for plant growth regulation, colonization, and biofilm formation. Overall, the characteristics and genomic features of *B*. *velezensis* IFST-221 indicate its potential as a beneficial bacterium for agricultural applications, such as biocontrol of plant pathogens and promotion of plant growth.

Chapter 5

Antifungal mechanism of *Bacillus velezensis* IFST-221 against *Fusarium verticillioides*: transcriptomic insights and surfactin contribution

Abstract

Bacillus velezensis is a widely studied plant growth-promoting rhizobacterium with potential biocontrol activity against fungal pathogens. In this study, we explored the antifungal mechanism of *B. velezensis* IFST-221 against *Fusarium verticillioides*, the major pathogen of maize ear and stalk rot, by combining LC-MS/MS, targeted gene knockout, biocontrol assays conducted *in vitro* and *in vivo*, and transcriptome sequencing. LC-MS/MS analysis confirmed the presence of surfactins in the crude extract. Deletion of the *srfAA* gene significantly reduced antifungal activity in the crude extract but did not impair growth inhibition in the plate confrontation assay or maize kernels assays, suggesting that surfactins contribute to antifungal activity but are not the primary antifungal determinants. Transcriptomic profiling of *F. verticillioides* under IFST-221 challenge revealed extensive reprogramming of primary metabolism, particularly carbon metabolism and the tricarboxylic acid cycle, amino sugar and nucleotide sugar metabolism, alongside pronounced enrichment of ribosome-related genes. Stress-response pathways, including antioxidant enzymes, autophagy, and heat shock proteins, were also strongly activated, indicating multiple adaptive responses to bacterial pressure. Collectively, these findings demonstrate that IFST-221 antagonism involves interconnected processes such as primary metabolic disruption, cell wall and membrane remodeling, oxidative stress induction, and interference with ribosomal function. Surfactins contribute to this activity but are unlikely to act alone, highlighting the potential involvement of additional metabolites or regulatory shifts. This work provides mechanistic insights into IFST-221-mediated biocontrol and reinforces its promise as a sustainable strategy for maize disease management.

Keywords: *Bacillus velezensis*, LC-MS/MS, surfactins, transcriptomic analysis

1. Introduction

Bacillus spp. are widely distributed in nature and are aerobic or facultative anaerobic Gram-positive bacteria capable of forming endospores, which enable them to survive under adverse environmental conditions (Blanco Crivelli et al., 2024). Besides, *Bacillus* species play a crucial role in plant disease management by suppressing phytopathogens. This suppression is achieved through the production of diverse antimicrobial compounds, the induction of systemic resistance in host plants, and the competition for niches or nutrients (N. Zhang et al., 2023). The antimicrobial arsenal of *Bacillus* includes antimicrobial proteins, volatile organic compounds, and particularly bioactive metabolites, including polyketides (PKs), nonribosomal peptides (NRPs), ribosomally synthesized and post-translationally modified peptides (RiPPs), and terpenes with potent antimicrobial properties (Put et al., 2024). The major classes of antimicrobial lipopeptides include surfactins, fengycins, and iturins, which exhibit broad-spectrum activity against fungi, bacteria, viruses, and even mycoplasma. Due to their potent bioactivities, these compounds have been applied not only in agriculture, but also in medicine, food preservation, and environmental protection (Fira et al., 2018).

Fungi play prominent roles in agriculture, food production, and processing, but also cause crop loss. They are constantly exposed to a variety of environmental challenges, including biotic factors such as damage caused by competing microorganisms like bacteria, viruses, and fungi, and abiotic stresses (temperature, pH, nutrient availability, oxidative stress, osmotic stress, and UV radiation) (Aghcheh & Braus, 2018). To survive and maintain cellular homeostasis under these conditions, fungi have evolved diverse and complex regulatory networks that trigger specific stress responses. To mitigate oxidative stress, fungi employ four primary responses strategies: (1) Activation of chitinase and lipase, along with associated signaling pathways, to maintain cell wall and cell membrane integrity; (2) Induction of antioxidant enzymes such as peroxidase (POD), superoxide dismutase (SOD), and catalase (CAT), which function through the thioredoxin and glutathione cycles to detoxify reactive oxygen species; (3) Upregulation of primary metabolism to meet cellular energy demands under stress conditions; (4) Enhanced production of secondary metabolites that either scavenge excess oxygen and ROS directly or modulate their formation through cofactor binding and antioxidative mechanisms (Fountain et al., 2016).

RNA sequencing serves as a powerful tool to investigate how biocontrol bacteria influence pathogenic fungi by revealing changes in gene expression and underlying potential regulatory mechanisms. In this study, transcriptome analysis was used to explore the effects of *Bacillus velezensis* IFST-221 on *F. verticillioides*. The investigation focused on key biological processes, including cell wall and cell membrane integrity (e.g., β-glucan and ergosterol metabolic genes), ROS metabolism (involving SOD, CAT, and POD), as well as some traditional stress-response pathways such as autophagy-related genes (ATG) and heat shock proteins (HSP) expression. These insights provide a theoretical foundation to understand how *B.*

velezensis IFST-221 affects fungal growth and virulence, contributing to its potential as an effective biological control agent.

2. Materials and methods

2.1. Mutant construction

To get the knockout fragment, the 1000 bp upstream (srfAA_up-F and srfAA_up-Tet-R) and downstream fragments (srfAA_down_Tet-F and srfAA_down-R) of the *srfAA* gene were amplified from the *B. velezensis* IFST-221 genome, while the 1583 bp tetracycline resistance gene (Tet-srfAA_up-F and Tet-srfAA_down-R) was amplified from the pHY-p43 vector. The PCR reaction, in a 50 μL final volume, contained 25 μL PrimeSTAR® Max DNA Polymerase (Takara Biomedical Technology Co., Ltd., Beijing, China), 1 μL forward primer, 1 μL reverse primer, 1 μL template, and 22 μL ddH_2O under 35 cycles of 98 ℃ for 10 s, annealing at 55 ℃ for 15 s, and 72 ℃ for 15 s. After amplification, products were separated using 1% agarose gel electrophoresis and purified with HiPure Gel Pure DNA Mini Kit (Magen Biotech, Guangzhou, China). To overlap these fragments, a two-step PCR was performed. In the first step, 100-200 ng each of upstream, tetracycline resistance gene (Tet^R), and downstream fragments were mixed with 12.5 μL PrimeSTAR® Max DNA Polymerase and ddH_2O (to a final volume of 25 μL), followed by 15 cycles of 98 ℃ for 10 s, 58 ℃ for 15 s, and 72 ℃ for 25 s. In the second step, the product from the first step was used as a template, together with 12.5 μL PrimeSTAR® Max DNA Polymerase, primers srfAA_up-F and srfAA_down-R, and 10.5 μL ddH_2O, under 35 cycles of 98 ℃ for 10 s, annealing at 56 ℃ for 15 s, and 72 ℃ for 25 s. After amplification and purification, the PCR products were ligated into the pLB vector (Tiangen Biotech Co., Ltd., Beijing, China) and transformed into *E. coli* TG-1. Positive transformants were selected and sequenced by Sangon Biotech (Shanghai) Co., Ltd. using Sanger sequencing. Then the positive colony was selected by PCR identification and named as pLB_Tet_srfAA_UD, and then introduced into *B. velezensis* IFST-221 through electroporation.

To prepare to competent cell, a single colony of *B. velezensis* IFST-221 was cultured overnight in LB liquid medium, and then 1 mL of the culture was inoculated into 100 mL of fresh LB medium supplemented with sorbitol to a final concentration of 0.5 M. When the optical density at 600 nm (OD600) reached to 0.8 under 37 ℃ culture, the cells were collected through centrifugation (4 ℃, 5000g, 5 min). After washing four times with ice-cold electroporation buffer (0.5 M sorbitol, 0.5 M mannitol, and 10% glycerol), the cells were resuspended in 3 mL of ice-cold electroporation buffer and divided into aliquots of 100 μL per tube, followed by storage at -80 ℃ (Tian et al., 2021).

To transform the plasmid into *B. velezensis* IFST-221, according to Tian's research, a total of 1 μg pLB_Tet_srfAA_UD DNA was added to 100 μL of competent cells and incubated on ice for 2 min. The mixture was immediately transferred into a 1-mm ice-cold electroporation cuvette and treated with electrical pulses using a Bio-Rad electroporation pulser (Bio-Rad, Hercules, CA, USA) at 2.0 kV/cm, 200 Ω, and

25 μF. After pulsing, the mixture was added to 1 mL of recovery medium (LB containing 0.5 M sorbitol and 0.5 M mannitol) and then cultured at 37 ℃ for 3 h with shaking (200 rpm). Subsequently, the cultures were plated onto LB agar with 10 μg/mL tetracycline. Colonies appeared after overnight culturing, and the transformants were verified through PCR using the detection primers listed in Table 5-1.

Table 5-1 Primers used in this study.

Primer	Sequence (5'-3')
Primers used to get the knockout fragments	
srfAA_up-F	gaatagatgatgaccgtacaaa
srfAA_up-Tet-R	acaatatggcccgtttgttgaaatgtgtgcgcctccccttttaa
Tet-srfAA_up-F	ttaaaaaggggaggcgcacacatttcaacaaacgggccatattgt
Tet-srfAA_down-R	atatgtcacctctgtcttttctgttagaaatccctttgagaatg
srfAA_down_Tet-F	cattctcaaagggatttctaacagaaaagacagaggtgacatat
srfAA_down-R	gctcggcttccacggcgtttt
Primers used for the identification of positive transformants	
srfAA_up-det-F	agagtgccccgcatgttg
srfAA_tet-det-R	gctgtgttcacccagtttgt
srfAA_tet-det-F	accagctttttatcagaggg
srfAA_down-det-R	gcgaaagccgctccattg
del_Tet_det-F	caccagcttcctgctgtttc
del_Tet-det-R	ggaagcgtatcattaaccct
srfAA_CDS-det-F	atgttgtcggcctcagggaa
srfAA_CDS-det-R	gcagcgtcaataccggaa
Primers used for the validation of RNA-seq data	
FVCG_010660-F	GACTGTCAAGAAGTCCGCCA
FVCG_010660-R	GCAATCTTATTGCGGAGGCG
FVCG_005907-F	CCATACCACTCGAGCAGAGC
FVCG_005907-R	TACATCCCGCCAACTCCCTA
FVCG_001768-F	AAGGGCCAGAGAACGAGTTG
FVCG_001768-R	GCCCAGTGGTACTCCACTTC
FVCG_009136-F	CTGTAAGCACGCCTCAGTCA
FVCG_009136-R	CTCGTCTACCAGACCCTCCA
FVCG_011938-F	TTCGTCGATATCGGCCACAG
FVCG_011938-R	AAGTCACGACCACCGAAGTC
FVCG_007577-F	GAGTACGCCGATGTTCTGGA
FVCG_007577-R	CGAGAAGGCTGGAGACACTG
FVCG_002059-F	GTTGGGACGAGTGGAGAGTG
FVCG_002059-R	TCGCTTGTAGCACAGCAGAA
FVCG_013279-F	AGAAGAGGCGGAGGAGACTT
FVCG_013279-R	GTTGTCCGGCCATGAGAAGA
FVCG_002399-F	ATTGCCTGTCAACGCAACAC
FVCG_002399-R	AGCGCGAGACTTGAACTTGA

2.2. Lipopeptide extraction and analysis

The single clone was cultured in the 4 mL LB medium at 37 °C and 160 rpm for 16-18 h as a preculture. 10 mL of preculture was inoculated in a 500 mL shake flask containing 200 mL of complete media (CM) (yeast extract 6 g/L, casein acids hydrolysate 6 g/L, and sucrose 10 g/L) and then cultivated at 30 °C at 100 rpm for 72 h for the antimicrobial substance production. At the end of cultivation, the culture was centrifuged at 11,000 ×g for 15 min to remove bacterial cells. The pH of the supernatant was adjusted to 2.0 by adding 6 N HCl until a white precipitate appeared. Then the supernatant was centrifuged at 11,000 ×g for 10 min, and the precipitate was collected. The total amount of methanol added to the precipitation was 4 mL, and the pH was neutralized to 7.0 with 6 N NaOH. The precipitate was suspended in methanol several times and removed by centrifugation to obtain a lipopeptide extract, which dissolved in methanol (Wang et al., 2020).

The crude extract was filtered through a 0.22 μm membrane and stored at -20°C before analysis. The recovered fractions were then analyzed using liquid chromatography coupled with tandem mass spectrometry (LC-MS/MS) to separate and identify lipopeptide components. Chromatographic separation was performed on an Agilent 1290 Infinity II HPLC system equipped with a ZORBAX Eclipse Plus C18 column (2.1 × 50 mm, 1.8 μm), using a mobile phase of 0.1% formic acid in water (A) and 0.1% formic acid in acetonitrile (B) under a gradient elution program of 10% B (0-0.5 min), increasing to 90% B (0.5-1.5 min), holding at 90% B (1.5-2.0 min), and returning to 10% B (2.0-3.0 min). The column temperature was maintained at 40 °C, with a flow rate of 0.5 mL/min, and an injection volume of 5 μL. The eluate was directly introduced into an Agilent 6460A Triple Quadrupole Mass Spectrometer (Agilent Technologies, Santa Clara, CA, USA) equipped with an electrospray ionization (ESI) mode. The capillary voltage was set at 3.5 kV, with a nebulizer gas pressure of 35 psi and a desolvation temperature of 300°C. Data were acquired in full scan mode (m/z 400-2000), with a fragmentor voltage of 380V, detecting a characteristic m/z 1058.4 $[M+Na]^+$ peak corresponding to surfactin. Mass spectra were analyzed using MassHunter Workstation (Agilent Technologies), and surfactin identification was confirmed based on retention time, molecular ion peaks, and MS/MS fragmentation patterns compared with reference data (Zhao et al., 2014).

2.3. Maize kernels inoculation assay

To evaluate the antifungal activity of the Δ*srfAA* mutants against *F. verticillioides* in maize kernels, sterilized maize kernels were prepared following the previously described method (Liang et al., 2022). Briefly, bacterial cultures of wild-type IFST-221 and Δ*srfAA* mutants were grown overnight in LB broth at 37 °C with shaking (180 rpm). Cells were harvested by centrifugation (5,000 × g, 10 min), washed twice with sterile 0.9% NaCl, and resuspended in sterile 0.9% NaCl to a final concentration of 1×10^9 cfu/mL. Fifteen surface-sterilized maize kernels were immersed for 1 h in 10 mL of bacterial suspension or in sterile 0.9% NaCl as a negative control. After treatment, each kernel was inoculated with either 10 μL of *F. verticillioides* conidial

suspension (1×10^6 conidia/mL) or with 10 µL of sterile ddH_2O for negative controls. Each treatment included 15 kernels, replicated five times, and the entire experiment was repeated independently three times. The kernels were then incubated at 25 °C for five days in the dark, after which disease symptoms were observed and photographed.

2.4. Transcriptome sequencing and data analysis

2.4.1. Co-culture assay

The co-culture assay was performed following Bi et al. (2023) with minor modifications. The conidial suspension of *F. verticillioides* and IFST-221 suspension were prepared as described before. Fungal conidia and bacterial cells were then added simultaneously into CM medium to reach final concentrations of 1×10^6 conidia/mL and 1×10^6 cfu/mL, respectively. Cultures were incubated at 25 °C with shaking at 180 rpm for 3 days, while a pure culture of *F. verticillioides* in CM at the same conidial concentration served as the control. After incubation, fungal mycelia were collected by centrifugation, immediately frozen in liquid nitrogen, and stored at -80 °C until RNA extraction. In parallel, spore and hyphal morphology under the same conditions was observed using a BX61 microscope (Olympus, Japan).

2.4.2. RNA extraction and quality control

RNA extraction, sample quality control, library preparation, clustering, and sequencing were performed by Beijing Novogene Co., Ltd., according to the manufacturer's instructions.

Total RNA was extracted using Trizol reagent according to the manufacturer's instructions (ThermoFisher, USA). RNA concentration was measured using a Nanodrop spectrophotometer and an Agilent 5400 system (Agilent Technologies, CA, USA). RNA integrity and purity were assessed with the Agilent 5400, which provided capillary electrophoresis profiles. All samples showed RNA integrity number (RIN) values ≥ 9.7, confirming sufficient integrity for sequencing.

2.4.3. Library preparation and sequencing

Poly(A)$^+$ mRNA was purified from total RNA using Oligo(dT) magnetic beads. The enriched mRNA was fragmented in NEB fragmentation buffer under divalent cation conditions and used for first-strand cDNA synthesis with random hexamer primers and M-MuLV reverse transcriptase (RNase H–). For strand-specific library preparation, dUTP was incorporated instead of dTTP during second-strand cDNA synthesis with DNA polymerase I (Parkhomchuk et al., 2009). After end repair, A-tailing, and adaptor ligation, ~250-300 bp cDNA fragments were size-selected with AMPure XP beads. USER enzyme digestion was performed to degrade the U-containing strand before PCR amplification.

Library concentration was initially measured using a Qubit 2.0 Fluorometer, and insert size distribution was analyzed with an Agilent 5400 system, and effective concentration was further quantified by qPCR (>1.5 nM). Qualified libraries were pooled and sequenced on an Illumina NovaSeq 6000 platform to generate 150 bp paired-end reads.

2.4.4. Data processing and read mapping

Raw reads in fastq format were processed with fastp (v0.19.7) to remove reads containing adaptor sequences, reads with ambiguous bases ("N"), and low-quality reads in which more than 50% of bases had a Phred quality score ⩽ 5. Sequencing quality was evaluated in terms of error rate, Q20, Q30, and GC content, all of which met the requirements for high-throughput sequencing.

The reference genome of *F. verticillioides* LNF15-11 (BioProject PRJNA1166641) was used for alignment. Clean reads were mapped to the reference genome using HISAT2 (v2.0.5) with the parameters --rna-strandness RF --dta. Mapping statistics showed > 94% uniquely mapped reads across all samples, consistent with the strand-specific dUTP/USER library preparation method.

2.4.5. Quantification of gene expression

Gene-level read counts were calculated based on the alignment results using featureCounts (v1.5.0-p3) (Liao et al., 2014), after filtering out reads with mapping quality < 10, discordant pairs, or multiple mapping loci. Expression levels were normalized as FPKM (Fragments Per Kilobase of transcript per Million mapped reads) values to construct the expression matrix for downstream analyses (Bray et al., 2015).

Correlations, principal component analysis (PCA), and Venn diagrams between Fv and Fv+221 were generated in R (v4.0.2) to assess the reproducibility of biological replicates and visualize gene expression patterns across samples.

2.4.6. Differential expression and enrichment analyses

Differentially expressed analysis between Fv and Fv+221 was performed using the DESeq2 R package (v1.20.0). Gene-level read counts were normalized to account for sequencing depth, and the statistical significance of differential expression was assessed using a negative binomial distribution model. Resulting *p*-values were adjusted for multiple testing using the Benjamini–Hochberg method to control the false discovery rate (FDR). Genes with $|\log_2(\text{FoldChange})| \geq 1$ and adjusted $p < 0.05$ were considered differentially expressed.

GO and KEGG enrichment analyses were performed using clusterProfiler v3.8.1, with adjusted $p < 0.05$ as the cutoff. Visualization of DEGs, enriched pathways, and heatmaps was conducted using seaborn v0.11.2 in Python.

2.5. Quantitative real-time polymerase chain reaction

qRT-PCR was performed to validate the DEGs identified from the transcriptomic analysis. Total RNA was extracted from two groups using Trizol reagent according to the manufacturer's instructions (ThermoFisher, USA). First-strand cDNA was synthesized from 1 μg of total RNA with the EasyScript cDNA Synthesis SuperMix Kit (TransGen, Beijing, China), following the manufacturer's instructions. Primers were designed using 2 × Universal SYBR qPCR Mix (GeneBetter, Beijing, China) on a Quant Studio™ 6 Flex System Cycler (Applied Biosystems, Waltham, MA, USA). Relative expression levels were calculated using the $2^{-\Delta\Delta Ct}$ method with *Fv_β-tubulin*

as the internal reference. Data were obtained from three independent biological replicates (each with three technical replicates) and expressed as mean ± SE.

3. Results

3.1. srfAA was knocked out from B. velezensis IFST-221

According to the genomic prediction of secondary metabolites, *B. velezensis* IFST-221 possesses the capability to synthesize surfactin, fengycin, bacillibactin, macrolactin H, difficidin, bacillaene, bacilysin, butirosin A/B, and andalusicin A/B (Liang et al., 2024). Following the extraction and detection of IFST-221 culture, the sodiated molecules $[M + H]^+$ at *m/z* 994.3, 1008.3, 1022.4, 1036.4, $[M + Na]^+$ at *m/z* 1044.3, 1058.4, and $[M+K]^+$ *m/z* 1074.3 are obtained. All molecular weights differ by 14 Da ($-CH_2$). These data indicate that IFST-221 produces surfactins, which may be identified as C_{13} surfactin, C_{14} surfactin, and C_{15} surfactin (Table 5-2).

Table 5-2 The active peaks and their assignments

m/z	Assignments
994.3	Surfactin B C13 $[M+H]^+$
1008.3	Surfactin A C13 $[M+H]^+$, Surfactin B C14 $[M+H]^+$
1022.4	Surfactin A C14 $[M+H]^+$, Surfactin B C15 $[M+H]^+$
1031.3	-
1036.4	Surfactin A C15 $[M+H]^+$
1044.3	Surfactin A C14 $[M+Na]^+$, Surfactin B C15 $[M+Na]^+$
1053.2	-
1058.4	Surfactin A C15 $[M+Na]^+$
1067.2	-
1074.3	Surfactin A C15 $[M+K]^+$

To identify the importance of surfactins in IFST-221, the surfactin non-ribosomal peptide synthetase *srfAA*, which is the first gene of the surfactins biosynthetic gene clusters (*srfAA*, *srfAB*, *srfAC*, and *srfAD*), was selected for deletion by replacing a tetracycline resistance (Tet^R) fragment (Figure 5-1A and B) (Qiao et al., 2024). As shown in Figure 5-1C and D, four primer pairs were used to detect the positive transformants: the first primer pair (P1, srfAA_up-det-F/srfAA_tet-det-R), the second primer pair (P2, srfAA_tet-det-F/srfAA_down-det-R), the third primer pair (P3, del_Tet_det- F/R), and the fourth primer pair (P4, srfAA_CDS-det-F/R). These primer pairs yielded amplicons of 1522 bp, 1453 bp, and 2843 bp, respectively, while the fourth primer pair did not produce an amplified band. Instead, in the wild-type IFST-

221, the fourth primer pair produced the expected amplified band. This confirmed that the *srfAA* gene was successfully knocked out in the strains of Δ*srfAA* 4# and 9#.

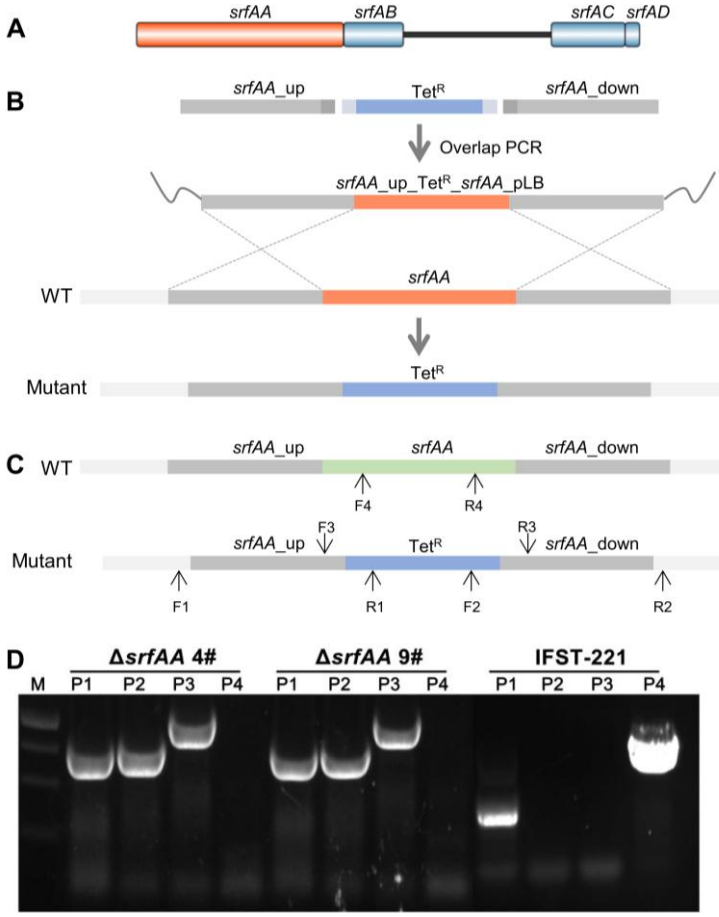

Figure 5-1 Generation of the *srfAA* deletion mutant by homologous recombination. (A) The key genes (*srfAA*, *srfAB*, *srfAC*, and *srfAD*) are related to surfactin production. (B) *srfAA* deletion strategy. *srfAA*_up, the upstream fragment of *srfAA* gene; *srfAA*_down, the downstream fragment of *srfAA* gene; Tet^R, tetracycline resistance gene cassette. (C) The location of detection primers to identify the *srfAA* mutant. (D) The PCR results were amplified by four detection primers. M, GeneRuler 1 kb DNA ladder.

3.2. Inhibitory ability of srfAA deletion mutants on the growth of F. verticillioides

Then, we test the antifungal activity of these mutants. As shown in Figure 5-2A, the mutants exhibited antifungal activity similar to that of the wild-type IFST-221 in the plate confrontation assay. Additionally, observation of bacterial morphology revealed that the wild-type strain exhibited a folded edge in long-term culture, distinguishing it from the mutants. Moreover, we tested the antifungal effect on *F.*

verticillioides-infected maize kernels. As shown in Figure 5-2B, maize kernels infected with *F. verticillioides* exhibited severe symptoms, while those treated with IFST-221 showed no signs of infection. The mutants Δ*srfAA* 4# and 9# strains also showed almost no symptoms.

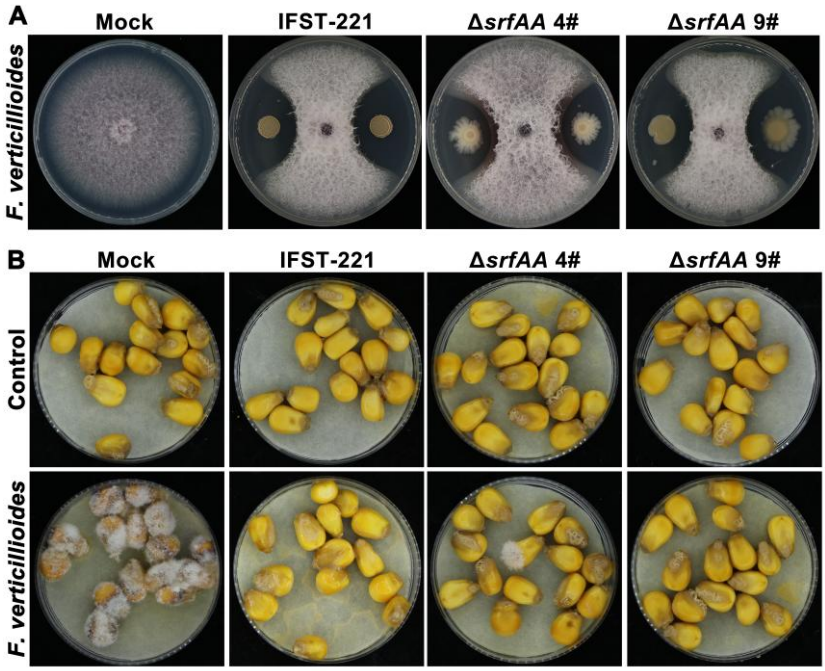

Figure 5-2 The biological activity of IFST-221 and its *srfAA* mutants (Δ*srfAA* 4# and 9#). (A) The antifungal activity of these strains *in vitro*. (B) Effect of these strains on the development of *F. verticillioides* in maize kernels. Maize kernels pretreated with ddH_2O or the strain's culture were then inoculated with *F. verticillioides* or ddH_2O. Representative photos were captured at 5 days post-inoculation.

However, the crude lipopeptide extract from IFST-221 and mutants Δ*srfAA* 4# and 9# exhibited different antifungal activities. As shown in Figure 5-3, the inhibition zone of mutants Δ*srfAA* 4# and 9# was smaller compared to that of the wild-type strain IFST-221. To further investigate surfactin production in these three strains, we analyzed their metabolite profiles. As shown in Figure 5-3, the wild-type IFST-221 exhibited sodiated molecules $[M + H]^+$ at *m/z* 1036.4, $[M + Na]^+$ at *m/z* 1044.3 and 1058.4, whereas none of these were detected in the mutants Δ*srfAA* 4# and 9#. This further confirmed the successful deletion of *srfAA* and the mutants' loss of surfactins production efficiency.

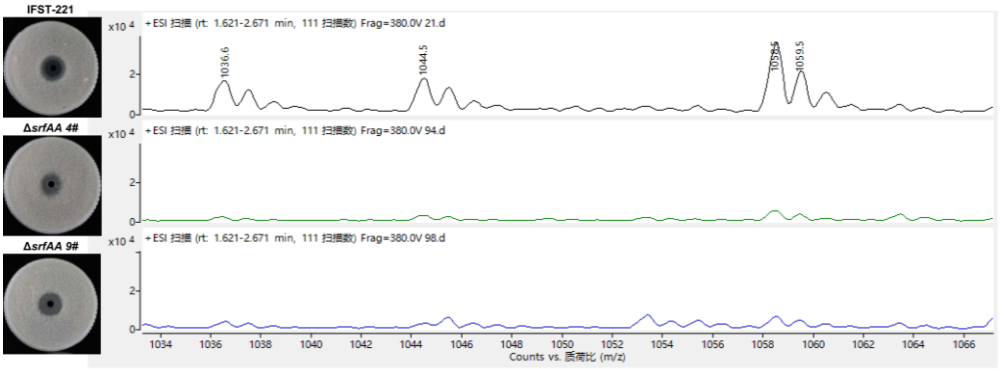

Figure 5-3 The antifungal activity and mass spectrum of the crude extract of IFST-221 and its *srfAA* mutants (Δ*srfAA* 4# and 9#).

3.3. Transcriptome sequencing of F. verticillioides under IFST-221 treatment

3.3.1. Data quality assessment and overall gene expression

(1) Sequencing data quality

Sequencing data quality was evaluated to ensure the reliability of downstream analysis. Each library generated ~13-17 million raw reads (3.93-5.07 Gb), of which ~12-16 million high-quality clean reads (3.68-4.79 Gb) were retained after filtering (Table 5-3). The overall error rate was below 0.01%, and Q20 and Q30 values exceeded 99% and 97%, respectively. GC content was stable across samples (52.74%-53.13%). These results indicate that the sequencing data were of high quality and suitable for subsequent transcriptomic analyses.

Table 5-3 Summary of RNA-seq data quality and read statistics for Fv and Fv+221 samples.

Sample	Raw reads (M)	Raw bases (G)	Clean Reads (M)	Clean bases (G)	Error rate (%)	Q20 (%)	Q30 (%)	GC (%)
Fv_1	15.80	4.74	15.40	4.62	0.01	99.29	97.69	52.92
Fv_2	15.60	4.68	15.11	4.53	0.01	99.30	97.75	52.76
Fv_3	16.26	4.88	15.76	4.73	0.01	99.32	97.80	52.74
Fv+221_1	16.68	5.01	15.98	4.79	0.01	99.28	97.68	52.98
Fv+221_2	16.89	5.07	15.81	4.74	0.01	99.28	97.71	53.13
Fv+221_3	13.11	3.93	12.28	3.68	0.01	99.29	97.70	52.87

(2) Mapping statistics

After quality filtering, clean reads were mapped to the *F. verticillioides* LNF15-11 reference genome using HISAT2. The overall alignment quality was high, with > 94.83% of reads successfully mapped and 94.29–96.59% uniquely aligned across all samples (Table 5-4). More than 90.19% of reads were properly paired, confirming the

accuracy of alignment. Approximately half of the reads aligned to each strand (positive vs. negative), consistent with the strand-specific RNA-seq protocol.

Table 5-4 Summary of read mapping statistics for Fv and Fv+221 samples.

Sample	Total reads (M)	Mapped reads (%)	Uniquely mapped (%)	Properly paired (%)	Strand distribution (pos/neg, %/%)
Fv_1	15.40	96.71	96.50	92.01	48.25/48.25
Fv_2	15.11	96.84	96.59	93.55	48.30/48.29
Fv_3	15.76	96.87	96.58	94.08	48.29/48.29
Fv+221_1	15.98	95.05	94.47	91.02	47.24/47.23
Fv+221_2	15.81	95.53	95.14	91.71	47.57/47.57
Fv+221_3	12.28	94.83	94.29	90.19	47.15/47.14

(3) Expression distribution and sample relationships

To investigate gene expression characteristics of *F. verticillioides* under stress from *B. velezensis* IFST-221, transcriptome-wide expression levels were quantified. Comparative analysis of FPKM values showed that the overall distribution and density curves were consistent between samples, suggesting that the datasets were comparable across replicates (Figure 5-4). Hierarchical clustering analysis (HCA) based on the expression of 8,290 genes demonstrated that the three biological replicates of each treatment clustered together into distinct branches, confirming high reproducibility (Figure 5-5A). Principal component analysis (PCA) further supported this result, showing tight grouping of replicates within each treatment and clear separation between Fv and Fv+221 samples (Figure 5-5B).

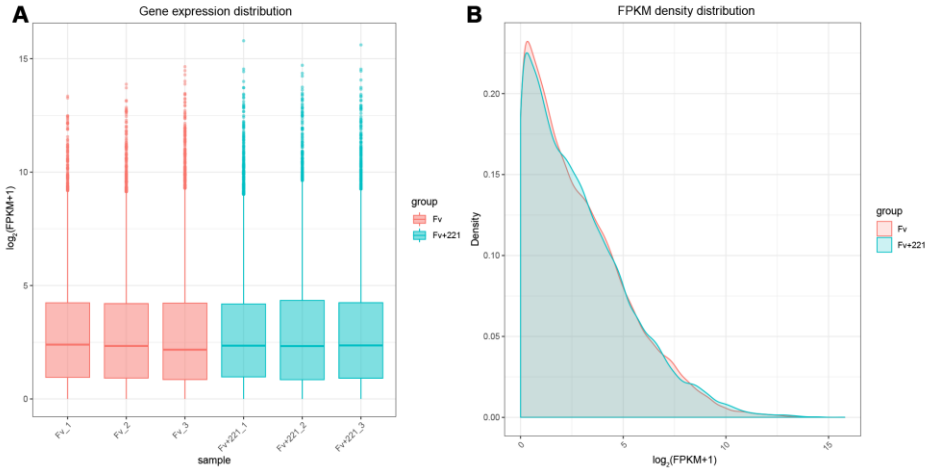

Figure 5-4 The gene expression distribution across samples, shown as boxplots (A) and density plots (B) of log_2(FPKM+1).

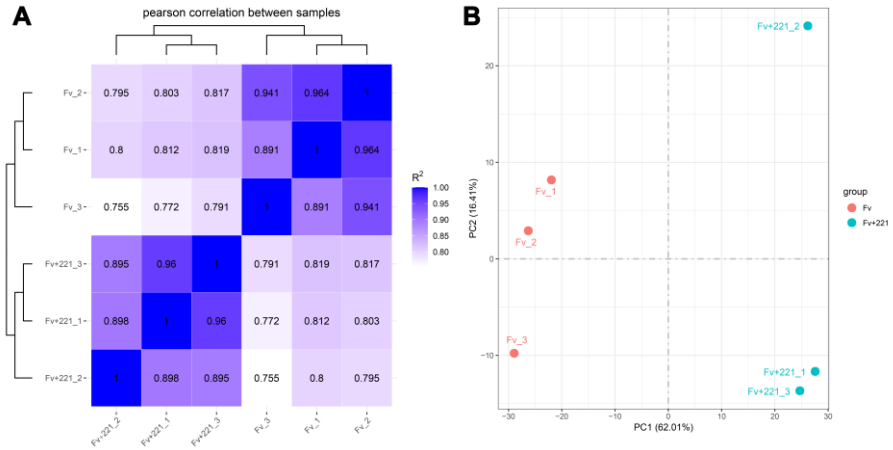

Figure 5-5 Sample-to-sample relationship of gene expression profiles between Fv and Fv+221 groups.

(A) Correlation heatmap of biological replicates. (B) Principal component analysis (PCA) of gene expression profiles.

In total, 8,290 expressed genes were expressed in the Fv group and 8,367 in the Fv+221 group. Among these, 7,468 genes were co-expressed across all samples, while 822 and 899 genes were uniquely expressed in the Fv and Fv+221 groups, respectively (Figure 5-6).

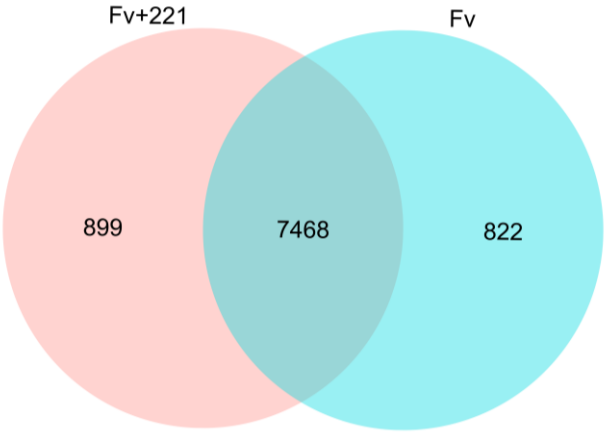

Figure 5-6 Venn diagram of total expressed genes in Fv and Fv+221 groups.

3.3.2. Differential expression analysis

(1) Overview of DEGs

Expressed genes with a fold change ≥ 2 and FDR < 0.05 were designated as differentially expressed genes. A total of 2,713 DEGs were identified in Fv vs. Fv+221 comparison, including 1,347 upregulated and 1,366 downregulated genes (Figure 5-7A). Among these comparisons, a total of 4,165 genes were differentially expressed, indicating a substantial reprogramming of the *F. verticillioides* transcriptome in response to IFST-221(Figure 5-7B). These results suggest that *B. velezensis* IFST-221 exerts a significant impact on fungal gene expression. Further functional enrichment analysis of these DEGs was performed to explore the molecular mechanisms underlying the antifungal activity of IFST-221.

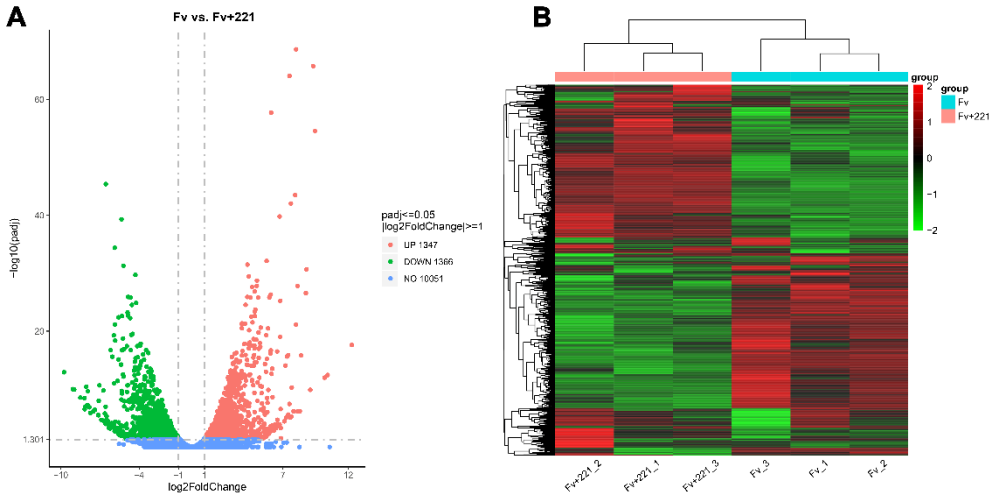

Figure 5-7 Differential expression analysis in the Fv vs. Fv+221 comparison. (A) Volcano plot showing significantly upregulated and downregulated genes. (B) Heatmap of hierarchical clustering of DEGs across biological replicates.

(2) GO enrichment analysis

Gene ontology analysis was performed to classify the functions of DEGs. A total of 2,713 DEGs from the Fv vs. Fv+221 comparison were categorized into 529 GO terms, which belong to three major GO categories: biological process (BP), cellular component (CC), and molecular function (MF) (Figure 5-8A). Among them, 11 GO terms were significantly enriched. Notably, although these terms were distributed across different GO categories, they could be included in protein biosynthesis and ribosome function. In BP, peptide biosynthetic process, translation, and related peptide/amide metabolic processes were among the most significant terms. In CC, the ribosome showed the strongest significance, followed by the ribonucleoprotein complex; broader terms (non-membrane-bounded organelle and intracellular non-membrane-bounded organelle) also appeared due to their large gene coverage. In MF, the structural constituent of ribosome and structural molecule activity were the most significant. This cross-category consistency indicates that the translational machinery was the most prominently affected process under IFST-221 treatment.

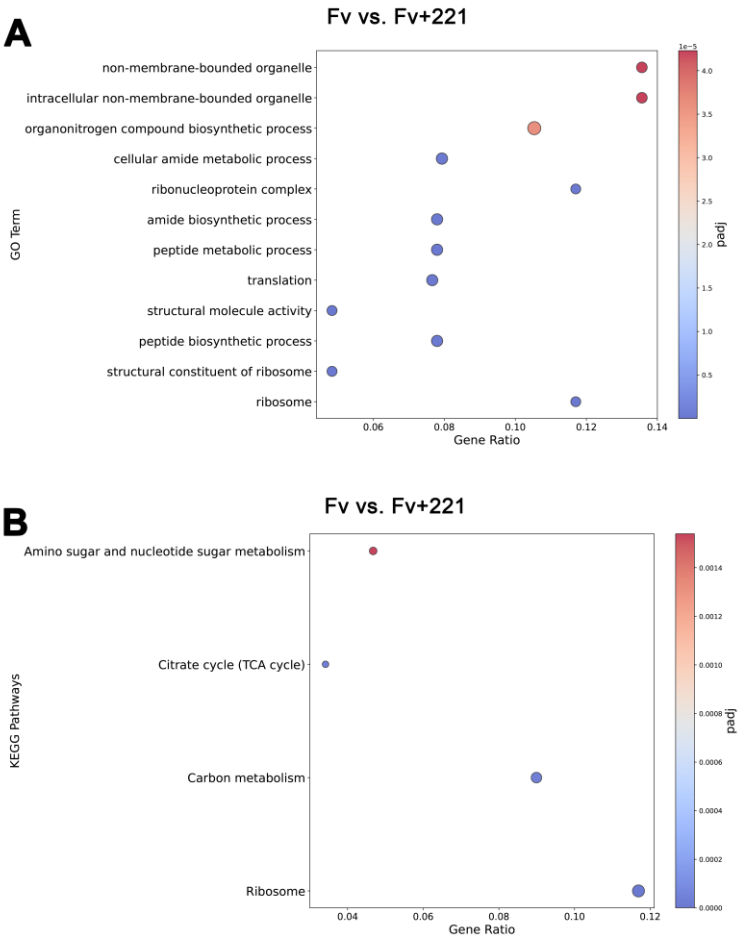

Figure 5-8 The GO (A) and KEGG (B) enrichment analyses in the Fv vs. Fv+221 comparison.

(3) KEGG enrichment analysis

To further examine the functional classifications and pathway assignments of DEGs, KEGG enrichment analysis was performed. Out of 2,713 DEGs, 108 pathways were annotated. Of these, four pathways were significantly enriched (*padj* < 0.05), including ribosome, carbon metabolism, TCA cycle, and amino sugar and nucleotide sugar metabolism (Figure 5-8B). Among them, the ribosome pathway was the most significantly enriched, in agreement with the GO results. The enrichment of carbon metabolism and TCA cycle indicates reprogramming of central energy metabolism, while amino sugar and nucleotide sugar metabolism points to potential remodeling of cell wall precursors. Together, these results highlight translational reprogramming as the most prominent effect of IFST-221 treatment, accompanied by adjustments in energy and cell wall-related metabolic pathways.

3.3.3. Functional categories of DEGs in the Fv vs. Fv+221 comparison

Comparative analysis of DEGs in the Fv vs. Fv+221 comparison was first carried out through GO and KEGG enrichment. GO enrichment revealed significant overrepresentation of ribosome- and translation-related terms, while KEGG pathway analysis highlighted ribosome, carbon metabolism, TCA cycle, and amino sugar and nucleotide sugar metabolism as significantly enriched pathways. In addition to these statistically enriched categories, we also examined stress-responsive processes in fungi, including cell wall and membrane integrity, antioxidant, and heat shock proteins, in which multiple DEGs were identified.

(1) Ribosome and translation-related DEGs

GO and KEGG enrichment analyses consistently highlighted ribosome- and translation-related categories as the most significantly affected in Fv vs. Fv+221 comparison (Figure 5-8). A total of 65 DEGs associated with ribosome structure and function were identified, including 24 small ribosomal subunit proteins, 39 large ribosomal subunit proteins, and two ubiquitin-ribosomal proteins (Supplementary Table A2-1). Most of these genes exhibited moderate but consistent upregulation ($1.01 < \log_2FC < 2.06$).

In addition to ribosomal structural components, GO terms such as translation, peptide metabolic process, and organonitrogen compound biosynthetic process were also significantly enriched, suggesting broader regulation of protein synthesis pathways. Furthermore, enrichment of structural molecule activity and ribonucleoprotein complex terms indicated coordinated changes in translation factors and ribonucleoprotein assembly. Together, these results suggest that IFST-221 treatment triggers pronounced translational reprogramming in *F. verticillioides*, which may represent an adaptive strategy to maintain protein synthesis under antifungal stress.

(2) Carbon metabolism and TCA cycle-related DEGs

KEGG pathway analysis revealed that carbon metabolism and citrate cycle (TCA cycle) were significantly enriched among the DEGs (Figure 5-8B). A total of 60 DEGs were mapped to these pathways (Supplementary Table A2-2). These genes are mainly involved in glycolysis, the TCA cycle, and associated metabolic branches.

In the glycolytic branch, fructose-bisphosphate aldolase (*fbaA*), pyruvate kinase (*pki1*), and mitochondrial malic enzyme (*mae1*) were significantly upregulated, suggesting an enhanced glycolytic flux and pyruvate conversion capacity. In contrast, phosphoenolpyruvate synthase (*ppsA*) was strongly downregulated, indicating restricted gluconeogenic potential.

For the TCA cycle, core enzymes including citrate synthase (*cit1*, *gltA*), aconitate hydratase (*acoA*), succinate dehydrogenase (*sdh1*, *sdh2*, *sdh3*), and malate dehydrogenase (*mdh1*) were markedly induced, consistent with an accelerated oxidative TCA cycle. By contrast, pyruvate carboxylase (*pyc*) was repressed, suggesting reduced anaplerotic replenishment of oxaloacetate.

Together, these transcriptional changes point to a reprogramming of central carbon fluxes, favoring energy and NAD(P)H production via glycolysis and the oxidative TCA cycle, while limiting gluconeogenic and anaplerotic pathways. Such adjustments likely support fungal stress adaptation by prioritizing redox balance and ATP supply over metabolic flexibility.

(3) Amino sugar and nucleotide sugar metabolism DEGs

KEGG analysis also revealed significant enrichment of DEGs in the amino sugar and nucleotide sugar metabolism pathway (Figure 5-8B). A total of 26 DEGs were mapped to this pathway (Supplementary Table A2-3), many of which are directly associated with chitin metabolism and cell wall biosynthesis. Genes involved in UDP-sugar precursor synthesis, such as *uap1* (UDP-N-acetylglucosamine pyrophosphorylase), *agm1* (phosphoacetylglucosamine mutase), and *uge1* (UDP-glucose 4-epimerase), were strongly upregulated, suggesting enhanced production of activated sugar donors.

For genes related to chitin metabolism, a mixed regulatory pattern was observed. Several chitinases, including acidic mammalian-like chitinase and chitotriosidase-1 (*chit1*), were strongly induced, whereas others, such as endochitinase B1 and additional endochitinase isoforms, were downregulated. Similarly, chitin synthases exhibited divergent expression: *chs1* and *chs3* were repressed, while *chsD* showed moderate upregulation. This combination of both induction and repression among members of the same functional family suggests that IFST-221 treatment caused a reprogramming of chitin degradation and synthesis in a gene-specific manner, rather than a uniform shift.

(4) Stress-responsive gene categories

In addition to the statistically enriched pathways described above, several DEGs were found to cluster into functional categories that are well known to contribute to fungal stress adaptation. Although these categories were not always enriched as complete pathways in the GO or KEGG analysis, manual inspection of DEG annotations revealed substantial transcriptional changes in genes involved in cell wall biosynthesis and remodeling, membrane sterol metabolism, antioxidant defense, autophagy, and heat shock protein chaperone systems. These stress-responsive categories represent core protective strategies that fungi deploy under environmental challenges and biocontrol pressure, and thus provide important insights into how *F. verticillioides* responds to *B. velezensis* IFST-221 treatment.

- Cell wall-related DEGs

Cyclic lipopeptide produced by *Bacillus* disrupts fungal cell wall synthesis, weakening cell wall strength under osmotic pressure (Q. Zhang et al., 2023). In this study, fungal mycelia treated with IFST-221 exhibited a similar balloon-like morphology, indicating significant cell wall damage, likely due to the stress induced by cyclic lipopeptides secreted by *B. velezensis* (Figure 5-10). Transcriptomic analysis revealed significant changes in genes associated with fungal cell wall biosynthesis and degradation in response to *B. velezensis* IFST-221. Multiple β-glucanase genes

involved in cell wall degradation were strongly downregulated, including exo-1,3-β-glucanase D (FVCG_014472), endo-1,6-β-glucanase (FVCG_009945), and endo-1,3(4)-β-glucanase (FVCG_004800), suggesting suppression of internal glucan breakdown. In contrast, genes encoding xylanase B (FVCG_007577) and lytic cellulose monooxygenase (FVCG_006024) were highly upregulated, indicating potential activation of hemicellulose and cellulose degradation pathways.

Regarding chitin metabolism, several chitinase genes (FVCG_012548 and FVCG_010163) were upregulated, while others (FVCG_000873, FVCG_014464, FVCG_013222, and FVCG_011221) were downregulated, reflecting a dynamic and possibly compensatory remodeling of the chitin network. Similarly, chitin synthase genes showed mixed regulation: FVCG_011937 and FVCG_011953 were upregulated, whereas others, such as FVCG_007902, FVCG_007672, and FVCG_008394, were downregulated. These results indicate a complex restructuring of the cell wall in response to bacterial antagonism, possibly aimed at reinforcing cell wall integrity or recycling wall components under stress.

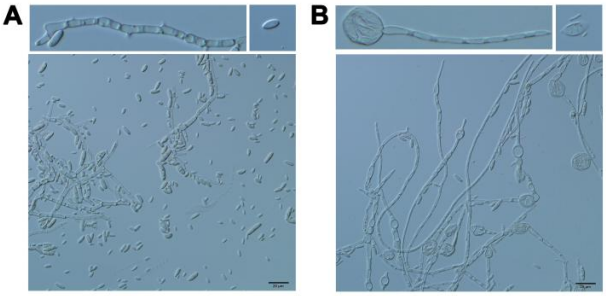

Figure 5-9 Hyphal and conidia morphology of *F. verticilllioides* co-cultivated with (B) or without (A) strain IFST-221. Scale bar, 20 μm.

- Cell membrane-related DEGs

Several differentially expressed genes involved in sterol and membrane lipid metabolism were identified in the comparison between Fv and Fv+221. The *erg4* gene (FVCG_007965), encoding sterol C-24 reductase responsible for the final step in ergosterol biosynthesis, was significantly downregulated. In contrast, the *cyp51* gene (FVCG_013279), encoding sterol 14-alpha demethylase (a key rate-limiting enzyme in the pathway), was highly upregulated (Eliaš et al., 2024). The regulatory gene *KES1* (FVCG_010334), which modulates sterol transport and homeostasis, was also strongly downregulated (Schulz & Prinz, 2007). Notably, a gene encoding sterol 3-β-glucosyltransferase (FVCG_012070) was upregulated, suggesting a shift toward sterol glucoside formation, possibly to regulate free sterol levels. Additionally, *PDAT* (FVCG_006349), encoding phospholipid: diacylglycerol acyltransferase, was upregulated, indicating enhanced phospholipid remodeling under bacterial stress. These alterations likely represent a stress adaptation strategy in response to *B. velezensis* IFST-221, aiming to modify the cell membrane under biotic stress.

- Antioxidant-related DEGs

Under the biotic and abiotic stress conditions, fungi activate antioxidant defense enzymes to eliminate reactive oxygen species, including superoxide dismutase, catalase, peroxidase, thioredoxin reductases, and glutathione reductases (Venkatarayappa & Dakshayini, 2023). Transcriptomic analysis revealed significant alterations in genes associated with reactive oxygen species (ROS) detoxification in *F. verticillioides* under *B. velezensis* IFST-221 stress. Two superoxide dismutase genes, *sod2* (FVCG_012854) and *sod5* (FVCG_001087), showed strong upregulation, suggesting enhanced dismutation of superoxide radicals. Among catalase-related genes, *cat1* (FVCG_002399) and *pod1* (FVCG_015156) were upregulated, while *cat2* (FVCG_005314) and *pod2* (FVCG_014928) were significantly downregulated, indicating a complex regulatory response to hydrogen peroxide stress. In addition, *ccp1* (FVCG_006740), encoding a mitochondrial cytochrome c peroxidase, was markedly upregulated, reflecting a mitochondrial ROS-scavenging response. The gene *ppoC* (FVCG_011260), putatively encoding a fatty acid oxygenase, also exhibited elevated expression, potentially linked to oxidative lipid metabolism or ROS signaling. The increased expression of these antioxidant genes suggests that *F. verticillioides* activates its oxidative stress response machinery as a defense mechanism to counteract the ROS accumulation triggered by IFST-221 treatment.

- Autophagy-related DEGs

Autophagy is required for proper vegetative growth, asexual/sexual reproduction, and full virulence in *Fusarium*, acting as a cellular response to stress by degrading damaged proteins and organelles via lysosomal pathways (Lv et al., 2017; H. Wang et al., 2025). Several autophagy-related genes were significantly upregulated in *F. verticillioides* upon treatment with *B. velezensis* IFST-221, suggesting activation of autophagic processes in response to bacterial stress. The core autophagy genes *atg*3 (FVCG_009136), *atg*9 (FVCG_006385), and *atg*29 (FVCG_003316) showed notable upregulation, indicating enhanced autophagosome formation and membrane recycling. *Atg*26 (FVCG_012070), a protein implicated in autophagosome maturation and possibly linked to sterol glucosylation, was also upregulated. Additionally, *Atg*22 (FVCG_000750), associated with vacuolar efflux of autophagic breakdown products, was moderately upregulated. These results suggest that autophagy may play a role in maintaining cellular homeostasis and mitigating damage under antagonistic stress.

-Heat shock protein-related DEGs

Heat shock proteins are highly conserved across all living organisms and are expressed in response to stress, with molecular weights ranging from 14 to 120 kDa (Jeyachandran et al., 2023). Exposure to *B. velezensis* IFST-221 led to a broad upregulation of heat shock protein (Hsp) genes in *F. verticillioides*, suggesting activation of protein quality control and stress response systems. Notably, several key molecular chaperones, including *Hsp90* (FVCG_011753), *Hsp88* (FVCG_011938), *Hsp98* (FVCG_010833), and *Hsp78* (FVCG_000976), were significantly upregulated. Mitochondrial chaperonins *Hsp60* (FVCG_006208) and *Hsp10* (FVCG_002597) also showed increased expression, indicating a potential role in maintaining mitochondrial protein homeostasis. Additionally, small heat shock protein (sHsp) domain-containing genes (e.g., FVCG_000828 and FVCG_001108) were upregulated, along with *STIP1* (FVCG_001717), a cochaperone that coordinates Hsp70-Hsp90 function. These results suggest that *F. verticillioides* responds to bacterial stress by enhancing its protein folding and refolding capacity, likely to mitigate damage caused by oxidative or structural stress.

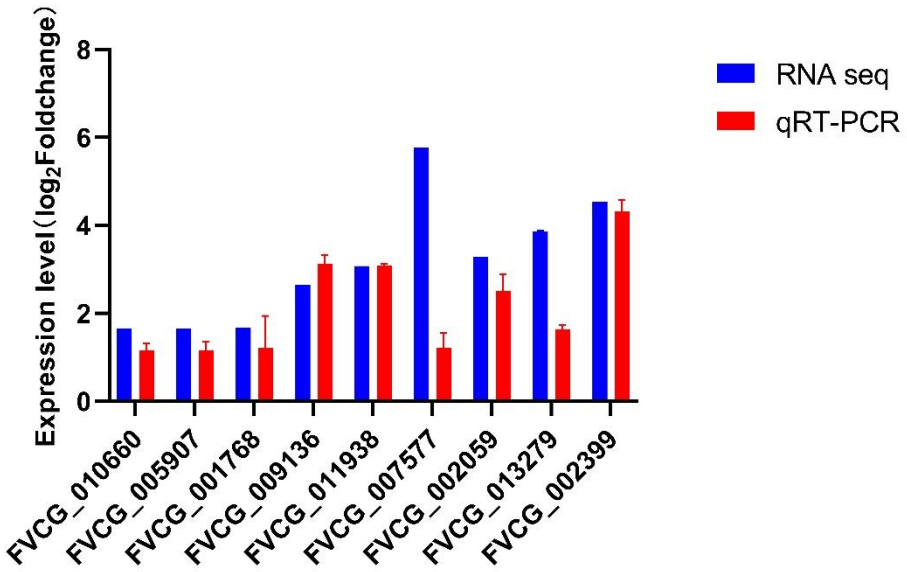

Figure 5-10 qRT-PCR was performed to validate the RNA-Seq-based differential gene expression analysis in *F. verticillioides* following exposure to *B. velezensis* IFST-221. A subset of DEGs was selected for validation based on their biological significance and expression patterns. The relative expression levels were normalized against an internal reference gene and calculated using the $2^{-\Delta\Delta Ct}$ method.

3.3.4. Integrated transcriptomic response model

To integrate the enriched pathways and stress-responsive categories, we constructed a model summarizing the transcriptomic reprogramming of *F. verticillioides* under IFST-221 treatment (Figure 5-11). The results indicate that primary metabolism was

markedly altered, particularly in amino sugar and nucleotide sugar metabolism, carbon metabolism, and the TCA cycle. Amino sugar and nucleotide sugar metabolism contributed to changes in cell-wall precursor supply, consistent with the observed remodeling of cell-wall-related enzymes such as chitin synthases and glucanases. Carbon metabolism and the TCA cycle were extensively reprogrammed, including glycolytic, pyruvate, and succinate dehydrogenase genes, suggesting altered energy fluxes and shifts in reducing equivalents production. These metabolic shifts are likely linked to enhanced ROS generation, which in turn triggers the induction of antioxidant enzymes, autophagy, and heat shock proteins.

In parallel, a lot of ribosome biogenesis and translation-related genes were strongly upregulated. This translational reprogramming may serve as a central hub, enabling the accelerated synthesis of essential proteins required for various stress responses, including antioxidant enzymes, heat shock proteins, autophagy components, and cell wall remodeling enzymes. Together, these findings suggest that IFST-221 imposes combined metabolic and oxidative stresses, to which *F. verticillioides* responds by reconfiguring its primary metabolism, activating stress defense systems, and reinforcing translational capacity.

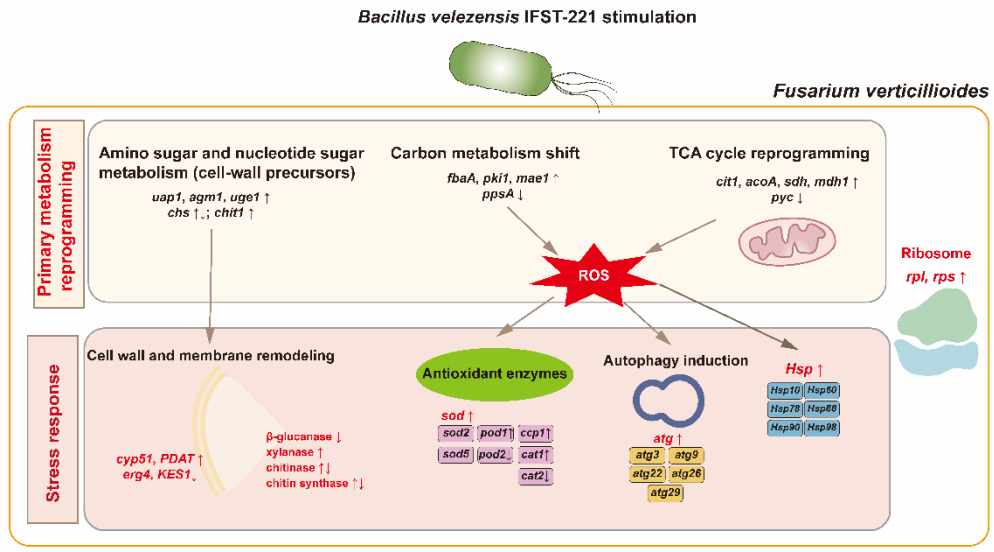

Figure 5-11 Integrated transcriptomic response model of *F. verticillioides* under IFST-221 treatment.

4. Discussion

B. velezensis IFST-221 has the potential for antifungal activity against *F. verticillioides* and biocontrol activity against maize ear rot. In this study, LC-MS/MS confirmed the production of surfactin by *B. velezensis* IFST-221, a well-known cyclic lipopeptide with broad-spectrum antimicrobial properties. Given the established roles of surfactin in disrupting cell membranes and inducing systemic resistance in plants,

its presence suggested a potential contribution to the observed antifungal effects against *F. verticillioides* (Jiang et al., 2016; Liu et al., 2012). Surprisingly, deletion of *srfAA*, a key gene for surfactin biosynthesis, did not impair the antagonistic effect in plate confrontation assays, while significantly reducing the antifungal activity of crude extracts. This suggests that surfactin, although an important component of *B. velezensis* IFST-221-derived lipopeptides, may not be the sole factor responsible for fungal inhibition under our experimental conditions. This observation is consistent with previous reports that iturins and fengycins are the major antifungal lipopeptides, especially *Fusarium* strains, whereas surfactins play more complementary roles (Cawoy et al., 2015; Falardeau et al., 2013; Ongena & Jacques, 2008).

In addition, the genetic architecture of the *srfA* operon should be considered when interpreting the phenotype of the *ΔsrfAA* mutant. In *B. velezensis* IFST-221, the competence gene *comS* is located entirely within the coding sequence of *srfAB,* and the srfA operon is transcribed from a single upstream promoter. Consequently, disruption of *srfAA* may exert a polar effect on downstream gene expression, potentially impairing *srfAB* transcription and abolishing *comS* production. Given the central role of ComS in competence development and global regulatory regulation (Danevčič et al., 2021), the observed phenotypes of the *ΔsrfAA* mutant may therefore reflect combined effects of surfactin deficiency and altered regulatory signaling. This genomic organization highlights an important limitation of full-gene knockout strategies within large NRPS operons and suggests that caution is required when attributing phenotypic changes exclusively to surfactin loss.

Genome mining with antiSMASH predicted gene clusters for surfactin and fengycin, while no typical iturin cluster was predicted as a famous lipopeptide of *Bacillus*. This may reflect either natural variation among *B. velezensis* strains or annotation ambiguity due to high similarity in NRPS domains. Consistent with these predictions, LC-MS/MS analysis detected surfactin under the tested conditions, whereas neither iturin nor fengycin peaks were observed, likely due to low production levels, conditional regulation of biosynthesis, or methodological sensitivity. For example, fengycin biosynthesis has been reported to be strongly induced in the presence of fungal pathogens (Cawoy et al., 2015), suggesting that IFST-221 might produce higher levels of these compounds under plant- or pathogen-associated conditions than under the culture conditions tested here. In addition to their individual effects, synergistic interactions between surfactin and other lipopeptides should also be considered, as surfactin has been shown to facilitate the insertion of iturins and fengycins into fungal membranes, thereby enhancing their antifungal potency (Cawoy et al., 2015). This may explain why deletion of *srfAA* reduced the activity of crude extracts but did not abolish antagonism in confrontation assays, as other lipopeptides could still act, potentially with reduced synergy. To establish causal links between individual lipopeptides and antifungal activity, further functional validation is required. Complementation of the *ΔsrfAA* mutants would help clarify the specific contribution of surfactin, while targeted deletion or inhibition of *fen* (fengycin) and *itu* (iturin) could provide direct evidence for their roles in fungal suppression.

Moreover, supplementation with purified surfactin or fengycin could test whether these compounds restore antifungal activity in deprived conditions. Although not included in this study, such experiments represent an essential next step toward defining the individual and cooperative contributions of the different lipopeptides of *B. velezensis* IFST-221.

The transcriptomic analysis provided mechanistic insights into how *F. verticillioides* responds to *B. velezensis* IFST-221. One of the most striking features was the strong enrichment of ribosome-related pathways. The activation of ribosome biogenesis and translation-associated processes is often considered a compensatory mechanism to sustain protein synthesis and safeguard essential functions under stress (Shore et al., 2021). Similar ribosomal upregulation has been observed in *Aspergillus niger* SICU-33 under alkaline stress (Zhang et al., 2024) and *Metarhizium anisopliae* exposed to heat (Wang et al., 2014), highlighting the conserved nature of this response across fungal species.

In addition to ribosomal adaptation, IFST-221 triggered broad metabolic reprogramming. Carbon metabolism and the TCA cycle were extensively reshaped, likely altering cellular energy fluxes and increasing mitochondrial activity (Nunes-Nesi et al., 2013). Such changes are tightly linked to ROS accumulation, which was consistent with the observed upregulation of antioxidant enzymes (*sod2*, *sod5*, *cat1*, and *ccp1*). At the same time, amino sugar and nucleotide sugar metabolism were significantly affected, suggesting a direct impact on the synthesis of structural precursors for chitin and glucans (Seifert, 2004). These alterations were accompanied by evidence of cell wall remodeling, including mixed regulation of chitin synthase genes and suppression of endogenous glucanases, which was consistent with the ballone-like hyphae observed microscopically in IFST-221-treated *F. verticillioides.*

The disturbance of central metabolism and redox homeostasis appears to have triggered secondary protective responses. Autophagy-related genes (*atg3*, *atg9*, *atg22*, *atg26*, *atg29*) were strongly upregulated, reflecting the need to recycle damaged organelles and maintain cellular viability. These autophagy components play essential roles in removing damaged organelles, particularly mitochondria, and recycling intracellular components to maintain homeostasis under stress conditions (Q. Wang et al., 2019). Similarly, heat shock proteins (*hsp90*, *hsp88*, *hsp60*, and several small HSPs) were induced, underscoring the importance of protein quality control during bacterial challenge (Tiwari et al., 2015). Together, these responses support a model in which metabolic imbalance, particularly in carbon and TCA cycle reprogramming, acts upstream to promote oxidative stress, which in turn activates antioxidant defenses, autophagy, and heat shock responses.

Finally, we validated selected DEGs by qRT-PCR. While the overall expression trends were consistent with RNA-seq, discrepancies in fold-change magnitude were observed for several genes (Figure 5-9). Such differences are commonly reported and may reflect technical factors such as the absence of primer efficiency determination and standard curve calibration, as well as biological factors such as reference-gene stability or post-transcriptional regulation. These limitations are acknowledged, and future work will incorporate efficiency testing and reference-gene validation

following Minimum Information for Publication of Quantitative Real-Time PCR Experiments (MIQE) guidelines to strengthen qRT-PCR validation (Bustin et al., 2009; Bustin et al., 2025). Despite these limitations, the RNA-seq data provide a robust overview of the major transcriptional adjustments induced by IFST-221.

Overall, the transcriptomic responses of *F. verticillioides* under IFST-221 challenge are consistent with those observed in fungi treated with purified CLPs. For example, iturin A inhibited *Aspergillus carbonarius* growth and ochratoxin A production, with transcriptome data revealing broad downregulation of genes involved in membrane function, transport capacity, osmotic regulation, redox balance, and energy metabolism, while morphological analysis showed cell swelling, thinning of cell wall and membrane, and mitochondrial damage (Jiang et al., 2020). These findings underscore that CLPs act not only through membrane disruption but also by perturbing core metabolic and transport processes, leading to systemic stress and organelle dysfunction. Our dataset, showing reprogramming of sterol biosynthesis, amino sugar metabolism, antioxidant defenses, autophagy, and TCA cycle, aligns with these observations and highlights that IFST-221 imposes a multi-layered pressure through CLP-driven mechanisms.

5. Conclusion

This study provides comprehensive insights into the antifungal mechanism of *B. velezensis* IFST-221 against *F. verticillioides*, a major pathogen of maize. By integrating LC-MS/MS analysis, gene knockout experiments, plate confrontation experiments, and transcriptomic profiling, we demonstrated that IFST-221 suppresses the pathogen through a multifaceted mechanism. Although surfactin was the only soluble metabolite detected under the tested conditions, deletion of *srfAA* only reduced extract-based antifungal activity without compromising overall inhibition in dual-culture or maize kernel assays, indicating the contribution of additional metabolites and complementary mechanisms. Transcriptome analysis further revealed that *F. verticillioides* adapts to bacterial antagonism by reprogramming primary metabolism (carbon metabolism, the TCA cycle, and amino sugar and nucleotide sugar pathway), together with ribosome biogenesis, cell wall and membrane remodeling, and stress-related pathways such as oxidative defense and proteostasis. Collectively, these findings advance our understanding of fungal adaptive responses to biocontrol agents and provide a molecular framework that may inform the future application of IFST-221 in the sustainable management of maize ear rot. Further functional validation of secondary metabolites and optimization of delivery strategies will be essential steps toward field translation.

Chapter 6

General discussion, conclusion, and perspectives

1. General discussion

1.1. Context

The purpose of this section is to integrate the findings of Chapters 3 to 5 and to assess whether their conclusions are consistent with each other and with the overarching objectives presented in Chapter 2. Chapter 3 established a rapid and field-deployable detection system for *F. verticillioides* based on an RPA-CRISPR/Cas12a assay targeting the *FUM1* gene, combined with a simple Chelex-100 DNA extraction protocol. Chapter 4 focused on the characterization of *B. velezensis* IFST-221, revealing strong antifungal activity against *F. verticillioides*, plant growth-promoting traits, and genome analysis enriched in plant growth-promoting related gene clusters. Chapter 5 further dissected the antifungal mechanism of IFST-221, showing that while surfactin was the lipopeptide detected under the test conditions, its deletion only moderately affected inhibition. Transcriptomic analysis of *F. verticillioides* revealed both reprogramming of primary metabolism, including carbon metabolism, the TCA cycle, and amino sugar and nucleotide sugar metabolism, and extensive stress responses involving oxidative stress adaptation, cell wall remodeling, ribosome-associated processes, autophagy, and heat shock proteins.

Collectively, the conclusions from these chapters are broadly consistent with one another and reinforce the strategy of rapid detection and effective biocontrol outlined in the objectives of this thesis. The diagnostic assay (Chapter 3) meets the need for timely identification of toxigenic *F. verticillioides*, while the characterization and mechanistic insights into IFST-221 (Chapters 4 and 5) highlight its potential as a sustainable control agent. Some apparent discrepancies, such as the limited contribution of surfactin compared to the genomic potential for other metabolites, do not contradict the overall conclusions but instead emphasize the multifaceted nature of the antagonistic interaction. Transcriptomic insights reinforce this view by revealing fungal stress responses cannot be attributed to a single metabolite but rather reflect combined or complementary effects. At the same time, the absence of detectable compounds beyond surfactin under the tested conditions reflects methodological and environmental constraints, underscoring the importance of context-dependent metabolite expression. Taken together, these observations indicate directions for future research while confirming the overall coherence of the thesis.

1.2. Rapid detection of F. verticillioides

1.2.1. Chelex-100-based DNA extraction for field-adaptable diagnostics

DNA extraction is a critical step in nucleic acid-based diagnostics, yet most existing methods depend on commercial kits designed for laboratory use. These kits typically employ silica gel column-based purification involving centrifugation and protein precipitation, which, although yielding high-purity DNA, are not suitable for on-site or low-resource settings due to their operational complexity (Claassen et al., 2013). Alternative fast extract methods, such as NaOH, rapid one-step extraction, Chelex 100, and proteinase K, have been proposed to simplify the procedure (Osmundson et

al., 2013). However, strong alkalinity of high NaOH levels posed a substantial risk to DNA integrity, compromising amplification efficiency or completely inhibiting enzymatic reactions (Bivehed et al., 2023). For instance, Xiao et al. evaluated the TPS solution (containing Tris, NaCl, and EDTA) combined with magnetic beads for fast DNA extraction from maize, which improved stability and yield for LAMP detection (Xiao et al., 2024). Compared to these approaches, the Chelex-100-based protocol developed in this study requires only heating in water, avoiding multiple high-speed centrifugations and minimizing inhibitor release. It successfully yielded DNA of sufficient quality to support downstream RPA amplification within 20 minutes, making it a robust and field-friendly solution.

Although the Chelex-100 protocol enabled successful amplification from naturally infected maize samples in this study, its robustness under broader conditions remains uncertain. Different maize tissues, storage states, and environmental conditions may contain varying levels of amplification inhibitors, and heterogeneous microbial communities may introduce additional complexity. While Chelex provides a rapid and low-cost alternative to kit-based extraction, further optimization and large-scale validation are required to ensure its stability and reproducibility across diverse sample types and field conditions.

As an angiosperm, the maize grain exhibits a unique structural composition that includes the pericarp, seed coat, endosperm, and embryo. Notably, the pericarp and seed coat derived from the maternal tissues are tightly fused in the mature grain, making them difficult to separate (Luo et al., 2023). This anatomical complexity, combined with the hard and fibrous nature of mature kernels and stalk tissues, necessitates the physical grinding of samples before crude DNA extraction. Moreover, *F. verticillioides* primarily colonizes internal tissues of maize stalks and roots, which are often asymptomatic in early stages (Xiong et al., 2024). Therefore, efficient tissue homogenization is critical for releasing sufficient quantities of pathogen DNA for successful amplification and detection. Although Chelex-100 enables crude DNA extraction without the need for multiple centrifugation or precipitation steps, optimizing field-compatible sample preparation for maize stalks and kernels remains a key area for further improvement. Future field implementations should explore portable grinding devices to ensure consistent and efficient processing across variable field conditions.

1.2.2. Specificity, sensitivity, and comparison with other detection methods

The assay showed strict specificity for *F. verticillioides*, with no cross-reactivity observed with other fungal pathogens. By targeting the *FUM1* gene, the system not only ensures species-level recognition but also directly links diagnosis with fumonisin biosynthesis, thereby providing unique relevance to food safety monitoring. This focus strengthens the assay for applications such as grain quality monitoring, export inspection, and toxin risk assessment.

In terms of sensitivity, the assay consistently detected about one genome copy per reaction, which is more sensitive than conventional PCR (0.1-1 ng, ~270 min), qPCR (13 fg, ~270 min), and LAMP (100fg, ~190 min), while requiring only about 73 min

(Nutz et al., 2011; Patiño et al., 2004; Zeng et al., 2018). The combination of RPA and CRISPR/Cas12a provides high amplification efficiency and signal specificity, but the ultra-high sensitivity also increases the risk of false positives. Therefore, careful handling and strict prevention of cross-contamination remain essential to ensure reliable results.

However, reliance on *FUM1* alone also imposes important limitations. Some *F. verticillioides* isolates carry the *FUM* cluster but do not produce fumonisins (Stępień et al., 2011). While some such isolates may not contribute to fumonisin contamination, they are still capable of causing ear and stalk rot and yield loss in maize. Moreover, fumonisin biosynthesis is not unique to *F. verticillioides*; other members in the *Fusarium fujikuroi* species complex, such as *F. fujikuroi*, *F. globosum*, *F. proliferatum*, *F. nygamai*, and *F. oxysporum,* also harbor the *FUM* cluster and represent significant contributors to fumonisin contamination (Plattner et al., 2004; Stępień et al., 2011). Multiplex or multi-species detection using RAA-CRISPR/Cas12a has already been demonstrated for *F. verticillioides*, *F. graminearum*, and *F. oxysporum*, confirming the feasibility of this approach for broader *Fusarium* surveillance (Su et al., 2025). In the present study, however, we deliberately focused on *F. verticillioides*-specific detection by targeting the *FUM1* gene, which directly links diagnosis to fumonisin biosynthesis and food safety monitoring. While our assay was implemented as a singleplex system, the platform is inherently compatible with multiplexing by integrating additional crRNAs and spatially separated read-outs on lateral flow strips. Such improvements remain perspectives for future development and were beyond the scope of this work.

1.2.3. Practicality and field applicability

The developed CRISPR/Cas12a assay demonstrated excellent analytical performance, with a detection limit of about one genome copy, strict specificity for *F. verticillioides*, and a total turnaround time of 73 minutes from crude sample to result. These features highlight its strong potential for early detection in field-oriented diagnostics, where rapid and sensitive pathogen identification is critical.

However, practical deployment of such assays is strongly influenced by cost considerations. The estimated per-sample cost includes approximately USD 4.3 for RPA reagents and an additional USD 6 for the lateral flow dipstick (Daher et al., 2016). Cheaper visual alternatives such as SYBR green I dye with UV visualization have been proposed, but they still require external equipment and may not be suitable in all field conditions (Zheng et al., 2021).

Moreover, the current system was validated under laboratory-optimized conditions and has not yet been deployed under real field circumstances. Its robustness under variable field environments, across diverse tissue types, and in the presence of heterogeneous microbial communities remains to be tested. In addition, several practical barriers must be considered for true field use: RPA and Cas12a reagents generally require cold-chain storage, raising concerns about stability during long-distance transport or under unstable ambient temperatures (Liu & Tsutsui, 2023); operation currently depends on pipettes and basic laboratory equipment like a heating

device and a small centrifuge; and visualization requires either the enspensives lateral flow strips or UV devices. These factors limit accessibility for farmers or non-specialist users.

With regard to the application stage, the current assay is most realistically suited for grain inspection and storage monitoring, where rapid screening for fumonisin-producing *F. verticillioides* is essential for food safety and trade. Although field-based surveillance is theoretically possible, further validation under variable environmental conditions would be required. Compared to Fumonisin ELISA Kits and LC-MS, which directly quantify fumonisins levels for regulatory purposes (S. Zhang et al., 2022), the RPA-CRISPR/Cas12a assay does not measure toxins; it detects *FUM1*-positive *F. verticillioides* as an upstream risk indicator, enabling rapid triage and selection of samples for confirmatory toxin testing. Accordingly, the two approaches are complementary rather than interchangeable. Relative to PCR and qPCR, the assay achieves comparable or higher sensitivity in a much shorter timeframe and without sophisticated equipment, making it particularly attractive for use in small laboratories, quarantine services, and grain inspection stations rather than direct farmer-level deployment.

1.3. Biocontrol potential of B. velezensis IFST-221

1.3.1. Antifungal and fumonisin-suppressing activity

The strain IFST-221 was originally isolated from the maize rhizosphere through antifungal screening against *F. verticillioides*. Consistent with this origin, IFST-221 exhibited robust inhibition of *F. verticillioides* growth in plate confrontation assays, with inhibition levels falling within the upper range typically reported for *Bacillus* spp. (28-78%) (Cavaglieri et al., 2005). Importantly, beyond restricting mycelial proliferation, IFST-221 also markedly suppressed FB_1 accumulation in maize kernels. While some *Bacillus* strains like *Bacillus* sp. 3 with high antifungal activity have paradoxically been associated with increased fumonisin levels (Cavaglieri et al., 2005), IFST-221 achieved an early and dramatic FB_1 reduction of more than 99% within five days of infection. In maize kernel assays, this suppression was closely correlated with reduced fungal biomass, indicating that toxin reduction was largely a consequence of growth inhibition. Nevertheless, the absence of *FUM* cluster induction in transcriptomic analyses suggests that IFST-221 does not provoke fumonisin biosynthesis under co-culture conditions, and may even interfere with secondary metabolic regulation in addition to limiting biomass. In addition to inoculation assays, soaking treatment of maize kernels with IFST-221 also effectively reduced FB_1 accumulation, highlighting seed- or kernel-based delivery as a feasible application strategy. Such approaches may enhance early colonization of the seed surface by beneficial bacteria, thereby protecting against fungal invasion at the earliest stages of infection.

From a mechanistic perspective, mass spectrometry analysis confirmed the presence of surfactins in IFST-221. However, deletion of the surfactin synthase gene *srfAA* markedly reduced the antifungal activity of crude extracts but did not impair growth inhibition in confrontation or kernel assays. This indicates that surfactins contribute

to extracellular activity but are not the primary antifungal determinants under direct interaction conditions. Similar observations have been reported for *B. subtilis* subsp. *krictiensis* ATCC55079, where an *srfAB* mutant showed significantly higher antifungal activity against *F. oxysporum* than the wild-type strain, which produced both iturin and surfactin (Kim et al., 2017). Moreover, the type and abundance of cyclic lipopeptides (CLPs) produced by *Bacillus* are context-dependent. For example, *B. amyloliquefaciens* subsp. *plantarum* S299 produced surfactin, fengycin, and iturin in LB medium, whereas maize root exudates induced much higher fengycin production, demonstrating that the culture environment can strongly alter the CLP profile, often with surfactin occupying a larger proportion even in different cultures (Zihalirwa Kulimushi et al., 2017). In addition, the combined application of surfactin and fengycin was reported to reduce antifungal activity against *Verticillium dahliae* and *Rhizopus stolonifer* (Liu et al., 2014). Two mechanisms have been proposed to explain this phenomenon: surfactin may stabilize fungal membranes in a way that counteracts the pore-forming activity of fengycin, or surfactin and fengycin may co-aggregate under certain conditions to form inactive complexes (Albarracín Orio et al., 2020; Zihalirwa Kulimushi et al., 2017). Together, these findings suggest that while surfactins are abundant and bioactive, their role in antifungal activity is complex and context-dependent. For IFST-221, the lack of impaired antagonism in the *srfAA* mutant implies that fengycins and iturins likely play more central roles in suppressing *F. verticillioides*, because their biosynthetic clusters are intact in the genome.

Collectively, these findings highlight IFST-221's distinctive dual capacity to suppress both fungal growth and fumonisin biosynthesis, distinguishing it from *Bacillus* strains that exhibit antagonism but fail to reduce toxin accumulation. Such dual functionality makes IFST-221 a particularly promising candidate for the sustainable management of maize ear rot and fumonisin contamination.

1.3.2. Plant growth-promoting potential of *B. velezensis* IFST-221

In addition to its antifungal activity, IFST-221 also exhibited plant growth-promoting (PGP) potential, particularly by enhancing aboveground biomass in seedling assays. Nutrient-deficient culture tests indicated multiple beneficial traits, including nitrogen fixation, phosphate and potassium solubilization, and biofilm formation, and genomic analysis further supported the partial presence of biosynthetic and functional pathways for these traits.

However, such characteristics were preliminarily tested under controlled laboratory conditions, typically on the culture media, and their expression in the complex rhizosphere environment remains uncertain. The realization of PGP traits in soil depends on multiple factors, such as microbial competition, soil physicochemical properties, and interactions with host plant root exudates. For example, biofilm formation can be triggered by specific plant polysaccharides such as pectin, xylan, and arabinogalactan (Beauregard et al., 2013), rather than by root exudates. Likewise, IAA production, another common PGPR trait, is typically tryptophan-dependent and partially regulated by plant-exuded tryptophan, like *B. velezensis* FZB42, although some *Bacillus* strains have been shown to possess tryptophan-independent pathways

(Goud et al., 2025; Idris et al., 2007; Persello-Cartieaux et al., 2003). Notably, IAA-deficient mutants of *B. velezensis* SQR9 still retained partial plant growth-promoting ability, suggesting that other factors, such as volatile compounds and extracellular enzymes, also contribute (Shao et al., 2015).

Therefore, while IFST-221 displays promising PGP features *in vitro*, future studies are needed to evaluate its ecological fitness, rhizosphere colonization capacity, and functional expression of key PGP traits under realistic soil conditions. Such work will be essential to determine its reliability and effectiveness as a biofertilizer in field applications. In this study, preliminary greenhouse pot experiments with maize, cotton, tomato, and broccoli seedlings further indicated growth promotion by IFST-221 under non-sterile substrate conditions. However, as the bacterial suspension was applied directly from culture broth without cell washing, potential contributions of residual medium nutrients cannot be fully excluded. Although control treatments received equivalent volumes of balanced NPK fertilizer solution to minimize confounding effects, more rigorous future assays should employ washed cell suspensions and field soils to better reflect ecological relevance.

1.3.3. Application practices and challenges

In this work, different application methods were employed depending on the experimental system. In plant growth promotion assays, IFST-221 was delivered to the rhizosphere by soil drenching, ensuring direct interaction with the maize root system. For maize kernel assays, the bacterial suspension was applied through spraying or kernel soaking to achieve effective contact between the inoculant and infection sites. In the greenhouse experiment against *Verticillium dahliae* on cotton plants, soil drenching was also adopted as the delivery method. These approaches were effective for validating the beneficial effects of IFST-221 under controlled conditions, but they required relatively high inoculum densities (10^9 CFU/mL) and large volumes of liquid suspension, a limitation common to many laboratory studies of beneficial *Bacillus* spp. (Chaurasia et al., 2020; Rahman et al., 2018). An additional limitation of the *Verticillium* wilt assay is the bacterial treatment contained in the culture medium. Although our results clearly indicated a protective effect of IFST-221, we cannot entirely exclude nutritional contributions, a similar limitation common to many laboratory studies of beneficial *Bacillus* spp. (L. Wang et al., 2025). Future assays should therefore incorporate matrix-matched medium controls to rigorously separate nutrient effects from biocontrol activity.

Although *Bacillus* species are generally capable of persisting in soil through endospore formation, their colonization dynamics are strongly influenced by soil type, crop growth stage, and microbial competition. Commercial examples, such as *B. subtilis* QST713 (marketed as SERENADE®), have demonstrated that *Bacillus*-based biocontrol products can be safe, effective, and capable of providing season-long disease protection (EPA, 2006). Nevertheless, even such well-established products must undergo extensive regulatory evaluation, including assessments of human health risks, environmental hazards, and risk mitigation strategies, before registration and commercialization (EPA, 2000).

Recent studies further highlight the complexity of rhizosphere colonization. For instance, a microfluidics-based iRhizo-Chip platform revealed that *B. subtilis* exhibits diurnal fluctuations in rhizosphere colonization, primarily driven by dissolved oxygen and pH (Dai et al., 2024). These findings underscore that the persistence and efficacy of IFST-221 in the field will depend not only on its intrinsic traits but also on fluctuating environmental conditions. In parallel, the biocontrol potential of *B. velezensis* IFST-221 emerges as a multifactorial trait resulting from the combined action of antimicrobial metabolites, regulatory networks, and ecological adaptability. Genome mining, chemical profiling, and functional analyses collectively indicate that antifungal activity cannot be attributed to a single dominant compound, such as surfactin, but rather reflects the coordinated contribution of multiple lipopeptides and their context-dependent regulation. Moreover, the genetic organization of large biosynthetic operons underscores the need for cautious interpretation of mutant phenotypes, as operon-level effects may influence both metabolite production and regulatory pathways. Taken together, while IFST-221 shows strong promise in laboratory and greenhouse assays, translating it into a registered biocontrol product will require overcoming challenges in formulation, application strategy, ecological monitoring, and regulatory approval, highlighting the long path from experimental validation to sustainable field deployment.

1.4. Fungal transcriptomic responses

Building on the results presented in Chapter 5, here we further interpret the transcriptomic responses of *F. verticillioides* to *B. velezensis* IFST-221 challenge and compare them with reported *Bacillus* cyclic lipopeptide (CLP) activities. Our dataset revealed broad transcriptional reprogramming across multiple cellular processes. Ribosome-related pathways were strongly enriched, including ribosome biogenesis, peptide metabolism, and structural ribosomal RNA components. Such upregulation is generally viewed as a compensatory strategy to sustain protein synthesis under stress. Comparable ribosomal activation has been reported in *Aspergillus niger* and *Metarhizium anisopliae* exposed to abiotic stresses, suggesting that ribosome biogenesis is a conserved fungal stress adaptation (Chen et al., 2024; Pava-Ripoll et al., 2011).

Primary metabolism was also markedly affected. Genes in carbon metabolism, the TCA cycle, and amino sugar and nucleotide sugar metabolism were differentially regulated, indicating disturbances in energy production and precursor supply. Because amino sugar pathways provide substrates for chitin and glucan biosynthesis, their alteration is consistent with structural remodeling of the fungal cell wall (Verbančič et al., 2018). Enhanced TCA cycle activity further links to ROS accumulation, and indeed, strong induction of antioxidant enzymes, autophagy genes, and multiple heat shock proteins was observed, pointing to oxidative stress and the activation of cellular quality-control mechanisms.

Many of these changes align with known CLP activities (Jiang et al., 2020; Yuan et al., 2025; D. Zhang et al., 2022). Iturins and fengycins disrupt fungal membranes by binding ergosterol and other lipids; correspondingly, sterol biosynthesis genes (erg4,

cyp51) were upregulated in *F. verticillioides*, echoing previous findings in *Aspergillus carbonarius* under iturin A (Jiang et al., 2020). In addition, CLPs have been shown to interfere with fungal cell wall metabolism, and our data similarly revealed altered expression of chitinase and glucanase genes along with enrichment of amino sugar pathways. The hallmark induction of oxidative stress by CLPs through mitochondrial disturbance was also evident in our dataset, as reflected by antioxidant, autophagy, and HSP responses. Moreover, carbon and TCA cycle rewiring may represent secondary adjustments to meet elevated energy demands under CLP-induced stress, consistent with observations in *F. graminearum* treated with iturins and fengycins (Yuan et al., 2025).

Taken together, the transcriptomic data indicate that IFST-221 imposes multifaceted pressures, including membrane and cell wall perturbation, metabolic imbalance, and oxidative stress, which converge on a coordinated fungal response integrating ribosome activation, metabolic rewiring, antioxidant defenses, and protein stabilization. Consistent with our genetic evidence that surfactin plays only a limited role, these broad transcriptional changes point to the combined impact of multiple *Bacillus*-derived metabolites. By documenting transcriptome-wide changes in pathways spanning primary metabolism, structural integrity, and stress adaptation, this work refines the mechanistic framework of *Bacillus-Fusarium* interactions.

2. Conclusion

This study developed and validated an integrated strategy for the sustainable management of *F. verticillioides* in maize, combining rapid field-deployable detection with biological control. A CRISPR/Cas12a-based assay was established that enables highly sensitive and specific diagnosis within a short time frame and without reliance on sophisticated laboratory infrastructure, demonstrating strong potential for early warning and on-site surveillance.

In parallel, *B. velezensis* IFST-221 was characterized as a promising biocontrol agent with both antifungal and plant growth-promoting capacities. The strain inhibited fungal growth, markedly reduced fumonisin accumulation in maize kernels, and exhibited multiple genomic traits, supported by genome mining and manual curation, consistent with secondary metabolite biosynthesis and rhizosphere adaptation.

Mechanistic insights further highlighted the multifactorial nature of IFST-221-mediated antagonism. Although surfactins were detected and contributed to extracellular antifungal activity, functional analysis revealed that they were not the sole determinants, implying a broader metabolite network. Transcriptomic profiling of *F. verticillioides* under bacterial challenge revealed reprogramming of primary metabolism, cell wall and membrane-related genes, and stress-adaptive pathways such as antioxidant defense, autophagy, and heat shock proteins. These findings illustrate the dynamic interaction between *B. velezensis* IFST-221 and its fungal target and provide a molecular framework for optimizing biocontrol efficacy.

Collectively, this work establishes a dual approach, including early pathogen detection and effective biological suppression, which contributes to sustainable maize protection and food safety. The originality of this thesis lies less in describing entirely

new mechanisms than in refining and contextualizing them for the *F. verticillioides*. Specifically, the RPA-CRISPR/Cas12a assay was tailored to the *FUM1* gene and combined with a simplified extraction method to strengthen its relevance for fumonisin risk assessment. In parallel, the systematic evaluation of *B. velezensis* IFST-221 linked genome-level evidence with antagonistic and plant growth-promoting traits, while the integration of gene knockout and transcriptomics provided a more nuanced view of lipopeptide contributions, showing the limited role of surfactin and highlighting broader fungal metabolic and stress responses.

3. Perspectives

3.1. Practical challenges and validation needs for assay deployment

For the RPA-Cas12a-LFD assay developed in this study to achieve practical impact, extensive field validation is required. Although the use of Chelex-100 resin provides a rapid, equipment-free DNA extraction method, maize tissues pose notable challenges for field application. Mature kernels and stalks are structurally complex and often colonized internally by *F. verticillioides*, especially at asymptomatic stages, making efficient tissue homogenization essential for releasing detectable DNA. While Chelex 100-based extraction avoids laborious centrifugation steps, further optimization of field-compatible sample preparation will be necessary to ensure consistent assay performance, such as portable grinding devices under variable field conditions.

In addition, broader validation is critical to confirm the robustness and applicability of the assay. A key limitation of the present study is that field validation was restricted to maize ear samples collected from Shanxi Province, China. Given that *F. verticillioides* is widely distributed across diverse agroecological zones in China and worldwide, and can colonize not only maize tissues but also stored grains and processed food products, multi-provincial and multi-matrix validation will be essential to establish generalizability. Moreover, *F. verticillioides* populations exhibit considerable genomic diversity, and fumonisin biosynthetic genes show evolutionary divergence among different *Fusarium* species (Stępień et al., 2011). Standardized protocols for sampling, DNA extraction, and assay execution should therefore be tested across multiple geographic regions, maize varieties, and natural infection contexts, particularly in grain storage and export monitoring. Such efforts will be essential to establish the robustness, sensitivity, and applicability of the assay for large-scale agricultural deployment.

3.2. Clarifying the role of iturin and fengycin in IFST-221 antagonism

Although surfactins were confirmed in IFST-221 and shown to contribute to extracellular antifungal activity, genomic analysis also revealed intact biosynthetic clusters for other lipopeptides, including iturin and fengycin. These compounds are well recognized as major antifungal determinants in *Bacillus* spp., yet they were not

detected under the extraction conditions applied in this study. Future work should optimize extraction and detection (e.g., resin/SPE enrichment coupled to LC-MS/MS) under plant-mimicking conditions (maize root exudates, or separated co-culture with *F. verticillioides*) to improve recovery of non-surfactin CLPs.

In parallel, functional genetics (targeted deletion and complementation of *fen* and *itu* biosynthesis genes), including the construction of double and triple mutants (e.g., *ΔituΔfen*, *ΔituΔfenΔsrfAA*), together with activity-guided fractionation/reconstitution, can causally link specific molecules to antifungal and FB_1-suppressing effects, while also testing reported interactions between surfactin and fengycin. Given the operon architecture of the *srfA* locus in IFST-221, future genetic designs should also minimize polar effects (e.g., in-frame domain deletions or regulatory-gene complementation) to disentangle surfactin loss from operon-level regulatory consequences. Such approaches will clarify whether these metabolites act independently, synergistically, or redundantly with surfactin and will provide a more complete understanding of the multifactorial antagonistic mechanism of IFST-221. Finally, these insights will support rational improvement of strain performance.

3.3. Toward practical application strategies of IFST-221

In this study, IFST-221 was applied as a liquid suspension, either through soil drenching in plant growth and *Verticillium dahliae* assays or by soaking maize kernels to protect against *F. verticillioides*. These approaches ensured effective contact between the bacterium and the host plant or infection sites, leading to clear antifungal and growth-promoting effects. However, they relied on relatively high inoculum densities, which may limit scalability and economic feasibility for large-scale agricultural deployment. Optimizing the minimal effective dose, therefore, represents an immediate priority for bridging laboratory efficacy with field application.

Beyond dosage, the application method is equally important for the practical deployment of IFST-221. Soil drenching represents a feasible strategy for root-associated pathogens, whereas seed soaking demonstrates the potential of seed-based delivery. Building on these results, seed-coating formulations represent a logical next step, offering controlled bacterial application while maintaining seed germination and early seedling vigor. Seed coating is particularly advantageous because it allows uniform delivery of bacterial spores at low doses, facilitates handling and storage, and can be readily integrated into existing seed treatment practices used by farmers and seed companies (Rocha et al., 2019). However, to move toward practical application, further work is needed to determine the minimal effective dose compatible with coating, to ensure long-term viability of IFST-221 spores on seeds, and to confirm that seed germination and early growth are not negatively affected under diverse storage and field conditions. Recent advances in microbial seed coating emphasize that successful deployment requires not only demonstrating efficacy but also ensuring microbial survival on seeds, compatibility with germination, stability during storage, and consistent field performance under variable conditions (Paravar et al., 2023).

While seed coating appears as the most realistic short-term strategy, soil application may represent a longer-term possibility. Before large-scale deployment, however,

several aspects would need to be addressed. First, root colonization and persistence of IFST-221 in the soil-plant interface should be confirmed through strain-specific molecular assays and culture-based recovery. Second, impacts on the soil microbiome need to be evaluated, since *Bacillus* spp. are known to modulate microbial community composition and interactions, which may have both beneficial and unintended outcomes (Sun et al., 2022). Third, plant-mediated effects such as ISR and plant growth promotion should be validated under field conditions, as these functions are context-dependent and may vary across soil types and crop genotypes (Xia et al., 2024). Finally, potential influences on soil physicochemical properties (e.g., nutrient cycling, pH, enzyme activities) should be monitored to ensure compatibility with sustainable soil management (Xia et al., 2025). Moreover, the background state of field microbial communities will strongly influence the establishment and performance of IFST-221, underscoring the need for multi-location trials and long-term ecological assessment.

Together, these findings suggest that near-term development should concentrate on improving liquid application methods and advancing seed treatment strategies, both of which are directly supported by current experimental evidence. Broader formulation technologies or synergistic combinations with other agents remain attractive in the long term, but their development requires additional optimization and validation.

3.4. Future directions for omics integration and functional validation

Our metabolomics survey did not detect significant changes in fumonisin levels under the current assay conditions, suggesting that host context may be essential to reveal toxin modulation. To resolve this, co-culture integrating *B. velezensis*, *F. verticillioides*, and maize should be considered. Combining transcriptomics with proteomics and metabolomics to better capture plant-mediated effects and distinguish between contact-dependent and secreted-factor interactions (Du Toit, 2025; Sanches et al., 2024).

On the bacterial side, prior evidence suggests that perturbation of one lipopeptide pathway can be accompanied by shifts in the production of other secondary metabolites; however, whether such compensatory changes occur in IFST-221 remains to be tested. Importantly, because large NRPS operons can show polar effects, transcriptomic and metabolomic profiling of mutants should be interpreted alongside verification of downstream gene expression (e.g., *srfAB* and *comS*), especially when using *srfAA*-targeted mutants. Addressing these questions will require multi-omics analyses in combination with targeted mutants (Δ*srfAA*, Δ*fen*, Δ*itu,* and combinations), chemical complementation, and investigation of regulatory pathways controlling cyclic lipopeptide biosynthesis to explain potential re-wiring.

On the fungal side, our transcriptomic analysis revealed that the response of *F. verticillioides* to IFST-221 treatment involves primary metabolism, cell wall remodeling, membrane sterol metabolism, oxidative stress resistance, ribosome

biogenesis, and heat shock proteins. Future work should integrate transcriptomics with proteomics and metabolomics to validate whether these transcriptional changes are reflected at protein and metabolite levels (Gallart et al., 2025). Targeted functional validation, such as gene knockouts in *F. verticillioides*, will be crucial to establish causal links between adaptive responses and bacterial inhibition.

Collectively, plant-contextualized multi-omics combined with mutant validation will enable rigorous evaluation of when and whether fumonisin is modulated in realistic host environments, the extent to which lipopeptide networks contribute to antifungal and FB_1-suppressing effects, and specific, testable molecular targets on both partners that can guide dosage and delivery strategy optimization.

Chapter 7

References

Abdel-Aziz, S. M., Abo Elsoud, M. M., & Anise, A. A. H. (2017). Chapter 2 - microbial biosynthesis: A repertory of vital natural products. In A. M. Grumezescu & A. M. Holban (Eds.), *Food biosynthesis* (pp. 25-54). Academic Press.

Accinelli, C., Abbas, H., & Shier, W. (2018). A bioplastic-based seed coating improves seedling growth and reduces production of coated seed dust. *Journal of Crop Improvement*, *32*, 1-13.

Adeniji, A. A., & Babalola, O. O. (2022). Evaluation of *Pseudomonas fulva* PS9.1 and *Bacillus velezensis* NWUMFKBS10.5 as candidate plant growth promoters during maize-*Fusarium* interaction. *Plants*, *11*(3), 324.

Aghcheh, R. K., & Braus, G. H. (2018). Importance of stress response mechanisms in filamentous fungi for agriculture and industry. In M. Skoneczny (Ed.), *Stress response mechanisms in fungi: Theoretical and practical aspects* (pp. 189-222). Springer International Publishing.

Ajayi, O. O. (2024). Chapter 19 - toxicity and safety of essential oil. In C. O. Adetunji & J. Sharifi-Rad (Eds.), *Applications of essential oils in the food industry* (pp. 235-241). Academic Press.

Ajuna, H. B., Lim, H.-I., Moon, J.-H., Won, S.-J., Choub, V., Choi, S.-I., Yun, J.-Y., & Ahn, Y. S. (2023). The prospect of hydrolytic enzymes from *Bacillus* species in the biological control of pests and diseases in forest and fruit tree production. *International Journal of Molecular Sciences*, *24*(23), 16889.

Akohoue, F., & Miedaner, T. (2022). Meta-analysis and co-expression analysis revealed stable QTL and candidate genes conferring resistances to *Fusarium* and *Gibberella* ear rots while reducing mycotoxin contamination in maize. *Frontiers in Plant Science*, *13*, 1050891.

Albarracín Orio, A. G., Petras, D., Tobares, R. A., Aksenov, A. A., Wang, M., Juncosa, F., Sayago, P., Moyano, A. J., Dorrestein, P. C., & Smania, A. M. (2020). Fungal-bacterial interaction selects for quorum sensing mutants with increased production of natural antifungal compounds. *Communications Biology*, *3*(1), 670.

Alikhan, N.-F., Petty, N. K., Ben Zakour, N. L., & Beatson, S. A. (2011). Blast ring image generator (BRIG): Simple prokaryote genome comparisons. *BMC Genomics*, *12*(1), 402.

Almeida, N. A., Freire, L., Carnielli-Queiroz, L., Bragotto, A. P. A., Silva, N. C. C., & Rocha, L. O. (2024). Essential oils: An eco-friendly alternative for controlling toxigenic fungi in cereal grains. *Comprehensive Reviews in Food Science and Food Safety*, *23*(1), e13251.

Anju, S., Aparna, Y., Bhima, B., & Sarada, J. (2018). Novel insights on the *Bacillus* quorum sensing mechanism: Its role in competence, virulence, sporulation and biofilm formation. In B. Pallaval Veera (Ed.), *Implication of quorum sensing system in biofilm formation and virulence* (pp. 313-327). Springer Singapore.

Assena, M. W., Pfannstiel, J., & Rasche, F. (2024). Inhibitory activity of bacterial lipopeptides against *Fusarium oxysporum* f.sp. *Strigae*. *BMC Microbiology*, *24*(1), 227.

Ayer, K. M., Strickland, D. A., Choi, M., & Cox, K. D. (2021). Optimizing the integration of a biopesticide (*Bacillus subtilis* QST 713) with a single-site fungicide (benzovindiflupyr) to reduce reliance on synthetic multisite fungicides (captan and mancozeb) for management of apple scab. *Plant Disease*, *105*(11), 3545-3553.

Ayesha, M. S., Suryanarayanan, T. S., Nataraja, K. N., Prasad, S. R., & Shaanker, R. U. (2021). Seed treatment with systemic fungicides: Time for review. *Frontiers in Plant Science*, *12*, 654512.

Bai, J., Lin, H., Li, H., Zhou, Y., Liu, J., Zhong, G., Wu, L., Jiang, W., Du, H., Yang, J., Xie, Q., & Huang, L. (2019). Cas12a-based on-site and rapid nucleic acid detection of African Swine Fever. *Frontiers in Microbiology*, *10*, 2830.

Barahona, E., Navazo, A., Martínez-Granero, F., Zea-Bonilla, T., Pérez-Jiménez, R. M., Martín, M., & Rivilla, R. (2011). *Pseudomonas fluorescens* F113 mutant with enhanced competitive colonization ability and improved biocontrol activity against fungal root pathogens. *Applied Environmental Microbiology*, *77*(15), 5412-5419.

Barker, B. (2007). *Irrigation management to prevent Fusarium*. Retrieved 18 September from https://www.topcropmanager.com/irrigation-management-to-prevent-fusarium-850/

Beauregard, P. B., Chai, Y., Vlamakis, H., Losick, R., & Kolter, R. (2013). *Bacillus subtilis* biofilm induction by plant polysaccharides. *Proceedings of the National Academy of Sciences*, *110*(17), 1621-1630.

Berghetti, J., Casa, R. T., Coelho, A. E., Sangoi, L., da Silva, F. N., Scheidt, B. T., Martins, F. C., & Ludwig, A. H. (2020). Grain quality of maize hybrids submitted to different sowing times and nitrogen rates. *Revista de Ciências Agroveterinárias*, *19*(1), 26-34.

Bi, Q., Liu, P., Wu, J., Lu, F., Han, X., Wang, W., & Zhao, J. (2023). Transcriptomic and metabolomic analysis of the mechanism by which *Bacillus tequilensis* inhibits *Alternaria alternata* to control pear black spot. *Biological Control*, *187*, 105394.

Biermann, R., & Beutel, S. (2023). Endospore production of *Bacillus* spp. for industrial use. *Engineering in Life Sciences*, *23*(11), e2300013.

Bivehed, E., Hellman, B., Fan, Y., Haglöf, J., & Buratovic, S. (2023). DNA integrity under alkaline conditions: An investigation of factors affecting the comet assay. *Mutation Research/Genetic Toxicology and Environmental Mutagenesis*, *891*, 503680.

Blacutt, A. A., Gold, S. E., Voss, K. A., Gao, M., & Glenn, A. E. (2017). *Fusarium verticillioides*: Advancements in understanding the toxicity, virulence, and niche adaptations of a model mycotoxigenic pathogen of maize. *Phytopathology*, *108*(3), 312-326.

Blanco Crivelli, X., Cundon, C., Bonino, M. P., Sanin, M. S., & Bentancor, A. (2024). The complex and changing genus *Bacillus*: A diverse bacterial powerhouse for many applications. *Bacteria*, *3*(3), 256-270.

Blandino, M., Scarpino, V., Giordano, D., Sulyok, M., Krska, R., Vanara, F., & Reyneri, A. (2017). Impact of sowing time, hybrid and environmental conditions

on the contamination of maize by emerging mycotoxins and fungal metabolites. *Italian Journal of Agronomy*, *12*(3), 928.

Blin, K., Medema, M. H., Kazempour, D., Fischbach, M. A., Breitling, R., Takano, E., & Weber, T. (2013). AntiSMASH 2.0--a versatile platform for genome mining of secondary metabolite producers. *Nucleic Acids Research*, *41*, 204-212.

Blin, K., Shaw, S., Kloosterman, A. M., Charlop-Powers, Z., van Wezel, G. P., Medema, Marnix H., & Weber, T. (2021). AntiSMASH 6.0: Improving cluster detection and comparison capabilities. *Nucleic Acids Research*, *49*(1), 29-35.

Borriss, R., Chen, X.-H., Rueckert, C., Blom, J., Becker, A., Baumgarth, B., Fan, B., Pukall, R., Schumann, P., Spröer, C., Junge, H., Vater, J., Pühler, A., & Klenk, H.-P. (2011). Relationship of *Bacillus amyloliquefaciens* clades associated with strains DSM 7^T and FZB42^T: A proposal for *Bacillus amyloliquefaciens* subsp. *amyloliquefaciens* subsp. nov. and *Bacillus amyloliquefaciens* subsp. *plantarum* subsp. nov. based on complete genome sequence comparisons. *International Journal of Systematic and Evolutionary Microbiology*, *61*(8), 1786-1801.

Bragulat, M. R., Martínez, E., Castellá, G., & Cabañes, F. J. (2004). Selective efficacy of culture media recommended for isolation and enumeration of *Fusarium* spp. *Journal of Food Protection*, *67*(1), 207-211.

Braun, M. S., & Wink, M. (2018). Exposure, occurrence, and chemistry of fumonisins and their cryptic derivatives. *Comprehensive Reviews in Food Science and Food Safety*, *17*(3), 769-791.

Bray, N., Pimentel, H., Melsted, P., & Pachter, L. (2015). Near-optimal RNA-seq quantification. *ArXiv e-prints*, *arXiv*.

Buddhachat, K., Sripairoj, N., Ritbamrung, O., Inthima, P., Ratanasut, K., Boonsrangsom, T., Rungrat, T., Pongcharoen, P., & Sujipuli, K. (2022). RPA-assisted Cas12a system for detecting pathogenic *Xanthomonas oryzae*, a causative agent for bacterial leaf blight disease in rice. *Rice Science*, *29*(4), 340-352.

Bustin, S. A., Benes, V., Garson, J. A., Hellemans, J., Huggett, J., Kubista, M., Mueller, R., Nolan, T., Pfaffl, M. W., Shipley, G. L., Vandesompele, J., & Wittwer, C. T. (2009). The miqe guidelines: Minimum information for publication of quantitative real-time PCR experiments. *Clinical Chemistry*, *55*(4), 611-622.

Bustin, S. A., Ruijter, J. M., van den Hoff, M. J. B., Kubista, M., Pfaffl, M. W., Shipley, G. L., Tran, N., Rödiger, S., Untergasser, A., Mueller, R., Nolan, T., Milavec, M., Burns, M. J., Huggett, J. F., Vandesompele, J., & Wittwer, C. T. (2025). Miqe 2.0: Revision of the minimum information for publication of quantitative real-time pcr experiments guidelines. *Clinical Chemistry*, *71*(6), 634-651.

Butcher, R. A., Schroeder, F. C., Fischbach, M. A., Straight, P. D., Kolter, R., Walsh, C. T., & Clardy, J. (2007). The identification of bacillaene, the product of the pksx megacomplex in *Bacillus subtilis*. *Proceedings of the National Academy of Sciences*, *104*(5), 1506-1509.

Campos, M. D., Patanita, M., Campos, C., Materatski, P., Varanda, C. M. R., Brito, I., & Félix, M. d. R. (2019). Detection and quantification of *Fusarium* spp. (*F.*

oxysporum, *F. verticillioides*, *F. graminearum*) and *Magnaporthiopsis maydis* in maize using real-time PCR targeting the its region. *Agronomy*, *9*(2), 45.

Cantalapiedra, C. P., Hernández-Plaza, A., Letunic, I., Bork, P., & Huerta-Cepas, J. (2021). Eggnog-mapper v2: Functional annotation, orthology assignments, and domain prediction at the metagenomic scale. *Molecular Biology and Evolution*, *38*(12), 5825-5829.

Cavaglieri, L., Orlando, J., Rodríguez, M. I., Chulze, S., & Etcheverry, M. (2005). Biocontrol of *Bacillus subtilis* against *Fusarium verticillioides in vitro* and at the maize root level. *Research in Microbiology*, *156*(5), 748-754.

Cawoy, H., Debois, D., Franzil, L., De Pauw, E., Thonart, P., & Ongena, M. (2015). Lipopeptides as main ingredients for inhibition of fungal phytopathogens by *Bacillus subtilis*/*amyloliquefaciens*. *Microbial Biotechnology*, *8*(2), 281-295.

Charron-Lamoureux, V., Lebel-Beaucage, S., Pomerleau, M., & Beauregard, P. B. (2024). Rooting for success: Evolutionary enhancement of *Bacillus* for superior plant colonization. *Microbial Biotechnology*, *17*(9), e70001.

Chaurasia, L. K., Tamang, B., Tirwa, R. K., & Lepcha, P. L. (2020). Influence of biosurfactant producing *Bacillus tequilensis* LK5.4 isolate of kinema, a fermented soybean, on seed germination and growth of maize (*Zea mays* L.). *3 Biotech*, *10*(7), 297.

Chen, C., Wu, Y., Li, J., Wang, X., Zeng, Z., Xu, J., Liu, Y., Feng, J., Chen, H., He, Y., & Xia, R. (2023). Tbtools-II: A "one for all, all for one" bioinformatics platform for biological big-data mining. *Molecular Plant*, *16*(11), 1733-1742.

Chen, J., Wen, J., Tang, Y., Shi, J., Mu, G., Yan, R., Cai, J., & Long, M. (2021). Research progress on fumonisin B1 contamination and toxicity: A review. *Molecules*, *26*(17), 5238.

Chen, J. S., Ma, E., Harrington, L. B., Da Costa, M., Tian, X., Palefsky, J. M., & Doudna, J. A. (2018). CRISPR-Cas12a target binding unleashes indiscriminate single-stranded DNase activity. *Science*, *360*(6387), 436-439.

Chen, Q., Hu, H.-y., Gao, M., Xu, J., Zhou, Y.-q., & Sun, J.-g. (2011). Screening and identification of a nitrogen fixing bacteria with 1-aminocyclopropane-1-carboxylate deaminase activity. *Journal of Plant Nutrition and Fertilizers*, *17*(6), 1515-1521.

Chen, W., Wei, L., Hou, R., Zhao, Y., Zhao, Y., & Liu, F. (2022). Sterol demethylation inhibitor fungicide resistance in *Colletotrichum siamense* from chili is caused by mutations in CYP51a and CYP51b. *Phytopathology Research*, *4*(1), 41.

Chen, X.-H., Vater, J., Piel, J., Franke, P., Scholz, R., Schneider, K., Koumoutsi, A., Hitzeroth, G., Grammel, N., Strittmatter Axel, W., Gottschalk, G., Süssmuth Roderich, D., & Borriss, R. (2006). Structural and functional characterization of three polyketide synthase gene clusters in *Bacillus amyloliquefaciens* FZB42. *Journal of Bacteriology*, *188*(11), 4024-4036.

Chen, X., Pan, B., Yu, L., Wang, B., & Pan, L. (2024). Enhancement of protein production in *Aspergillus niger* by engineering the antioxidant defense metabolism. *Biotechnology for Biofuels and Bioproducts*, *17*(1), 91.

Chen, X. H., Koumoutsi, A., Scholz, R., Eisenreich, A., Schneider, K., Heinemeyer, I., Morgenstern, B., Voss, B., Hess, W. R., Reva, O., Junge, H., Voigt, B., Jungblut, P. R., Vater, J., Süssmuth, R., Liesegang, H., Strittmatter, A., Gottschalk, G., & Borriss, R. (2007). Comparative analysis of the complete genome sequence of the plant growth-promoting bacterium *Bacillus amyloliquefaciens* FZB42. *Nature Biotechnology*, *25*(9), 1007-1014.

Chen, Y., Yang, H., Shen, Z., & Ye, J. (2022). Whole-genome sequencing and potassium-solubilizing mechanism of *Bacillus aryabhattai* SK1-7. *Frontiers in Microbiology*, *12*, 722379.

Cheng, W., Yan, X., Xiao, J., Chen, Y., Chen, M., Jin, J., Bai, Y., Wang, Q., Liao, Z., & Chen, Q. (2020). Isolation, identification, and whole genome sequence analysis of the alginate-degrading bacterium *Cobetia* sp. cqz5-12. *Scientific Reports*, *10*(1), 10920.

Chin, A. W. T. F., Bloemberg, G. V., Mulders, I. H., Dekkers, L. C., & Lugtenberg, B. J. (2000). Root colonization by phenazine-1-carboxamide-producing bacterium *Pseudomonas chlororaphis* PCL1391 is essential for biocontrol of tomato foot and root rot. *Molecular Plant-Microbe Interactions*, *13*(12), 1340-1345.

Chowdhury, S. P., Hartmann, A., Gao, X., & Borriss, R. (2015). Biocontrol mechanism by root-associated *Bacillus amyloliquefaciens* FZB42 - a review. *Frontiers in Microbiology*, *6*, 780.

Claassen, S., du Toit, E., Kaba, M., Moodley, C., Zar, H. J., & Nicol, M. P. (2013). A comparison of the efficiency of five different commercial DNA extraction kits for extraction of DNA from faecal samples. *Journal of Microbiological Methods*, *94*(2), 103-110.

Cochrane, S. A., & Vederas, J. C. (2016). Lipopeptides from *Bacillus* and *Paenibacillus* spp.: A gold mine of antibiotic candidates. *Medicinal Research Reviews*, *36*(1), 4-31.

Comba-González, N. B., Chaves-Moreno, D., Santamaría-Vanegas, J., & Montoya-Castaño, D. (2024). A pan-genomic assessment: Delving into the genome of the marine epiphyte *Bacillus altitudinis* strain 19a and other very close *Bacillus* strains from multiple environments. *Heliyon*, *10*(7), e27820.

Cornforth, D. M., & Foster, K. R. (2013). Competition sensing: The social side of bacterial stress responses. *Nature Reviews Microbiology*, *11*(4), 285-293.

Cotten, T. K., & Munkvold, G. P. (1998). Survival of *Fusarium moniliforme*, *F. proliferatum*, and *F. subglutinans* in maize stalk residue. *Phytopathology*, *88*(6), 550-555.

Cowger, C., Patton-Özkurt, J., Brown-Guedira, G., & Perugini, L. (2009). Post-anthesis moisture increased *Fusarium* head blight and deoxynivalenol levels in North Carolina winter wheat. *Phytopathology*, *99*(4), 320-327.

Cui, Y., Wang, S., Ding, S., Shen, J., & Zhu, K. (2020). Toxins and mobile antimicrobial resistance genes in *Bacillus* probiotics constitute a potential risk for one health. *Journal of Hazardous Materials*, *382*, 121266.

Daher, R. K., Stewart, G., Boissinot, M., & Bergeron, M. G. (2016). Recombinase polymerase amplification for diagnostic applications. *Clin Chem*, *62*(7), 947-958.

Dai, H., Wu, B., Zhuang, Y., Ren, H., Chen, Y., Zhang, F., Chu, C., Lv, X., Xu, J., & Ma, B. (2024). Dynamic in situ detection in IRHIZO-chip reveals diurnal fluctuations of *Bacillus subtilis* in the rhizosphere. *Proceedings of the National Academy of Sciences*, *121*(40), e2408711121.

Dale, M., & Ogle, H. (1997). Disease management: Cultural practices. In J. F. Brown, and Ogle, H.J., (eds.) (Ed.), *Plant pathogens and plant diseases* (pp. 390-404). Rockvale Publications.

Danevčič, T., Dragoš, A., Spacapan, M., Stefanic, P., Dogsa, I., & Mandic-Mulec, I. (2021). Surfactin facilitates horizontal gene transfer in *Bacillus subtilis*. *Frontiers in Microbiology*, *Volume 12 - 2021*.

Deepa, N., & Sreenivasa, M. Y. (2019). Molecular methods and key genes targeted for the detection of fumonisin producing *Fusarium verticillioides* - an updated review. *Food Bioscience*, *32*, 100473.

Deng, C., Zeng, N., Li, C., Pang, J., Zhang, N., & Li, B. (2024). Mechanisms of ROS-mediated interactions between *Bacillus aryabhattai* LAD and maize roots to promote plant growth. *BMC Microbiology*, *24*(1), 327.

Dimkić, I., Janakiev, T., Petrović, M., Degrassi, G., & Fira, D. (2022). Plant-associated *Bacillus* and *Pseudomonas* antimicrobial activities in plant disease suppression via biological control mechanisms - a review. *Physiological and Molecular Plant Pathology*, *117*, 101754.

Ding, L., Wang, X., Chen, X., Xu, X., Wei, W., Yang, L., Ji, Y., Wu, J., Xu, J., & Peng, C. (2025). Development of a novel Cas13a/Cas12a-mediated 'one-pot' dual detection assay for genetically modified crops. *Journal of Advanced Research*, *72*, 97-106.

Ding, Y., Ma, N., Haseeb, H. A., Dai, Z., Zhang, J., & Guo, W. (2024). Genome-wide transcriptome analysis of toxigenic *Fusarium verticillioides* in response to variation of temperature and water activity on maize kernels. *International Journal of Food Microbiology*, *410*, 110494.

Dinolfo, M. I., Martínez, M., Castañares, E., & Arata, A. F. (2022). *Fusarium* in maize during harvest and storage: A review of species involved, mycotoxins, and management strategies to reduce contamination. *European Journal of Plant Pathology*, *164*(2), 151-166.

Doležel, J., Bartoš, J., Voglmayr, H., & Greilhuber, J. (2003). Letter to the editor. *Cytometry Part A*, *51A*(2), 127-128.

dsm-firmenich. (2022). Dsm-firmenich world mycotoxin survey 2022.

dsm-firmenich. (2024). *Dsm-firmenich world mycotoxin survey 2024*. https://www.dsm-firmenich.com/anh/products-and-services/tools/mycotoxin-contamination/mycotoxin-survey/mycotoxin-survey-report-q4-2024.html

Du Toit, A. (2025). Bacterial contact killing. *Nature Reviews Microbiology*, *23*(3), 143-143.

Duan, C., Qin, Z., Yang, Z., Li, W., Sun, S., Zhu, Z., & Wang, X. (2016). Identification of pathogenic *Fusarium* spp. causing maize ear rot and potential mycotoxin production in China. *Toxins (Basel)*, *8*(6), 186.

Duncan, K. E., & Howard, R. J. (2009). Biology of maize kernel infection by *Fusarium verticillioides*. *Molecular Plant-Microbe Interactions*, *23*(1), 6-16.

Dunlap, C. A., Bowman, M. J., & Rooney, A. P. (2019). Iturinic lipopeptide diversity in the *Bacillus subtilis* species group - important antifungals for plant disease biocontrol applications. *Frontiers in Microbiology*, *10*, 1794.

Dunlap, C. A., Kim, S.-J., Kwon, S.-W., & Rooney, A. P. (2016). *Bacillus velezensis* is not a later heterotypic synonym of *Bacillus amyloliquefaciens*; *Bacillus methylotrophicus*, *Bacillus amyloliquefaciens* subsp. *plantarum* and '*Bacillus oryzicola'* are later heterotypic synonyms of *Bacillus velezensis* based on phylogenomics. *International Journal of Systematic and Evolutionary Microbiology*, *66*(3), 1212-1217.

Duré, L. M. M., Mascarin, G. M., & Bettiol, W. (2025). Optimization of endospore production by solid and liquid fermentation for the development of effective formulations of *Bacillus velezensis*-based products. *Brazilian Journal of Microbiology*, *56*(2), 1253-1261.

Einloft, T. C., Hartke, S., de Oliveira, P. B., Saraiva, P. S., & Dionello, R. G. (2021). Selection of rhizobacteria for biocontrol of *Fusarium verticillioides* on non-rhizospheric soil and maize seedlings roots. *European Journal of Plant Pathology*, *160*(3), 503-518.

Ekwomadu, T. I., Akinola, S. A., & Mwanza, M. (2021). *Fusarium* mycotoxins, their metabolites (free, emerging, and masked), food safety concerns, and health impacts. *International Journal of Environmental Research and Public Health*, *18*(22), 11741.

Ekwomadu, T. I., & Mwanza, M. (2023). *Fusarium* fungi pathogens, identification, adverse effects, disease management, and global food security: A review of the latest research. *Agriculture*, *13*(9), 1810.

El-Aswad, A. F., Aly, M. I., Alsahaty, S. A., & Basyony, A. B. A. (2023). Efficacy evaluation of some fumigants against *Fusarium oxysporum* and enhancement of tomato growth as elicitor-induced defense responses. *Scientific Reports*, *13*(1), 2479.

Eliaš, D., Tóth Hervay, N., & Gbelská, Y. (2024). Ergosterol biosynthesis and regulation impact the antifungal resistance and virulence of *Candida* spp. *Stresses*, *4*(4), 641-662.

Elnahal, A. S. M., El-Saadony, M. T., Saad, A. M., Desoky, E.-S. M., El-Tahan, A. M., Rady, M. M., AbuQamar, S. F., & El-Tarabily, K. A. (2022). The use of microbial inoculants for biological control, plant growth promotion, and sustainable agriculture: A review. *European Journal of Plant Pathology*, *162*(4), 759-792.

EPA, U. (2000). *Guidelines for health risk assessment of chemical mixtures*. EPA. https://www.epa.gov/risk/guidelines-health-risk-assessment-chemical-mixtures

EPA, U. (2006). *Bacillus subtilis strain QST 713: Biopesticide registration action document*. E. B. a. P. P. Division). https://www3.epa.gov/pesticides/chem_search/reg_actions/registration/decision_PC-006479_9-Aug-06.pdf

Falardeau, J., Wise, C., Novitsky, L., & Avis, T. J. (2013). Ecological and mechanistic insights into the direct and indirect antimicrobial properties of *Bacillus subtilis* lipopeptides on plant pathogens. *Journal of Chemical Ecology*, *39*(7), 869-878.

Fan, B., Blom, J., Klenk, H.-P., & Borriss, R. (2017). *Bacillus amyloliquefaciens*, *Bacillus velezensis*, and *Bacillus siamensis* form an "operational group *B. amyloliquefaciens*" within the *B. subtilis* species complex. *Frontiers in Microbiology*, *8*, 22.

Fang, Z. D. (1998). *Zhibing yanjiu fangfa [plant pathology research methods]*. China Agriculture Press.

FAOStat. (2023). *FAO statistics* http://www.fao.org/faostat.

Faria, C. B., Abe, C. A. L., Silva, C. N. d., Tessmann, D. J., & Barbosa-Tessmann, I. P. (2012). New pcr assays for the identification of *Fusarium verticillioides*, *Fusarium subglutinans*, and other species of the *Gibberella fujikuroi* complex. *International Journal of Molecular Sciences*, *13*(1), 115-132.

Fierro-Coronado, R. A., Quiroz-Figueroa, F. R., García-Pérez, L. M., Ramírez-Chávez, E., Molina-Torres, J., & Maldonado-Mendoza, I. E. (2014). IAA-producing rhizobacteria from chickpea (*Cicer arietinum* L.) induce changes in root architecture and increase root biomass. *Canadian Journal of Microbiology*, *60*(10), 639-648.

Fira, D., Dimkić, I., Berić, T., Lozo, J., & Stanković, S. (2018). Biological control of plant pathogens by *Bacillus* species. *Journal of Biotechnology*, *285*, 44-55.

Fountain, J. C., Bajaj, P., Pandey, M., Nayak, S. N., Yang, L., Kumar, V., Jayale, A. S., Chitikineni, A., Zhuang, W., Scully, B. T., Lee, R. D., Kemerait, R. C., Varshney, R. K., & Guo, B. (2016). Oxidative stress and carbon metabolism influence *Aspergillus flavus* transcriptome composition and secondary metabolite production. *Scientific Reports*, *6*, 38747.

Gai, X., Dong, H., Wang, S., Liu, B., Zhang, Z., Li, X., & Gao, Z. (2018). Infection cycle of maize stalk rot and ear rot caused by *Fusarium verticillioides*. *PLoS One 13*(7), e0201588.

Gallart, M., Dow, L., Nowak, V., Belt, K., Sabburg, R., Gardiner, D. M., & Thatcher, L. F. (2025). Multi-omic investigation identifies key antifungal biochemistry during fermentation of a Streptomyces biological control agent. *Microbiological Research*, *292*, 128032.

Gao, X., Shim, W.-B., Göbel, C., Kunze, S., Feussner, I., Meeley, R., Balint-Kurti, P., & Kolomiets, M. (2007). Disruption of a maize 9-lipoxygenase results in increased resistance to fungal pathogens and reduced levels of contamination with mycotoxin fumonisin. *Molecular Plant-Microbe Interactions*, *20*(8), 922-933.

Gelderblom, W. C., Jaskiewicz, K., Marasas, W. F., Thiel, P. G., Horak, R. M., Vleggaar, R., & Kriek, N. P. (1988). Fumonisins--novel mycotoxins with cancer-promoting activity produced by *Fusarium moniliforme*. *Applied and Environmental Microbiology, 54*(7), 1806-1811.

González-Estrada, R. R., Blancas-Benitez, F. J., Aguirre-Güitrón, L., Hernandez-Montiel, L. G., Moreno-Hernández, C., Cortés-Rivera, H. J., Herrera-González, J. A., Rayón-Díaz, E., Velázquez-Estrada, R. M., Santoyo-González, M. A., &

Gutierrez-Martinez, P. (2021). Chapter 5 - alternative management technologies for postharvest disease control. In C. M. Galanakis (Ed.), *Food losses, sustainable postharvest and food technologies* (pp. 153-190). Academic Press.

Gootenberg, J. S., Abudayyeh, O. O., Kellner, M. J., Joung, J., Collins, J. J., & Zhang, F. (2018). Multiplexed and portable nucleic acid detection platform with Cas13, Cas12a, and Csm6. *Science*, *360*(6387), 439-444.

Goud, M. S., Sharma, S. K., Kharbikar, L. L., Prasanna, R., Sangwan, S., Dahuja, A., & Dixit, A. (2025). *Bacillus* species consortium with tryptophan-dependent and -independent pathways mediated production of IAA and its derivatives modulates soil biological properties, growth and yield of wheat. *Plant and Soil*, *508*(1), 71-97.

Grigoreva, A., Andreeva, J., Bikmetov, D., Rusanova, A., Serebryakova, M., Garcia, A. H., Slonova, D., Nair, S. K., Lippens, G., Severinov, K., & Dubiley, S. (2021). Identification and characterization of andalusicin: N-terminally dimethylated class III lantibiotic from *Bacillus thuringiensis* sv. *andalousiensis*. *iScience*, *24*(5), 102480.

Guadet, J., Julien, J., Lafay, J. F., & Brygoo, Y. (1989). Phylogeny of some *Fusarium* species, as determined by large-subunit rRNA sequence comparison. *Molecular Biology and Evolution*, *6*(3), 227-242.

Guarro, J., & Gené, J. (1992). *Fusarium* infections. Criteria for the identification of the responsible species. *Mycoses*, *35*(5-6), 109-114.

Gundlach, J., Herzberg, C., Kaever, V., Gunka, K., Hoffmann, T., Weiß, M., Gibhardt, J., Thürmer, A., Hertel, D., Daniel, R., Bremer, E., Commichau, F. M., & Stülke, J. (2017). Control of potassium homeostasis is an essential function of the second messenger cyclic di-AMP in *Bacillus subtilis*. *Science Signaling*, *10*(475), 3011.

Gupta, K., Dubey, N. K., Singh, S. P., Kheni, J. K., Gupta, S., & Varshney, A. (2021). Plant growth-promoting rhizobacteria (PGPR): Current and future prospects for crop improvement. In A. N. Yadav, J. Singh, C. Singh, & N. Yadav (Eds.), *Current trends in microbial biotechnology for sustainable agriculture* (pp. 203-226). Springer Singapore.

Gupta, M., Topgyal, T., Zahoor, A., & Gupta, S. (2021). Chapter 15 - Rhizobium: Eco-friendly microbes for global food security. In A. Kumar & S. Droby (Eds.), *Microbial management of plant stresses* (pp. 221-233). Woodhead Publishing.

Guzmán-Guzmán, P., Kumar, A., de los Santos-Villalobos, S., Parra-Cota, F. I., Orozco-Mosqueda, M. D., Fadiji, A. E., Hyder, S., Babalola, O. O., & Santoyo, G. (2023). *Trichoderma* species: Our best fungal allies in the biocontrol of plant diseases-a review. *Plants*, *12*(3), 432.

Hammami, I., Siala, R., Jridi, M., Ktari, N., Nasri, M., & Triki, M. A. (2013). Partial purification and characterization of chiIO8, a novel antifungal chitinase produced by *Bacillus cereus* IO8. *Journal of Applied Microbiology*, *115*(2), 358-366.

Harwood, C. R., Mouillon, J.-M., Pohl, S., & Arnau, J. (2018). Secondary metabolite production and the safety of industrially important members of the *Bacillus subtilis* group. *FEMS Microbiology Reviews*, *42*(6), 721-738.

Haskett, T. L., Tkacz, A., & Poole, P. S. (2021). Engineering rhizobacteria for sustainable agriculture. *The ISME Journal*, *15*(4), 949-964.

He, D. C., He, M. H., Amalin, D. M., Liu, W., Alvindia, D. G., & Zhan, J. (2021). Biological control of plant diseases: An evolutionary and eco-economic consideration. *Pathogens*, *10*(10), 1311.

He, H., Hu, Q., Li, R., Pan, X., Huang, B., & He, Q. (2020). Regional gap in maize production, climate and resource utilization in China. *Field Crops Research*, *254*, 107830.

Heifetz, C. L., Fisher, M. W., Chodubski, J. A., & DeCarlo, M. O. (1972). Butirosin, a new aminoglycosidic antibiotic complex: Antibacterial activity *in vitro* and in mice. *Antimicrobial Agents and Chemotherapy*, *2*(2), 89-94.

Humpf, H. U., & Voss, K. A. (2004). Effects of thermal food processing on the chemical structure and toxicity of fumonisin mycotoxins. *Molecular Nutrition & Food Research*, *48*(4), 255-269.

Idris, E. E., Iglesias, D. J., Talon, M., & Borriss, R. (2007). Tryptophan-dependent production of indole-3-acetic acid (IAA) affects level of plant growth promotion by *Bacillus amyloliquefaciens* FZB42. *Molecular Plant-Microbe Interactions*, *20*(6), 619-626.

Ivanov, A. V., Safenkova, I. V., Zherdev, A. V., & Dzantiev, B. B. (2021). The potential use of isothermal amplification assays for in-field diagnostics of plant pathogens. *Plants*, *10*(11), 2424.

Jannat, M., Auyon, S. T., Tushar, A. S. M., Tonny, S. H., Hasan, M. H., Shahi, M., Singha, U. R., Sultana, A., Akter, S., & Islam, M. R. (2024). Seed priming with rhizospheric *Bacillus subtilis*: A smart strategy for reducing fumonisin contamination in pre-harvest maize. *Toxins (Basel)*, *16*(8), 337.

Jeyachandran, S., Chellapandian, H., Park, K., & Kwak, I.-S. (2023). A review on the involvement of heat shock proteins (extrinsic chaperones) in response to stress conditions in aquatic organisms. *Antioxidants*, *12*(7), 1444.

Jiang, C., Li, Z., Shi, Y., Guo, D., Pang, B., Chen, X., Shao, D., Liu, Y., & Shi, J. (2020). *Bacillus subtilis* inhibits *Aspergillus carbonarius* by producing iturin A, which disturbs the transport, energy metabolism, and osmotic pressure of fungal cells as revealed by transcriptomics analysis. *International Journal of Food Microbiology*, *330*, 108783.

Jiang, J., Gao, L., Bie, X., Lu, Z., Liu, H., Zhang, C., Lu, F., & Zhao, H. (2016). Identification of novel surfactin derivatives from nrps modification of *Bacillus subtilis* and its antifungal activity against *Fusarium moniliforme*. *BMC Microbiology*, *16*(1), 31.

Jin, X., Zhou, X., Wu, F., Xiang, W., & Pan, K. (2023). Biochar amendment suppressed *Fusarium* wilt and altered the rhizosphere microbial composition of tomatoes. *Agronomy*, *13*(7), 1811.

Kachhadia, R., Kapadia, C., Singh, S., Gandhi, K., Jajda, H., Alfarraj, S., Ansari, M. J., Danish, S., & Datta, R. (2022). Quorum sensing inhibitory and quenching activity of *Bacillus cereus* RC1 extracts on soft rot-causing bacteria *Lelliottia amnigena*. *ACS Omega*, *7*(29), 25291-25308.

Kang, M., Chanderbali, A., Lee, S., Soltis, D. E., Soltis, P. S., & Kim, S. (2023). High-molecular-weight DNA extraction for long-read sequencing of plant genomes: An optimization of standard methods. *Applications in Plant Sciences*, *11*(3), e11528.

Kant, P., Reinprecht, Y., Martin, C. J., Islam, R., & Pauls, K. P. (2017). 4.65 - disease resistance. In M. Moo-Young (Ed.), *Comprehensive biotechnology (third edition)* (pp. 789-805). Pergamon.

Kaspar, F., Neubauer, P., & Gimpel, M. (2019). Bioactive secondary metabolites from *Bacillus subtilis*: A comprehensive review. *Journal of Natural Products*, *82*(7), 2038-2053.

Keawmanee, P., Rattanakreetakul, C., & Pongpisutta, R. (2021). Microbial reduction of fumonisin B1 by the new isolate *Serratia marcescens* 329-2. *Toxins (Basel)*, *13*(9).

Keswani, C., Singh, S. P., Cueto, L., García-Estrada, C., Mezaache-Aichour, S., Glare, T. R., Borriss, R., Singh, S. P., Blázquez, M. A., & Sansinenea, E. (2020). Auxins of microbial origin and their use in agriculture. *Applied Microbiology and Biotechnology*, *104*(20), 8549-8565.

Kim, Y. T., Park, B. K., Kim, S. E., Lee, W. J., Moon, J. S., Cho, M. S., Park, H.-Y., Hwang, I., & Kim, S. U. (2017). Organization and characterization of genetic regions in *Bacillus subtilis* subsp. *krictiensis* ATCC55079 associated with the biosynthesis of iturin and surfactin compounds. *PLoS One*, *12*(12), e0188179.

Kloepper, J. W., Leong, J., Teintze, M., & Schroth, M. N. (1980). Enhanced plant growth by siderophores produced by plant growth-promoting rhizobacteria. *Nature*, *286*(5776), 885-886.

Knoester, M., Pieterse, C. M. J., Bol, J. F., & Van Loon, L. C. (1999). Systemic resistance in *Arabidopsis* induced by rhizobacteria requires ethylene-dependent signaling at the site of application. *Molecular Plant-Microbe Interactions*, *12*(8), 720-727.

Kocevski, D., Du, M., Kan, J., Jing, C., Lačanin, I., & Pavlović, H. (2013). Antifungal effect of *Allium tuberosum*, *Cinnamomum cassia*, and *Pogostemon cablin* essential oils and their components against population of *Aspergillus* species. *Journal of Food Science*, *78*(5), 731-737.

Krnjaja, V., Mandić, V., Bijelić, Z., Stanković, S., Obradović, A., Caro Petrović, V., & Gogić, M. (2022). Influence of sowing time on *Fusarium* and fumonisin contamination of maize grains and yield component traits. *Agriculture*, *12*(7), 1042.

Krnjaja, V., Mandić, V., Stanković, S., Obradović, A., Vasić, T., Lukić, M., & Bijelić, Z. (2019). Influence of plant density on toxigenic fungal and mycotoxin contamination of maize grains. *Crop Protection*, *116*, 126-131.

Kujawa, M. (1994). Some naturally occurring substances: Food items and constituents, heterocyclic aromatic amines and mycotoxins. *IARC Monographs on the Evaluation of Carcinogenic Risks to Humans*, *38*(3), 351-351.

Li, B., Li, Q., Xu, Z., Zhang, N., Shen, Q., & Zhang, R. (2014). Responses of beneficial *Bacillus amyloliquefaciens* SQR9 to different soilborne fungal

pathogens through the alteration of antifungal compounds production. *Frontiers in Microbiology*, *5*, 636.

Li, L., Qu, Q., Cao, Z., Guo, Z., Jia, H., Liu, N., Wang, Y., & Dong, J. (2019). The relationship analysis on corn stalk rot and ear rot according to *Fusarium* species and fumonisin contamination in kernels. *Toxins (Basel)*, *11*(6), 320.

Li, Q., Shi, J., He, K., & Wang, Z. (2021). Effects of chemical control of ear borers on reducing *Fusarium verticillioides* ear rot and fumonisin level. *Scientia Agricultura Sinica*, *54*(17), 3702-3711.

Li, S.-Y., Cheng, Q.-X., Wang, J.-M., Li, X.-Y., Zhang, Z.-L., Gao, S., Cao, R.-B., Zhao, G.-P., & Wang, J. (2018). CRISPR-Cas12a-assisted nucleic acid detection. *Cell Discovery*, *4*(1), 20.

Li, Y., Jiang, D., Xu, L., Zhang, S., Ji, P., Pan, H., Jiang, B., & Shen, Z. (2019). Evaluation of diversity and resistance of maize varieties to *Fusarium* spp. causing ear rot in maize under conditions of natural infection. *Czech Journal of Genetics and Plant Breeding*, *55*, 131-137.

Li, Y., Zhang, Y., Kong, F., Wang, C., Chen, S., Wang, J., & Wang, D. (2023). Visual detection of *Fusarium temperatum* by using CRISPR-Cas12a empowered LAMP assay coupled with AuNPs-based colorimetric reaction. *LWT-Food Science and Technology*, *185*, 115190.

Liang, N., Charron, J.-B., & Jabaji, S. (2023). Comparative transcriptome analysis reveals the biocontrol mechanism of *Bacillus velezensis* E68 against *Fusarium graminearum* DAOMC 180378, the causal agent of *Fusarium* head blight. *PLoS One*, *18*(1), e0277983.

Liang, X., Ishfaq, S., Liu, Y., Jijakli, M. H., Zhou, X., Yang, X., & Guo, W. (2024). Identification and genomic insights into a strain of *Bacillus velezensis* with phytopathogen-inhibiting and plant growth-promoting properties. *Microbiological Research*, *285*, 127745.

Liang, X., Zhang, X., Haseeb, H. A., Tang, T., Shan, J., Yin, B., & Guo, W. (2022). Development and evaluation of a novel visual and rapid detection assay for toxigenic *Fusarium graminearum* in maize based on recombinase polymerase amplification and lateral flow analysis. *International Journal of Food Microbiology*, *372*, 109682.

Liao, Y., Smyth, G. K., & Shi, W. (2014). Featurecounts: An efficient general purpose program for assigning sequence reads to genomic features. *Bioinformatics*, *30*(7), 923-930.

Lin, F., Xue, Y., Huang, Z., Jiang, M., Lu, F., Bie, X., Miao, S., & Lu, Z. (2019). Bacillomycin D inhibits growth of *Rhizopus stolonifer* and induces defense-related mechanism in cherry tomato. *Applied Microbiology and Biotechnology*, *103*(18), 7663-7674.

Liu, C.-W., & Tsutsui, H. (2023). Sample–to-answer sensing technologies for nucleic acid preparation and detection in the field. *SLAS Technology*, *28*(5), 302-323.

Liu, J., Hagberg, I., Novitsky, L., Hadj-Moussa, H., & Avis, T. J. (2014). Interaction of antimicrobial cyclic lipopeptides from *Bacillus subtilis* influences their effect

on spore germination and membrane permeability in fungal plant pathogens. *Fungal Biology*, *118*(11), 855-861.

Liu, J., Han, Y., Li, W., Qi, T., Zhang, J., & Li, Y. (2022). Identification of pathogens and evaluation of resistance and genetic diversity of maize inbred lines to stalk rot in Heilongjiang province, China. *Plant Disease*, *107*(2), 288-297.

Liu, X., Ren, B., Gao, H., Liu, M., Dai, H., Song, F., Yu, Z., Wang, S., Hu, J., Kokare, C. R., & Zhang, L. (2012). Optimization for the production of surfactin with a new synergistic antifungal activity. *PLoS One*, *7*(5), e34430.

Liu, Y., Ma, L., Liu, W., Xie, L., Wu, Q., Wang, Y., Zhou, Y., Zhang, Y., Jiao, B., & He, Y. (2023). RPA-CRISPR/Cas12a combined with rolling circle amplification-enriched DNAzyme: A homogeneous photothermal sensing strategy for plant pathogens. *Journal of Agricultural and Food Chemistry*, *71*(11), 4736-4744.

Liu, Y., Xu, Z., Chen, L., Xun, W., Shu, X., Chen, Y., Sun, X., Wang, Z., Ren, Y., Shen, Q., & Zhang, R. (2024). Root colonization by beneficial rhizobacteria. *FEMS Microbiology Reviews*, *48*(1), fuad066.

Lobato, I. M., & O'Sullivan, C. K. (2018). Recombinase polymerase amplification: Basics, applications and recent advances. *Trends in Analytical Chemistry*, *98*, 19-35.

Lugtenberg, B., & Kamilova, F. (2009). Plant-growth-promoting rhizobacteria. *Annual Review of Microbiology*, *63*, 541-556.

Luo, B., & Ning, Y. (2022). Comprehensive overview of carboxamide derivatives as succinate dehydrogenase inhibitors. *Journal of Agricultural and Food Chemistry*, *70*(4), 957-975.

Luo, T., Li, L., Wang, S., & Cheng, N. (2023). Research progress of nucleic acid detection technology for genetically modified maize. *International Journal of Molecular Sciences*, *24*(15).

Lv, W., Wang, C., Yang, N., Que, Y., Talbot, N. J., & Wang, Z. (2017). Genome-wide functional analysis reveals that autophagy is necessary for growth, sporulation, deoxynivalenol production and virulence in *Fusarium graminearum*. *Scientific Reports*, *7*(1), 11062.

Ma, P., Li, H., Liu, E., He, K., Song, Y., Dong, C., Wang, Z., Zhang, X., Zhou, Z., Xu, Y., Wu, J., & Zhang, H. (2022). Evaluation and identification of resistance lines and QTLs of maize to seedborne *Fusarium verticillioides*. *Plant Disease*, *106*(8), 2066-2073.

Ma, R.-y., Zhang, A.-m., Hui, X.-s., Dai, M., Wang, W., & Zhu, B.-c. (2013). Screening, identification and sporulation conditions optimization of nx-11 strain having the ability of solubilizing phosphorus and potassium. *Acta Agriculturae Boreali-Sinica*, *28*(2), 6.

Macar, O., Kalefetoğlu Macar, T., Yalçın, E., & Çavuşoğlu, K. (2022). Acute multiple toxic effects of trifloxystrobin fungicide on *Allium cepa* L. *Scientific Reports*, *12*(1), 15216.

Machado, J., Machado, A., Pozza, E., Machado, C., & Zancan, W. (2013). Inoculum potential of *Fusarium verticillioides* and performance of maize seeds. *Tropical Plant Pathology*, *38*, 213-217.

Madigan, M. T., & Imhoff, J. F. (2001). Phylum bxiii. Firmicutes. In D. R. Boone, R. W. Castenholz, & G. M. Garrity (Eds.), *Bergey's manual of systematic bacteriology: Volume one: The archaea and the deeply branching and phototrophic bacteria* (pp. 625-637). Springer New York.

Mahas, A., Hassan, N., Aman, R., Marsic, T., Wang, Q., Ali, Z., & Mahfouz, M. M. (2021). LAMP-coupled CRISPR–Cas12a module for rapid and sensitive detection of plant DNA viruses. *Viruses*, *13*(3).

Manzoni, C., Kia, D. A., Vandrovcova, J., Hardy, J., Wood, N. W., Lewis, P. A., & Ferrari, R. (2018). Genome, transcriptome and proteome: The rise of omics data and their integration in biomedical sciences. *Brief Bioinform*, *19*(2), 286-302.

Markakis, E. A., Fountoulakis, M. S., Daskalakis, G. C., Kokkinis, M., & Ligoxigakis, E. K. (2016). The suppressive effect of compost amendments on *Fusarium oxysporum* f.sp. *radicis-cucumerinum* in cucumber and *Verticillium dahliae* in eggplant. *Crop Protection*, *79*, 70-79.

Marqués, M.-C., Sánchez-Vicente, J., Ruiz, R., Montagud-Martínez, R., Márquez-Costa, R., Gómez, G., Carbonell, A., Daròs, J.-A., & Rodrigo, G. (2022). Diagnostics of infections produced by the plant viruses TMV, TEV, and PVX with CRISPR-Cas12 and CRISPR-Cas13. *ACS Synthetic Biology*, *11*(7), 2384-2393.

Masiello, M., Somma, S., Ghionna, V., Logrieco, A. F., & Moretti, A. (2019). *In vitro* and in field response of different fungicides against *Aspergillus flavus* and *Fusarium* species causing ear rot disease of maize. *Toxins (Basel)*, *11*(1), 11.

Matos, D., Cardoso, P., Almeida, S., & Figueira, E. (2024). Challenges in maize production: A review on late wilt disease control strategies. *Fungal Biology Reviews*, *50*, 100396.

Matthews, M. C., van der Linden, J., Robène, I., Rozsasi, S., Coetzee, B., Campa, M., Burger, J., Akwuruoha, U. N., Madufor, N. J., Perold, W., Opara, U. L., Viljoen, A., & Mostert, D. (2025). A combined recombinase polymerase amplification CRISPR/Cas12a assay for detection of *Fusarium oxysporum* f. sp. *cubense* tropical race 4. *Scientific Reports*, *15*(1), 2436.

Mesterházy, Á., Lemmens, M., & Reid, L. M. (2012). Breeding for resistance to ear rots caused by *Fusarium* spp. in maize – a review. *Plant Breeding*, *131*(1), 1-19.

Mongkolthanaruk, W. (2012). Classification of *Bacillus* beneficial substances related to plants, humans and animals. *Journal of Microbiology and Biotechnology*, *22*(12), 1597-1604.

Moreno-Letelier, A., Olmedo, G., Eguiarte, L. E., Martinez-Castilla, L., & Souza, V. (2011). Parallel evolution and horizontal gene transfer of the PST operon in firmicutes from oligotrophic environments. *International Journal of Evolutionary Biology*, 1, 781642.

Mu, K., Ren, X., Yang, H., Zhang, T., Yan, W., Yuan, F., Wu, J., Kang, Z., Han, D., Deng, R., & Zeng, Q. (2022). CRISPR-Cas12a-based diagnostics of wheat fungal diseases. *Journal of Agricultural and Food Chemistry*, *70*(23), 7240-7247.

Mulè, G., Susca, A., Stea, G., & Moretti, A. (2004). A species-specific PCR assay based on the calmodulin partial gene for identification of *Fusarium verticillioides*,

F. proliferatum and *F. subglutinans*. *European Journal of Plant Pathology*, *110*(5), 495-502.

Munkvold, G. P. (2003). Epidemiology of *Fusarium* diseases and their mycotoxins in maize ears. *European Journal of Plant Pathology*, *109*(7), 705-713.

Murillo-Williams, A., & Munkvold, G. P. (2008). Systemic infection by *Fusarium verticillioides* in maize plants grown under three temperature regimes. *Plant Disease*, *92*(12), 1695-1700.

N, D., Achar, P. N., & Sreenivasa, M. Y. (2021). Current perspectives of biocontrol agents for management of *Fusarium verticillioides* and its fumonisin in cereals-a review. *Journal of Fungi*, *7*(9).

Nagaraj, D. (2017). *Fusarium verticillioides* a globally important pathogen of agriculture and livestock: A review. *Journal of Veterinary Medicine and Research*, *4*(4), 1084.

Nagaraj, D., Adkar-Purushothama, C. R., & Sreenivasa, M. (2016). Nested PCR method for early detection of fumonisin producing *Fusarium verticillioides* in pure cultures, cereal samples and plant parts. *Food Biotechnology*, *30*, 18-29.

Nautiyal, C. S. (1999). An efficient microbiological growth medium for screening phosphate solubilizing microorganisms. *FEMS Microbiology Letters*, *170*(1), 265-270.

Nguyen, T. T. X., Dehne, H.-W., & Steiner, U. (2016a). Histopathological assessment of the infection of maize leaves by *Fusarium graminearum*, *F. proliferatum*, and *F. verticillioides*. *Fungal Biology*, *120*(9), 1094-1104.

Nguyen, T. T. X., Dehne, H.-W., & Steiner, U. (2016b). Maize leaf trichomes represent an entry point of infection for *Fusarium* species. *Fungal Biology*, *120*(8), 895-903.

Noman, E., Al-Gheethi, A., Rahman, N. K., Talip, B., A., Radin Mohamed, R. M. S., & Kadir, O. A. (2018). *Single spore isolation as a simple and efficient technique to obtain fungal pure culture* IOP Conf. Series: Earth and Environmental Science, *140*, 012055.

Nunes-Nesi, A., Araújo, W. L., Obata, T., & Fernie, A. R. (2013). Regulation of the mitochondrial tricarboxylic acid cycle. *Current Opinion in Plant Biology*, *16*(3), 335-343.

Nutz, S., Döll, K., & Karlovsky, P. (2011). Determination of the LOQ in real-time PCR by receiver operating characteristic curve analysis: Application to qPCR assays for *Fusarium verticillioides* and *F. proliferatum*. *Analytical and Bioanalytical Chemistry*, *401*(2), 717-726.

Nzelu, C. O., Kato, H., & Peters, N. C. (2019). Loop-mediated isothermal amplification (LAMP): An advanced molecular point-of-care technique for the detection of leishmania infection. *PLoS Neglected Tropical Diseases*, *13*(11), e0007698.

O'Donnell, K. (1996). Progress towards a phylogenetic classification of *Fusarium*. *Sydowia*, *48*, 57-70.

O'Donnell, K., & Cigelnik, E. (1997). Two divergent intragenomic rDNA ITS2 types within a monophyletic lineage of the fungus *Fusarium* are nonorthologous. *Molecular Phylogenetics and Evolution*, *7*(1), 103-116.

O'Donnell, K., Cigelnik, E., & Nirenberg, H. I. (1998). Molecular systematics and phylogeography of the *Gibberella fujikuroi* species complex. *Mycologia*, *90*(3), 465-493.

O'Donnell, K., Rooney, A. P., Proctor, R. H., Brown, D. W., McCormick, S. P., Ward, T. J., Frandsen, R. J. N., Lysøe, E., Rehner, S. A., Aoki, T., Robert, V. A. R. G., Crous, P. W., Groenewald, J. Z., Kang, S., & Geiser, D. M. (2013). Phylogenetic analyses of RPB1 and RPB2 support a middle Cretaceous origin for a clade comprising all agriculturally and medically important fusaria. *Fungal Genetics and Biology*, *52*, 20-31.

O'Donnell, K., Ward, T. J., Robert, V. A. R. G., Crous, P. W., Geiser, D. M., & Kang, S. (2015). DNA sequence-based identification of *Fusarium*: Current status and future directions. *Phytoparasitica*, *43*(5), 583-595.

Omori, A. M., Ono, E. Y. S., Bordini, J. G., Hirozawa, M. T., Fungaro, M. H. P., & Ono, M. A. (2018). Detection of *Fusarium verticillioides* by PCR-ELISA based on Fum21 gene. *Food Microbiology*, *73*, 160-167.

Omotayo, O. P., & Babalola, O. O. (2023). *Fusarium verticillioides* of maize plant: Potentials of propitious phytomicrobiome as biocontrol agents. *Front Fungal Biol*, *4*, 1095765.

Ongena, M., & Jacques, P. (2008). *Bacillus* lipopeptides: Versatile weapons for plant disease biocontrol. *Trends in Microbiology*, *16*(3), 115-125.

Ongena, M., Jourdan, E., Adam, A., Paquot, M., Brans, A., Joris, B., Arpigny, J. L., & Thonart, P. (2007). Surfactin and fengycin lipopeptides of *Bacillus subtilis* as elicitors of induced systemic resistance in plants. *Environmental Microbiology*, *9*(4), 1084-1090.

Ons, L., Bylemans, D., Thevissen, K., & Cammue, B. P. A. (2020). Combining biocontrol agents with chemical fungicides for integrated plant fungal disease control. *Microorganisms*, *8*(12), 1930.

Osmundson, T. W., Eyre, C. A., Hayden, K. M., Dhillon, J., & Garbelotto, M. M. (2013). Back to basics: An evaluation of naoh and alternative rapid DNA extraction protocols for DNA barcoding, genotyping, and disease diagnostics from fungal and Oomycete samples. *Molecular Ecology Resources*, *13*(1), 66-74.

Pahlich, E., & Gerlitz, C. (1980). A rapid DNA isolation procedure for small quantities of fresh leaf tissue. *Phytochemistry*, *19*, 11-13.

Paravar, A., Piri, R., Balouchi, H., & Ma, Y. (2023). Microbial seed coating: An attractive tool for sustainable agriculture. *Biotechnology Reports*, *37*, e00781.

Parkhomchuk, D., Borodina, T., Amstislavskiy, V., Banaru, M., Hallen, L., Krobitsch, S., Lehrach, H., & Soldatov, A. (2009). Transcriptome analysis by strand-specific sequencing of complementary DNA. *Nucleic Acids Research*, *37*(18), e123.

Patiño, B., Mirete, S., González-Jaén, M. T., Mulé, G., Rodríguez, M. T., & Vázquez, C. (2004). PCR detection assay of fumonisin-producing *Fusarium verticillioides* strains. *Journal of Food Protection*, *67*(6), 1278-1283.

Pava-Ripoll, M., Angelini, C., Fang, W., Wang, S., Posada, F. J., & St Leger, R. (2011). The rhizosphere-competent entomopathogen *Metarhizium anisopliae* expresses a specific subset of genes in plant root exudate. *Microbiology*, *157*(1), 47-55.

Pereira, P. C. G., Parente, C. E. T., Carvalho, G. O., Torres, J. P. M., Meire, R. O., Dorneles, P. R., & Malm, O. (2021). A review on pesticides in flower production: A push to reduce human exposure and environmental contamination. *Environmental Pollution*, *289*, 117817.

Perrony, P. E. P., Guimarães, R. A., Reis, L. O., Gomes, L. B., da Silva, L. J., de Albuquerque Correa, C. M., da Silva, J. C. P., & de Medeiros, F. H. V. (2023). Selectivity of chemical and biological foliar treatments on the phyllosphere communities of bacteria and fungi antagonistic to *Fusarium verticillioides* in maize. *Journal of Phytopathology*, *171*(11-12), 656-672.

Persello-Cartieaux, F., Nussaume, L., & Robaglia, C. (2003). Tales from the underground: Molecular plant-rhizobacteria interactions. *Plant, Cell & Environment*, *26*(2), 189-199.

Piepenburg, O., Williams, C. H., Stemple, D. L., & Armes, N. A. (2006). DNA detection using recombination proteins. *PLoS Biology*, *4*(7), e204.

Pieterse, C. M., van Wees, S. C., Hoffland, E., van Pelt, J. A., & van Loon, L. C. (1996). Systemic resistance in Arabidopsis induced by biocontrol bacteria is independent of salicylic acid accumulation and pathogenesis-related gene expression. *The Plant Cell*, *8*(8), 1225-1237.

Plattner, R., Brown, D., Seo, J.-A., & Lee, Y.-W. (2004). Discontinuous distribution of fumonisin biosynthetic genes in the *Gibberella fujikuroi* species complex. *Mycological research*, *108*, 815-822.

Put, H., Gerstmans, H., Vande Capelle, H., Fauvart, M., Michiels, J., & Masschelein, J. (2024). *Bacillus subtilis* as a host for natural product discovery and engineering of biosynthetic gene clusters. *Natural Product Reports*, *41*(7), 1113-1151.

Qi, X., Liu, W., He, X., & Du, C. (2023). A review on surfactin: Molecular regulation of biosynthesis. *Archives of Microbiology*, *205*(9), 313.

Qiao, J., Borriss, R., Sun, K., Zhang, R., Chen, X., Liu, Y., & Liu, Y. (2024). Research advances in the identification of regulatory mechanisms of surfactin production by *Bacillus*: A review. *Microbial Cell Factories*, *23*(1), 100.

Qin, Z., Ren, X., Jiang, K., Wu, X., Yang, Z., & Wang, X. (2014). Identification of *Fusarium* species and *F. graminearum* species complex causing maize ear rot in China. *Acta Phytophylacica Sinica*, *5*, 589-596.

Qiu, J., Jiang, C., Wang, S., He, C., Chen, D., Lan, J., Xu, J., Lee, Y.-W., & Shi, J. (2025). Geographic variations in the *Fusarium* species and toxins associated with maize ear rot in China. *International Journal of Food Microbiology*, *436*, 111208.

Qiu, J., Lu, Y., He, D., Lee, Y. W., Ji, F., Xu, J., & Shi, J. (2020). *Fusarium fujikuroi* species complex associated with rice, maize, and soybean from Jiangsu province, China: Phylogenetic, pathogenic, and toxigenic analysis. *Plant Disease*, *104*(8), 2193-2201.

Qiu, J., Xu, J., Dong, F., Yin, X., & Shi, J. (2015). Isolation and characterization of *Fusarium verticillioides* from maize in eastern China. *European Journal of Plant Pathology*, *142*(4), 791-800.

Qu, Z., Ren, X., Du, Z., Hou, J., Li, Y., Yao, Y., & An, Y. (2024). *Fusarium* mycotoxins: The major food contaminants. *mLife*, *3*(2), 176-206.

Rahman, M., Sabir, A. A., Mukta, J. A., Khan, M. M. A., Mohi-Ud-Din, M., Miah, M. G., Rahman, M., & Islam, M. T. (2018). Plant probiotic bacteria *Bacillus* and *Paraburkholderia* improve growth, yield and content of antioxidants in strawberry fruit. *Scientific Reports*, *8*(1), 2504.

Rajapaksha, P., Elbourne, A., Gangadoo, S., Brown, R., Cozzolino, D., & Chapman, J. (2019). A review of methods for the detection of pathogenic microorganisms. *Analyst*, *144*(2), 396-411.

Rani, A., Rana, A., Dhaka, R. K., Singh, A. P., Chahar, M., Singh, S., Nain, L., Singh, K. P., & Minz, D. (2023). Bacterial volatile organic compounds as biopesticides, growth promoters and plant-defense elicitors: Current understanding and future scope. *Biotechnology Advances*, *63*, 108078.

Riley, R. T., & Voss, K. A. (2006). Differential sensitivity of rat kidney and liver to fumonisin toxicity: Organ-specific differences in toxin accumulation and sphingoid base metabolism. *Toxicological Sciences*, *92*(1), 335-345.

Rocha, I., Ma, Y., Souza-Alonso, P., Vosátka, M., Freitas, H., & Oliveira, R. S. (2019). Seed coating: A tool for delivering beneficial microbes to agricultural crops. *Frontiers in Plant Science*, *10*, 1357.

Roussin-Léveillée, C., Mackey, D., Ekanayake, G., Gohmann, R., & Moffett, P. (2024). Extracellular niche establishment by plant pathogens. *Nature Reviews Microbiology*, *22*(6), 360-372.

Ruiz-García, C., Béjar, V., Martínez-Checa, F., Llamas, I., & Quesada, E. (2005). *Bacillus velezensis* sp. nov., a surfactant-producing bacterium isolated from the river vélez in málaga, southern Spain. *International Journal of Systematic and Evolutionary Microbiology*, *55*(Pt 1), 191-195.

Ryu, M.-H., Zhang, J., Toth, T., Khokhani, D., Geddes, B. A., Mus, F., Garcia-Costas, A., Peters, J. W., Poole, P. S., Ané, J.-M., & Voigt, C. A. (2020). Control of nitrogen fixation in bacteria that associate with cereals. *Nature Microbiology*, *5*(2), 314-330.

Sahane, P. (2020). In vitro efficacy of fungicides against *Fusarium oxysporum* f. sp. *ciceri*. *Journal of Pharmacognosy and Phytochemistry*, *10*(1), 978-984.

Samyal, S., & Sharma, A. (2023). Mycotoxins: Structure, biosynthesis, health effects, and their biological detoxification. In I. Singh, V. R. Rajpal, & S. S. Navi (Eds.), *Fungal resources for sustainable economy: Current status and future perspectives* (pp. 479-508). Springer Nature Singapore.

Sanches, P. H. G., de Melo, N. C., Porcari, A. M., & de Carvalho, L. M. (2024). Integrating molecular perspectives: Strategies for comprehensive multi-omics integrative data analysis and machine learning applications in transcriptomics, proteomics, and metabolomics. *Biology*, *13*(11), 848.

Saravanakumari, K., Thiruvudainambi, s. T., Ebenezar, E., & Natesan, S. (2019). Efficacy of some fungicides and oil cake extracts against basal rot of onion caused by *Fusarium oxysporum*. *International Journal of Farm Sciences*, *9*, 93.

Savary, S., Willocquet, L., Pethybridge, S. J., Esker, P., McRoberts, N., & Nelson, A. (2019). The global burden of pathogens and pests on major food crops. *Nature Ecology & Evolution*, *3*(3), 430-439.

Schalk, I. J. (2025). Bacterial siderophores: Diversity, uptake pathways and applications. *Nature Reviews Microbiology*, *23*(1), 24-40.

Schulz, T. A., & Prinz, W. A. (2007). Sterol transport in yeast and the oxysterol binding protein homologue (OSH) family. *Biochimica et Biophysica Acta (BBA) - Molecular and Cell Biology of Lipids*, *1771*(6), 769-780.

Seifert, G. J. (2004). Nucleotide sugar interconversions and cell wall biosynthesis: How to bring the inside to the outside. *Current Opinion in Plant Biology*, *7*(3), 277-284.

Shao, J., Li, Y., Li, Z., Xu, Z., Xun, W., Zhang, N., Feng, H., Miao, Y., Shen, Q., & Zhang, R. (2021). Participating mechanism of a major contributing gene ysne for auxin biosynthesis in *Bacillus amyloliquefaciens* SQR9. *Journal of Basic Microbiology*, *61*(6), 569-575.

Shao, J., Xu, Z., Zhang, N., Shen, Q., & Zhang, R. (2015). Contribution of indole-3-acetic acid in the plant growth promotion by the rhizospheric strain *Bacillus amyloliquefaciens* SQR9. *Biology and Fertility of Soils*, *51*(3), 321-330.

Shao, M.-W., Chen, H.-J., Huang, A.-Q., Zheng, L., Li, C.-j., Qin, D., Sun, Y.-H., Lin, Z., Fu, G., Chen, Y.-H., Li, Y.-J., Dong, Z.-Y., Cheng, P., Pramono, H., Yu, G.-H., Xu, Z.-M., Miao, S., & Hyde, K. D. (2025). Modulation of rhizosphere microbiota by *Bacillus subtilis* R31 enhances long-term suppression of banana *Fusarium* wilt. *iMetaOmics*, *2*(2), e70006.

Shin, K., Kwon, S.-H., Lee, S.-C., & Moon, Y.-E. (2021). Sensitive and rapid detection of citrus scab using an RPA-CRISPR/Cas12a system combined with a lateral flow assay. *Plants*, *10*(10), 2132.

Shore, D., Zencir, S., & Albert, B. (2021). Transcriptional control of ribosome biogenesis in yeast: Links to growth and stress signals. *Biochemical Society Transactions*, *49*(4), 1589-1599.

Sobek, E. A., & Munkvold, G. P. (1999). European corn borer (Lepidoptera: Pyralidae) larvae as vectors of *Fusarium moniliforme*, causing kernel rot and symptomless infection of maize kernels. *Journal of Economic Entomology*, *92*(3), 503-509.

Spears, J. L., Kramer, R., Nikiforov, A. I., Rihner, M. O., & Lambert, E. A. (2021). Safety assessment of *Bacillus subtilis* MB40 for use in foods and dietary supplements. *Nutrients*, *13*(3).

Sreedharan, S. M., Rishi, N., & Singh, R. (2023). Microbial lipopeptides: Properties, mechanics and engineering for novel lipopeptides. *Microbiological Research*, *271*, 127363.

Sritongon, N., Boonlue, S., Mongkolthanaruk, W., Jogloy, S., & Riddech, N. (2023). The combination of multiple plant growth promotion and hydrolytic enzyme

producing rhizobacteria and their effect on *Jerusalem artichoke* growth improvement. *Scientific Reports*, *13*(1), 5917.

Stępień, Ł., Koczyk, G., & Waśkiewicz, A. (2011). FUM cluster divergence in fumonisins-producing *Fusarium* species. *Fungal Biology*, *115*(2), 112-123.

Stincone, P., Veras, F. F., Pereira, J. Q., Mayer, F. Q., Varela, A. P. M., & Brandelli, A. (2020). Diversity of cyclic antimicrobial lipopeptides from *Bacillus* p34 revealed by functional annotation and comparative genome analysis. *Microbiological Research*, *238*, 126515.

Su, F., Wang, S., Gao, W., Sun, M., Li, X., Zhao, Y., Zhao, L., Wei, J., Liu, Z., & Zhao, B. (2025). Visual detection of multiple *Fusarium* species via RAA-CRISPR/Cas12a dual fluorescence–lateral flow assay. *Journal of Future Foods*.

Sun, H., Zhang, H., Guo, N., Shi, J., Chen, D., & Ma, H. (2017). Isolation and identification of pathogens causing maize ear rot in Huang-huai-hai summer corn region. *Journal of Plant Protection*, *44*(5), 796-802.

Sun, X., Xu, Z., Xie, J., Hesselberg-Thomsen, V., Tan, T., Zheng, D., Strube, M. L., Dragoš, A., Shen, Q., Zhang, R., & Kovács, Á. T. (2022). *Bacillus velezensis* stimulates resident rhizosphere *Pseudomonas stutzeri* for plant health through metabolic interactions. *The ISME Journal*, *16*(3), 774-787.

Tabassum, B., Khan, A., Tariq, M., Ramzan, M., Iqbal Khan, M. S., Shahid, N., & Aaliya, K. (2017). Bottlenecks in commercialisation and future prospects of PGPR. *Applied Soil Ecology*, *121*, 102-117.

Tan, M., Liao, C., Liang, L., Yi, X., Zhou, Z., & Wei, G. (2022). Recent advances in recombinase polymerase amplification: Principle, advantages, disadvantages and applications. *Frontiers in Cellular and Infection Microbiology*, *12*, 1019071.

Tanaka, H., & Watanabe, T. (1995). Glucanases and chitinases of *Bacillus circulans* WL-12. *Journal of Industrial Microbiology and Biotechnology*, *14*(6), 478-483.

Tang, T., Ding, Y., & Guo, W. (2024). Development of an efficient CRISPR/Cas9 system in *Fusarium verticillioides* and its application in reducing mycotoxin contamination. *Journal of Agricultural and Food Chemistry*, *72*(25), 14229-14240.

Tao, C., Li, R., Xiong, W., Shen, Z., Liu, S., Wang, B., Ruan, Y., Geisen, S., Shen, Q., & Kowalchuk, G. A. (2020). Bio-organic fertilizers stimulate indigenous soil pseudomonas populations to enhance plant disease suppression. *Microbiome*, *8*(1), 137.

Tariq, M., Amir, K., Mohd, A., Faryad, K., Taruba, A., Mohammad, S., & Siddiqui, M. A. (2020). Biological control: A sustainable and practical approach for plant disease management. *Acta Agriculturae Scandinavica, Section B - Soil & Plant Science*, *70*(6), 507-524.

Tian, H., Liu, B., Yang, J., Zhou, C., Xu, X., Zhang, Y., Lu, Z., & Zhang, W. (2021). Genetic transformation system for *Bacillus velezensis* NSZ-YBGJ001 and curing of the endogenous plasmid pBV01. *Biotechnology Letters*, *43*(8), 1595-1605.

Tiwari, S., Thakur, R., & Shankar, J. (2015). Role of heat-shock proteins in cellular function and in the biology of fungi. *Biotechnology Research International*, *2015*(1), 132635.

Torres, P., Altier, N., Beyhaut, E., Fresia, P., Garaycochea, S., & Abreo, E. (2024). Phenotypic, genomic and in planta characterization of *Bacillus sensu* lato for their phosphorus biofertilization and plant growth promotion features in soybean. *Microbiological Research*, *280*, 127566.

Tsegaye, Z., Assefa, F., Genene, T., Tenkegna, T., Gizaw, B., & Abatenh, E. (2018). Concept, principle and application of biological control and their role in sustainable plant diseases management strategies. *International Journal of Research Studies in Biosciences*, *6*(4), 18-34.

Tunsagool, P., Jutidamrongphan, W., Phaonakrop, N., Jaresitthikunchai, J., Roytrakul, S., & Leelasuphakul, W. (2019). Insights into stress responses in mandarins triggered by *Bacillus subtilis* cyclic lipopeptides and exogenous plant hormones upon *Penicillium digitatum* infection. *Plant Cell Reports*, *38*(5), 559-575.

Tyagi, A., Lama Tamang, T., Kashtoh, H., Mir, R. A., Mir, Z. A., Manzoor, S., Manzar, N., Gani, G., Vishwakarma, S. K., Almalki, M. A., & Ali, S. (2024). A review on biocontrol agents as sustainable approach for crop disease management: Applications, production, and future perspectives. *Horticulturae*, *10*(8), 805.

Vasilchenko, A. S., Lukyanov, D. A., Dilbaryan, D. S., Usachev, K. S., Poshvina, D. V., Taldaev, A. K., Nikandrova, A. A., Imamutdinova, A. N., Garaeva, N. S., Bikmullin, A. G., Klochkova, E. A., Rusanov, A. L., Romashin, D. D., Luzgina, N. G., Osterman, I. A., Sergiev, P. V., & Teslya, A. V. (2025). Macrolactin A is an inhibitor of protein biosynthesis in bacteria. *Biochimie*, *232*, 25-34.

Vela-Corcía, D., Romero, D., de Vicente, A., & Pérez-García, A. (2018). Analysis of β-tubulin-carbendazim interaction reveals that binding site for mbc fungicides does not include residues involved in fungicide resistance. *Scientific Reports*, *8*(1), 7161.

Venkatarayappa, N., & Dakshayini, M. (2023). Potential antioxidant enzymes from fungi and their clinical significance. In I. Singh, Rajpal, V.R., Navi, S.S. (eds) (Ed.), *Fungal resources for sustainable economy.* (pp. 147-177). Springer.

Verbančič, J., Lunn, J. E., Stitt, M., & Persson, S. (2018). Carbon supply and the regulation of cell wall synthesis. *Molecular Plant*, *11*(1), 75-94.

Voss, K. A., Smith, G. W., & Haschek, W. M. (2007). Fumonisins: Toxicokinetics, mechanism of action and toxicity. *Animal Feed Science and Technology*, *137*(3), 299-325.

Wajid, K., Gull-e-Laala, Haneef, N., Khalid, A.-u.-R., Irshad, G., Shakeel, S., & Saghir, N. (2024). Screening of systemic fungicides against *Fusarium verticilloides* initiating stalk rot of maize. *Agricultural and Biological Research*, *40*(3), 1160-1163.

Wang, B., Wang, R., Wang, D., Wu, J., Li, J., Wang, J., Liu, H., & Wang, Y. (2019). Cas12avdet: A CRISPR/Cas12a-based platform for rapid and visual nucleic acid detection. *Analytical Chemistry*, *91*(19), 12156-12161.

Wang, C., Wang, X., Jin, Z., Müller, C., Pugh, T. A. M., Chen, A., Wang, T., Huang, L., Zhang, Y., Li, L. X. Z., & Piao, S. (2022). Occurrence of crop pests and diseases has largely increased in China since 1970. *Nature Food*, *3*(1), 57-65.

Wang, C., Zhao, D., Qi, G., Mao, Z., Hu, X., Du, B., Liu, K., & Ding, Y. (2019). Effects of *Bacillus velezensis* FKM10 for promoting the growth of *Malus hupehensis* Rehd. and inhibiting *Fusarium verticillioides*. *Food Microbiology*, *10*, 2889.

Wang, D. C., Jiang, C. H., Zhang, L. N., Chen, L., Zhang, X. Y., & Guo, J. H. (2019). Biofilms positively contribute to *Bacillus amyloliquefaciens* 54-induced drought tolerance in tomato plants. *International Journal of Molecular Sciences*, *20*(24), 6271.

Wang, F., Xiao, J., Zhang, Y., Li, R., Liu, L., & Deng, J. (2021). Biocontrol ability and action mechanism of *Bacillus halotolerans* against *Botrytis cinerea* causing grey mould in postharvest strawberry fruit. *Postharvest Biology and Technology*, *174*, 111456.

Wang, H., Sun, P., Yuan, X., Xu, Z., Jiang, X., Xiao, M., Yao, X., & Shi, Y. (2025). Autophagy in tumor immune escape and immunotherapy. *Molecular Cancer*, *24*(1), 85.

Wang, L., Jia, S., Du, Y., Cao, H., Zhang, K., Xing, J., & Dong, J. (2025). Biocontrol potential of *Bacillus subtilis* A3 against corn stalk rot and its impact on root-associated microbial communities. *Agronomy*, *15*(3), 706.

Wang, L., Zhang, L., Liu, Z., Zhao, D., Liu, X., Zhang, B., Xie, J., Hong, Y., Li, P., Chen, S., Dixon, R., & Li, J. (2013). A minimal nitrogen fixation gene cluster from *Paenibacillus* sp. WLY78 enables expression of active nitrogenase in *Escherichia coli*. *PLoS Genetics*, *9*(10), e1003865.

Wang, L. T., Lee, F. L., Tai, C. J., & Kasai, H. (2007). Comparison of *gyrB* gene sequences, 16s rRNA gene sequences and DNA-DNA hybridization in the *Bacillus subtilis* group. *International Journal of Systematic and Evolutionary Microbiology*, *57*(8), 1846-1850.

Wang, L. T., Lee, F. L., Tai, C. J., & Kuo, H. P. (2008). *Bacillus velezensis* is a later heterotypic synonym of *Bacillus amyloliquefaciens*. *International Journal of Systematic and Evolutionary Microbiology*, *58*(3), 671-675.

Wang, Q., Liu, H., Xu, H., Hei, R., Zhang, S., Jiang, C., & Xu, J. R. (2019). Independent losses and duplications of autophagy-related genes in fungal tree of life. *Environmental Microbiology*, *21*(1), 226-243.

Wang, S., Sun, L., Zhang, W., Chi, F., Hao, X., Bian, J., & Li, Y. (2020). *Bacillus velezensis* BM21, a potential and efficient biocontrol agent in control of corn stalk rot caused by *Fusarium graminearum*. *Egyptian Journal of Biological Pest Control*, *30*(1), 9.

Wang, Z.-X., Zhou, X.-Z., Meng, H.-M., Liu, Y.-J., Zhou, Q., & Huang, B. (2014). Comparative transcriptomic analysis of the heat stress response in the filamentous fungus *Metarhizium anisopliae* using RNA-seq. *Applied Microbiology and Biotechnology*, *98*(12), 5589-5597.

Wei, F., Ma, N., Haseeb, H. A., Gao, M., Liu, X., & Guo, W. (2022). Insights into structural and physicochemical properties of maize starch after *Fusarium verticillioides* infection. *Journal of Food Composition and Analysis*, *114*, 104819.

Wigmann, É. F., Meyer, K., Cendoya, E., Maul, R., Vogel, R. F., & Niessen, L. (2020). A loop-mediated isothermal amplification (LAMP) based assay for the rapid and sensitive group-specific detection of fumonisin producing *Fusarium* spp. *International Journal of Food Microbiology*, *325*, 108627.

Wimalasekera, R. (2015). Role of seed quality in improving crop yields. In K. R. Hakeem (Ed.), *Crop production and global environmental issues* (pp. 153-168). Springer International Publishing.

Wu, G., Liu, Y., Xu, Y., Zhang, G., Shen, Q., & Zhang, R. (2018). Exploring elicitors of the beneficial rhizobacterium *Bacillus amyloliquefaciens* SQR9 to induce plant systemic resistance and their interactions with plant signaling pathways. *Molecular Plant-Microbe Interactions*, *31*(5), 560-567.

Wu, L., Wu, H., Chen, L., Yu, X., Borriss, R., & Gao, X. (2015). Difficidin and bacilysin from *Bacillus amyloliquefaciens* FZB42 have antibacterial activity against *Xanthomonas oryzae* rice pathogens. *Scientific Reports*, *5*, 12975.

Wu, Q., Xu, H., Chen, G., Mao, Y., Xue, L., Hao, D., Chen, G., Zhang, Z., Lu, H., Shi, M., Huang, X., & Zhou, G. (2018). Screening of maize germplasms for stem rot resistance and classification of heterotic groups. *Journal of Jinling institute of technology*, *34*(4), 67-70.

Xi, J. (2016). *Study on integrated control techniques of corn stalk rot.* Shandong Agricultural University. Shandong province, China.

Xi, K., Shan, L., Yang, Y., Zhang, G., Zhang, J., & Guo, W. (2021). Species diversity and chemotypes of *Fusarium* species associated with maize stalk rot in Yunnan province of southwest China. *Frontiers in Microbiology*, *12*, 652062.

Xia, H., Liu, H., Gong, P., Li, P., Xu, Q., Zhang, Q., Sun, M., Meng, Q., Ye, F., & Yin, W. (2025). Study of the mechanism by which *Bacillus subtilis* improves the soil bacterial community environment in severely saline-alkali cotton fields. *Science of the Total Environment*, *958*, 178000.

Xia, X., Wei, Q., Wu, H., Chen, X., Xiao, C., Ye, Y., Liu, C., Yu, H., Guo, Y., Sun, W., & Liu, W. (2024). *Bacillus* species are core microbiota of resistant maize cultivars that induce host metabolic defense against corn stalk rot. *Microbiome*, *12*(1), 156.

Xiao, B., Wang, M., Zhang, J., Wang, N., Fu, W., Chen, H., Wang, H., Li, L., Pang, X., Liu, C., Huang, F., & Chen, A. (2024). Rapid DNA extraction and microfluidic lamp system in portable equipment for GM crops detection. *Sensors and Actuators B: Chemical*, *411*, 135716.

Xiong, H., Xing, X., Liu, M., Zhang, Z., Wang, Q., Zhang, X., Gou, X., Lu, Y., & Feng, X. (2024). Stalks and roots are the main battlefield for the coevolution between maize and *Fusarium verticillioides*. *Frontiers in Plant Science*, *15*, 1461896.

Xiong, W., Guo, S., Jousset, A., Zhao, Q., Wu, H., Li, R., Kowalchuk, G. A., & Shen, Q. (2017). Bio-fertilizer application induces soil suppressiveness against *Fusarium* wilt disease by reshaping the soil microbiome. *Soil Biology and Biochemistry*, *114*, 238-247.

Xu, J., Yang, X., Wu, C., Chen, Z., & Dai, T. (2022). Recombinase polymerase amplification–lateral flow dipstick assay for rapid detection of *Fusarium circinatum* based on a newly identified unique target gene. *Plant Disease*, *107*(4), 1067-1074.

Xu, L., Dong, Z., Fang, L., Luo, Y., Wei, Z., Guo, H., Zhang, G., Gu, Y. Q., Coleman-Derr, D., Xia, Q., & Wang, Y. (2019). Orthovenn2: A web server for whole-genome comparison and annotation of orthologous clusters across multiple species. *Nucleic Acids Research*, *47*(1), 52-58.

Xu, T., Zhu, T., & Li, S. (2016). B-1,3-1,4-glucanase gene from *Bacillus velezensis* ZJ20 exerts antifungal effect on plant pathogenic fungi. *World Journal of Microbiology and Biotechnology*, *32*(2), 26.

Xu, Y., Zhang, Z., Lu, P., Li, R., Ma, P., Wu, J., Li, T., & Zhang, H. (2023). Increasing *Fusarium verticillioides* resistance in maize by genomics-assisted breeding: Methods, progress, and prospects. *The Crop Journal*, *11*(6), 1626-1641.

Xu, Z., Shao, J., Li, B., Yan, X., Shen, Q., & Zhang, R. (2013). Contribution of bacillomycin D in *Bacillus amyloliquefaciens* SQR9 to antifungal activity and biofilm formation. *Applied and Environmental Microbiology*, *79*(3), 808-815.

Yamamoto, S., & Harayama, S. (1995). PCR amplification and direct sequencing of *gyrB* genes with universal primers and their application to the detection and taxonomic analysis of *Pseudomonas putida* strains. *Applied and Environmental Microbiology*, *61*(3), 1104-1109.

Yu, S., Jia, B., Liu, N., Yu, D., Zhang, S., & Wu, A. (2021). Fumonisin B1 triggers carcinogenesis via HDAC/PI3K/AKT signalling pathway in human esophageal epithelial cells. *Science of The Total Environment*, *787*, 147405.

Yu, X., Ai, C., Xin, L., & Zhou, G. (2011). The siderophore-producing bacterium, *Bacillus subtilis* CAS15, has a biocontrol effect on *Fusarium* wilt and promotes the growth of pepper. *European Journal of Soil Biology*, *47*(2), 138-145.

Yu, Y., Gui, Y., Li, Z., Jiang, C., Guo, J., & Niu, D. (2022). Induced systemic resistance for improving plant immunity by beneficial microbes. *Plants*, *11*(3), 386.

Yuan, Q. S., Yang, P., Liu, Y. K., Tabl, K. M., Guo, M. W., Zhang, J. B., Wu, A. B., Liao, Y. C., Huang, T., & He, W. J. (2025). Iturin and fengycin lipopeptides inhibit pathogenic *Fusarium* by targeting multiple components of the cell membrane and their regulative effects in wheat. *Journal of Integrative Plant Biology*, *67*(8), 2184-2197.

Yuan, X., Hong, S., Xiong, W., Raza, W., Shen, Z., Wang, B., Li, R., Ruan, Y., Shen, Q., & Dini-Andreote, F. (2021). Development of fungal-mediated soil suppressiveness against *Fusarium* wilt disease via plant residue manipulation. *Microbiome*, *9*(1), 200.

Zawadzka, A. M., Kim, Y., Maltseva, N., Nichiporuk, R., Fan, Y., Joachimiak, A., & Raymond, K. N. (2009). Characterization of a *Bacillus subtilis* transporter for petrobactin, an anthrax stealth siderophore. *Proceedings of the National Academy of Sciences*, *106*(51), 21854-21859.

Zeng, D., Rong, Z., Yuan, Y., Wang, X., & Zheng, X. (2018). Rapid diagnosis of rice bakanae disease caused by *Fusarium verticillioides* using a loop-mediated isothermal amplification assay. *Journal of Nanjing Agricultural University*, *41*(2), 286-292.

Zhang, D., Qiang, R., Zhou, Z., Pan, Y., Yu, S., Yuan, W., Cheng, J., Wang, J., Zhao, D., Zhu, J., & Yang, Z. (2022). Biocontrol and action mechanism of *Bacillus subtilis* lipopeptides' fengycins against *Alternaria solani* in potato as assessed by a transcriptome analysis. *Frontiers in Microbiology*, *13*, 861113.

Zhang, F., Tang, T., Li, F., & Guo, W. (2023). Characterization of mating type, spore killing, and pathogenicity of *Fusarium verticillioides* populations from maize in China. *Phytopathology Research*, *5*(1), 40.

Zhang, H., Luo, W., Pan, Y., Xu, J., Xu, J. S., Chen, W. Q., & Feng, J. (2014). First report of *Fusarium* ear rot of maize caused by *Fusarium andiyazi* in China. *Plant Disease*, *98*(10), 1428-1428.

Zhang, J., Cui, W., Abdul Haseeb, H., & Guo, W. (2020). VdNOP12, containing two tandem rna recognition motif domains, is a crucial factor for pathogenicity and cold adaptation in *Verticillium dahliae*. *Environmental Microbiology*, *22*(12), 5387-5401.

Zhang, N., Wang, Z., Shao, J., Xu, Z., Liu, Y., Xun, W., Miao, Y., Shen, Q., & Zhang, R. (2023). Biocontrol mechanisms of *Bacillus*: Improving the efficiency of green agriculture. *Microbial Biotechnology*, *16*(12), 2250-2263.

Zhang, N., Yang, D., Wang, D., Miao, Y., Shao, J., Zhou, X., Xu, Z., Li, Q., Feng, H., Li, S., Shen, Q., & Zhang, R. (2015). Whole transcriptomic analysis of the plant-beneficial rhizobacterium *Bacillus amyloliquefaciens* SQR9 during enhanced biofilm formation regulated by maize root exudates. *BMC Genomics*, *16*(1), 685.

Zhang, Q., Lin, R., Yang, J., Zhao, J., Li, H., Liu, K., Xue, X., Zhao, H., Han, S., & Zhao, H. (2023). Transcriptome analysis reveals that c17 mycosubtilin antagonizes *Verticillium dahliae* by interfering with multiple functional pathways of fungi. *Biology*, *12*(4), 513.

Zhang, R., Chen, Y., Wang, W., Chen, J., Liu, D., Zhang, L., Xiang, Q., Zhao, K., Ma, M., Yu, X., Chen, Q., Penttinen, P., & Gu, Y. (2024). Combined transcriptomic and metabolomic analysis revealed that pH changes affected the expression of carbohydrate and ribosome biogenesis-related genes in *Aspergillus niger* SICU-33. *Frontiers in Microbiology*, *15*, 1389268.

Zhang, S., Zhou, S., Yu, S., Zhao, Y., Wu, Y., & Wu, A. (2022). LC-MS/MS analysis of fumonisin B1, B2, B3, and their hydrolyzed metabolites in broiler chicken feed and excreta. *Toxins (Basel)*, *14*(2), 131.

Zhao, Y., Chen, F., Li, Q., Wang, L., & Fan, C. (2015). Isothermal amplification of nucleic acids. *Chemical Reviews*, *115*(22), 12491-12545.

Zhao, Y., Selvaraj, J. N., Xing, F., Zhou, L., Wang, Y., Song, H., Tan, X., Sun, L., Sangare, L., Folly, Y. M. E., & Liu, Y. (2014). Antagonistic action of *Bacillus subtilis* strain SG6 on *Fusarium graminearum*. *PLoS One*, *9*(3), e92486.

Zheng, Y., Hu, P., Ren, H., Wang, H., Cao, Q., Zhao, Q., Li, H., Zhang, H., Liu, Z., Li, Y., Wang, C., Liu, Z., & Lu, S. (2021). RPA-SYBR green I based instrument-

free visual detection for pathogenic *Yersinia enterocolitica* in meat. *Analytical Biochemistry*, *621*, 114157.

Zhu, H.-Q., Feng, Z.-L., Li, Z.-F., Shi, Y.-Q., Zhao, L.-H., & Yang, J.-R. (2013). Characterization of two fungal isolates from cotton and evaluation of their potential for biocontrol of *Verticillium* wilt of cotton. *Journal of Phytopathology*, *161*(2), 70-77.

Zhu, L., Huang, J., Lu, X., & Zhou, C. (2022). Development of plant systemic resistance by beneficial rhizobacteria: Recognition, initiation, elicitation and regulation. *Frontiers in Plant Science*, *13*, 952397.

Zihalirwa Kulimushi, P., Argüelles Arias, A., Franzil, L., Steels, S., & Ongena, M. (2017). Stimulation of fengycin-type antifungal lipopeptides in *Bacillus amyloliquefaciens* in the presence of the maize fungal pathogen *Rhizomucor variabilis*. *Frontiers in Microbiology*, *8*, 850.

Appendix 1

Gene-by-gene annotation of biosynthetic gene clusters predicted by antiSMASH in *B. velezensis* IFST-221

Table A1-1 Gene-level annotation of the andalusicin A/B biosynthetic gene cluster

Identifier	Length (aa)	Function	Best BLASTP hit (NCBI nr)	Identity (%)
ctg1_188	600	biosynthetic-additional	Glutamine--fructose-6-phosphate transaminase (isomerizing)	95.17
ctg1_191	869	biosynthetic	Class III lanthionine synthetase LanKC	100.00
ctg1_192	45	biosynthetic-additional	MULTISPECIES: class III lanthipeptide	100.00
ctg1_193	280	biosynthetic-additional	Class I SAM-dependent methyltransferase	95.39
ctg1_194	281	biosynthetic-additional	Aldo/keto reductase	98.58
ctg1_199	461	biosynthetic-additional	MULTISPECIES: amino acid permease [*Bacillus*]	100.00
ctg1_200	237	biosynthetic-additional	YjjG family noncanonical pyrimidine nucleotidase [*Bacillus amyloliquefaciens*]	96.62

Table A1-2 Gene-level annotation of the surfactin biosynthetic gene cluster

Identifier	Length (aa)	Function	Best BLASTP hit (NCBI nr)	Identity (%)
ctg1_300	336	biosynthetic-additional	NAD(P)/FAD-dependent oxidoreductase [*Bacillus velezensis*]	94.81
ctg1_301	479	biosynthetic-additional	Uroporphyrinogen-III C-methyltransferase [*Bacillus velezensis*]	98.12
ctg1_303	805	biosynthetic-additional	NADPH-nitrite reductase [*Bacillus siamensis*]	96.77
ctg1_304	710	biosynthetic-additional	Assimilatory nitrate reductase catalytic subunit NasC [*Bacillus velezensis*]	97.04
ctg1_305	775	biosynthetic-additional	MULTISPECIES: nitrite reductase large subunit NirB [*Bacillus amyloliquefaciens* group]	96.52
ctg1_307	400	biosynthetic-additional	GTP-binding protein [*Bacillus amyloliquefaciens*]	97
ctg1_308	378	biosynthetic-additional	Zinc-dependent alcohol dehydrogenase [*Bacillus velezensis*]	98.68
ctg1_317	3584	biosynthetic	Surfactin non-ribosomal peptide synthetase SrfAA [*Bacillus velezensis*]	98.21
ctg1_318	3586	biosynthetic	Surfactin non-ribosomal peptide synthetase SrfAB [*Bacillus velezensis*]	98.8
ctg1_319	1278	biosynthetic	MULTISPECIES: surfactin non-ribosomal peptide synthetase SrfAC [*Bacillus*]	99.3
ctg1_320	243	biosynthetic-additional	MULTISPECIES: surfactin biosynthesis thioesterase SrfAD [*Bacillus*]	99.18
ctg1_321	436	biosynthetic-additional	Aminotransferase class I/II-fold pyridoxal phosphate-dependent enzyme [*Bacillus* sp. UNC69MF]	98.62
ctg1_322	224	biosynthetic-additional	MULTISPECIES: 4'-phosphopantetheinyl transferase family protein [*Bacillus*]	99.55
ctg1_326	265	biosynthetic-additional	Cystine ABC transporter substrate-binding lipoprotein TcyA [*Bacillus velezensis*]	98.87
ctg1_328	192	biosynthetic-additional	Non-oxidative hydroxyarylic acid decarboxylases subunit B [*Bacillus velezensis*]	99.47
ctg1_338	440	biosynthetic-additional	LLM class flavin-dependent oxidoreductase [*Bacillus subtilis*]	92.24

Table A1-3 Gene-level annotation of the macrolactin biosynthetic gene cluster

Identifier	Length (aa)	Function	Best BLASTP hit (NCBI nr)	Identity (%)

ctg1_1362	303	biosynthetic-additional	MULTISPECIES: 1-phosphofructokinase [*Bacillus*]	98.35
ctg1_1375	577	biosynthetic-additional	MULTISPECIES: adenine deaminase [*Bacillus*]	98.61
ctg1_1378	257	biosynthetic-additional	Cof-type HAD-IIB family hydrolase [*Bacillus amyloliquefaciens*]	98.83
ctg1_1379	184	biosynthetic-additional	MULTISPECIES: peptide deformylase [*Bacillus*]	99.46
ctg1_1382	768	biosynthetic	ACP S-malonyltransferase [*Bacillus amyloliquefaciens*], mlnA	98.31
ctg1_1383	4086	biosynthetic	SDR family NAD(P)-dependent oxidoreductase [*Bacillus velezensis*], mlnB	97.36
ctg1_1384	1586	biosynthetic	Type I polyketide synthase [*Bacillus velezensis*], mlnC	97.42
ctg1_1385	2901	biosynthetic	MULTISPECIES: type I polyketide synthase [*Bacillus*], mlnD	97.11
ctg1_1386	2334	biosynthetic	SDR family NAD(P)-dependent oxidoreductase [*Bacillus velezensis*], mlnE	96.79
ctg1_1387	1903	biosynthetic	Type I polyketide synthase, partial [*Bacillus velezensis*], mlnF	98.1
ctg1_1388	2460	biosynthetic	Type I polyketide synthase [*Bacillus velezensis*], mlnG	97.85
ctg1_1389	1283	biosynthetic-additional	Alpha/beta fold hydrolase [*Bacillus velezensis*], mlnH	97.22
ctg1_1390	363	biosynthetic-additional	Serine hydrolase domain-containing protein [*Bacillus amyloliquefaciens*], mlnI	98.62
ctg1_1391	371	biosynthetic-additional	Pyruvate dehydrogenase (acetyl-transferring) E1 component subunit alpha [*Bacillus velezensis*]	99.46
ctg1_1392	325	biosynthetic-additional	Alpha-ketoacid dehydrogenase subunit beta [*Bacillus carboniphilus*]	89.85
ctg1_1394	470	biosynthetic-additional	Dihydrolipoyl dehydrogenase [*Bacillus spizizenii*]	97.45
ctg1_1396	266	biosynthetic-additional	Polysaccharide deacetylase family protein [*Bacillus velezensis*]	95.11
ctg1_1397	490	biosynthetic-additional	Aminotransferase class I/II-fold pyridoxal phosphate-dependent enzyme [*Bacillus velezensis*]	98.98
ctg1_1401	265	biosynthetic-additional	MULTISPECIES: inositol-1-monophosphatase [*Bacillus*]	97.37

Table A1-4 Gene-level annotation of the bacillaene biosynthetic gene cluster

Identifier	Length (aa)	Function	Best BLASTP hit (NCBI nr)	Identity (%)
ctg1_1622	393	biosynthetic-additional	MULTISPECIES: serine hydrolase domain-containing protein [*Bacillus amyloliquefaciens* group]	95.42
ctg1_1626	348	biosynthetic-additional	L-threonine 3-dehydrogenase [*Bacillus amyloliquefaciens*]	94.83
ctg1_1627	391	biosynthetic-additional	Glycine C-acetyltransferase [*Bacillus* sp. JNUCC-22]	99.74
ctg1_1628	509	biosynthetic-additional	MULTISPECIES: tRNA (N6-isopentenyl adenosine(37)-C2)-methylthiotransferase MiaB [*Bacillus*]	91.55
ctg1_1634	230	biosynthetic-additional	MBL fold metallo-hydrolase [*Bacillus amyloliquefaciens*], baeB	99.11
ctg1_1635	289	biosynthetic	ACP S-malonyltransferase [*Bacillus velezensis*], baeC	98.62
ctg1_1636	324	biosynthetic	Malonyl-CoA-[acyl-carrier-protein] transacylase [*Bacillus velezensis* FZB42], baeD	100
ctg1_1637	746	biosynthetic	MULTISPECIES: ACP S-malonyltransferase [*Bacillus*], baeE	93.43
ctg1_1638	82	biosynthetic-additional	Acyl carrier protein [*Bacillus amyloliquefaciens*], acpK	92.68

ctg1_1639	420	biosynthetic	MULTISPECIES: hydroxymethylglutaryl-CoA synthase family protein [*Bacillus*], baeG	99.28
ctg1_1640	257	biosynthetic-additional	Enoyl-CoA hydratase/isomerase [Bacillus velezensis] baeH	98.05
ctg1_1641	249	biosynthetic-additional	Polyketide synthase [*Bacillus velezensis*], baeI	99.6
ctg1_1642	4982	biosynthetic	Amino acid adenylation domain-containing protein [*Bacillus velezensis*], baeJ	98.31
ctg1_1643	4474	biosynthetic	SDR family NAD(P)-dependent oxidoreductase [*Bacillus velezensis*], baeL	98.17
ctg1_1644	3512	biosynthetic	SDR family NAD(P)-dependent oxidoreductase [*Bacillus velezensis*], baeM	98.41
ctg1_1645	5433	biosynthetic	Non-ribosomal peptide synthetase [*Bacillus velezensis*], baeN	98.77
ctg1_1646	2485	biosynthetic	Beta-ketoacyl synthase N-terminal-like domain-Containing protein [*Bacillus amyloliquefaciens*], baeR	90.99
ctg1_1647	403	biosynthetic-additional	Cytochrome P450 family protein [*Bacillus velezensis*], baeS	99.01
ctg1_1651	442	biosynthetic-additional	S8 family peptidase [*Bacillus velezensis*]	98.42
ctg1_1659	314	biosynthetic-additional	MULTISPECIES: tRNA (adenosine(37)-N6)-dimethylallyltransferase MiaA [*Bacillus amyloliquefaciens* group]	99.04

Table A1-5 Gene-level annotation of the fengycin biosynthetic gene cluster

Identifier	Length (aa)	Function	Best BLASTP hit (NCBI nr)	Identity (%)
ctg1_1738	339	biosynthetic-additional	MULTISPECIES: zinc-binding alcohol dehydrogenase family protein [*Bacillus amyloliquefaciens* group]	98.23
ctg1_1741	278	biosynthetic-additional	SDR family oxidoreductase [*Bacillus velezensis*]	97.12
ctg1_1757	2619	biosynthetic	MULTISPECIES: bacillomycin D non-ribosomal peptide synthetase BamC [*Bacillus*]	97.02
ctg1_1758	5363	biosynthetic	Bacillomycin D non-ribosomal peptide synthetase BamB [*Bacillus velezensis*]	98.62
ctg1_1759	3982	biosynthetic	Bacillomycin D hybrid PKS/NRPS BamA, partial [*Bacillus velezensis*]	97.29
ctg1_1760	400	biosynthetic	MULTISPECIES: bacillomycin D biosynthesis malonyl-CoA transacylase BamD [*Bacillus*]	95.05
ctg1_1761	261	biosynthetic-additional	MULTISPECIES: 3-hydroxybutyrate dehydrogenase [*Bacillus*]	97.32
ctg1_1765	398	biosynthetic-additional	MULTISPECIES: cytochrome P450 [*Bacillus*]	98.99
ctg1_1766	339	biosynthetic-additional	Biotin synthase BioB [*Bacillus siamensis*]	96.76
ctg1_1768	386	biosynthetic-additional	8-Amino-7-oxononanoate synthase [*Bacillus velezensis*]	98.96
ctg1_1769	448	biosynthetic-additional	Adenosylmethionine--8-amino-7-oxononanoate transaminase [*Bacillus velezensis*]	98.88
ctg1_1772	297	biosynthetic-additional	UTP--glucose-1-phosphate uridylyltransferase GalU [*Bacillus* sp. SL112]	97.29
ctg1_1774	509	biosynthetic-additional	MULTISPECIES: acyl-CoA carboxylase subunit beta [*Bacillus amyloliquefaciens* group]	98.43
ctg1_1775	259	biosynthetic-additional	MULTISPECIES: enoyl-CoA hydratase [*Bacillus amyloliquefaciens* group]	96.91
ctg1_1776	299	biosynthetic	MULTISPECIES: hydroxymethylglutaryl-CoA lyase [*Bacillus*]	99.67
ctg1_1778	449	biosynthetic-additional	Acetyl-CoA carboxylase biotin carboxylase subunit [*Bacillus velezensis*]	99.33

ctg1_1779	546	biosynthetic	AMP-binding protein [*Bacillus velezensis*]	98.53
ctg1_1780	380	biosynthetic-additional	Acyl-CoA dehydrogenase family protein [*Bacillus amyloliquefaciens*]	99.74
ctg1_1783	1267	biosynthetic	Fengycin non-ribosomal peptide synthetase FenB [*Bacillus mojavensis*]	62.46
ctg1_1784	3591	biosynthetic	Fengycin non-ribosomal peptide synthetase FenA [*Bacillus halotolerans*]	64.33
ctg1_1785	2549	biosynthetic	Fengycin non-ribosomal peptide synthetase FenE [*Bacillus halotolerans*]	68.01
ctg1_1786	2565	biosynthetic	Fengycin non-ribosomal peptide synthetase FenD [*Bacillus halotolerans*]	62.77
ctg1_1787	2552	biosynthetic	Fengycin non-ribosomal peptide synthetase FenC [*Bacillus halotolerans*]	63.92
ctg1_1794	588	biosynthetic-additional	Gamma-glutamyltransferase [*Bacillus velezensis*]	98.81
ctg1_1799	326	biosynthetic-additional	MULTISPECIES: zinc-binding dehydrogenase [*Bacillus*]	96.27
ctg1_1800	493	biosynthetic-additional	Glutamate synthase small subunit [*Bacillus spizizenii*]	91.68

Table A1-6 Gene-level annotation of the difficidin biosynthetic gene cluster

Identifier	Length (aa)	Function	Best BLASTP hit (NCBI nr)	Identity (%)
ctg1_2101	306	biosynthetic-additional	MULTISPECIES: aldo/keto reductase [*Bacillus*]	98.04
ctg1_2103	302	biosynthetic-additional	Alpha/beta hydrolase [*Bacillus velezensis*]	98.34
ctg1_2116	449	biosynthetic-additional	MULTISPECIES: D-serine ammonia-lyase [*Bacillus*]	96.21
ctg1_2117	258	biosynthetic-additional	MULTISPECIES: SDR family NAD(P)-dependent oxidoreductase [*Bacillus*]	97.67
ctg1_2118	319	biosynthetic-additional	MBL fold metallo-hydrolase [*Bacillus velezensis*]	98.11
ctg1_2120	248	biosynthetic-additional	Polyketide synthase [*Bacillus velezensis*], difO	98.79
ctg1_2121	415	biosynthetic-additional	Hydroxymethylglutaryl-CoA synthase family protein [*Bacillus siamensis*], difN	98.8
ctg1_2122	384	biosynthetic-additional	Cytochrome P450 [*Bacillus amyloliquefaciens*], difM	99.48
ctg1_2123	2071	biosynthetic	Beta-ketoacyl synthase N-terminal-like domain-containing protein [*Bacillus siamensis*], difL	97.4
ctg1_2124	2051	biosynthetic	MULTISPECIES: type I polyketide synthase [*Bacillus amyloliquefaciens* group], difK	97.17
ctg1_2125	2572	biosynthetic	Type I polyketide synthase [*Bacillus velezensis*], difJ	96.89
ctg1_2126	5204	biosynthetic	SDR family NAD(P)-dependent oxidoreductase [*Bacillus* sp. YBsi01], difI	96.87
ctg1_2127	1908	biosynthetic	Type I polyketide synthase [*Bacillus velezensis*], difH	94.83
ctg1_2128	2098	biosynthetic	MULTISPECIES: beta-ketoacyl synthase N-terminal-like domain-containing protein [*Bacillus*], difG	96.33
ctg1_2129	4197	biosynthetic	MULTISPECIES: type I polyketide synthase [*Bacillus*], difF	97.55
ctg1_2130	245	biosynthetic-additional	MULTISPECIES: SDR family oxidoreductase [*Bacillus*] difE	99.18
ctg1_2131	454	biosynthetic-additional	MULTISPECIES: long-chain fatty acid--CoA ligase [*Bacillus*], difD	98.46
ctg1_2132	90	biosynthetic-additional	Acyl carrier protein [*Bacillus velezensis*], difC	97.78

ctg1_2134	752	biosynthetic	ACP S-malonyltransferase [*Bacillus velezensis*], difA	98.94
ctg1_2138	338	biosynthetic-additional	MULTISPECIES: NADPH dehydrogenase NamA [*Bacillus*]	99.7
ctg1_2139	257	biosynthetic-additional	Alpha/beta fold hydrolase [*Bacillus velezensis*]	98.44
ctg1_2142	469	biosynthetic-additional	NADP-dependent phosphogluconate dehydrogenase [*Bacillus velezensis*]	99.57
ctg1_2146	371	biosynthetic-additional	M20/M25/M40 family metallo-hydrolase [*Bacillus velezensis*]	99.46
ctg1_2147	507	biosynthetic-additional	MULTISPECIES: acyl-CoA carboxylase subunit beta [*Bacillus amyloliquefaciens* group]	98.62
ctg1_2154	255	biosynthetic-additional	Transporter substrate-binding domain-containing protein [*Bacillus velezensis*]	99.22

Table A1-7 Gene-level annotation of the bacillibactin biosynthetic gene cluster

Identifier	Length (aa)	Function	Best BLASTP hit (NCBI nr)	Identity (%)
ctg1_2765	127	biosynthetic-additional	Hotdog fold thioesterase [*Bacillus velezensis*]	97.64
ctg1_2769	303	biosynthetic	MULTISPECIES: polyprenyl synthetase family protein [*Bacillus*]	99.01
ctg1_2775	183	biosynthetic-additional	Cysteine hydrolase family protein [*Bacillus velezensis*]	98.89
ctg1_2782	243	biosynthetic-additional	(S)-benzoin forming benzil reductase [*Bacillus velezensis*]	99.81
ctg1_2790	376	biosynthetic-additional	MULTISPECIES: alanine dehydrogenase [*Bacillus*]	99.73
ctg1_2792	71	biosynthetic-additional	MbtH family protein [*Bacillus velezensis*]	95.77
ctg1_2793	2375	biosynthetic	Amino acid adenylation domain-containing protein [*Bacillus siamensis*]	93.31
ctg1_2794	308	biosynthetic-additional	isochorismatase [*Bacillus siamensis*], DhbB	93.18
ctg1_2795	541	biosynthetic-additional	MULTISPECIES: (2,3-dihydroxybenzoyl)adenylate synthase [*Bacillus amyloliquefaciens* group], DhbE	99.08
ctg1_2796	398	biosynthetic	Isochorismate synthase DhbC [*Bacillus velezensis*], DhbC	98.49
ctg1_2797	261	biosynthetic	MULTISPECIES: 2,3-dihydro-2,3-dihydroxybenzoate dehydrogenase [*Bacillus*] dhbA	97.7
ctg1_2798	289	biosynthetic-additional	Alpha/beta hydrolase [*Bacillus velezensis*]	97.23
ctg1_2806	406	biosynthetic-additional	NAD(P)/FAD-dependent oxidoreductase [*Bacillus siamensis*]	97.78
ctg1_2807	331	biosynthetic-additional	Ferredoxin--NADP reductase 2 [*Bacillus amyloliquefaciens*]	99.7
ctg1_2814	112	biosynthetic	Uberolysin/carnocyclin family circular bacteriocin, partial [*Bacillus velezensis*]	98
ctg1_2816	181	biosynthetic-additional	MULTISPECIES: GNAT family N-acetyltransferase [*Bacillus*]	96.65
ctg1_2817	253	biosynthetic-additional	SDR family oxidoreductase [*Bacillus velezensis*]	98.42

Table A1-8 Gene-level annotation of the bacilysin biosynthetic gene cluster

Identifier	Length (aa)	Function	Best BLASTP hit (NCBI nr)	Identity (%)
ctg1_3351	460	biosynthetic-additional	Putative amino acid permease YhdG [*Bacillus velezensis*]	99.13

ctg1_3369	266	biosynthetic-additional	NADPH-dependent reductase BacG [*Bacillus subtilis*]	83.01
ctg1_3370	399	biosynthetic-additional	MULTISPECIES: transaminase BacF [*Bacillus*]	87.62
ctg1_3372	472	biosynthetic	L-alanine--L-anticapsin ligase [*Bacillus velezensis*], bacD	98.36
ctg1_3373	253	biosynthetic-additional	Dihydroanticapsin 7-dehydrogenase [*Bacillus amyloliquefaciens*], bacC	98.81
ctg1_3378	472	biosynthetic-additional	Amino acid permease [*Bacillus velezensis*]	99.15
ctg1_3380	515	biosynthetic-additional	L-glutamate gamma-semialdehyde dehydrogenase [*Bacillus nakamurai*]	95.73
ctg1_3387	151	biosynthetic-additional	L-glutamate gamma-semialdehyde dehydrogenase [*Bacillus nakamurai*]	94.7
ctg1_3388	282	biosynthetic-additional	dTDP-4-dehydrorhamnose reductase [*Bacillus siamensis*]	95.76
ctg1_3389	315	biosynthetic-additional	MULTISPECIES: dTDP-glucose 4,6-dehydratase [*Bacillus*]	96.82
ctg1_3390	245	biosynthetic-additional	Sugar phosphate nucleotidyltransferase [*Bacillus amyloliquefaciens*]	95.51

Appendix 2

Differentially expressed genes related to ribosome, carbon metabolism, amino sugar and nucleotide sugar metabolism, and stress responses

Table A2-1 Ribosome-related DEGs.

Gene ID	Log2FC	padj	Predicted protein or description
FVCG_008481	2.06	1.57E-05	Large ribosomal subunit protein eL28
FVCG_010813	1.96	2.05E-05	Small ribosomal subunit protein uS10
FVCG_004764	1.73	1.02E-04	Large ribosomal subunit protein uL1
FVCG_007762	1.75	1.20E-04	Large ribosomal subunit protein eL30
FVCG_011102	1.87	1.91E-04	Large ribosomal subunit protein uL24z
FVCG_000904	1.74	1.98E-04	Large ribosomal subunit protein uL5
FVCG_005927	1.87	2.70E-04	Small ribosomal subunit protein eS25
FVCG_008518	1.65	2.71E-04	Small ribosomal subunit protein uS11
FVCG_005907	1.65	2.79E-04	Large ribosomal subunit protein eL27A
FVCG_001768	1.67	2.90E-04	Small ribosomal subunit protein eS21
FVCG_005926	1.55	3.76E-04	Small ribosomal subunit protein uS7
FVCG_005785	1.62	4.48E-04	Large ribosomal subunit protein eL38
FVCG_004996	1.76	5.83E-04	Small ribosomal subunit protein eS12
FVCG_007624	1.60	6.04E-04	Large ribosomal subunit protein P1
FVCG_004756	1.54	7.69E-04	Large ribosomal subunit protein uL2
FVCG_010947	1.58	8.52E-04	Large ribosomal subunit protein eL29
FVCG_010660	1.66	9.39E-04	Small ribosomal subunit protein eS17
FVCG_011646	1.46	9.60E-04	Large ribosomal subunit protein uL13
FVCG_008472	1.55	0.001	Large ribosomal subunit protein uL23
FVCG_011848	1.51	0.001	Large ribosomal subunit protein uL22
FVCG_004613	1.51	0.001	Small ribosomal subunit protein uS15
FVCG_008168	1.53	0.001	Large ribosomal subunit protein eL18B
FVCG_013228	1.41	0.002	Large ribosomal subunit protein eL32
FVCG_010696	1.54	0.002	Large ribosomal subunit protein P2
FVCG_008013	1.86	0.002	Large ribosomal subunit protein uL18
FVCG_001276	1.48	0.002	Small ribosomal subunit protein uS19
FVCG_000832	1.50	0.002	Large ribosomal subunit protein uL6B
FVCG_004227	1.34	0.002	Small ribosomal subunit protein eS1
FVCG_010881	1.33	0.002	Small ribosomal subunit protein uS3
FVCG_008406	1.53	0.002	Small ribosomal subunit protein eS19
FVCG_012061	1.52	0.002	Large ribosomal subunit protein uL15A
FVCG_009293	1.49	0.002	Large ribosomal subunit protein eL13B
FVCG_000975	1.23	0.003	Large ribosomal subunit protein eL6y
FVCG_013215	1.41	0.003	Large ribosomal subunit protein eL34A
FVCG_004454	1.48	0.004	Large ribosomal subunit protein uL4B
FVCG_001775	1.46	0.004	Large ribosomal subunit protein uL14A
FVCG_013229	1.45	0.004	Small ribosomal subunit protein uS9
FVCG_004943	1.53	0.004	Large ribosomal subunit protein eL43
FVCG_006255	1.54	0.005	Large ribosomal subunit protein uL3
FVCG_001418	1.40	0.005	Large ribosomal subunit protein eL15
FVCG_011223	1.37	0.005	Small ribosomal subunit protein eS26
FVCG_009723	1.36	0.005	Large ribosomal subunit protein eL24
FVCG_000705	1.40	0.005	Small ribosomal subunit protein eS28
FVCG_006233	1.30	0.006	Small ribosomal subunit protein eS10A
FVCG_011897	1.60	0.006	Large ribosomal subunit protein uL11
FVCG_004794	1.29	0.006	Small ribosomal subunit protein uS13
FVCG_009765	1.22	0.007	Small ribosomal subunit protein eS4
FVCG_009418	1.49	0.007	Large ribosomal subunit protein eL14B
FVCG_001628	1.34	0.007	Small ribosomal subunit protein uS17A
FVCG_008160	1.10	0.009	Large ribosomal subunit protein eL19A
FVCG_011170	1.63	0.009	Small ribosomal subunit protein uS2

FVCG_000969	1.25	0.010	Large ribosomal subunit protein uL29
FVCG_009141	1.35	0.010	Small ribosomal subunit protein uS4
FVCG_004997	1.36	0.013	Small ribosomal subunit protein uS8
FVCG_007835	1.26	0.013	Large ribosomal subunit protein eL42
FVCG_015798	1.23	0.014	Ubiquitin-ribosomal protein eS31 fusion protein
FVCG_000445	1.25	0.014	Large ribosomal subunit protein eL31
FVCG_002920	1.06	0.016	Small ribosomal subunit protein eS27
FVCG_009715	1.24	0.016	Large ribosomal subunit protein eL37
novel.581	1.15	0.018	Ubiquitin-ribosomal protein eL40 fusion protein
FVCG_000420	1.22	0.023	Large ribosomal subunit protein eL20A
FVCG_004874	1.21	0.027	Large ribosomal subunit protein uL10
FVCG_000688	1.21	0.037	Large ribosomal subunit protein eL33A
FVCG_004767	1.09	0.040	Large ribosomal subunit protein eL39
FVCG_010971	1.01	0.044	Small ribosomal subunit protein uS12

Table A2-2 Carbon metabolism and TCA cycle DEGs.

Gene ID	Log2FC	padj	Predicted protein or description
FVCG_006044	4.69	3.78E-16	Formate dehydrogenase
FVCG_012454	-5.43	5.95E-15	Phosphoenolpyruvate synthase
FVCG_002399	4.54	1.03E-14	Peroxisomal catalase
FVCG_001778	4.44	2.9E-13	NAD-dependent malic enzyme, mitochondrial
FVCG_004585	-3.65	2.07E-12	Pyruvate carboxylase
FVCG_005314	-4.91	1.22E-08	Catalase-1
FVCG_007808	3.22	1.31E-07	S-(hydroxymethyl)glutathione dehydrogenase
FVCG_008204	2.52	3.63E-07	Fructose-bisphosphate aldolase
FVCG_002230	8.25	6.75E-07	6-phosphogluconate dehydrogenase, decarboxylating
FVCG_005135	3.23	3.57E-06	S-formylglutathione hydrolase
FVCG_010984	2.45	1.37E-05	Aspartate aminotransferase, mitochondrial
FVCG_000835	-1.98	1.04E-04	Probable aminomethyltransferase, mitochondrial
FVCG_009314	-2.78	1.26E-04	Putative serine hydroxymethyltransferase, mitochondrial
FVCG_007899	2.45	1.84E-04	Serine racemase
FVCG_011023	3.30	3.16E-04	Putative glutathione-dependent formaldehyde-activating enzyme
FVCG_009650	-1.71	3.31E-04	Hexokinase-1
FVCG_014899	-2.53	6.71E-04	Gluconolactonase
FVCG_009315	-2.07	0.001	Glycine cleavage system H protein 2, mitochondrial
FVCG_004889	1.72	0.001	Probable 3-hydroxybutyryl-CoA dehydrogenase
FVCG_014041	6.01	0.002	Alcohol oxidase
FVCG_003438	2.05	0.006	Fructose-1,6-bisphosphatase
FVCG_009461	1.56	0.009	Phosphoserine phosphatase
FVCG_011515	3.02	0.010	Probable methylmalonate-semialdehyde/malonate-semialdehyde dehydrogenase [acylating], mitochondrial
FVCG_014962	-1.55	0.015	Probable gluconokinase
FVCG_009316	-1.92	0.015	Putative glycine dehydrogenase (decarboxylating), mitochondrial
FVCG_000687	-1.54	0.015	Glucose-6-phosphate 1-dehydrogenase
FVCG_003461	1.07	0.020	Ribose-phosphate pyrophosphokinase 2
FVCG_001350	1.59	0.033	Acetyl-coenzyme A synthetase
FVCG_002787	1.23	0.038	Aspartate aminotransferase, cytoplasmic
FVCG_004176	1.68	0.038	Pyruvate kinase
FVCG_000875	1.27	0.039	6-phosphogluconate dehydrogenase, decarboxylating 1

FVCG_003048	1.78	0.041	Peroxisomal hydratase-dehydrogenase-epimerase
TCA cycle related-DEGs			
FVCG_001701	2.68	7.38E-10	Succinate dehydrogenase [ubiquinone] cytochrome b small subunit, mitochondrial
FVCG_013036	2.68	4.34E-08	2-oxoglutarate dehydrogenase, mitochondrial
FVCG_006402	2.71	9.96E-08	Dihydrolipoyllysine-residue succinyltransferase component of 2-oxoglutarate dehydrogenase complex, mitochondrial
FVCG_000522	2.45	4.33E-07	Citrate synthase, mitochondrial
FVCG_008368	2.26	4.84E-07	Malate dehydrogenase, mitochondrial
FVCG_011796	5.43	6.02E-07	Succinate dehydrogenase/Fumarate reductase transmembrane subunit
FVCG_011145	2.35	3.60E-06	Succinate--CoA ligase [ADP-forming] subunit beta, mitochondrial
FVCG_006944	3.13	8.61E-06	Aconitate hydratase, mitochondrial
FVCG_004375	2.06	1.34E-05	Probable succinate dehydrogenase [ubiquinone] flavoprotein subunit, mitochondrial
FVCG_006421	2.38	1.79E-05	Aconitate hydratase, mitochondrial
FVCG_010475	2.22	2.14E-05	Succinate dehydrogenase cytochrome B subunit, mitochondrial
FVCG_010691	2.02	2.55E-05	Succinate dehydrogenase [ubiquinone] iron-sulfur subunit, mitochondrial
FVCG_009877	2.13	8.62E-05	Fumarate hydratase, mitochondrial
FVCG_011734	2.03	5.62E-04	Succinate--CoA ligase [ADP-forming] subunit alpha, mitochondrial
FVCG_008482	2.02	9.13E-04	Malate dehydrogenase, cytoplasmic
FVCG_011231	2.05	0.007	Dihydrolipoyllysine-residue succinyltransferase component of 2-oxoglutarate dehydrogenase complex, mitochondrial
FVCG_012562	2.18	0.015	Citrate synthase
FVCG_006379	1.23	0.032	Dihydrolipoyl dehydrogenase, mitochondrial

Table A2-3 Amino sugar and nucleotide sugar metabolism DEGs.

Gene ID	Log_2FC	padj	Predicted protein or description
FVCG_000683	-4.33	1.99E-30	Beta-hexosaminidase ARB_07893
FVCG_001505	4.85	1.9E-24	UDP-N-acetylglucosamine pyrophosphorylase
FVCG_010163	3.71	3.26E-13	Acidic mammalian chitinase
FVCG_014852	4.06	1.13E-12	Alpha-L-arabinofuranosidase
FVCG_000852	2.94	6.38E-12	Phosphoacetylglucosamine mutase
FVCG_006702	-4.94	3.77E-07	UDP-glucuronate 4-epimerase 4
FVCG_002987	-3.67	5.5E-07	Mannose-6-phosphate isomerase
FVCG_012548	8.08	7.68E-07	Chitotriosidase-1
FVCG_000873	-2.33	1.73E-04	Endochitinase B1
FVCG_007902	-2.32	2.27E-04	Chitin synthase 1
FVCG_009650	-1.71	3.31E-04	Hexokinase-1
FVCG_009654	-1.59	0.001	Beta-hexosaminidase
FVCG_007672	-1.61	0.001	Chitin synthase 3
FVCG_010599	2.87	0.002	Bifunctional protein GAL10
FVCG_014464	-1.76	0.002	Endochitinase 1
FVCG_013222	-3.95	0.002	Endochitinase 1
FVCG_010600	3.11	0.005	UDP-glucose 4-epimerase uge1
FVCG_011937	1.92	0.005	Chitin synthase D
FVCG_004738	1.64	0.005	NADH-cytochrome b5 reductase 1

FVCG_009651	-1.50	0.008	Glucosamine-6-phosphate deaminase 1
FVCG_013285	1.55	0.010	Galactokinase
FVCG_011953	1.27	0.012	Chitin synthase 8
FVCG_001436	-1.17	0.017	NADH-cytochrome b5 reductase 2
FVCG_011221	-1.96	0.020	Endochitinase B1
FVCG_008394	-1.54	0.022	Chitin synthase 2
FVCG_004535	1.69	0.040	Phosphomannomutase

Table A2-4 Stress-responsive DEGs (cell wall, membrane, ROS, autophagy, HSP).

Gene_id	Log_2FC	padj	Predicted protein or description
Cell wall related-DEGs			
FVCG_002059	3.28	0.001	Cytosolic beta-glucosidase
FVCG_009945	-3.47	0.019	Endo-1,6-β-glucanase
FVCG_004800	-2.66	7.02E-10	Endo-1,3(4)-beta-glucanase
FVCG_014472	-6.45	3.50E-05	Exo-1,3-beta-glucanase D
FVCG_009842	-2.00	0.000156	Glucan endo-1,3-beta-D-glucosidase
FVCG_013827	-1.58	0.024	Glucan endo-1,3-beta-D-glucosidase
FVCG_007577	5.77	2.39E-08	Endo-1,4-beta-xylanase B
FVCG_006024	3.34	0.049	Lytic cellulose monooxygenase (c4-dehydrogenating)
FVCG_010163	3.71	3.26E-13	Chitinase
FVCG_012548	8.08	7.68E-07	Chitinase
FVCG_000873	-2.33	1.73E-4	Chitinase
FVCG_014464	-1.76	0.002	Chitinase
FVCG_013222	-3.95	0.002	Chitinase
FVCG_011221	-1.96	0.020	Chitinase
FVCG_007902	-2.32	2.27E-4	Chitin synthase
FVCG_007672	-1.61	0.001	Chitin synthase
FVCG_011937	1.92	0.005	Chitin synthase
FVCG_011953	1.27	0.012	Chitin synthase
FVCG_008394	-1.54	0.022	Chitin synthase
Cell membrane related-DEGs			
FVCG_007965	-1.42	0.017	Delta(24(24(1)))-sterol reductase
FVCG_013279	3.88	0.009	Sterol 14-alpha demethylase
FVCG_010334	-2.97	2.45E-06	KES1-involved in ergosterol biosynthesis
FVCG_012070	1.74	3.18E-4	sterol 3 beta-glucosyltransferase
FVCG_006349	1.30	0.011	Phospholipid: diacylglycerol acyltransferase
Antioxidant enzymes related-DEGs			
FVCG_012854	4.02	1.49E-18	Superoxide dismutase [Mn], mitochondrial
FVCG_001087	3.26	5.45E-13	Superoxide dismutase copper/zinc binding domain-containing protein
FVCG_015156	1.53	0.003	Catalase-peroxidase
FVCG_014928	-1.38	0.021	Catalase-peroxidase
FVCG_002399	4.54	1.03E-14	Catalase
FVCG_005314	-4.91	1.22E-08	Catalase
FVCG_006740	2.68	5.47E-06	Cytochrome c peroxidase, mitochondrial precursor
FVCG_011260	2.89	0.042	Hypothetical protein similar to fatty acid oxygenase

Autophagy related-DEGs			
FVCG_000750	1.19	0.033	Autophagy-like protein 22
FVCG_012070	1.74	3.18E-4	Autophagy-related protein 26
FVCG_003316	1.99	0.002	Autophagy-related protein 29
FVCG_006385	1.38	0.001	Autophagy-related protein 9
FVCG_009136	2.65	2.75E-08	Autophagy-related protein 3
Heat shock proteins related-DEGs			
FVCG_011938	3.08	1.55E-13	Hsp88-like protein
FVCG_011753	2.75	1.13E-12	Molecular chaperone HtpG/hsp90
FVCG_002597	2.76	9.47E-13	Hsp10-like protein
FVCG_000828	3.49	3.84E-12	SHSP domain-containing protein
FVCG_010833	2.86	2.52E-10	Hsp98-like protein
FVCG_000976	2.31	1.06E-05	Hsp78, mitochondrial
FVCG_006208	1.58	1.5E-4	Hsp60, mitochondrial
FVCG_001717	1.52	1.71E-4	Stress-induced-phosphoprotein 1
FVCG_001108	1.57	6.28E-4	SHSP domain-containing protein

Appendix 3

Scientific publications

1. **Xiaoyan Liang**, Shumila Ishfaq, Yang Liu, M. Hassiam Jijakli, Xueping Zhou, Xiuling Yang, and Wei Guo, 2024. Identification and genomic insights into a strain of *Bacillus velezensis* with phytopathogen-inhibiting and plant growth-promoting properties. *Microbiological Research*, *285*, 127745.

2. **Xiaoyan Liang**†, Xiu Zhang†, Kaifei Xi, Yang Liu, M. Haissam Jijakli, and Wei Guo, 2024. Development of an RPA-based CRISPR/Cas12a assay in combination with a lateral flow strip for rapid detection of toxigenic *Fusarium verticillioides* in maize. *Food Control*, *157*, 110172. (co-first author)

3. Shumila Ishfaq, **Xiaoyan Liang**, Yi Ding, Jun Zhang, Fengcheng Zhang, Arslan Anjum, and Wei Guo, 2025. Integrated transcriptomic and metabolomic analysis reveals the antifungal effects of myco-silver nanoparticles against toxigenic *Fusarium verticillioides*. *Journal of Environmental Management*, *390*, 126360.

4. Shumila Ishfaq, Yi Ding, **Xiaoyan Liang**, and Wei Guo, 2025. Advancing lodging resistance in maize: Integrating genetic, hormonal, and agronomic insights for sustainable crop productivity. *Plant stress*, *15*, 100777.

5. Huan Li, Shumila Ishfaq, **Xiaoyan Liang**, Rui Wang, Hailei Wei, and Wei Guo, 2025. A novel CFEM effector in *Fusarium verticillioides* required for virulence involved in plant immunity suppression and fungal cell wall integrity. *International Journal of Molecular Sciences*, *26*(9), 4369.

6. Kaihua Wu†, **Xiaoyan Liang**†, Xiu Zhang, Guoping Yang, Huaxiao Wang, Yining Xia, Shumila Ishfaq, Hongfei Ji, Yuxi Qi, and Wei Guo, 2024. Metabolomics analysis reveals enhanced salt tolerance in maize through exogenous Valine-Threonine-Isoleucine-Aspartic acid application. *Frontiers in Plant Science*, *15*, 1374142. (co-first author)

7. Jun Zhang†, **Xiaoyan Liang**†, Hao Zhang, Shumila Ishfaq, Kaifei Xi, Xueping Zhou, Xiuling Yang, and Wei Guo, 2023. Rapid and sensitive detection of toxigenic *Fusarium asiaticum* integrating recombinase polymerase amplification, CRISPR/Cas12a, and lateral flow techniques. *International Journal of Molecular Sciences*, *24*, 14134. (co-first author)

8. **Xiaoyan Liang**†, Xiu Zhang†, Abdul Haseeb Hafiz, Tingting Tang, Jihao Shan, Bo Yin, and Wei Guo, 2022. Development and evaluation of a novel visual and rapid detection assay for toxigenic *Fusarium graminearum* in maize based on recombinase polymerase amplification and lateral flow analysis. *International Journal of Food Microbiology*, *372*, 109682. (co-first author)